DISSOLUTION KINETICS OF CALCIUM CARBONATE

by

Padraig Joseph Daly

Thesis submitted in accordance with the requirements of the University of Liverpool for the degree of Doctor in Philosophy.

September 1985

ACKNOWLEDGEMENTS

I would like to thank my illustrious supervisor, Dr. R.G.Compton, and his ever present side kick, Mr. A.M.Waller, for their thought provoking insight into research, and life in the department in general, summing up the true spirit of research, especially that coming from a gin bottle! I would also like to thank the rest of the ex-electrochemistry group for the use of their equipment over the last four years. My thanks must be extended to the technical staff in the Department for their advice and understanding, and to my fellow denizens at 'Parkside' for their support, down the Masonic.

I wish to thank the S.E.R.C. and the Freshwater Biological Association for a CASE award, especially for the selubrious accommodation provided in Dorset.

Finally, I would like to express my appreciation to Mrs. Andrea Simpson for her unexpected ability to translate hyroglyphics.

ABSTRACT

A technique has been devised for fabricating single crystal rotating discs, and use has been made of the reproducible, well-defined hydrodynamics to separate the transport controlled reactions from those which are chemically controlled, in the dissolution of calcium carbonate. The dissolution has been studied over a range of pH_2 and pCO_2 values and in general the flux of dissolving Ca^{2+} is given by; $J = k_1 H^+ + k_3 H_2CO_3 + k_2$, where k_1 and k_3 are transport controlled rate constants and $k_2 = 2.1 \times 10^{-9}$ $mol.cm^{-2} s^{-1}$. In the case of a weak acid which dissociates H^+ is replaced by weak acid, and k_1 is changed accordingly.

However, the above value of k_2 only holds for pre-reacted surfaces. It has been shown that, for a flawless surface, either freshly cleaved or polished, k_2 is reduced by a factor of 10. This, it has been shown, is due to the lack of active sites, at which dissolution can occur. Further work on powders, both dissolution and precipitation, have confirmed this value of k_2 for flawless surfaces.

To overcome the intrinsic disadvantages of using the rotating disc, i.e., poor transient times and the difficulty in studying the action of inhibitors, the use of a channel electrode has been proposed. The theory for this system has been derived, and has been shown to be in good agreement with experiment.

CONTENTS PAGE

PAGE
MISSING
IN
ORIGINAL

CHAPTER 1

INTRODUCTION

Calcium carbonate is an important naturally occurring compound which, chiefly in its most stable form, calcite, makes up nearly 7% of the earth's crust, as limestone, marble, chalk and as the crystalline mineral calcite. Environmentally, it plays an important role in maintaining the balance of pH in rivers, lakes and oceans, through the carbon dioxide bicarbonate equilibria. Calcium carbonate enters the system by dissolution and leaves it *via* precipitation and both of these processes have been extensively studied giving rise to a number of kinetic models.

1.1 DISSOLUTION OF CALCIUM CARBONATE

The dissolution of calcium carbonate, in its various natural forms is of considerable interest geologically and extensive research has been carried out to investigate the mechanism and kinetics of the reaction. Researchers have used various techniques to measure the rate and it has been shown that the rate of dissolution in aqueous media is controlled by a mixture of transport and surface controlled steps. The particular rate determining step depends upon the experimental conditions, especially pH and pCO_2 flowing through the reaction mixture. It has further been shown that the different forms of calcium carbonate, i.e., marble, limestone, Iceland Spar, dolomite and olivine show different rates of reaction,[1] and this has been explained in terms of differing surface reactivity.

Miller[2] measured the solubility of various forms of calcium carbonate, (Iceland Spar, from Chihuahua, Mexico, Limestone from Solenhofen, Germany, and Venus Mercenaria shells), as a function of temperature and ρCO_2. He ground all three forms into pellets approximately 1 mm x 30 mm x 12 mm, washed the surface with dilute HCl and carefully weighed each sample! The samples were then placed in a glass container and sufficient water, either distilled, 0.5M NaCl, or sea water was added to cover the pellet. This container was then placed in a "bomb", the required temperature and ρCO_2 set, and the system was allowed to come to thermal equilibrium, (typically 6 - 8 hours). The solubility was found by reweighing the pellets, to find the weight loss (g), and dividing this by the volume of water (l). He found that the solubility of the Iceland Spar was less than that of the limestone, which was less than that of the Venus Mercenaria shells. He further found that the solubility of all three samples decreased with temperature, but increased with ρCO_2. He compared his results with those of earlier workers,[3-7] who had studied the solubility under similar conditions, and found that although his values were somewhat lower than the values reported, the shape of the plots of solubility versus ρCO_2 was similar. This he attributed to the difference in the calcium carbonate samples used and the difference in particle size, as smaller particles dissolve more rapidly and have a greater solubility.[8,9]

Miller then proceeded to calculate the equilibrium constant for the reaction:

$$CaCO_{3(s)} + CO_{2(g)} + H_2O_{(l)} \rightleftharpoons Ca(HCO_3)_2 \qquad 1.1$$

at various ρCO_2, and found good agreement between his results and those in the literature. At ρCO_2=0.1 bar he calculated the solubility to be 0.37g l^{-1} (c.f. 0.39 g^{-1} as found by Frear and Johnston[7]), and at ρCO_2 = 3.5×10^{-4}bar his valueof 0.044g l^{-1} compared well with that of 0.046g l^{-1} as found by Kendall.[10]

The actual kinetics of the reaction was studied in 1933 by King and Liu[11] who used a rotating marble cylinder to study the dissolution of hydrochloric acid (from pH 2.0 - pH 2.72) at various rotation speeds, between 15 - 25°C. As this work was carried out before the Levich theory of the rotating disc[12] the experiment consisted of weighing the marble cylinder, rotating it in the acid solution for four minutes and the reweighing the cylinder to find the dissolution rate!

They found that the rate of dissolution increased with $[H^+]$, temperature, and rotation speed. They also investigated the effects of viscosity on the reaction rate. To do this they dissolved inert salts and cane sugar into the acid, and found that the rate was inversely proportional to the viscosity of the solution. These results led them to propose that the rate of reaction was transport controlled, and that the chemical step was the attack of H^+ on the marble surface:

$$2H^+ + CaCO_3 \rightarrow Ca^{2+} + 2HCO_3^- \qquad 1.2$$

This experiment suffered from the drawback that the area of marble exposed changed as the reaction proceeded, and to overcome this Tominaga et al.,[13] used a marble rotating disc, in which the walls of the marble cylinder were coated in a non-reacting glue. Thus, the area could be considered to be constant. They rotated this disc at 485 rpm in various concentrations of HCl (pH = 0.41 - 0.88) and followed the reaction by measuring the volume of CO_2 released. They believed that the reaction was transport controlled.

The transport controlled nature of the reaction was also shown by Kaye[14] and by Weyl[15]. Kaye studied the dissolution of limestone and calcite crystals in dilute (10%) HCl. He allowed the acid to flow down the limestone blocks, and measured the depth dissolved. He varied the flow by increasing the angle of the block and found that by increasing the velocity of the acid, he increased the dissolution rate.

Weyl used a high powered jet of H_2O, saturated with CO_2 (pH $\sim$ 3.9), to study the dissolution of Iceland Spar. The velocity was varied from 1.8 - 3.7 $m.s^{-1}$ by adjusting the hydrostatic head of the reservoir. He directed the jet onto the crystals and measured the rate by the depth of solid dissolved. He showed that the rate was proportional to the jet velocity, for the values used, and he claimed that the rate of reaction was controlled by the diffusion of products away from the surface.

Erga and Terjesen[16] studied the dissolution of crushed limestone divided into particle sizes from 295 - 422 μm, which corresponds to a surface area of $\sim$125 $cm^2 g^{-1}$, assuming that all the particles are perfect rhombs. The experiments were carried out in a stainless steel vessel of 10 l capacity, thermostated at 25 $\pm$ 0.2°C. The vessel was filled with distilled water and carbon dioxide at 0.95 atm., was passed through the water, which was constantly stirred using baffles, until the system had reached equilibrium, as indicated by a steady conductivity value. 100g Of the limestone was weighed out and this was placed in the reaction vessel, and the reaction was allowed to proceed towards equilibrium.

They found that the presence of 10^{-5} mol dm^{-3} Cu^{2+} (present as an impurity in the distilled water) caused the system to approach a new equilibrium, approximately 20 - 30% below the true one. They claimed that the presence of small amounts of copper in the reaction solution accounted for the difficulties Frear and Johnston[7] and Shetermina and Frolova[17] had experienced in allowing their systems to reach equilibrium.

Erga and Terjesen then investigated whether the copper was adsorbed onto the calcite surface, or whether it remained in solution by:- (1) stopping the reaction, decanting the reaction solution, and then adding new crushed limestone and rerunning the reaction; and (2) decanting the solution and adding the particles to a copper free solution and re-running. In the first case the

reaction proceeded towards the new equilibrium, while in the second the expected equilibrium was approached. Thus, the Copper (II) ions remain in the solution.

To overcome these inhibitory effects, and to make sure that all their results could be directely compared with one another, the solution was pretreated with E.D.T.A. (ethyl-diamine-tetroacetic acid). This solution was then used to investigate the reaction with various values of ρCO_2 flowing through the system. They found a linear relationship between the reaction rate and the concentration of $Ca(HCO_3)_2$ and used the intercepts of their plots to find the equilibrium concentration of $Ca(HCO_3)_2$ at various ρCO_2 values, finding that the values of Miller[2] (who used a coarser material) was 4% lower, while those of Frear and Johnston[7] (who used a finer powder) were 6.2 - 9.8% higher.

The gradients of the graphs of rate versus $[Ca(HCO_3)_2]$ were plotted as function of equilibrium concentration of $Ca(HCO_3)_2$ and a linear relationship was shown. From this they derived the following relationship:

$$\frac{dc}{dt} = k\ C^*\ (C^* - C) \qquad 1.3$$

C = concentration of $Ca(HCO_3)_2$

C^* = equilibrium concentration of $Ca(HCO_3)_2$

Thus, the rate of reaction is proportional to the degree of undersaturation in the system.

Further experiments showed that the dissolution rate was proportional to area, but independant of the velocity of the CO_2. From this they concluded:

1. The rate was independant of CO_2 transfer between the gas phase into the liquid, and
2. The dissolution was independant of any chemical reaction occurring in the bulk of the solution.

Therefore, the reaction at the pH studied was assumed to occur at the calcite surface, or in the layer adjacent to it. This was verified by varying the stirring rate and finding the change in dissolution rate. It has been shown by Bircumshaw and Riddiford[18] that heterogeneous processes controlled by diffusion should show a stirring coefficient of 0.5 - 1.0, while Erga and Terjesen measured a value of 0.22, indicative of a surface controlled reaction.

Terjesen et al.,[19] investigated the inhibitory effects of Pb^{2+}, Cd^{2+} and Zn^{2+} respectively, on the dissolution rate of calcite, and Nestaas and Terjesen[20,21] studied the effects of Sc^{3+} on the dissolution of CaF_2. From this they derived the following empirical rate equation, describing the dissolution of calcite in the presence of inhibitors:

$$\text{rate} = k\left(C^*_{real} - \frac{CC^*_{real}}{C^*_{app}} \right) \qquad 1.4$$

C^*_{real} = real equilibrium concentration of $Ca(HCO_3)_2$

C^*_{app} = apparent equilibrium concentration of $Ca(HCO_3)_2$

They explained the inhibition by the impurity absorbing onto the calcite surface with equivalent amounts of CO_3^{2-}. So the role of the inhibitor in reducing the dissolution, is to promote the reverse reaction, i.e., the formation of solid carbonate on the lattice surface.

Nestaas and Terjesen[22] then proceeded to study the inhibitory effects of Sc^{3+} on the dissolution rate of calcite, measuring the surface concentration of Sc^{3+} by using ^{46}Sc, a radioactive isotope. They found agreement with Gorlich et al.,[23,24] that the adsorption was pH dependant and that only a small area of the calcite surface was covered (i.e., 1.4×10^{-10} moles Sc^{3+} per cm^2, 1% of the available area) in good agreement with the work of Ives[25] who studied the dissolution of LiF crystals in the presence of Fe^{3+}. They found that the inhibition observed was proportional to the number of Sc^{3+} ions per cm^2. These results give rise to the following empirical rate equation:

$$\text{rate} = k(C^*_{real} - C) - k' \bar{C}_{inh} \qquad 1.5$$

$\bar{C}_{inh}$ = surface concentration of Sc^{3+}

These results, based on the measurement of absorbed inhibitors led them to reject their earlier theory of the inhibitor being absorbed onto the lattice surface. They postulated that the reaction was governed by the simultaneous hydration of Ca^{2+} and CO_3^{2-} ions by water molecules present in the absorption layer. This layer also contains Ca^{2+} and inhibitor ions present in their hydrated forms. When the concentration of these ions increases then the quantity of free water available for the hydration of lattice ions falls, as does the rate of dissolution. This theory was also rejected as it could not explain how compounds could inhibit both dissolution and precipitation, as well as being unable to explain the promotion of rate noted by Nestaas and Terjesen.[20]

They therefore proposed a theory based on active sites or "kinks" to explain the observed inhibition (in agreement with Ives[25]). This suggested that dissolution occurs from active sites or "kinks" on the lattice surface, and that inhibitors block these sites by absorption. The rate of dissolution is, therefore, equal to the product of the number of kinks and the rate of movement of individual kinks. Thus, equation 1.5 can be rewritten:

$$\text{rate} = k(\bar{C}_o - \bar{C}_{Ca^{2+}} - \bar{C}_{inh}) \qquad 1.6$$

$\bar{C}_o$ = surface concentration of kinks

$\bar{C}_{Ca^{2+}}$ = surface concentration of kinks blocked by hydrated Ca^{2+} ions.

$\bar{C}_{inh}$ = surface concentration of kinks covered by inhibitor

Morse[26] (in 1974) developed a new technique for the study of dissolution (and precipitation) under conditions of steady state disequilibrium - the "pH-stat". He developed it for the study of $CaCO_3$ dissolution. Previous work had used the 'free drift' method in which $CaCO_3$ was added to the system, which was allowed to react towards equilibrium, the rate slowing down as the equilibrium state was approached. In the 'pH-stat' method the pH of the solution is kept constant by the automatic addition of acid or base, as soon as a pH electrode detects any change in the solution. (Figure 1.1 shows a schematic representation of the "pH-stat". The chart recorder shown has subsequently been replaced by a micro computer.)

In the 'free drift' method when the reaction was followed by measuring the change in pH,[27-29] the measured rate was dependant on calculating the H^+ consumption from the change in the slope of the pH *vs.* time plot. However, the pH change was not simply due to H^+ consumption,

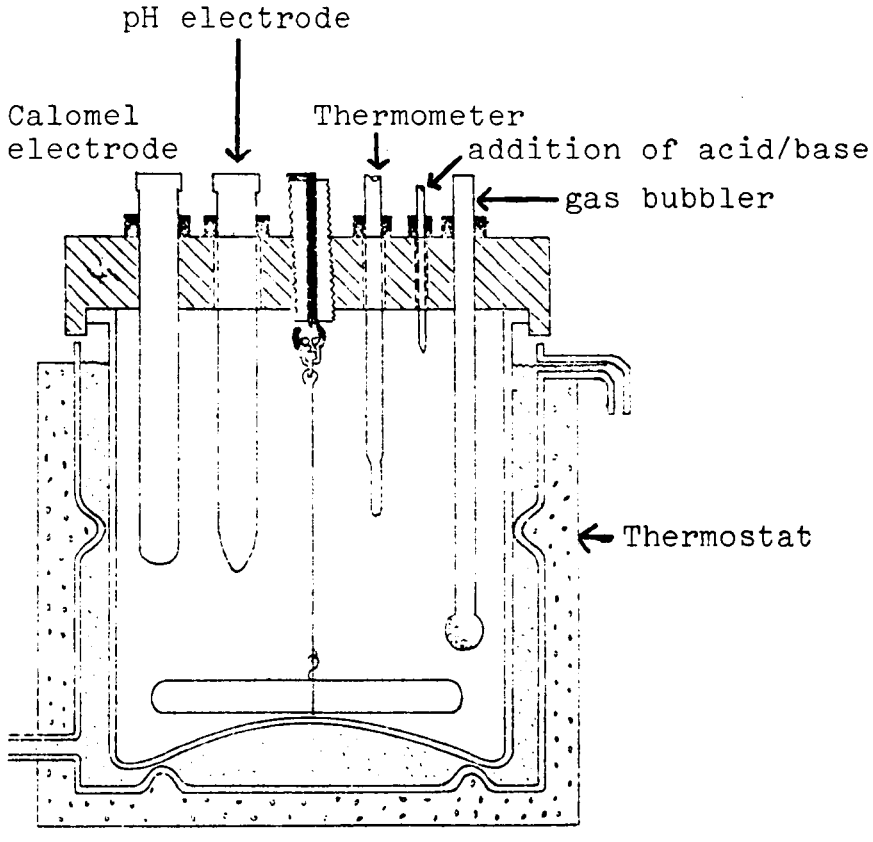

FIGURE 1.1 The pH stat

the CO_3^{2+} released effected the pH, and allowances had to be made for this via a consideration of the chemical equilibria set up in the system. With the 'pH-stat' the total alkalinity remains constant and the rate of addition of H^+ is a direct measure of the dissolution rate. Morse claimed that by keeping the system under constant conditions, it would be possible to obtain very accurate reaction rates and to study the effects of absorption, and of inhibitors under conditions of constant saturation.

Morse et al., used the apparatus shown in Figure 1.2, in conjunction with the 'pH-stat' to study the dissolution of calcite, comparing the determined rates with those found in the oceans, and published a series of papers.[30-34]

Their first experiments[32] consisted of trying to create oceanic conditions in the laboratory. They used constant stirring speed and constant pCO_2, thermostated the reaction vessel at 25°C and added 255 mg of calcite, consisting of rhombs ranging in size from 1 to 20 μm, to 300 ml of sea water. The measured dissolution rates were found to be higher than those found in the ocean, even when allowances were made for the difference in particle size and temperature (the ocean being typically 2°C). They assumed that this was due to differences between the surface of the calcite particles and those in the oceans:- probably due to absorption of naturally occurring organic compounds (e.g., humic acids) found in the oceans.

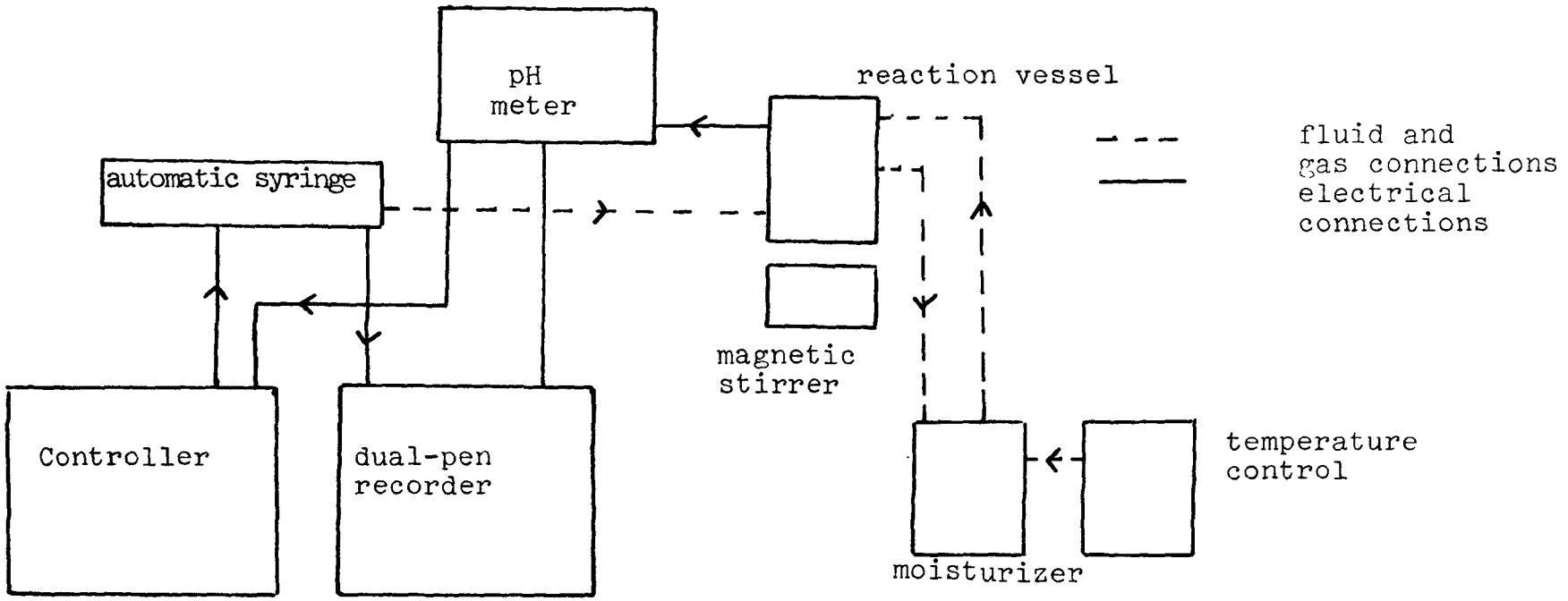

FIGURE 1.2 The experimental set-up as used by Morse.

They attempted to explain the measured dissolution rate in terms of the diffusion controlled model of Pond et al.,[35] and of Berner.[36] However, like Peterson[37] and Berger[38] they found that the measured rate was an order of magnitude less than the calculated value. This led them to propose (like Peterson[37]) that the rate of dissolution of calcite was controlled by the rate of detachment of ions from the lattice surface. Thus, the velocity and turbulance of the reaction solution did not affect the rate determining step.

The next area investigated[33] was the effect of pH (3.9 - 7.5) and pCO_2 ($1 - 10^{-4.5}$ atm.) on the dissolution rate. For this work they used synthetic calcite, formed from the crystalisation of sodium free aragonite, using the method of Katz.[39] This calcite was not sorted into size, instead the random distribution of particle size was measured and a computer programme was used to find the exposed reaction area. The reaction solution was 'pseudo sea-water', a solution of $NaCl$-$CaCl_2$ having the same ionic strength and calcium concentration as sea water.

They found that the dissolution of the calcite could be split up into 3 pH regions. The rate being proportional to the area of calcite in all cases. The first pH region (below pH 3.9) they found could be described in terms of a diffusion controlled reaction, using the following equation:[36,39,40]

$$R = \frac{D}{r} A (Cs-C) \qquad 1.7$$

D = diffusion coefficient

A = surface area

Cs = surface concentration

C = bulk concentration

r = spherical radius of crystals.

It should be noted that equation 1.7 only holds for small spherical particles (<10 μm in radius) for larger particles r must be replaced by L, the thickness of the stagnant boundary layer about each particle.

They found $D_{H^+} = 2.6 \times 10^{-5}$ cm^2s^{-1} compared to the literature value for D_{H^+} (in sea water) of $3.3 \times 10^{-5} cm^2s^{-1}$. They were also able to show that the rate was independant of ρCO_2 and $[H_2CO_3]$, despite the difficulty in maintaining the steady state conditions, due to the speed of the reaction. They attributed the rate determining step to be H^+ transfer across the stagnant layer.

Above pH 4 the rate measured was found to be an order of magnitude lower than that for diffusion control, thus the reaction was not controlled by H^+ transfer.

The rate of reaction in the third region was found to be independant of ρCO_2 and of stirring speed and they compared this region to that studied by Nestaas and Terjesen.[22] They assumed that the rate determining step in this region was the detachment of ions from the lattice surface, and they postulated that the detachment

occurred at kink sites,[43-46] explaining the inhibitory effect they had noted in the presence of phosphate.[31]

The boundary between the second and third region had no set pH transition point, but varied according to ρCO_2. In the second region the rate was faster than in the third and was found to be proportional to pH. However, above $\rho CO_2 = 10^{-2}$ atm., the rate became constant. They were unable to define the reaction occurring in this pH, but suggested that the rate determining step was the absorption of H^+ onto the calcite surface which created new kink sites by reaction with CO_3^{2-}. The absorbed H^+ could also increase the rate of reaction by chemically reacting with inhibitors bound to the kink sites.

In the final paper of the series,[34] they studied the effect of inhibitors, both organic and inorganic, present in the ocean, on the dissolution rate, following the observation of Chave and Suess[47] that absorbed ions and organic molecules played an important role in controlling the surface chemistry, and thus the dissolution, of minerals in sea water. They investigated the reduction in the reaction rate caused by the presence of a mixture of organic compounds (see Table 1.1), finding that 1000 µg/l of each compound reduced the rate by 25%. However, since the concentration of dissolved organic compounds rarely exceeded 1 mg/l they concluded that the presence of dissolved organic compounds was not responsible for the reduced rate found in the ocean.

They then turned to inorganic compounds, chiefly, phosphate, nitrate, and silica. They found that silica

TABLE 1.1 Composition of the organic mixture used by Morse

L-Cystine	Sodium stearate
Taurine	Cetyl alcohol
L-methionine	Cadavarine
Hydroquinone	Lauric acid
Lauric acid	Palmitric acid
Soluble starch	L-ascorbic acid
Sodium citrate	Glycogen
Sodium palmitate	Sucrose
Sodium oleate	Egg albumin

even at 400 μmol dm^{-3}, twice the levels found in the ocean, showed no inhibition, nitrate only produced a 6% reduction at twice its natural highest concentration, while phosphate again showed the large inhibition already demonstrated.

From this series of experiments they concluded:

1. The major inhibitor of calcite in the oceans was phosphate which acted by absorbing onto kinks on the lattice surface.
2. At high pH the rate determining step was not transport controlled, but consisted of the removal of Ca^{2+} and CO_3^{2-} ions from kink sites.
3. At lower pH the rate of reaction increased due to the formation of new kink sites, from the reaction of absorbed H^+ with CO_3^{2-} ions, and due to the increased rate of step spreading.

4. At pH <4 the surface detachment of Ca^{2+} and CO_3^{2-} became so fast that the rate limiting step became the diffusion of H^+ towards the calcite surface; thus this region showed transport control.

Plummer and Wigley[48] used the "free drift" method to study the dissolution of semi-optical Iceland Spar over the pH range 4 - 6. The Iceland Spar was washed and sorted into particle size by wet sieving, using a 325 mesh sieve (44 μm). The area was found from the weight of calcite used, assuming the particles were pefect rhombs and that no area change occurred during the reaction. To make this last assumption valid the weight of calcite exceeded its solubility by at least five times, and often by up to twenty times. The reaction was carried out in a reaction vessel thermostated at 25°C. 500 ml Of distilled water was placed in the vessel and carbon dioxide at a partial pressure of 0.92 atm., was bubbled through and the system was left to equilibrate, as indicated by a steady pH value. The calcite sample was weighed out and was washed in 10^{-3} mol dm^{-3} HCl, to dissolve any absorbed impurities, organic or inorganic, before being added to the reaction vessel. The reaction was followed by monitering the change in pH, and the calcium concentration was found using the pH and ρCO_2 values, <u>via</u> an iterative programme, utilising the extended Debye-Huckel theory.

They tested the rate of reaction for any transport controlled step, by altering the particle size, but while they found a slight dependance it was insufficient for the reaction to be controlled by H^+ transport. They, therefore, assumed the reaction was controlled by a surface reaction.

They found that the dissolution reaction could be divided into two pH regions; the boundary being at pH 5.9. At pH's lower than 5.9 they found the surface reaction to be second order with respect to $[H^+]$ and $[Ca^{2+}]$. This region they related to the second pH region of Berner and Morse,[30] and found good agreement with the measured rate constants. The rate of reaction was less in the second region and showed a higher order of reaction. They attributed this to trace inhibitors absorbed on reactive sites on the lattice surface.

Plummer et al.,[49] in a paper widely regarded as definitive, then proceeded to investigate the dissolution of calcite over a wider range of pH (2 - 7) and at variable pCO_2 (0 - 1 atm.), using a mixture of the 'pH-stat' and 'free drift' methods. The 'pH stat' method was used to investigate the reaction far from equilibrium, while the reaction was followed by the 'free drift' method when the system was near equilibrium.

Three regions of dissolution were found. The first region was found to be transport controlled and a plot of log rate vs. pH gave a slope of -1. They assigned the reaction in this region to be the transport

of H^+ to the calcite surface, but were unable to be more definite as they could not determine the H^+ transfer rate constant a priori for their system.

The reaction rate was shown to be independant of ρCO_2, though the transition point varied with ρCO_2. At ρCO_2 = 1 atm., the transition occurred at pH 3.5, while at ρCO_2 = 0, it occured at pH 4.5.

Thus, in this region the rate of reaction was given by:

$$\text{rate} = k_1 [H^+] \qquad 1.8$$

k_1 = H^+ transport coefficient.

The measured rate of dissolution in the second region was lower than in the first. It was found to be transport controlled and to depend upon both ρCO_2 and pH. At constant ρCO_2 the rate was proportional to pH. The exact boundaries of this region was found to depend upon ρCO_2. At ρCO_2 = 1 atm., the region extended from pH 3.5 - 5.5, while when ρCO_2 = 0 the region started at pH 4.5, but the transition to the third region could not be found.

They also found that in the near absence of both H^+ and CO_2 the reaction rate was constant and showed no transport control. This was assumed due to a surface reaction, which they assigned to the reaction of H_2O with the calcite surface.

Thus the overall reaction was described by:

$$R = k_1 [H^+] + k_3 [H_2CO_3] + k_2 \qquad 1.9$$

$k_1 + k_3$ are transport controlled rate constants.

k_2 = surface controlled rate constant.

In the third region (where the system was approaching equilibrium) they assumed that all three of the above reactions continued to occur, but the back reaction, precipitation, became significant, reducing the rate of dissolution. The overall reaction could, therefore, be defined by:

$$R = k_1 [H^+] + k_3 [H_2CO_3] + k_2 - k_4 [Ca^{2+}][HCO_3^-] \qquad 1.10$$

The value of k_4 being a function of ρCO_2 and temperature.

Using this rate equation they attempted to derive a mechanistic model which could explain their experimental results. They made the assumption that a very thin surface layer existed between the boundary layer and the solid surface, and assumed that the supply of aqueous CO_2, H_2CO_3, and of H_2O across the boundary layer was so fast that the concentration of these species at the

surface was equal to that at the bottom of the boundary layer. They further assumed that the surface layer was saturated with respect to calcite and that the surface H^+ concentration was equal to the calcite saturated value for a given surface concentration of H_2CO_3. They achieved good agreement between theory and experiment.

Sjöberg[50] studied the dissolution of calcite powder, using the free drift method, as a function of pH. The powder used had a specific surface area of 0.37 m^2g^{-1} (B.E.T. nitrogen absorption), and this was dissolved in 700 ml, 0.7 mol dm^{-3} HCl thermostated at 25°C, with a stream of pure nitrogen flowing through the solution. He investigated the stirring dependance finding a stirring coefficient of 0.33, indicative of a chemically controlled rate determining step.[18] He also found that the rate was proportional to the area of calcite and that above pH 7.5 the rate of reaction was independant of pH.

He then studied the reaction with various concentrations of calcium present in the original solution and when he plotted a graph of log (rate/area) versus log $[Ca^{2+}]_{initial}$ he found a straight line with a gradient of $-\frac{1}{2}$, indicating that the rate was proportional to the square root of the calcium concentration. He then plotted a graph of (rate/area) vs. $[Ca^{2+}] \times [CO_3^{2-}]$, and he found a straight line. Using these results he proposed the following equation to describe the rate of dissolution:

$$R = kA\ (K_{sp}^{\frac{1}{2}} - [Ca^{2+}]^{\frac{1}{2}}[CO_3^{2-}]^{\frac{1}{2}}) \qquad 1.11$$

A = area

K_{sp} = solubility product of calcite.

Further work[51] investigated the role inhibitors played on the observed rate. He redefined equation 1.11 in terms of the relative saturation, Ω, where:

$$\Omega = \frac{[Ca^{2+}]\,[CO_3^{2-}]}{K_{sp}} \qquad 1.12$$

giving:

$$R = kA\ (1 - \Omega^{\frac{1}{2}}) \qquad 1.13$$

He found that in the presence of inhibitors an improved description was:

$$R = k'A\ (1 - \Omega^{\frac{1}{2}})^n \qquad 1.14$$

where k' depended upon $[Ca^{2+}]$ and $[SO_4^{2-}]$

n depended upon the ratio $[Mg^{2+}] / [Ca^{2+}]$.

Thus, in KCl solution the equation reverted back to equation 1.13, while in phosphate-free sea water the rate was given by:

$$\text{rate} = k'A\,(1 - \Omega^{\frac{1}{2}})^2 \qquad 1.15$$

From his results he proposed that not all inhibitors acted similarly. His results with phosphate showed agreement with the work of Morse,[33] Terjessen et al.,[22] and Plummer et al.,[49] that phosphate acted by blocking kink sites, but he proposed the Mg^{2+} acted by forming a layer of Mg-calcite on the lattice surface. He also agreed with Christoffersen et al.,[52] that the presence of Ca^{2+} caused inhibition.

Equation 1.13 showed disagreement with the empirical equation of Morse[53] and with that of Keir.[54] Sjöberg (equation 1.13) found that the rate was proportional to the square root of the relative saturation, while Morse and Kier found that the rate was directly proportional to the relative saturation, i.e.,

$$R = kA\,(1 - \Omega)^2 \qquad 1.16$$

Rickard and Sjöberg[55] assumed that the differences in these empirical equations could be explained in terms of the contrasting hydrodyanmics of the different systems, and they proposed the use of a rotating disc[56] to study the reaction under conditions where the hydrodynamics had been exactly solved.[57,58]

They fabricated a rotating disc from a single crystal of calcite, and studied the dissolution of calcite as a function of pH[59,60] and of temperature.[61] They found that the dissolution reaction could be divided into 3 pH regions.

At low pH (<4), the reaction was found to be independant of ρCO_2, though the exact transition point was dependant upon ρCO_2. The rate of reaction was found to be directly proportional to $\omega^{\frac{1}{2}}$, indicative of a transport controlled reaction. The second region extended from pH 4.0 - 5.5 and again the rate was found to show a stirring dependance, as well as varying with pH and ρCO_2. The third region was found to show no rotational speed effect, and the rate was independant of $[H^+]$.

They varied the temperature of the reaction solution between 1 - 62°C and found that the boundary points between the three regions were temperature dependant, the boundary point moving to higher pH as the temperature decreased. This they attributed to the transport controlled reaction becoming less dominant as the temperature fell, in agreement with the work of Lund et al.[62]

The results of Sjöberg and Rickard will be discussed in detail later.

Lund et al.,[62] used a marble rotating disc, of approximately 1 cm diameter, to study the rate of calcite dissolution as a function of ; $[H^+]$, 9 - 0.1M HCl; temperature, 25 - -15.6°C; and rotation speed, 100 - 500 rpm. The disc was polished using a mixture of 400, 320, and 180 carborundum pads, and pure nitrogen was bubbled through the reaction solution at all times.

They found that at 25°C the dissolution rate was proportional to $\omega^{\frac{1}{2}}$ and they measured D_{H^+} to be 3.97 x $10^{-5} cm^2 s^{-1}$. However, at -15.6°C the reaction was found to

TABLE 1.2 The value of k_1 as measured by various workers.

RESEARCHER	pH	TYPE OF CALCITE	STIRRING	RATE/cm s^{-1}
King and Liu[11]	2.0 - 2.7	Marble cylinder	485 rpm	0.032
Tominaga et al.,[13]	0.41 - 0.88	Marble disc	4000 rpm	0.0073
Weyl[15]	3.9	Iceland Spar/ Limestone	1.8 - 3.7 ms^{-1}	0.15
Morse and Berner[33]	3.9 - 5.2	Calcite powder	Magnetic stirrer	0.038
Plummer et al.,[49]	2 - 4	Crushed Iceland Spar	1800 - 2300 rpm	0.051
Sjöberg[51]	2 - 4	Calcite powder	276 - 480 rpm	0.012
Lund et al.,[62]	1.0	Marble disc	100 - 500 rpm	0.016
Sverdrup and Bjerle[1]	2 - 5	Calcite powder	?	0.136

be controlled by a mixture of transport control and a surface reaction, as indicated by a curving Levich plot. This they claimed was due to the chemical reaction becoming dominant at low temperatures.

This section has outlined the major techniques used in the study of the dissolution of calcite, in its various forms, and has shown the various techniques and experimental conditions used. All workers have agreed that at low pH (<4) the reaction is governed by the transport of H^+ to the calcite surface, and that at high pH the reaction is controlled by a surface chemical reaction. In between these two extremes the reaction is controlled by mixed kinetics, though the exact mechanism has been a subject of debate.

In regions where the reaction is chemically controlled then the rate will differ for the various kinds of calcite. However, the transport controlled reaction should yield similar results. Table 1.2 lists the measured rate constants for this transport reaction, showing the type of calcite used and indicating the experimental conditions. The rate constants have all been defined in terms of Plummer's k_1.

1.2 THE PRECIPITATION OF CALCIUM CARBONATE

The precipitation of calcium carbonate has been extensively studied, and it has been shown[63] that the form of calcium carbonate preferably formed is calcite, though the presence of impurities has been shown to favour the formation of the thermodynamically less stable form,

aragonite.[63] Precipitation of calcium carbonate apart from being of interest geologically, is also of industrial interest, with much research being carried out to prevent the scaling of pipes, usually through the addition of small quantities of inhibitors.

Crystalisation can be categorised into two processes; nucleation and growth. Nucleation, known as spontaneous, or homogenous, crystalisation, is the generation of crystals from solution, onto which growth can occur. Growth is the process whereby solute is transported to the crystal surface, and then incorporated into the lattice. This process involves many steps including:-

1. The diffusion of the solute from the bulk of solution to the diffusion layer surrounding the particle.
2. The diffusion of the solute through the diffisuion layer to the crystal surface.
3. Adsorption onto the lattice surface.
4. Migration to a growth site and reorientation.
5. Incorporation into the lattice.

The order of these steps and their relative importance, in determining the rate of crystallisation are still undecided and this has given rise to a number of kinetic models.

Precipitation has been studied by many workers using spontaneous crystallisation,[64-67] though this method does not allow reliable, reproducible results to be obtained,[68,69] as nucleation is likely to occur on any impurity particles in solution, which will provide growth sites.

The work of Davies and Jones[70,71] was amongst the first to report the addition of seed crystals to stable supersaturated solutions in the study of precipitation. They prepared a stable supersaturated solution of AgCl by adding KCl solution, drop by drop, into a similar quantity of $AgNO_3$ solution, while stirring the solution continuously. Silver chloride seed crystals were then added to the solution, and the precipitation was followed by monitering the change in conductivity of the solution.

From their experiments they found that the rate was proportional to the area and to the square of supersaturation, and they drived the following equation:

$$R = K\gamma^2 A \left([Ag^+]^{\frac{1}{2}} [Cl^-]^{\frac{1}{2}} - (k_{sp}\gamma^2)^{\frac{1}{2}} \right)^2 \qquad 1.17$$

A = area of crystal surface

γ^2 = activity coefficient of the reacting ions.

Nancollas and Reddy[72,73] were the first workers to apply this seeded growth technique to the study of calcium carbonate precipitation. They formed their super-saturated solutions by the dropwise addition of 100 ml 0.2M $NaHCO_3$ to 100 ml 0.2M $CaCl_2$, in the thermostated reaction vessel. The solution being continually stirred with a Teflon coated bar magnet. The seed crystals were prepared by the slow addition of 0.2M $CaCl_2$ to 0.2M Na_2CO_3, at 25°C. The crystals formed were regular rhombs having an average edge length of 10 μm, giving an approximate

surface area of 0.3 $m^2 g^{-1}$. X-ray crystallography showed only calcite present.

When the stirred solution had reached equilibrium, as indicated by a steady pH value, a weighed amount of the seed crystal was added and the reaction was allowed to proceed towards equilibrium. The reaction was monitored by the change in pH and by the change in calcium ion concentration, which was found using atomic adsorption.

It was found that in the pH range 8.4 - 8.8 the rate of calcium removal from the solution was first order with respect to both $[Ca^{2+}]$ and $[CO_3^{2-}]$, and was proportional to the surface area of calcite seed. $[CO_3^{2-}]$ was found using an iterative method. They then proceeded to measure the activation energy for the reaction, finding a value of 46.2 kJ mol^{-1}, indicative of a surface controlled reaction. Further evidence of this was obtained when they found no change in the rate upon varying the rate of stirring. These results led them to suggest that the precipitation was controlled by a surface controlled reaction, and they gave the following rate equation:

$$R = ks \quad ([Ca^{2+}] [CO_3^{2-}] - k_{sp}/\gamma^2) \qquad 1.18$$

s = surface area of calcite.

i.e., the rate is proportional to the distance from equilibrium, in terms of the ionic product.

This equation was found to be valid in the calcium range 1.4×10^{-4} to 4.44×10^{-4} $mol.dm^{-3}$, and in the carbonate range 1.83×10^{-4} to 3.79×10^{-4} $mol.dm^{-3}$. The above theory assumes that the absorbed lattice ions collide directly with the growth sites and are incorporated separately into the lattice.

Wiechers et al.,[69] in their study of the precipitation of $CaCO_3$, found agreement with the above rate equation. They only measured the change in pH to moniter the reaction which involved lengthy computer calculations to find both $[Ca^{2+}]$ and $[CO_3^{2-}]$. They also found no stirring effect and measured the activation energy and found a value of 43.3 kJ mol^{-1}. They found that the rate constant changed with the composition of the initial reaction solution, those with a higher pH giving rise to a larger rate constant.

Further work by Reddy and Nancollas,[74,75] using the same technique, led them to rewrite their earlier equation. They found that the rate could be more accurately described by an equation which was second order with respect to calcium i.e.,:

$$R = ks\ (C_t - C_s)^2 \qquad 1.19$$

C_s = equilibrium concentration of calcium

C_t = calcium concentration at time t

$$R = KsN^2 \qquad 1.20$$

$$N = (C_t - C_s)$$

Reddy[76] investigated the role of inhibitors on the precipitation of $CaCO_3$. He added the inhibitors to the supersaturated solution before the addition of the seed crystal and found that very small quantities of inhibitor could show a dramatic effect on the rate. Thus, 1.6×10^{-5} $mol.dm^{-3}$ glycero phosphate reduced the precipitation by half, while the same reduction was achieved by the addition of only 2×10^{-6} $mol.dm^{-3}$ ortho-phosphate. These results, together with the consideration of equation 1.20, suggested that the inhibitors worked by blocking the growth sites available.

In order to understand his semi-empirical equation Reddy and Gaillard[77] investigated calcite growth over a wide range of seed solution concentrations, using super-saturated solutions made up as previously, but using commercial calcite, having a specific area of 0.228 m^2g^{-1}, (measured using nitrogen B.E.T. adsorption), as seed material. The experiments were carried out at 25°C, with a magnetic stirrer rotating at 200 rpm. The change in pH was measured continually, but the change in $[Ca^{2+}]$ was only measured at set time intervals. At these times, aliquots of reaction solution were removed *via* a millipore filter, to ensure that the amount of seed present was unchanged, and $[Ca^{2+}]$ was found from titrating with the sodium salt of E.D.T.A.

To analyse their results, they used the integrated form of equation 1.20, giving:

$$N^{-1} - N_o^{-1} = Kst$$

N_o = amount of calcite to be precipitated from the initial supersaturated solution.

They found that $(N^{-1} - N_o^{-1})$ was proportional to the time, which supported their theory that calcite growth involved chemical steps at growth sites. They then proceeded to examine the seed calcite under a scanning electron microscope, before and after reaction. They found that before precipitation the crystals were perfrect rhombs with no evidence of steps or terraces. After reaction the crystals showed well-developed macro growth steps. They therefore concluded that growth proceeded by the formation and movement of macro growth steps across the crystal faces, from elementary kink sites.

Nancollas[78] described a constant composition technique for the study of precipitation. Under this technique, instead of the reactants changing concentration rapidly with time, especially during the initial stages of crystallisation, as had been the case previously, the composition of the reactant solution was kept constant by the automatic addition of calcium chloride and a mixture of sodium carbonate - sodium bicarbonate. He claimed that this method gave rise to more reproducible

results, would enable a wider range of supersaturations to be studied, and would allow more material to grow than was present as original seed material.

He found that the rate of reaction could be described by the following equation:

$$R = ks \left[\left([Ca^{2+}][CO_3^{2-}] \right)^{\frac{1}{2}} - k_{sp}^{\frac{1}{2}} \right]^2 \qquad 1.21$$

which was similar in form to his earlier equation 1.19.

Nancollas[79] then proceeded to compare the results obtained from powdered calcite, to those obtained using a rotating calcite disc. He formed his disc by casting a single crystal of Iceland Spar (from Chihuahua, Mexico), of approximately 1 cm^2, in a self-setting resin. This was then machined into the bell shape, as recommended by Riddiford,[80] to avoid edge effects (see Chapter 3). This was then polished using 6 and 1 μm diamond sprays, and immediately before use the disc was polished using 0.05 μm alumina, and the disc was finally cleaned by washing it with distilled water in an ultrasonic bath for five minutes.

Nancollas studied the precipitation reaction in the pH range 8 - 9, for both powdered calcite (having a surface area of 5.00 cm^2) and the calcite disc. He found that the rate of reaction was proportional to the area of seed, and was constant during the experiment, despite the increasing surface area of the crystals. From this he concluded that the reaction was surface controlled with crystallisation confined to the initial growth sites of

the seed crystals, and that no secondary nucleation occurred on the seed crystals during the course of crystallisation. He found good agreement with the rates measured using powders to those measured on the rotating disc. He then examined the surface of the rotating disc after reaction, using an S.E.M., and found nucleated rhombohedral crystal growth on the surface, orientated along the original crystal lattice plane.

He then proceeded to study the effects of inhibitors on the crystallisation rate. He tried phosphate and 1-hydroxy-ethylidene-1,1-diphosphoric acid (HEDP), and found that both reduced the rate. The presence of 4×10^{-7} $mol.dm^{-3}$ phosphate reduced the rate by 13%, while in the case of H.E.D.P., he found that the addition of 1×10^{-5} $mol.dm^{-3}$ was sufficient to completely inhibit the rate for up to 100 hours, after which time the reaction proceeded at approximately the uninhibited rate. This, he claimed, was due to the H.E.D.P., being absorbed onto the kink sites, and that during the 100 hours the H.E.D.P., was covered by slow growth onto the crystal.

The various models for precipitation, described in this section, have been investigated by various workers. Plummer et al.,[81] compared the model of Nancollas and Reddy,[73] (equation 1.18) to his own mechanistic model.[49] This model was drawn up for dissolution, giving equation 1.10, i.e.,

$$R = k_1 [H^+] + k_3 [H_2CO_3] + k_2 - k_4 [Ca^{2+}][HCO_3^-]$$

at high pH (>7) and low ρCO_2, this equation becomes:

$$R = k_2 - k_4 [Ca^{2+}][HCO_3^-] \qquad 1.22$$

which can be rewritten[81] in terms of the relative saturation (Ω) as:

$$R = k_2 \left(1 - \frac{[H^+]}{[H^+]_s} \Omega\right) \qquad 1.23$$

$[H^+]_s$ = proton concentration at the calcite surface.

Calculation of the ratio $[H^+]/[H^+]_s$ at low ρCO_2 crystal growth experiments gives values of 0.93 at the start of the reaction which increases to 0.97 at the termination. Thus, equations 1.18 and 1.23 can be considered to be similar. Plummer et al.,[81] then proceeded to fit their mechanistic model to the experimental data. They found that if they assumed that ρCO_2 at the surface was equal to ρCO_2 in the bulk of solution, and that the calcite equilibrium determined the surface pH, then the calculated rate was, ~10 - 20 times too high. They therefore used the experimental data and used the model to predict ρCO_2 at the calcite surface and found that the initial ρCO_2 was 1/5 that of the bulk, and that this rose to ½ at the end of the reaction. They also found that the surface pH was 0.6 pH units less than the bulk pH. They then tried

to predict the rate at higher pCO_2 and found closer agreement.

House[82] investigated the model of Plummer et al.,[49] Nancollas and Reddy,[73] Reddy,[74] Davies and Jones,[70] and Nielsen.[83] Nielsen's theory is based upon the kinetics of the movement of a growth spiral, details of which can be found in reference 83. This gives rise to the following equation:

$$R = k\,[Ca^{2+}][CO_3^{2-}](\ln([Ca^{2+}][CO_3^{2-}]/K_{sp}))^2 \qquad 1.24$$

The equations used by House are listed in Table 1.3, the terms being as previously defined.

In order to compare the experiments performed on different substances, and to compare the rate equations obtained on the same substance, House made use of reduced growth curves, to present the crystal growth data. He followed the method of Leeuwen and Blomen[84] and used the growth affinity, β, and the reduced growth, S:

$$\beta = \ln\ (a_{Ca^{2+}}\ a_{CO_3^{2-}})\ K_{sp} \qquad 1.25$$
$$= 2.3026\ S$$

TABLE 1.3 The kinetic models tested by House.

WORKER	RATE EQUATION
Nancollas and Reddy[73]	$R = ks([Ca^{2+}][CO_3^{2-}] - k_{sp}/\gamma^2)$
Reddy[74]	$R = ks\ (C_t - C_s)^2$
Plummer et al.,[49]	$R = k_3 - k_4[Ca^{2+}][HCO_3^-]$
Davies and Jones[70]	$R = k\gamma^2 A([Ca^{2+}]^{\frac{1}{2}}[CO_3^{2-}]^{\frac{1}{2}} - (k_{sp}\gamma^2)^{\frac{1}{2}})^2$
Nielsen [83]	$R = k[Ca^{2+}][CO_3^{2-}](\ln([Ca^{2+}][CO_3^{2-}]/k_{sp}))^2$

He then rewrote the rate equations in terms of these parameters.

For his experiments, House introduced calcite seed, having a specific surface area of 0.5 m^2g^{-1}, into a supersaturated $Ca(HCO_3)_2$ solution at 25 $\pm$ 0.002°C. He prepared his solution by dissolving a known weight of calcite in distilled water, under conditions of constant stirring, and with a constant stream of CO_2 flowing through the solution. This solution was made supersaturated by bubbling through N_2 and thus degassing the CO_2. He monitored the reaction by pH and conductivity, the concentrations being found using an iterative programme.

He found that the models of Nancollas and Reddy, Reddy ,and Nielsen, were unsatisfactory, while that of Davies

and Jones could be fitted to his data when the extent of precipitation was between 0.1 and 0.45. The mechanistic model of Plummer et al., was shown to give good agreement.

In a later paper,[85] House et al., investigated the temperature dependance of calcite precipitation, between 5 and 20°C, for two different calcite samples, and interpreted the results using the models of Plummer et al., and Davies and Jones. The two calcite samples were found to have specific surface areas of 0.22 m^2g^{-1}, and 5.65 m^2g^{-1}, respectively. The two samples were found to react at different rates and this was attributed to the reaction site density of the two samples differing.

They found that at low growth rate ($<5 \times 10^{-6}$ $mol.dm^{-3}$ min^{-1}) the Davies-Jones equation produced agreement. With the mechanistic model, they found that the best agreement with their results was obtained by assuming that the growth step involved the reaction between, the $(Ca - HCO_3)^-$ ion pair and CO_3^{2-} anion sites on the lattice surface.

1.3 AIMS OF THIS RESEARCH

The aims of this research were to fabricate a rotating calcite disc and to use it in the study of the kinetics of dissolution of calcium carbonate as a function of pH and pCO_2, utilising the well defined hydrodynamics to differentiate between the acknowledged chemical and transport controlled steps. From measurement of these rate constants it was hoped that it would be possible to

define the exact mechanism at dissolution, and from this to understand the effects of inhibitors on the rate, and also the effects of differing surface morphology.

1. H.Sverdrup, I.Bjerle, *Vatten*, 38, 59 (1982).

2. J.P.Miller, *Am.J.Sci.*, 250, 161 (1953).

3. A.Cossa, *Zeitschr.Anal.Chemica*, 8, 145 (1869).

4. M.Engle, *Annales.Chim.Paris*, 6, 344 (1888).

5. N.H.McCoy, *J.Am.Chem.Soc.*, 33, 468 (1911).

6. A.E.Mitchell, *J.Chem.Soc., London*, 123, 1887 (1923).

7. G.L.Frear, J.J.Johnston, *J.Am.Chem.Soc.*, 51, 2082 (1929).

8. J.Hullet, *J.Am.Chem.Soc.*, 27, 49 (1905).

9. W.Stumm, J.J.Morgan, In: "Aquatic Chemistry", p.295, J.Wiley and Sons, New York, 1981.

10. J.Kendell, *Philos.Mag.*, 23, 958 (1912).

11. C.V.King, C.L.Liu, *J.Am.Chem.Soc.*, 55, 1928 (1933).

12. G.V.Levich, *Acta Phys.Chim., U.R.R.S.*, 17, 257 (1942).

13. H.Tominaga, H.Adzumi, T.Isobe, *Chem.Soc., Japan Bull.*, 14, 348 (1938).

14. C.A.Kaye, *Jour.Geol.*, 65, 34 (1957).

15. P.K.Weyl, *Jour.Geol.*, 66, 163 (1958).

16. O.Erga, S.G.Terjesen, *Acta Chem.Scand.*, 10, 872, (1956).

17. E.B.Shtermina, E..Frolova, *Doklady Akad.Nauk, S.S.S.R.*, 21, 271 (1952).

18. L.L.Bircumshaw, A.C.Riddiford, *Quart.Rev., London*, 6, 137 (1952).

19. S.G.Terjesen, O.Erga, G.Thorse, A.Ve., *Chem.Eng.Sci.*, 14, 277 (1961).

20. I.Nestaas, S.G.Terjesen, *Acta Chem.Scand.*, 22, 2101 (1968).

21. I.Nestaas, S.G.Terjesen, *Acta Chem.Scand.*, 22, 2111 (1968).

22. I.Nestaas, S.G.Terjesen, *Acta Chem.Scand.*, 23, 2519 (1969).

23. E.Gorlich, Z.Gorlich, *Z.Bull.Acad.Polon.Sci., Ser.Sci. Chim.Geol.Geogrph.*, 6, 669 (1958).

24. E.Gorlich, Z.Gorlich, A.Szwaja , *ibid.*, 8, 75 (1960).

25. M.B.Ives, *Ind.Eng.Chem.*, 57, 34 (1965).

26. J.W.Morse, *Am.J.Sci.*, 274, 97 (1974).

27. P.K.Weyl, *Shell Development Company, E.P.R. Pub.*, 428, 1 (1967).

28. L.N.Plummer, Ph.D. Thesis, 1972, North Western University.

29. I.Presret, M.S ., Dissertation, 1972, North Western University.

30. See 23.

31. R.A.Berner, P.Wilde, *Am.J.Sci.*, 272, 826 (1972).

32. J.W.Morse, R.A.Berner, *Am.J.Sci.*, 272, 840 (1972).

33. R.A.Berner, J.W.Morse, *Am.J.Sci.*, 274, 108 (1974).

34. J.W.Morse, *Am.J.Sci.*, 274, 638 (1974).

35. S.Pond, R.M.Pythowicz, J.E.Hawley, *Deep Sea Research*, 18, 1135 (1971).

36. R.A.Berner, In: "Principles of Chemical Sedimentology", McGraw Hill, Book Company, New York (1971).

37. M.N.A.Peterson, *Science*, 154, 1542 (1966).

38. W.H.Berger, *Marine Geology*, 8, 111 (1970).

39. F.C.Frank, *Faraday Soc.Discussions*, 5, 48 (1949).

40. A.E.Nielsen, In: "Kinetics of Precipitation", MacMillan, New York (1964).

41. Ben-Yarkov, *Geochim et Cosmochim Acta*, 36, 1395 (1971).

42. G.H.Nancollas, N.Purdie, *Chem.Soc., (London)*, 18, 1 (1964).

43. See 22.

44. W.K.Barton, N.Cabrera, *Faraday Soc.Discussions*, 5, 33 (1949).

45. W.K.Barton, N.Cabrera, F.C.Frank, *Royal Soc.London Philos.Trans.*, A243, 299 (1951).

46. See 19.

47. K.E.Chave, E.Suess, *Limnology and Oceanography*, 15, 633 (1970).

48. L.N.Plummer, T.M.L.Wigley, *Geochim.et Cosmochim. Acta*, 40, 191 (1976).

49. L.N.Plummer, T.M.L.Wigley, P.L.Parkhurst, *Am.J. Sci.*, 278, 179 (1978).

50. E.L.Sjöberg, *Geochim.et Cosmochim.Acta*, 40, 461 (1976).

51. E.L.Sjöberg, *Stockholm Contr.Geology*, 32, 1 (1978).

52. J.Christoffersen, M.R.Christoffersen, J.Arends, *Croatica Chimica Acta, CCACAA*, 56, 769 (1983).

53. J.W.Morse, *Am.J.Sci.*, 278, 344 (1978).

54. R.S.Keir, *Geochim.et Cosmochim.Acta*, 44, 241 (1980).

55. D.Rickard, E.L.Sjöberg, *Am.J.Sci.*, 283, 815 (1983).

56. E.L.Sjöberg, D.Rickard, *Geochim.et Cosmochim.Acta*, 47, 2281 (1983).

57. See 18.

58. Y.V. Pleskov, V.Y.Filinovski, In: "The Rotating Disc Electrode", Plenum Press, New York, 1976.

59. D.Rickard, E.L.Sjöberg, *Am.J.Sci.*, 283, 815 (1983).

60. E.L.Sjöberg, D.Rickard, *Chem.Geol.*, 42, 119 (1984).

61. E.L.Sjöberg, D.T.Rickard, *Geochim.et Cosmochim. Acta*, 48, 485 (1984).

62. K.Lund, H.S.Foyler, C.C.McCure, S.W.Ault, *Chem.Eng. Sci.*, 30, 825 (1975).

63. See p.286 of reference 9.

64. R.Brooks, L.M.Clark, E.F.Thurston, *Phil.Soc.Roy. Soc., London, Ser.A*, 243, 145 (1950).

65. Y.Kitano, D.W.Hooda, *Geochim.et Cosmochim. Acta*, 29, 29, (1965).

66. P.M.Gruzensky, *J.Phy.Chem.Solid Suppl.*, 1, 365 (1967).

67. A.Packter, *Kristall und Technik.*, 10, 11 (1975).

68. See 42.

69. H.N.S.Wiechers, P.Sturrock, G.V.R.Marais, *Water Research*, 9, 835 (1975).

70. C.W.Davies, A.L.Jones, *Faraday Soc.Discussions*, 5, 103 (1949).

71. C.W.Davies, A.L.Jones, *Faraday Soc.Trans.*, 51, 166 (1971).

72. M.M.Reddy, G.H.Nancollas, *J.Colloid.Interface Sci.*, 36, 166 (1971).

73. G.H.Nancollas, M.M.Reddy, *J.Colloid.Interface Sci.*, 37, 824 (1971).

74. M.M.Reddy, G.H.Nancollas, *Desalination*, 12, 61 (1973).

75. M.M.Reddy, *Internat.Assoc.Theoret.Appl.Limnol.*, 19, 429 (1975).

76. M.M.Reddy, *J.Crystal.Growth*, 41, 287 (1977).

77. M.M.Reddy, W.D.Gaillard, *J.Colloid.Interface Sci.*, 80, 171 (1981).

78. G.H.Nancollas, *Advances in Colloid.Sci.*, 19, 215, (1979).

79. G.H.Nancollas, *Corrosion*, 12, 76 (1981).

80. A.C.Riddiford, In: "Advances in Electrochemistry and Electrochemical Engineering", (P.Delahay and C.W. Tobias, Eds.), Vol. 4, p.47, Wiley Interscience, New York, 1966.

81. N.L.Plummer, T.M.L.Wigley, P.L.Parkhurst, *Am.Chem.Soc., Symposium Ser.*, 93, 538 (1979).

82. W.A.House, *J.Chem.Soc., Faraday I*, 77, 341 (1981).

83. A.E.Nielsen, In: "Kinetics of Precipitation", Ch.5, Pergamon Press, Oxford, 1964.

84. C.van Leeuman, L.J.M.J.Blomen, *J.Crystal.Growth*, 46, 96 (1979).

85. G.E.Cassford, W.A.House, A.D.Pethybridge, *J.Chem. Soc., Faraday Trans. I*, 79, 1617 (1983).

CHAPTER 2

ION SELECTIVE ELECTRODES

2.1 INTRODUCTION

The reason for the use of a calcium ion selective electrode (Ca. I.S.E.) in measuring the dissolution of $CaCO_3$.

For any analytical system to be suitable for use in a laboratory, the system must incorporate certain features including:-

1. The system must be accurate.
2. It must only require a small volume for testing, especially when many readings are to be taken.
3. It must give a quick response, a pre-requisite for any rapidly changing situation.
4. It must give an immediate value, to enable the reaction to be monitored and controlled as it proceeds,

   and
5. It must be easy to use.

In the particular case of calcium detection, five main systems are in use; (1) Atomic Adsorption; (2) fluorimetry, after complexation of the calcium ions by a suitable ligand; (3) Titration, generally using the sodium salt of E.D.T.A.; (4) An Iterative method, which involves the measurement of the solution pH and conductivity values, at known time intervals, together with a knowledge of the chemical equilibria established in the calcium bicarbonate water system; and (5) Potentiometry, using a Ca.I.S.E. Table 2.1 shows how each of these detection systems compare against the desirable characteristics.

TABLE 2.1 The features of the common systems for the detection of calcium

	ACCURACY	VOLUME REQUIRED	SPEED OF RESPONSE	DETERMINATION TIME	EASE OF USE
Atomic Adsorption	✓	✓	✓	x	✓
Fluormetry	x	x	✓	x	✓
Titration	✓	x	✓	x	?
Iterative method	✓	✓	✓	x	x
Ca.I.S.E.	✓	✓	✓	✓	✓

As shown only the Ca.I.S.E. fulfils all of the requirements. Atomic Adsorption suffers from not giving an on-line value, since the exact concentration is not known until after taking the sample. This makes it difficult to continuously moniter the progress of the experiment. The fluorimetric method also suffers from this problem, and has the additional drawbacks that before the calcium concentration can be determined the approximate concentration of the sample must be known, and the sample must be pretreated with the ligand, which is time consuming and cumbersome. This method also suffers from a lack of sensitivity (see Section 4.1.3.1). Using an iterative method has two drawbacks, namely; the calcium concentration is not immediately known, and while this method is easy to use once set up, complex computer programmes have to be written, and the analysis is time consuming. The titration method is time consuming and fails to give an immediate value. Because the Ca.I.S.E. fulfils all of the required characteristics, this was the method used for the detection of calcium in the work described in this thesis. This Chapter will describe the theory of Ion Selective Electrodes (I.S.E.).

2.2 THEORETICAL ASPECTS

I.S.E.'s consist of a membrane composed of either a solid or a liquid phase, to which only one ionic species is permeable. The membrane must, therefore, exhibit ionic conductance, as opposed to purely electronic conductance,

as electronic conductors are sensitive to redox systems and not to individual ions. The membrane in an I.S.E. separates the solution to be tested from an internal reference solution, of constant composition, and an internal reference electrode.

When such an electrode is placed in a solution containing ions to which it is sensitive, a small number of these ions pass through the membrane, from the solution of higher concentration to that of lower. As this diffusion process occurs, a concentration gradient is built up in the membrane which generates a transmembrane potential, which hinders further passage of ions, and finally stops it entirely.

Thus, electrical potentials are established on both sides of the membrane (η_{ref} and η_{test}) and at equilibrium $\eta_{ref} = \eta_{test}$. Assuming that the electrode responds solely to the ion of interest, then these electrical potentials can be expressed in terms of the standard electrical potentials, the activity of the ions, and the inner potential differences between the membrane and the solutions, i.e.,

$$\eta_{ref} = U_{ref} + RT \ln a_{ref} + ZF\Psi_{ref} \qquad 2.1$$

$$\eta_{test} = U_{test} + RT \ln a_{test} + ZF\Psi_{test} \qquad 2.2$$

where Z = charge on ion

U = Standard electrical potential

F = Faraday's constant

T = Absolute temperature

a = activity of ion

Ψ = inner potential difference between membrane and solution.

Now at equilibrium,

$$\eta_{ref} = \eta_{test} \qquad 2.3$$

therefore, the potential difference across the membrane, $(\Psi_{ref} - \Psi_{test})$, is given by:-

$$\Delta\Psi = \frac{U_{test} - U_{ref}}{ZF} + \frac{RT}{ZF} \ln \left(\frac{a_{test}}{a_{ref}}\right) \qquad 2.4$$

$$\Delta\Psi = C + 2.303 \frac{RT}{ZF} \log \left(\frac{a_{test}}{a_{ref}}\right) \qquad 2.5$$

Since the reference solution is of constant composition, equation 2.5 can be rewritten:-

$$\Delta\Psi = C + 2.303 \frac{RT}{ZF} \log a_{test} \qquad 2.6$$

Equation 2.6 shows that the potential difference established across the membrane is governed purely by the activity of the ion being measured in the test solution.

This potential difference ($\Delta\Psi$) is measured relative to the internal reference electrode of the I.S.E. ($E_{ref.\ int}$) and this potential difference is compared to that of an external reference electrode ($E_{ref.ext}$). The observed potential difference ($E_{obs.}$) is therefore given by:-

$$E_{obs.} = (E_{ref.ext} + E_{ref.int}) + \Delta\Psi \qquad 2.7$$

substituting for $\Delta\Psi$, equation 2.6 gives:

$$E_{obs.} = k + (C + 2.303 \frac{RT}{ZF} \log a_{test}) \qquad 2.8$$

therefore,

$$E_{obs.} = K + 2.303 \frac{RT}{ZF} \log a_{test} \qquad 2.9$$

Thus, from equation 2.9, it can be seen that, in theory, the observed potential difference depends only upon the activity of the ion in the test solution, and that a Nernstein response of 59 mV/decade is expected for a monovalent ion, while a divalent ion should show a calibration slope of 29.5 mV/decade.

2.2.1 SELECTIVITY COEFFICIENTS AS OF I.S.E.'s

The above derivation has assumed that the electrode is totally selective, i.e., it responds solely to the ion being determined, and that its response is totally independant of other ions present in the test solution. In practical I.S.E.'s however, some response is shown towards impurity ions, and the extent to which the electrode responds to these ions is measured in terms of the selectivity coefficient.

In the case of an I.S.E., designed to measure ion i^z, but also showing some response to an impurity ion j^y, being immersed in a solution containing both i^z and j^y ions, then at the membrane an exchange recurs between i^z ions in the membrane and j^y ions, as impurity ions compete for vacant sites i.e.,

$$i^z_{(m)} + j^y_{(s)} \underset{}{\overset{k_{ij}}{\rightleftharpoons}} i^z_{(s)} + j^y_{(m)}$$

where (m) and (2) refer to the membrane and solution respectively.

In the above case $E_{obs.}$ is defined by the following equation:

$$E_{obs.} = K + 2.303 \frac{RT}{ZF} \log (a_i + k_{ij} (a_j)^{z/Y}) \qquad 2.10$$

k_{ij} = selectivity coefficient.

The selectivity coefficient is a measure of the extent to which an I.S.E. determining the primary ion (i^z) also responds to an impurity ion (j^y), the higher the value of k_{ij} the less selectivity the electrode exhibits.

In cases where many impurities (to which the electrode responds) are present in the test solution, equation 2.10 can be rewritten as:-

$$E_{obs.} = K + 2.303 \frac{RT}{ZF} \log \left(a_i + \sum_{i=1}^{m} k_{im} (a_m)^{Z/m}\right) \quad 2.11$$

Selectivity coefficients are determined experimentally for each electrode and the literature contains reports from numerous workers.[1-12] The reported values of k depend upon both the electrode used and upon the experimental conditions, especially the relative concentrations of the primary and impurity ions. Thus, the selectivity coefficient (k_{ij}) found for ion i with various concentrations of ion j may well be different from the k_{ij} value found at a different concentration of i and vice versa. Table 2.2 lists the selectivity coefficients for the two Ca.I.S.E.'s used in this work, though it should be noted that the experimental conditions are not reported.

Broadly speaking there are two ways to determine k_{ij}; firstly, by making measurements in two different solutions,

TABLE 2.2 Selectivity coefficients for Ca.I.S.E.'s

IMPURITY	RADIOMETER F2112 Ca	BECKMAN
Na^+	3.98×10^{-6}	1.46×10^{-4}
K^+	1.58×10^{-6}	$> 1 \times 10^{-6}$
Li^+	6.31×10^{-5}	-
Mg^{2+}	4.32×10^{-6}	2.51×10^{-4}
Ba^{2+}	2.21×10^{-5}	3.02×10^{-3}
Pb^{2+}	-	0.101
Zn^{2+}	2.32×10^{-3}	1.04

one consisting of impurity ion and the other of the primary ion of interest; and secondly, by taking measurements in a single solution.

Eisemann et al.,[1,2] and Hepp[3] used the first method. They chose an impurity ion with the same ionic charge as the primary ion and produced two solutions of equal activities. They then measured the response of the electrode in both solutions.

From equation 2.9 the potential of the primary ion solution (E_p) is given by:-

$$E_p = K + 2.303 \frac{RT}{ZF} \log a_i \qquad 2.12$$

whilst from equation 2.10 that of the impurity ion solution (E_i) is given by:-

$$E_i = K + 2.303 \frac{RT}{ZF} \log (0 + k_{ij}a_j) \qquad 2.13$$

subtracting equation 2.12 from 2.13, and considering that the activities of both samples are equal, gives:-

$$(E_p - E_i) = 2.303 \frac{RT}{ZF} \log k_{ij} \qquad 2.14$$

and thus k_{ij} can be found.

Rechnitz et al.,[4,5] Pouget[6] and Verloo and Cottenie[7] used a slightly different method. Instead of keeping both solutions at the same activity, they varied the activity of the impurity ion until $E_p = E_i$, defining the selectivity coefficient as the ratio at which equipotentiality was achieved. Again, ions with the same charges were used. From equation 2.9:

$$E_p = K + 2.303 \frac{RT}{ZF} \log (a_i)$$

and from equation 2.13:

$$E_i = K = 2.303 \frac{RT}{ZF} \log (k_{ij}a_j)$$

therefore, if $E_p = E_i$

$$k_{ij} = \frac{a_i}{a_j} \qquad 2.15$$

This method of using two separate solutions has been criticised[8-11] because during the potential measurement of the impurity ion solution, an equilibrium is set up between the primary ions in the membrane and impurity ions in solution, so an unknown concentration of primary ions appears at the membrane surface, leading to errors in the determination of the coefficient. It has further been criticised on the grounds that the situation does not occur when the electrode is being used practically. However, despite these criticisms this method yields similar results to the one solution method.

Two variations of the single solution method exist for determining the selectivity coefficient; keeping the primary ion constant and adding the impurity ion, and vice versa. Tůsl[8] kept the primary ion constant and added impurity ions to the test solution. He found the critical value of a_j from the intersection of the extrapolated linear branches (Figure 2.1). He then used this value, together with the known activity of the primary ion, and found k_{ij} using equation 2.15.

The alternative method of adding primary ion to a solution of impurity ions is again analysed graphically[9-13]

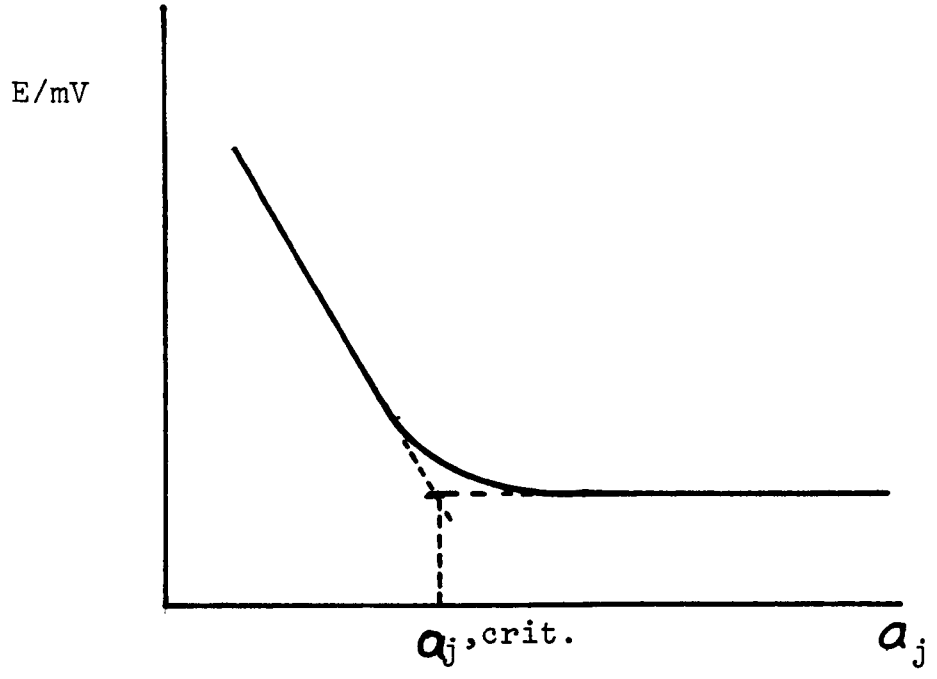

FIGURE 2.1 Determination of k_{ij} by addition of secondary ion.

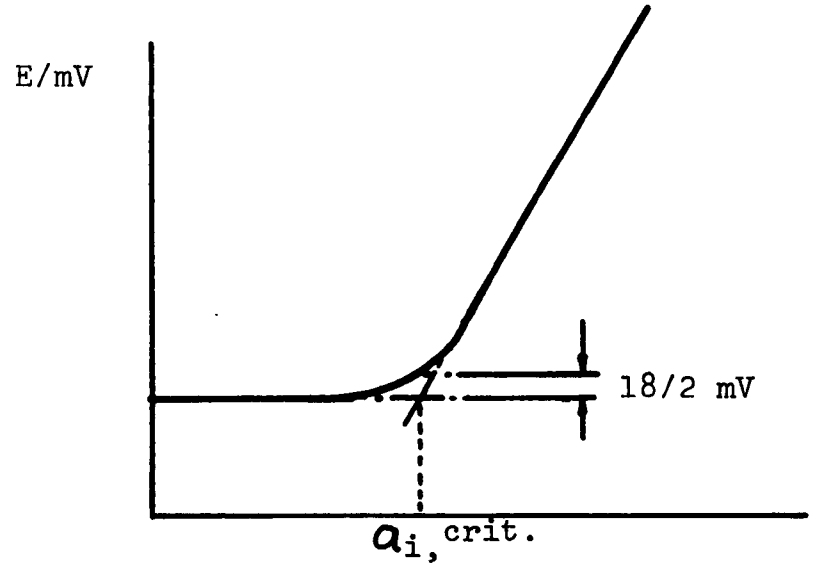

FIGURE 2.2 Determination of k_{ij} by addition of primary ion

(Figure 2.2). However, the initial part of the curve, that with a low concentration of the primary ion, is very susceptible to electrode drift and liable to give unreproducible results. To overcome this inherent unreproducibility, the "critical" activity is defined as the point at which the extrapolated Nernstian region of the slope and the experimental slope differ by (18/Z)mV, where Z is the charge on the primary ion. k_{ij} is found using equation 2.15.

2.3 THE RESPONSE TIME OF AN I.S.E.

An important quantity in I.S.E.'s is the response time (τ) which describes how fast the electrode responds to a change in concentration. It has been demonstrated experimentally[14] that the response time is exponential in form. Toth derived the following equation to describe the transience :

$$E_t = E_o + k_1 (1 - \exp(-k_2 t)) \qquad 2.16$$

E_t = potential at time t

E_o = potential at time 0

t = time

k_1 and k_2 are constants

This equation has subsequently been rewritten by Koryta[15] as:

$$E_t = E_o + (E_f - E_o) \exp(-t/\tau) \qquad 2.17$$

E_f = final potential

τ = time constant.

The exact definition of response time varies according to the worker. Rechnitz and co-workers[16,17] defined it as the time interval taken for half of the total electrode change to have occurred.

Fleet et al.,[18] claimed that a more reproducible value, and one more relevant to analytical situations, was the time taken for 95% of the response to have occurred.

Moody and Thomas[19] defined τ as the time taken for the potential to be within 1mV of the final equilibrium potential. Of these three definitions, that of Fleet is the most widely used.

Two ways of determining the response time are used; firstly, rapidly transfering the I.S.E. and reference electrode between solutions of differing strengths, taking care to clean the electrodes before insertion; and secondly, injecting a concentrated solution of primary ion into the sample solution. In both cases the electrode response is measured and later analysed. Most workers have employed chart recorders to record the transient, though Pungor[20] used an oscilloscope, in order to avoid the relatively high time constant associated with chart recorders.

The response time is very dependant upon experimental conditions, especially the stirring rate. Scrinvasan and Rechnitz[21] studied the difference between stirred and unstirred solutions, finding that stirred solutions showed

a shorter response time, and Rechnitz,[22] showed that the actual stirring rate was also important, the faster the stirring rate the faster the response. This has been attributed[23,24] to the diffusion of primary ions across the stagnant layer around the membrane. They claimed that since the response time of an I.S.E. is governed by the diffusion of primary ions from the bulk of the solution to the membrane, the rate determining step is transport across the stagnant layer. Thus, since a faster stirring rate reduces the size of the stagnant layer, it also reduces the response time.

τ is also strongly influenced by the order in which the transition is made, a change from high to low concentrations takes a far longer time to reach equilibrium than vice versa. This has been pointed out by many workers, and Simon et al.,[24] were the first to explain this phenomena. They considered the case of a neutral membrane I.S.E., in which diffusion occurred both inside the membrane and in the test solution.

At t = 0 a steady state has been established between the membrane and the external solution, the flux of the solution in the boundary layer being equal to that inside the membrane, as no electrolyte is lost at the interface, i.e.,:

$$J_t = J_m \qquad 2.18$$

J_t = flux within boundary layer solution

J_m = flux inside membrane.

When the activity of the external solution is suddenly changed from a_o to a_f (Figure 2.3) the activity of the solution next to the membrane is a_t.

The flux of test solution towards the membrane is given by:-

$$J_t = D_t \left(\frac{a_f - a_t}{\delta}\right) \qquad 2.19$$

D_t = diffusion coefficient of the test solution.

From equation 2.18 and 2.19 the concentration gradient set up can be related to the diffusion occurring within the membrane. To solve this situation, and derive an analytical description of the dynamic response, they used Carslaw and Jaeger's extensive heat conduction theory,[35] and obtained:

$$(a_t - a_o) = (a_f - a_o)\left(1 - \frac{1}{(\sqrt{(t/\tau)} + 1)}\right) \qquad 2.20$$

where τ = response time

$$= \frac{D_m K^2 \delta^2}{\pi D_t^2} \qquad 2.21$$

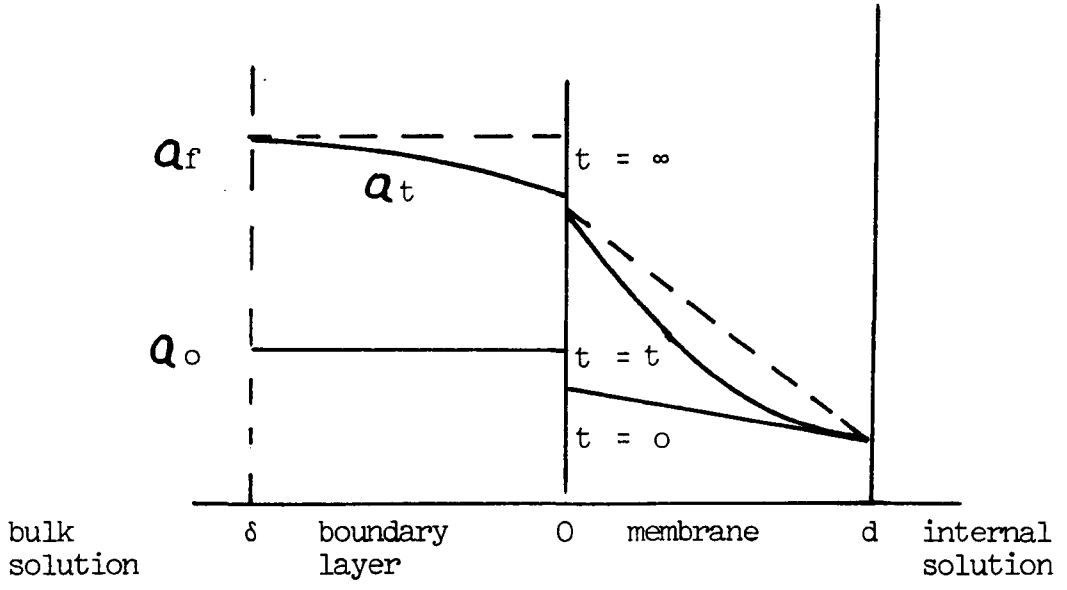

FIGURE 2.3 Response of an I.S.E. to a change in concentration

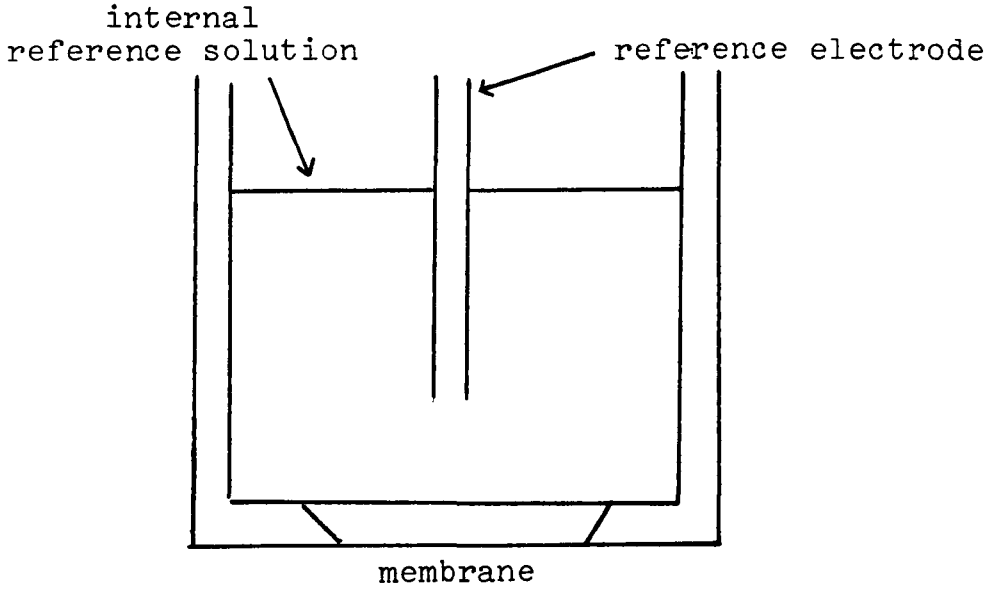

FIGURE 2.4 I.S.E. with a solid ion-exchange membrane.

K = constant

D_m = diffusion coefficient in the membrane.

Rearranging equation 2.20 gives:

$$\frac{a_t}{a_f} = 10^{(Et-Ef/s)} = 1 - (1\frac{a_o}{a_f})\left(\frac{1}{\sqrt{t/\tau + 1}}\right) \qquad 2.22$$

E_f = final potential

E_t = potential at time T

s = calibration slope of electrode.

Thus, equation 2.22 shows that the response time will be shorter for a change from low to high concentrations, than vice versa.

The response time has also been shown to be effected by the presence of impurity ions.[26-30]

It has also been pointed[31] out that the response time actually measures the response for an electrochemical cell, I.S.E. and reference, and that the response time measured is actually the response of the whole cell, and thus only in cases where the response of the I.S.E. is slow can that of the reference electrode be ignored.

2.4 TYPES OF ION SELECTIVE ELECTRODES

This chapter has dealt with the theoretical aspects of I.S.E.'s. The different types of practical electrodes will now be discussed, I.S.E.'s can be divided up into five main classes; (1) glass membrane electrodes; (2) Solid

ion exchange membranes; (3) solid state I.S.E.'s using a non-porous slightly soluble salt as a membrane (either a compact poly-crystalline material, or a single crystal); (4) liquid ion-exchange membranes - using an ion exchanger dissolved in a water immiscible solvent; and (5) neutral membrane, formed using for example, a polycyclic polyether dispersed in a P.V.C. membrane.

2.4.1 GLASS ELECTRODES

The first I.S.E. developed, and still the most widely used, was the glass pH electrode. At first it was thought that the potential was set up by protons passing through the thin glass membrane, but it has been shown,[32,33] that the potential is set up by an ion exchange reaction occurring between the glass and the solution, i.e.,

$$J^+ (m) + K^+ (s) \overset{Keq}{\rightleftharpoons} J^+ (s) + K^+ (m)$$

When the electrode is placed in a solution containing ions to which it is sensitive, then this exchange takes place until equilibrium is achieved.

Ions also diffuse from the solution of higher concentration to that of lower, setting up a concentration gradient which generates a transmembrane potential, which stops further diffusion. Thus the total potential measured is given by the sum of these two potentials, the concentration potential, set up by diffusion, and the potential set up by ion exchange. Glass electrodes combine

high sensitivity and a fast response. They show Nernstian response up to pH 11 or 12, after which they show deviation as they respond to the cations present, especially sodium and other monovalent ions. This deviation has been used as the basis for the development of glass electrodes sensitive to alkali metals and silver ions.[36] Since then work has involved alteration of the composition of the glass to produce increased sensitivity and further the range of metals which can be detected. This has been reviewed by Simon et al.[35] The only restriction on the use of glass electrodes is the limited range of ions for which they can be designed.

2.4.2 SOLID ION-EXCHANGE MEMBRANES

These electrodes use a membrane incorporating an ion exchanger and utilise an ion exchange between the ions in solution and those in the membrane to set up the potential. This class incorporates glass electrode and the full potential is established as described previously.

These electrodes are easy to construct and Figure 2.4 shows a typical electrode. They can be designed to cover a range of ions, e.g., fluoride,[43] chloride[44] and chromate[45] but they lack sensitivity and selectivity and generally show inferior performance to solid state electrodes. Also, the active ion exchanger becomes depleted in the membrane with time, and the electrode has to be regenerated by soaking it in a solution containing the ion exchanger.

2.4.3 SOLID STATE ION-SELECTIVE ELECTRODES

These consist of a non-porous membrane of a sparingly soluble salt, cemented into a chemically inert body (such as P.V.C.) ensuring that no leakage occurs into the inner space from the test solution (see Figure 2.5). The membrane consists of a single crystal or polycrystalline material. The potential is set up by an ion exchange reaction occurring on the surface and the charge is carried through the crystal according to the Frenkel mechanism, via holes. Since the ion of interest is left at the surface no diffusion potential arises, and the potential set up is solely due to the ion exchange mechanism.

The most widely used electrode of this class is the fluoride electrode, which uses as a membrane a single crystal of LaF_3, activated by the small addition of EuF_2. The change is carried across the membrane by a combination of LaF_3 holes and LaF_3 units, i.e.,

$$\left| LaF_3 \right| + LaF_3 \rightleftharpoons LaF_2^+ + F^-$$

The particles formed, LaF_2^+ and F^-, occupy the same lattice space as LaF_3. The charge is carried by movement of F^- from LaF_3 to neighbouring LaF_2^+.

The first electrode of this class was that of Frant and Ross[36] and since then the electrode has been further developed and is widely used in the determination of F^- ions, showing extremely high sensitivity.[37,38]

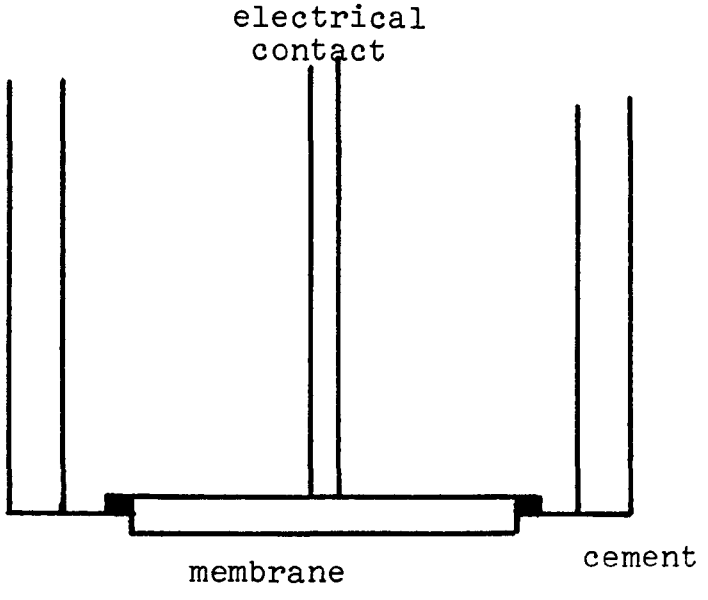

FIGURE 2.5 Solid state membrane

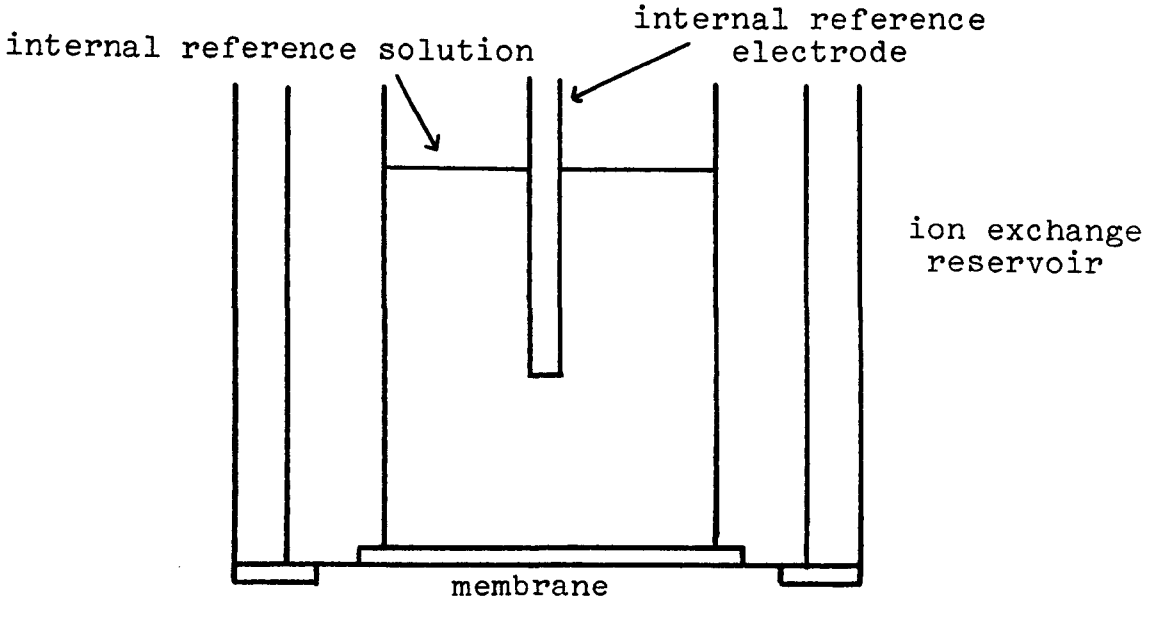

FIGURE 2.6 Liquid ion selective electrode

Other solid state electrodes include the silver halide I.S.E. which shows high selectivity and can be used over a wide range of pH, and the silver sulphide I.S.E., which employs a membrane of silver sulphide and silver iodide. These show high selectivity towards sulphide ions, but also show Nernstian response to both cyanide ions,[40] and silver ions,[41,42] and have been used to detect these ions, to within 0.2% accuracy.

Solid state electrodes tend to be robust, very selective and to show Nernstian response over a large timescale, showing almost no drift. The only drawback in their use is the lack of suitable material from which to fabricate them.

2.4.4 LIQUID ION EXCHANGE MEMBRANES

The membranes used in these electrodes consist of a water immiscible organic solvent containing the ion exchanger of interest. The liquid membrane, which is held in pores, separates the test solution from an internal reference solution (see Figure 2.6). As in the case of the solid state ion exchange membrane, a potential is set up due to the ion exchange, and the diffusion of ions also creates a potential. However, in this case due to the higher mobility of the exchanger the diffusion term is far larger, and dominates the potential set up.

The electrode suffers from the gradual loss of the ion exchanger in the pores and this is replaced by the ion-exchange material held in a reservoir.

The first liquid I.S.E. was described by Ross[46] who developed a calcium ion selective electrode. This showed a fast response time (30 sec.) in pure solutions, but was severely effected by the presence of impurities, the response time being up to 10 min., in the presence of Mg^{2+}. Calcium selective electrodes have subsequently been improved,[47] and electrodes have been developed sensitive to other ions, e.g., antimony,[48] ceasium,[49] gold,[50] lithium[51] and sodium.[52] All these electrodes, however, suffer from low sensitivity and slow response times in the presence of impurities.

2.4.5 NEUTRAL MEMBRANES

These membranes consist of polycyclic poly ethers dispersed in a matrix, usually P.V.C. The internal arrangement of the oxygens in the poly ether , whilst having no formal charge, is able to chelate to the cations and replace their hydrated shells. This ionic charge complex is then transported in the direction of decreasing electrochemical potential. The poly ether itself does not move, but the cation is moved by rapid exchange.

In the membrane the poly ether carriers are bound in a complex with the cation from the internal reference solution. This means that the positive charge of the matrix stops transport of like charge ions through the membrane by all processes, apart from ionic exchange, and with the cyclic poly ether chelating to one ion preferentially, this explains the selectivity of the membrane.

The first electrode of this kind was described by Ross[46] who formed a calcium selective electrode. He dissolved di-(n-decyl)-phosphoric acid in di-(n-octyl)-phenyl phosphate, and dispersed this solution in a porous membrane. This electrode suffered from poor selectivity and from a short lifetime. The electrode was subsequently improved by Moody et al.,[52,53] who dissolved a matrix of P.V.C. and the ester of alkyl phosphoric acid in tetrahydrofuran, and formed a thin membrane as the solvent evaporated. This gave longer lifetimes and improved the sensitivity. Further work involved the incorporation of polycyclic poly ether in the P.V.C. matrix,[54,55] which improved the sensitivity and gave shorter response times.[56] Other electrodes of this kind have since been fabricated for detecting other ions including Ag^+,[57] and F^- and Cl^-.[58] These electrodes show high sensitivity and long lifetimes, and have frequently been used for analytical and control work.

REFERENCES

1. G.Eisenman, G.Szabo, S.Cianni, S.McLaughlin, S.Krasme, In: "Ion binding and Ion Transport produced by neutral lipid soluble membranes", in "Progresses in Surface and Membrane Science", Vol. 6, (Ed., D.A. Cadendend, J.F.Danielle, M.D. Rosenberg), Academic Press, New York, 1973, p.139.
2. F.Conti, G.Eisenman, *Biophysics. J.*, 5, 511 (1965).
3. E.Hepp, *Apothekerf Tidds*, 80, 327 (1972).
4. G.A.Rechnitz, Z.F.Liu,*Anal.Chem.*, 40, 696 (1968).
5. G.A.Rechnitz, M.K.Kresz, S.B.Zamochnik, *Anal.Chem.*, 38, 973 (1966).
6. R.Pouget, *Chin.Anal., (Paris)*, 53, 479 (1971).
7. M.Verloo, A.Cottenie, *Med.Fac.Landb.Uni.Ghent*, 34, 137 (1969).
8. J.Tusl, *Chem.Listy.*, 64, 322 (1970).
9. E.Pungor, K.Toth, *Anal.Chim.Acta*, 47, 291 (1969).
10. E.Pungor, K.Toth, *Analyst.*, 95, 625 (1970).
11. E.J.Duff, S.L.Stuart, *Talanta*, 19, 76 (1972).
12. D.E.Jordan, *J.Assoc.Of Anal.Chem.*, 53, 467 (1970).
13. E.J.Duff, S.L.Stuart, *Anal.Chim.Acta*, 52, 155 (1970).
14. K.Toth, I.Gaveller, E.Pungor, *Anal.Chim.Acta*, 57, 131 (1971).
15. J.Koryta, In: "Ion Selective Electrodes", p.38, Cambridge University Press, Cambridge, 1975.
16. G.A.Rechnitz, M.R.Kresz, *Anal.Chem.*, 38, 1786 (1966).
17. See 5.

18. B.Fleet, T.H.Ryan, M.J.Brans, *Anal.Chem.*, 46, 12 (1974).

19. G.J.Moody, J.D.R.Thomas, *Talanta*, 19, 623 (1972).

20. E.Pungor, K.Toth, *Anal.Chim.Acta*, 64, 417 (1973).

21. K.Scrinvason , G.A.Rechnitz, *Anal.Chem.*, 40, 509 (1968).

22. G.A.Rechnitz, T.M.Hsea, *Anal.Chem.*, 41, 111 (1969).

23. P.L.Markovic, T.O.Osburn, *A.I.Ch.E.J.*, 19, 504 (1973).

24. W.E.Morf, E.Lindner, W.Simon, *Anal.Chem.*, 47, 1596 (1975).

25. H.S.Carshaw, J.C.Jaeger, In: "Conduction of heat in Solids", Oxford University Press, Oxford 1959.

26. See 18.

27. See 4.

28. G.J.Moody, D.R.Thomas, *Lab.Practices*, 20, 307 (1971).

29. W.E.Morf, D.Ammann, W.Simon, *Chemica*, 28, 65 (1974).

30. G.J.Moody, R.Oke, J.Thomas, J.Davies, *Analyst.*, 97, 87 (1972).

31. E.Pungor, Y.Umezawa, *Anal.Chem.*, 55, 1432 (1983).

32. M.Dole, *J.Chem.Phys.*, 2, 862 (1934).

33. B.P.Nikolsky, *Zh.Fiz.Khim.*, 10, 495 (1957).

34. B.Lengyd, E.Blan, *Trans.Faraday Soc.*, 30, 461 (1934).

35. W.Simon, H.R.Wuhrman, M. Vasak, L.A.Piode, R.Dohner, Z.Stefac, *Angew.Chemie.*, 82, 433 (1972).

36. E.Pungor, J.Havas, *Acta Chem.Hung.*, 50, 77 (1966).

37. J.Sapio, J.Colaruotolo, J.Bobbit, *Anal.Chim.Acta*, 71, 222 (1974).

38. U.Lukkari, *Acta Chem.Fenn.*, 45, 182 (1972).

39. M.S.Frant, J.W.Ross, *Science*, 154, 1553 (1966).

40. See references in J.Koryata, "Ion Selective Electrodes", Chapter 5, Cambridge University Press, Cambridge, 1973.

41. See references in T.S.Ma and S.S.M.Hassan, "Organic Analysis using Ion Selective Electrodes", Vol. 1, Chapter 2, Academic Press, New York, 1983.

42. E.Pungor, K.Toth, *Analyst.*, 95, 625 (1970).

43. H.Clysters, F.Adams, *Anal.Chim.Acta*, 83, 27 (1976).

44. A.Allan, G.Patts, J.Hollis, *Soil Sci.*, 114, 456 (1972).

45. D.Muller, P.West, R.Muller, *Anal.Chem.*, 41, 2038 (1969).

46. J.W.Ross, *Science*, 156, 1378 (1967).

47. D.Midgley, *Analyst*, 100, 386 (1975).

48. A.F.A.Al-Sibarai, C.Burgess, *Anal.Lett.*, 8, 129 (1975).

49. C.Coetzes, A.Basson, *Anal.Chim.Acta*, 83, 361 (1976).

50. A.Fogg, A.Al-Sibarai, *Anal.Lett.*, 9, 33 (1976).

51. W.Hildebrant, K.Pool, *Talanta*, 23, 469 (1976).

52. G.J.Moody, R.B.Oke, J.D.R.Thomas, *Analyst*, 95, 910 (1970).

53. G.H.Griffiths, G.J.Moody, J.D.R.Thomas, *Analyst*, 97, 420 (1972).

54. O.Ryba, J.Petranek, *J.Electroanal.Chem.*, 44, 425 (1973).

55. J.Stepanova, R.Vaduse, *Chem.Listy.*, 68, 853 (1974).

56. A.Craggs, B.Boyle, S.K.A.G.Hassan, G.J.Moody, *Talanta*, 27, 277 (1980).

57. V.V.Cosofret, C.Stefanesca, A.A.Bunaui, *Talanta*, 26, 1035 (1979).

58. V.Majer, K.Stulik, *Talanta*, 29, 145 (1982).

CHAPTER 3

THE ROTATING DISC

3.1 INTRODUCTION

A major problem in understanding dissolution processes is that most of the studies undertaken have used suspensions of powders. Such experiments suffer from the intrinsic disadvantage that it is impossible to define the hydrodynamics of such a system, which means that transport controlled reactions cannot be satisfactorily modelled.

To study transport reactions properly, well-defined hydrodynamics are essential. A system in which the hydrodynamic and convective diffusion equations have been solved exactly is the rotating disc system. This chapter will describe the theory of the rotating disc showing the exact solution of transport processes to the rotating disc surface.

3.2 THEORY OF THE ROTATING DISC ELECTRODE (R.D.E.)

The first mathematical description of the rotating disc hydrodynamics was that of von Karman[1] who solved the flow pattern to a spinning disc. Because of cylindrical ~~co-ordinates~~ symmetry it is easier to use polar co-ordinates to describe the system (Figure 3.1).

von Karman used the Navier-Stokes equation (which describes the functional dependance of the fluid velocity upon the co-ordinates of the system) and defined the three component equations as:-

$$V_r \frac{\partial V_r}{\partial r} + V_y \frac{\partial V_r}{\partial y} - \frac{V_\phi^2}{r} = \nu\{\frac{\partial^2 V_r}{\partial r^2} + \frac{\partial}{\partial r}(\frac{V_r}{r}) + \frac{\partial^2 V_r}{\partial y^2}\} \quad 3.1$$

$$V_r \frac{\partial}{\partial r} V_\phi + V_y \frac{\partial}{\partial y} V_\phi + \frac{V_r}{r} V_\phi =$$

$$\nu \{\frac{\partial^2}{\partial r^2} V_\phi + \frac{\partial}{\partial r}(\frac{V_\phi}{r}) + \frac{\partial^2}{\partial y^2} V_\phi\} \quad 3.2$$

$$V_y \frac{\partial V_y}{\partial y} = \frac{-1}{\rho} \frac{\partial}{\partial y} p + \frac{\nu \partial^2}{\partial y^2} V_y \quad 3.3$$

Where V_r, V_y, V_ϕ are as shown in Figure 3.1

ρ = density

ν = kinematic viscosity.

with the equation of continuity:

$$\frac{\partial V_r}{\partial r} + \frac{V_r}{r} + \frac{\partial V_y}{\partial y} = 0 \quad 3.4$$

He then set the boundary conditions:

$$V_r = 0 \quad V_\phi = Wr \quad V_y = 0 \quad y = 0 \quad 3.5$$

W = rotation speed in radians

$$V_r = 0 \quad V_\phi = 0 \quad y = \infty \quad 3.6$$

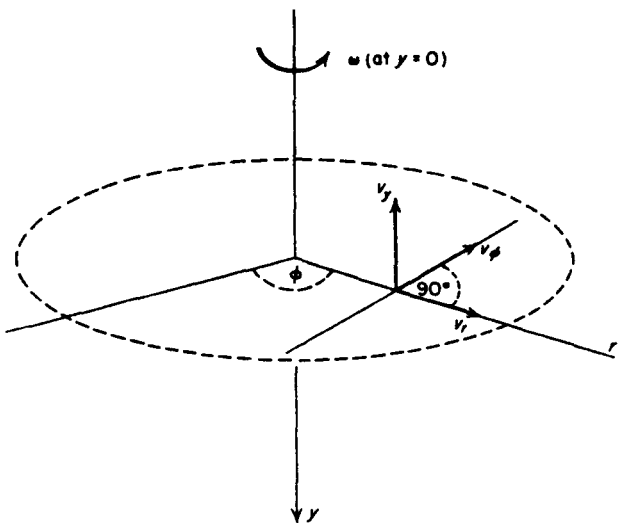

FIGURE 3.1 Polar co-ordinates

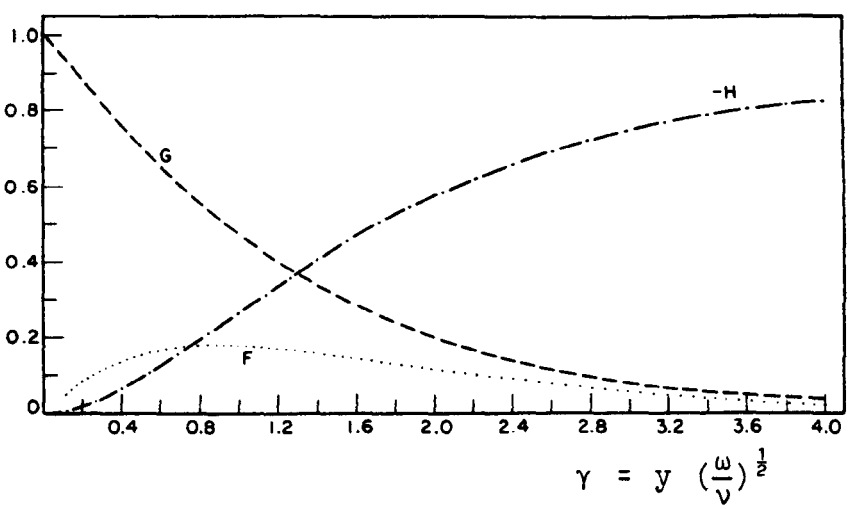

FIGURE 3.2 Plot of Cochran's non-dimensional functions vs. γ

since close to the disc fluid acquired radical and tangential motion and is thrown radically outwards by centrifugal force. Fresh solution is then drawn up to replace it at a constant velocity when a steady state is achieved.

To solve these equations von Karman cast them into the following non-dimensional forms:-

$$V_r = rWF(\gamma) \qquad 3.7$$

$$V_\phi = rWG(\gamma) \qquad 3.8$$

$$V_y = (W\nu)^{\frac{1}{2}} H(\gamma) \qquad 3.9$$

$$p = -\rho\nu WP(\gamma) \qquad 3.10$$

Where $(\gamma) = \left(\frac{W}{\nu}\right)^{\frac{1}{2}} y$

p = pressure.

These equations were then solved using von Karman's approximate integral method.

These approximations were removed by Cochran[2] who used a numerical integration method, expressing the above non-dimensional function (F, G, H, P) as power series.

These functions are plotted in Figure 3.2. Note from the figure that at $\gamma = 2.8$, $G \approx 0.1 G_{(o)}$, $H \approx 0.72\ H_{(o)}$, thus this value ($y = 2.8\ (\frac{\nu}{W})^{\frac{1}{2}}$) is the approximate thickness of the solution caused to rotate by the spinning disc. Also, from equation (3.9) we see that the velocity of fluid flow to the disc is independant of r, this means that all parts of the disc are uniformly accessible.

The problem of transport to the spinning disc was solved by Levich.[3,4,5] Transport to the disc is by convection and diffusion and the rate of change of concentration with time is given by:

$$\frac{\partial c}{\partial t} = D \left| \frac{\partial^2 c}{\partial y^2} + \frac{\partial^2 c}{\partial r^2} + \frac{1}{r} \frac{\partial c}{\partial r} + \frac{1}{r^2} \left(\frac{\partial^2 c}{\partial \phi^2} \right) \right| -$$

(diffusion term)

$$\left| V_r \left(\frac{\partial c}{\partial r} \right) + V_\phi \left(\frac{\partial c}{\partial \phi} \right) + V_y \left(\frac{\partial c}{\partial y} \right) \right| \qquad 3.11$$

(convective term)

D = diffusion coefficient.

When a steady state is set up then:

$$\frac{\partial c}{\partial t} = 0$$

From symmetry c is not a function of Ø and from equation 3.9 V_y is independent of r.

Applying the boundary conditions that:

at y = 0, c = o

equation 3.11 becomes:

$$V_y \left(\frac{\partial c}{\partial y} \right) = \frac{D \partial^2 c}{\partial y^2} \qquad 3.12$$

V_y can be found from equation 3.9:

$$V_y = -0.51 \, W^{3/2} \nu^{-\frac{1}{2}} \, y^2 \qquad 3.13$$

substituting and rearranging gives:

$$\frac{\partial^2 c}{\partial y^2} = - \frac{y^2 \partial c}{\partial y} \times \left(\frac{1}{DW^{-3/2} \nu^{\frac{1}{2}} / 0.51} \right) \qquad 3.14$$

$$= \frac{-y^2}{B} \frac{\partial c}{\partial y} \qquad 3.15$$

Applying boundary conditions that: $y \to \infty \quad c \to c_\infty$

i.e., at distances far from the electrode then the concentration is equal to the bulk concentration, and defining:

$$X = \frac{\partial c}{\partial y} \qquad 3.16$$

$$\therefore \quad y = o \qquad \chi = \chi_o = \left(\frac{\partial c}{\partial y}\right)_{y = o}$$

which gives equation 3.15 as:

$$\frac{\partial \chi}{\partial y} = \left(\frac{-y^2}{B}\right)\chi \qquad 3.17$$

$$\int_{\chi_o}^{\chi} \left(\frac{d\chi}{\chi}\right) = \frac{-1}{B} \int_{o}^{y} y^2 dy \qquad 3.18$$

$$\frac{\chi}{\chi_o} = \exp\left(\frac{-y^3}{3B}\right) \qquad 3.19$$

$$\frac{\partial c}{\partial y} = \left(\frac{\partial c}{\partial y}\right)_{y=o} \left(\exp\left(\frac{-y^3}{3B}\right)\right) \qquad 3.20$$

integrating gives:

$$\int_{o}^{c_\infty} dc = \left(\frac{\partial c}{\partial y}\right)_{y=o} \int_{o}^{\infty} \exp\left(\frac{-y^3}{3B}\right) dy \qquad 3.21$$

and substituting:

$$Z = \frac{y^3}{3B}$$

$$\int_0^\infty \exp Z = (3B)^{1/3} \times 0.8934 \qquad 3.22$$

$$= 1.288\ B^{1/3} \qquad 3.23$$

$$\therefore \quad c_\infty = \left(\frac{\partial c}{\partial y}\right)_{y=o} 1.288\ B^{1/3} \qquad 3.24$$

$$= \left(\frac{\partial c}{\partial y}\right)_{y=o} 1.613\ (DW^{3/2}\nu^{-\frac{1}{2}})^{1/3} \qquad 3.25$$

From Fick's first law:

$$J = D\left(\frac{\partial c}{\partial y}\right) \qquad 3.26$$

$$= \frac{Dc_\infty}{1.613\ D^{1/3}\ W^{-\frac{1}{2}}\ \nu^{1/6}} \qquad 3.27$$

$$J = 1.554\ c_\infty D^{2/3}\omega^{\frac{1}{2}}\nu^{-1/6} \qquad 3.28$$

J = flux/mole $cm^{-2}s^{-1}$

c_∞ = bulk concentration/mol cm^{-3}

ω = rotation speed/Hz

ν = kinematic viscosity/cm^2s^{-1}

D = diffusion coefficient/cm^2s^{-1}

Equation 3.28 is known as the Levich equation.

The concentration profile with distance from the electrode surface can be calculated from equation 3.21, integrating between 0 and c_y. The profile is as shown in Figure 3.3. As can be seen, beyond the distance known as y_D, ($y_D = 0.643\omega^{-\frac{1}{2}}\nu^{1/6}D^{1/3}$) the solution is well stirred and the concentration is equal to the bulk concentration (c_∞). However, for $y < y_D$ then transport is by diffusion across the stagnant layer of solution swept around by the electrode. This distance (y_D) is called the thickness of the diffusion layer.

3.3 THE ROTATING DISC : EXPERIMENT

The first workers to verify the Levich theory were Siver and Kabanov.[6] They used a silver electrode to study the cathodic reduction of oxygen in dilute sulphuric acid solution, using the relationship:-

$$i_{lim} = J_{lim} A n F \qquad 3.29$$

i_{lim} = limiting current

J_{lim} = limiting flux

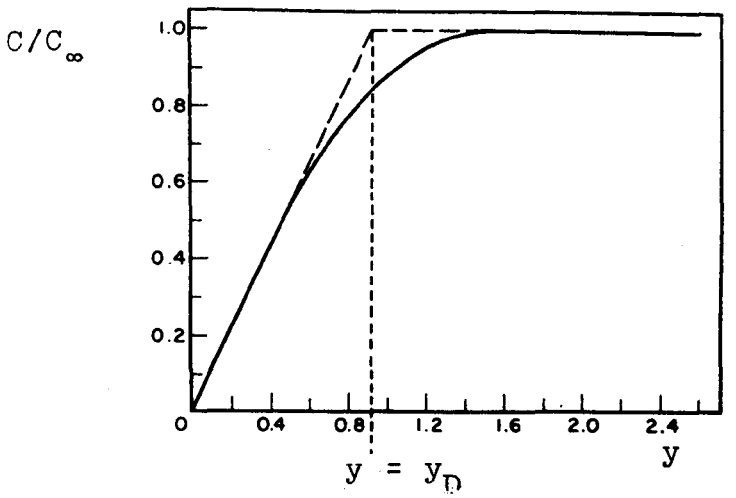

FIGURE 3.3 Concentration profile as a function of distance from the electrode surface.

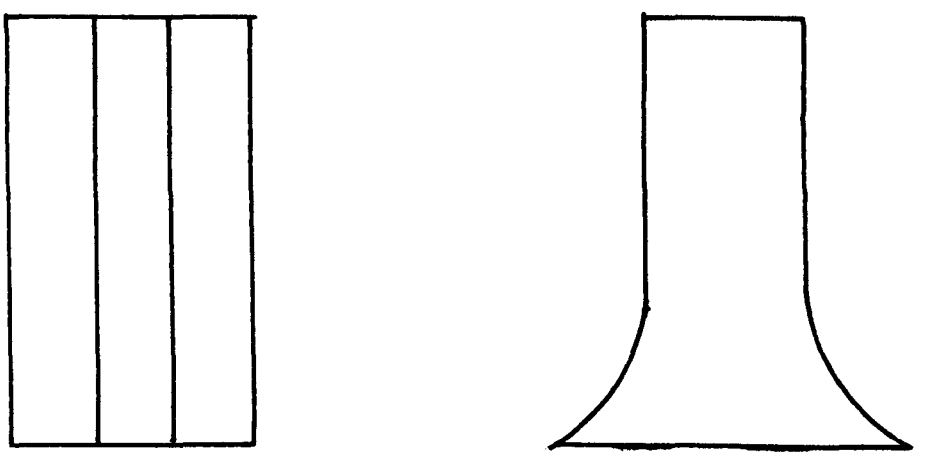

FIGURE 3.4 Differing shapes for the rotating disc (a) with only the central area active, and (b) with curving edges.

A = area of electrode/cm^2

n = number of electrons passed

F = Faraday's constant

and they found agreement between theory and experiment, assuming a literature value of 1.98×10^{-5} $cm^2 s^{-1}$ for the diffusion coefficient of oxygen.

Extensive studies have subsequently been reported using rotating discs, and the later development of rotating-ring discs, and these have been reviewed.[7,8,9] General agreement has been shown with the Levich theory, though some[10,11] claimed that a plot of i vs. $\sqrt{\omega}$ while varying linearly, did not pass through the origin but give a positive intercept. This variation has been put down by Riddiford[12] to the electrode shape not fulfilling the theoretical requirements.

Many electrode shapes have been used and the individual shapes have been discussed by Azim and Riddiford.[13] To fulfil the theoretical conditions then the disc must firstly be horizontal, of minimum eccentricity and be smooth to the extent that the maximum height of undulation is far less than the boundary layer. Secondly, the active part of the rotating disc must be free from edge effects which may introduce turbulance into the hydrodynamics.

Many ways have been suggested to ensure that these edge effects do not become important:-

1. Use a disc with only the central area being active (Figure 3.4a).
2. Use a guard ring[14]
3. Use a rotating disc with curving sides (Figure 3.4b).

Of these Riddiford[7,13] suggested the latter as the second method was difficult to construct and the first kind he considered to act as a rotating cylinder, which are prone to fluid mixing above and below the disc plane, which introduces turbulance. However, many workers have since used electrodes of similar shape to that shown in Figure 3.4a, and have shown[15-18] that satisfactory hydrodynamic behaviour is established.

Further recomendations involved the positioning of the rotating disc in relation to the reaction vessel's walls and base, and to the liquid surface. The theory demands an infinite volume of solution. Gregory and Riddiford[19] reported that the results were independant of the vessel dimensions providing that the electrode was at least 0.5 cm away from the walls and base of the reaction vessel. Prater and Adams[20] then showed that there was practically no effect on the limiting current measured in changing from a 100 ml beaker to a 9 litre laboratory bucket!

Thus, the rotating disc electrode has been shown to be a useful tool in the measurements of fluxes and currents, where the well defined hydrodynamics allow these to be measured and quoted with great confidence.

3.4 MEASUREMENT OF CHEMICAL RATE CONSTANTS USING R.D.E.

The theory outlined so far in this chapter has dealt with reactions involving electron transfer with no preceding chemical steps. If, however, a chemical step does proceed electron transfer (such as the dissociation of a weak acid), then modifications have to be introduced into the theory. Levich and Koutecky[21,22] derived and solved the mathematical model, and this was given a more rigerous treatment by Dogonadze[23].

Consider the case of an acid (HA) dissociating into its component acid and base ($H^+ + \bar{A}$):

$$HA \underset{k_{-1}}{\overset{k_1}{\rightleftharpoons}} H^+ + A^-$$

$$K_A = \frac{k_1}{k_{-1}}$$

before reaction occurs at the electrode surface

$$H^+ + e \xrightarrow{\text{electrode}} 1/2\ H_2$$

Making the assumption that H^+ and A^- are in equilibrium throughout the bulk of solution, then the equilibrium is maintained as HA diffusses across the boundary layer. However, near the electrode H^+ is removed which leads to an unbalance between A^- and H^+, and more HA dissociates than is reformed.

The distance at which the equilibrium is no longer maintained is known as the reaction layer (y_r).

Since electron transfer is considered to be fast then the maximum flux of protons is given by diffusion of HA across the diffusion layer. From equation 3.28:

$$J_{HA} = 1.554\ D_{HA}^{2/3}\ \nu^{-1/6}\ \omega^{\frac{1}{2}}\ (C_{HA,\infty} - C_{HA,r})$$

$$= \frac{D_{HA}}{y_D}\ (C_{HA,\infty} - C_{HA,r}) \qquad 3.30$$

where $C_{HA,\infty}$ = bulk concentration of HA

$C_{HA,r}$ = concentration of HA at reaction layer.

At the reaction layer the rate of change of concentration of HA with time can be described by a combination of Fick's second law and homogeneous kinetics:

$$\frac{\partial c_{HA}}{\partial t} = D_{HA} \frac{\partial^2 c_{HA}}{\partial y^2} - k_1 c_{HA} + k_{-1} c_H c_A \qquad 3.31$$

where c_H, c_A are concentrations of $H^+ + A^-$

when a steady state is set up at the electrode then equation 3.31 becomes:

$$D_{HA} \frac{\partial^2 c_{HA}}{\partial y^2} = k_1 c_{HA} - k_{-1} c_H c_A \qquad 3.32$$

A similar equation can be drawn up for H^+, i.e.,

$$D_{H^+} \frac{\partial^2 c_H}{\partial y^2} = k_1 c_{HA} - k_{-1} c_H c_A \qquad 3.33$$

Applying the boundary conditions $y = 0$, $c_H = 0$

$y = 0$, $\frac{\partial c_{HA}}{\partial t} = 0$ since HA does not react at the surface

also just outside the reaction layer ($y > y_r$),

$$c_{HA} = c_{HA,\infty}$$

and

$$c_H = \frac{k_1 \cdot c_{HA}}{k_{-1} \cdot c_A}$$

c'is defined as the loss of equilibrium between HA and H^+

$$c' = \left(\frac{k_1 \cdot c_{HA}}{k_{-1} \cdot c_A} \right) - c_H \qquad 3.34$$

at $y = \infty$, $c' = 0$ (solution is in equilibrium)

$$y = 0, \; c' = c'_o = \left(\frac{k_1 \cdot c_{HA}}{k_{-1} \cdot c_A} \right)$$

This has been solved giving:

$$c' = c'_o \exp - \left(\frac{y}{y_r}\right) \qquad 3.35$$

$$\text{where } y_r = \sqrt{\frac{D_{H^+}}{k_{-1}}}\, c_A \qquad 3.36$$

Using Fick's first law:

$$J = D_{H^+} \left(\frac{\partial c_H}{\partial y}\right)_{y=0} \qquad 3.37$$

$$= -D_{H^+} \left(\frac{\partial c'}{\partial y}\right)_{y=0} = \frac{D_{H+} K_A c_{HA}}{c_A y_r} \qquad 3.38$$

substituting for y_r

$$J = D_H^{\frac{1}{2}+} \cdot c_A^{-\frac{1}{2}} \cdot c_{HA} \cdot k_1^{\frac{1}{2}} \cdot K_A^{\frac{1}{2}} \qquad 3.39$$

$$= A\ c_{HA} \qquad 3.40$$

From equation 3.30

$$D_{HA} \left(\frac{c_{HA,\infty} - c_{HA,r}}{y_D}\right) = A\, c_{HA} \qquad 3.41$$

eliminating $c_{HA,r}$ gives:

$$\frac{1}{J} = \left(\frac{y_D A - D_{HA}}{D_{HA} c_{HA,\infty} A} \right) \qquad 3.42$$

$$= \frac{1}{c_{HA,\infty}} \left[\frac{y_D}{D_{HA}} - \frac{1}{A} \right] \qquad 3.43$$

substituting gives:

$$\frac{1}{J} = \frac{1}{c_{HA,\infty}} \left[\frac{0.64\ \nu^{1/6}}{D_{HA}^{2/3} \cdot \sqrt{\omega}} + \sqrt{\left(\frac{c_A}{D_{H^+} \cdot k_1 K_A} \right)} \right] \qquad 3.44$$

The above equation is known as the Koutecky-Levich equation. Its form has been verified by many workers, including Albery and Bell,[24] and Vielstich et al.[25-27] Albery[28] however, pointed out that this equation only held for reaction solutions with sufficient background electrolyte present to be able to ignore the effects of the electric field in the diffuse part of the double layer. Otherwise corrections have to be allowed for.

3.5 ESTIMATION OF DIFFUSION COEFFICIENT

Both theLevich equation 3.28 and the Koutecky-Levich equation 3.44 contain the diffusion coefficient (D) and the concentration (c). This has enabled many workers to use the rotating disc as an analytical tool, using the slope of the Levich plots to find the bulk concentration, knowing the diffusion coefficient. Levich plots have

also been used to measure the diffusion coefficients of species in solution, and this has often been used as a check on the hydrodynamics of the experimental system. In cases where the diffusion coefficient is unknown it can be approximated to within 10% using the Wilke-Chang equation.[29,30]

They empirically plotted experimental data against various functions and derived the following equation:

$$D = \alpha \left| \frac{(\chi M)^{\frac{1}{2}} T}{V^{0.6}} \right| \qquad 3.45$$

D = diffusion coefficient/$cm^2.s^{-1}$

α = constant (7.4×10^{-8})

M = molecular weight of solvent/$g.mol^{-1}$

T = absolute temperature/K

η = solvent viscosity/cP

χ = association parameter characteristic of the solvent, describing how associated the solvent is, i.e., for non-associated solvents $\chi = 1$, for water $\chi = 2.6$.

V = molecular volume of diffusing species.

V can be found using the method of Le Bas[31].

Bidstrup and Geankoplis[32] measured the diffusion coefficients of carboxylic acids, using diaphragm cells, and found that the Wilke-Chang equation give constantly higher values ($\sim$11%) than they found by experiment. They redefined the equation changing α from 7.4×10^{-8} to 6.6×10^{-8}.

3.6 APPLICATION OF R.D.E.

Since their development rotating discs have been extensively used as analytical tools, and have replaced to a certain extent the dropping mercury electrode (D.M.E.), as developed earlier by Heyrovsky[33] and described mathematically by Ilkovic.[34,35] This is because the D.M.E. is far more complex to describe mathematically, and because that instead of a true steady state being set up, as in the R.D.E., in the D.M.E. a cyclic pattern is set up in which the concentration varies with both time and distance. D.M.E.'s do, however, have the advantage that the electrode surface is continuously being replaced and, therefore, the electrode surface does not suffer from the effects of fouling, as species become absorbed onto the surface.

R.D.E.'s have been used with high accuracy to find the bulk concentration of solutions knowing the diffusion coefficients, and vice versa. They have also been used to determine homogeneous rate constants (such as systems showing Koutecky Levich behaviour). Normally $i_{lim} \alpha \sqrt{\omega}$ (equations 3.28 and 3.29) for a simple n electron transfer process without homogeneous chemical coupling, but, if a chemical step proceeds the electron transfer step, then the Levich plot appears as in Figure 3.5. As can be seen at high rotation speeds the limiting current falls off as the rate of electron transfer (and thus i_{lim}) is limited by the rate of the proceeding chemical process. This type of reaction is

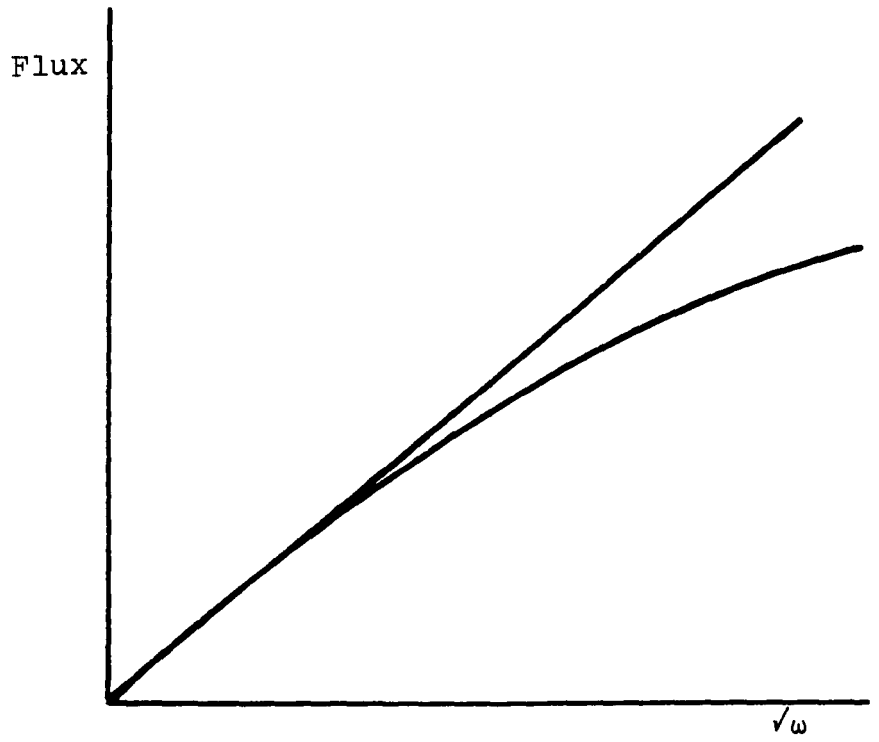

FIGURE 3.5 Levich plot for E.C.E reaction

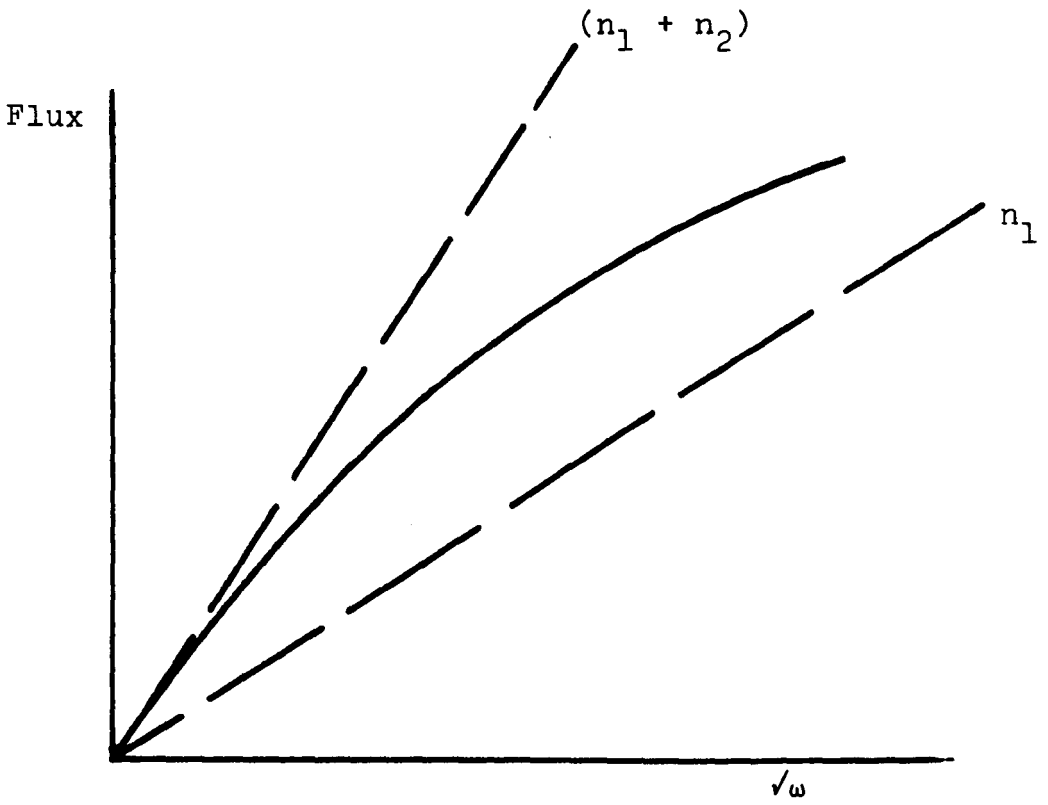

FIGURE 3.6 Levich plot for E.C.E. reaction.

known as a "C.E." process (a chemical reaction followed by electron transfer). As well as measuring dissociation constants, other C.E. reactions include:

$$H_2C(OH)_2 \underset{k_{-1}}{\overset{k_1}{\rightleftharpoons}} H_2C=O + H_2O$$

non-electro active electro active

and

$$R_2CH - NO_2 + OH^- \underset{k_{-1}}{\overset{k_1}{\rightleftharpoons}} R^-C\,NO_2$$

electro active non-electro active

In both these cases the rate constants can be found using the Koutecky-Levich equation.

Another reaction which can be followed, and the rate constants measured, is the E.C.E. reaction (an electron transfer followed by a chemical step and then by a second electron transfer) i.e.,

$$O_1 + n_1e \rightarrow R_1 \qquad (E)$$

$$R_1 \xrightarrow[k]{+s} O_2 \qquad (C)$$

$$O_2 + n_2e \rightarrow R_2 \qquad (E)$$

In such a case if i_{lim} is measured as a function of ω and a Levich plot drawn up, then the following is seen (Figure 3.6). At low rotation speeds the experimental plot lies close to the line expected for a $(n_1 + n_2)$ electron transfer process. However, at high rotation speeds the experimentally determined time lies close to that expected for a n_1 electron transfer process. This is because while at low ω the species O_2 remains close enough to the electrode surface to be further reduced to R_2, at high ω O_2 is swept away from the electrode surface too quickly for the second electrode process to occur.

Further developments of the R.D.E. include the use of pulse and A.C. voltametries to improve the sensitivity. In normal voltametry the potential of the electrode is linearly swept from E_b (Figure 3.7). In pulse voltametry, however, the electrode is held at E_b, at which no electrochemical reaction is seen, the potential is then suddenly changed and is held at $(E_b + E)$ for approximately 50 m.s. before being returned to E_b (see Figure 3.7). This sequence is repeated at set time intervals, E increasing each time. Sampling is taken near the end of each pulse after capacidance charging processes have occurred. This increases the sensitivity because of the large concentration gradients induced by jumping from E_b to the sampling potential. Sensitivity is improved down to approximately 10^{-7} mol dm^{-3}.

In A.C. voltametry a sine wave is superimposed upon the linear sweep (Figure 3.7). The current response is

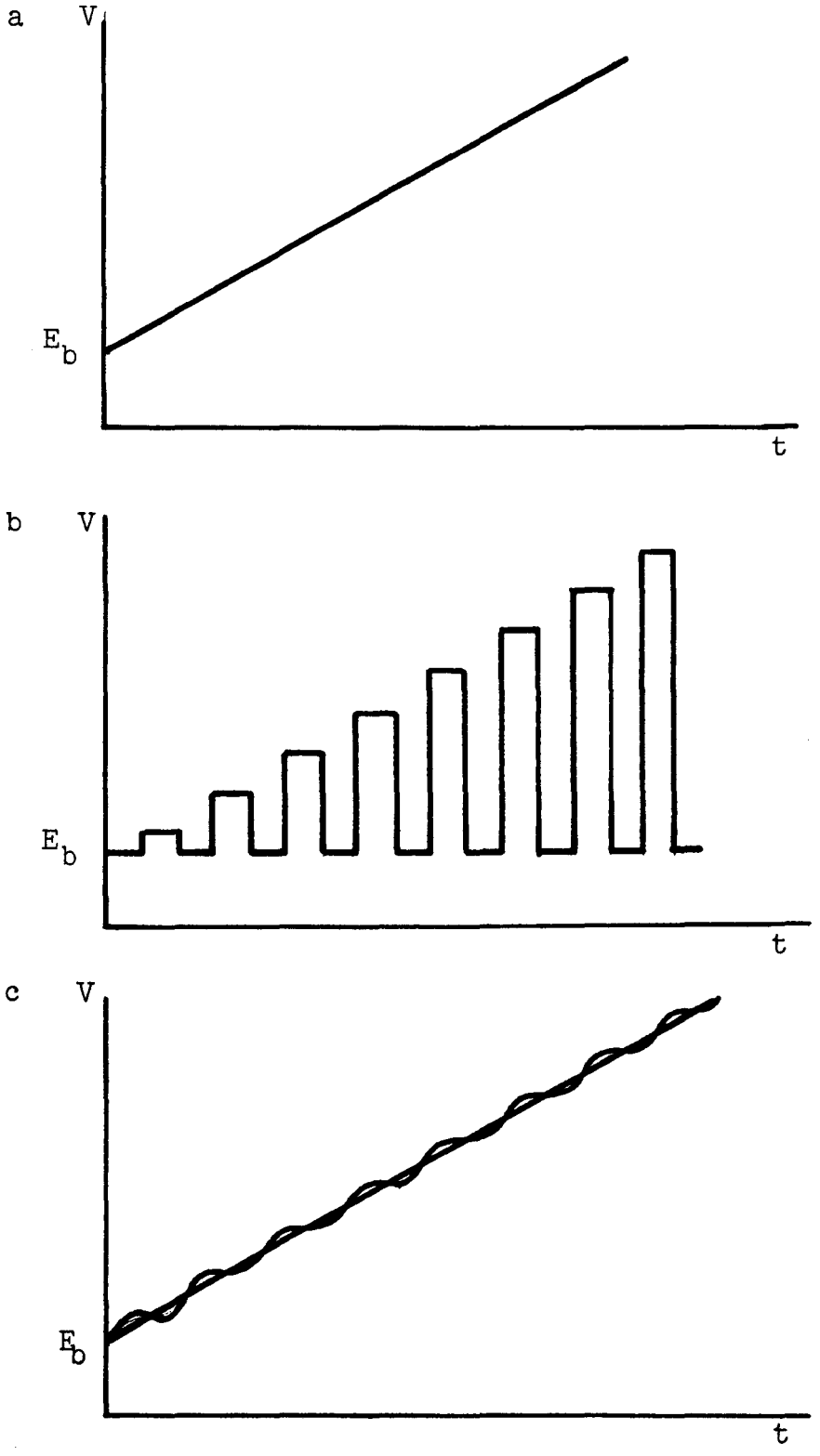

FIGURE 3.7 Voltage time curves for (a) normal voltammetry, (b) potential step voltammetry (c) AC voltammetry.

measured via a lock-in amplifier which separates the A.C. response from the D.C. voltamagram. Figure 3.8 shows a typical D.C. voltamagram and Figure 3.8b shows the corresponding A.C. voltamagram. As can be seen in the regions a and c the D.C. current is practically constant and thus no change in the Faradaic A.C. current is seen as the potential is modulated. In region b however, the D.C. current is rapidly changing and a large A.C. current is seen. The concentration $\propto$ i max.. A.C. voltametry improves the sensitivity because the lock-in amplifier will only detect signals which have the same modulation as the potential, thus it will not pick up any background noise. Sensitivity is again improved down to 10^{-7} mol dm^{-3}.

3.7 ROTATING RING-DISC ELECTRODES R.R.D.E.

A development that enhanced the use of R.D.E.'s for use in investigating the kinetics of multistep electrode processes was the introduction of R.R.D.E.'s. The theory for such electrodes was developed by Levich and Inanov,[36,37] and the first system described was that of Frumkin.[38,39]

As shown in Figure 3.9 a R.R.D.E. consists of a central disc electrode separated from an outer surrounding ring electrode by an insulating gap. The supporting electronics are designed so that the voltage of both electrodes can be swept separately and each current response measured separately. Species formed at the

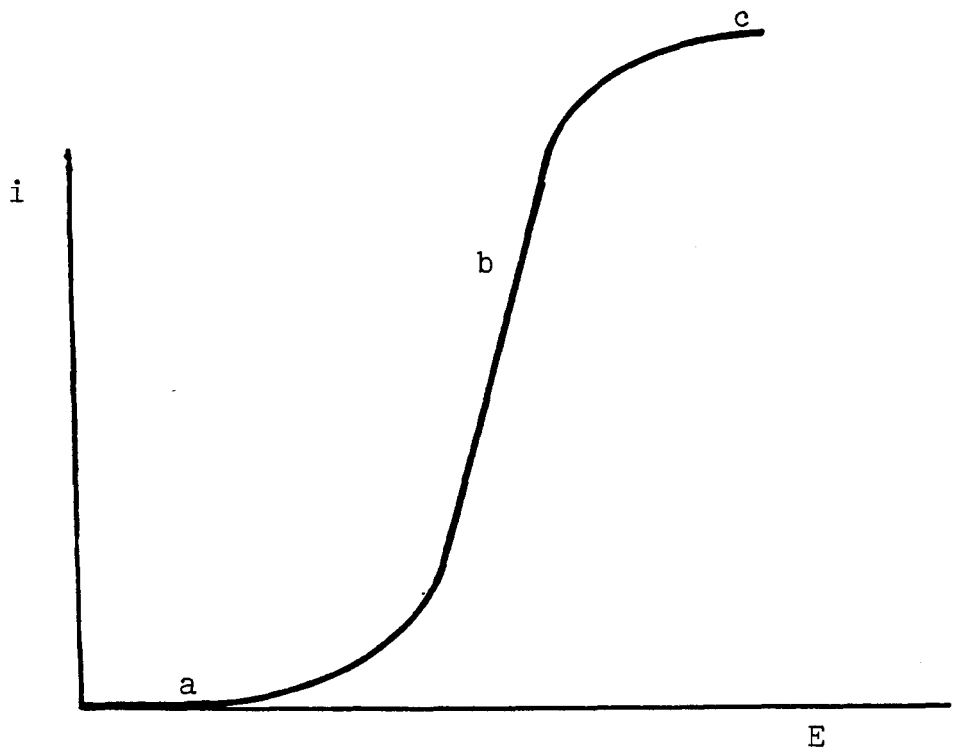

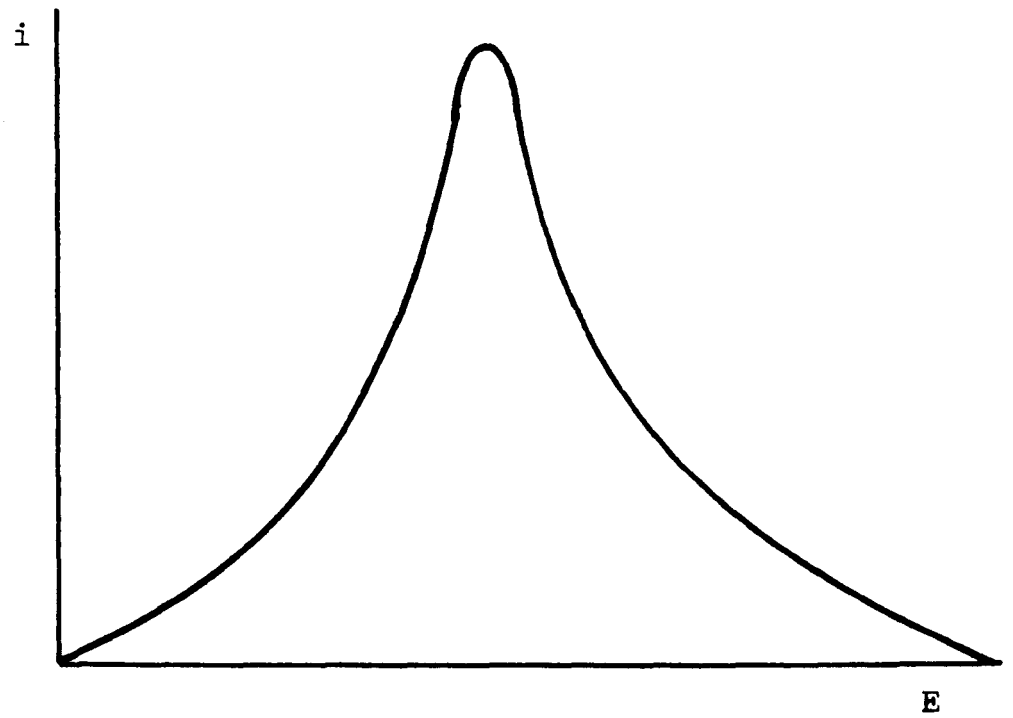

FIGURE 3.8 Voltammagrams (a) D.C., (b) A.C.

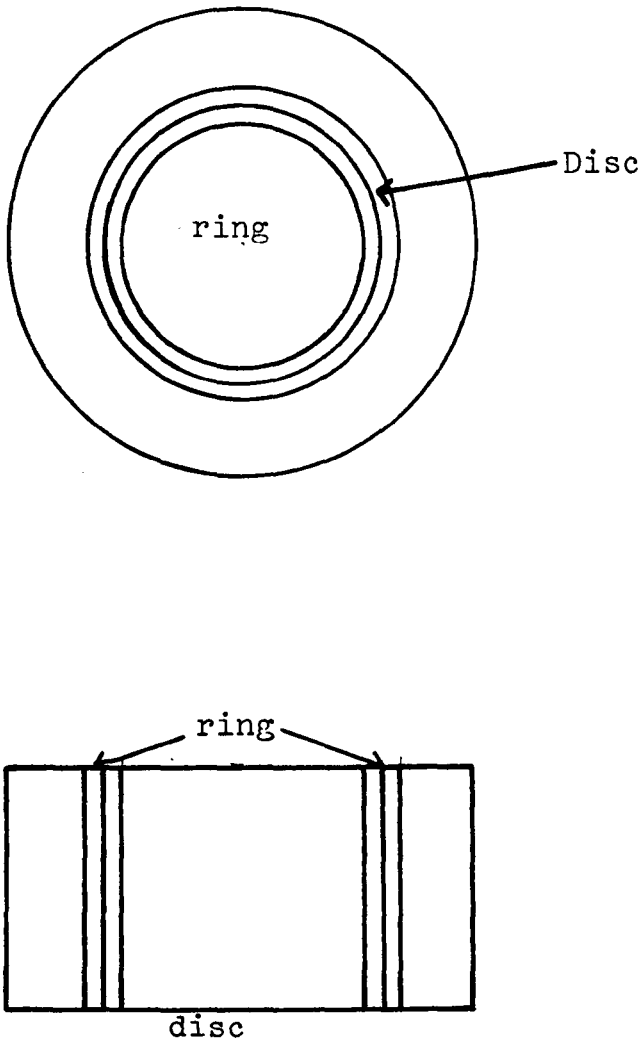

FIGURE 3.9 A rotating ring-disc electrode

inner disc electrode are swept outwards, and only a fraction reaches the ring (Figure 3.10). The ring is set at such a potential as to destroy any species arriving. Levich showed that the fraction of species arriving at the ring is independant of rotation speed (for stable species) and is a constant (N) governed only by the geometry of the system.

This, however, only holds for stable species, if the electrochemically generated species is short lived then the fraction arriving at the ring is less than would be calculated, and the measured current at the ring (i_r) will fall. The reduction will be greatest for low rotation speeds as species will have longer to react. If a plot is drawn up of i_r vs. i_d (current measured at the disc), then the following (Figure 3.11) would be seen. All of the plots fall below the theoretical ratio N, but as ω increases then the ratio approaches this theoretical value.

Ivanov and Levich solved this situation, enabling the chemical rate constant to be found by measuring the variation of N with ω. Their solution has subsequently been used by many workers[40-42] in the determination of rate constants.

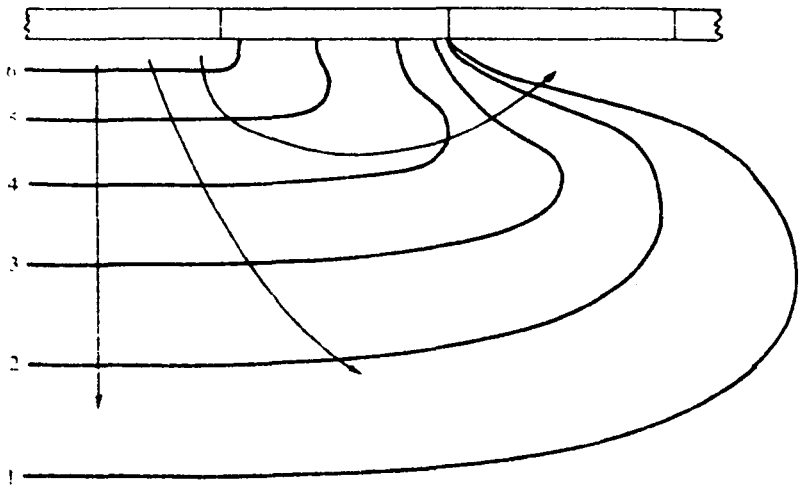

FIGURE 3.10 The flow pattern in a rotating disc solid lines represent points of equal concentration

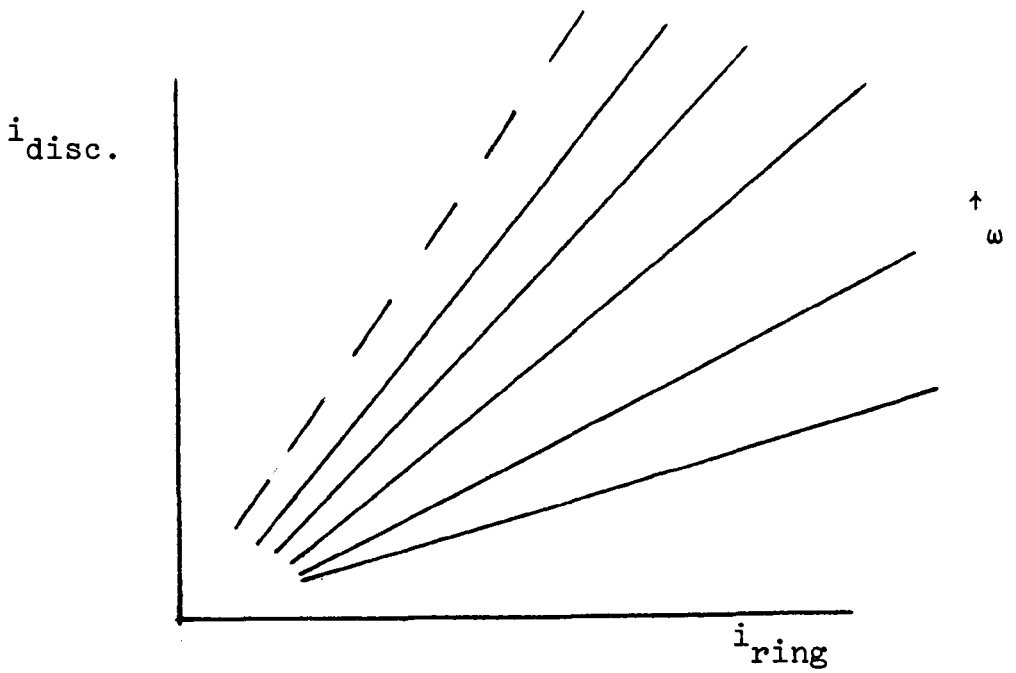

FIGURE 3.11 Collection efficiency for reactive species. N increases with ω but never reaches N_o.

REFERENCES

1. T.von Karman, *Z.Angew.Math.Mech.*, 1, 837 (1921).
2. W.G.Cochran, *Proc.Cambridge Phil.Soc.*, 30, 365 (1934).
3. V.G.Levich, In: "Physiochemical Hydrodynamics", Prentice Hall Inc., Englewood Cliffs, New Jersey, 1962.
4. V.G.Levich, *Acta Physiochem., U.R.S.S.*, 17, 257 (1942).
5. V.G.Levich, *Zh.Fiz.Khim.*, 18, 335 (1944).
6. G.Yu.Siver, B.N.Kabanov, *Zh.Fiz.Khim.*, 22, 53 (1948).
7. A.C.Riddiford in "Advances in Electrochemistry and Electrochemical Engineering", (P.Delahay and C.W.Tobias Eds.,), Vol. 4, p.47, Wiley Interscience, New York, 1966.
8. R.N.Adams, In: "Electrochemistry of Solid Electrodes", Ch. 4, Marcel Dekker Inc., New York, 1969.
9. Yu.V.Pleskov, V.Yu.Filinovski, In: "The Rotating Disc Electrode", Plenum Press, New York, 1976.
10. S.V.Gorbachev, V. A.Belyaeva, *Zh.Fiz.Khim.*, 35, 2158 (1961).
11. Z.Galus, C.Olson, H.Y.Lee, R.N.Adams, *Anal.Chem.*, 34, 164, (1962).
12. See 7.
13. S.Azim., A.C.Riddiford, *Anal.Chem.*, 34, 1023 (1962).
14. E.Cubb., O.A.Saunders, *Proc.Roy.Soc., (London)*, A236, 343 (1956).
15. See 9.

16. W.J.Albery, M.L.Hitchman, In: "Ring Disc Electrodes", p.17, Oxford University Press, Oxford, 1971.

17. K.B.Prater, R.N.Adams, *Anal.Chem.*, 38, 153 (1966).

18. W.J.Albery, S.Bruckenstein, *T.Faraday Soc.*, 62, 1920, (1966).

19. D.P.Gregory, A.C.Riddiford, *J.Chem.Soc.*, 3756 (1956).

20. See 17.

21. J.Koutecky, V.G.Levich, *Zh.Fiz.Khim.*, 30, 1565, (1956).

22. See 3.

23. R.R.Dogonadze, *Zh.Fiz.Khim.*, 32, 2437 (1958).

24. W.J.Albery, R.P.Bell, *Proc.Chem.Soc.*, 169 (1963).

25. W.Vielstich, D.Jahn, In: "Advances in Polarography", Vol. 1, (I.S.Longmuir Ed.,) p.281 Pergamon Press, New York, 1960.

26. W.Vielstich, D.Jahn, *Z.Electrochem.*, 64, 43 (1960).

27. M. von Stackelberg, W.Vielstich, D.Jahn, *Anales. Real.Soc.Espan.Fiz.Quim., (Madrid)*, B56, 475 (1960).

28. W.J.Albery, *Trans.Faraday Soc.*, 61, 2063 (1965).

29. C.R.Wilke, P.Chang, *A.I.Ch.E.J.*, 1, 264 (1955).

30. P.Chang , C.R.Wilke, *J.Phy.Chem.*, 59, 592 (1935).

31. G.Le Bas: "The molecular volumes of liquid chemical compounds", Longmans, London 1915.

32. D.E.Bidstrup, J.G.Geankoplis, *J.Chem.Eng.Data*, 8, 170 (1963).

33. J.Hegrovsky, *Chem.Listy.*, 16, 256 (1922).

34. D.Ilkovic, *Collect.Czech.Chem.Commun.*, 6, 498 (1934).

35. D.Ilkovic, *J.Chim.Phys.*, 35, 129 (1938).

36. Yu.V.Inanov, V.G.Levich, *Dokl.Akad.Nauk. S.S.S.R.*, 126, 1029 (1956).

37. Y.V. Inanov, V.G.Levich, In: "Some problems of theoretical physics - Atomiz Dat Moscow", 1958.

38. A.N.Frumkin, L.N.Nekrasov, *D kl.Akad.Nauk, S.S.S.R.*, 129, 115, (1959).

39. A.N.Frumkin, L.N.Nekrasov, V.G.Levich, Y.V.Inanov, *J.Electroanal.Chem.*, 1, 84 (1959).

40. W.J.Albery, S.Bruckenstein, *Trans.Faraday Soc.*, 62, 1920 (1966).

41. W.J.Albery, M.L.Hitchman, J.Utstrup, *Trans.Faraday Soc.*, 64, 2831 (1968).

42. See 16.

CHAPTER FOUR

EXPERIMENTAL

In this Chapter the experimental detail for all the work carried out will be described.

4.1 ROTATING DISC EXPERIMENTS

To define the hydrodynamics of the system which is essential if transport controlled reactions are involved, a rotating disc was used, because as described in Chapter 3, the pattern of flow to a rotating disc surface has been solved exactly.

4.1.1 FABRICATION OF THE ROTATING DISC

Five different types of rotating discs were used in the experimentation, and their fabrication will be described below.

4.1.1.1 POWDERED PELLETS

To form powdered pellets powdered Analar calcium carbonate (B.D.H.) was used. The powder was first dried in an oven overnight and then approximately 2g of powder was placed in a 15 mm Beckman Press (K3 pellet press). At first this was simply compressed to a pressure of two tons, using an Aprex Hydraulic press, for five minutes, but it was subsequently found that a harder pellet was formed if the Beckman Pellet Press was evacuated before the compressing, and this was the procedure subsequently adopted. Pellets thus formed were approximately 15 mm in diameter and 0.3 cm thick, and were stored in a vacuum

desiccator until use.

Smaller powdered pellets were formed using a smaller pellet press and to this end a Beckman K5 adaptor (Fife, Scotland) was purchased. This was a conversion kit and changed the pellet size from 7.5 to 2.5 mm radius, the adaptor fitting inside the old pellet press. The pellet press was evacuated and compressed to a pressure of two tons for five minutes, before the pellets were removed and stored in a vacuum desiccator. To form rotating discs, the pellets were placed in the base of a mould (Figure 4.1), the top was screwed on and a cast was made of a cylinder of araldite epoxy resin (Resin MY 753 with hardener HY 951, from Ciba-Geigy, Cambridge, England). One part of the hardener was mixed with ten parts of the resin and after mixing well, the araldite was poured into the mould and was left to set overnight. The mould was made of stainless steel and was built in the departmental mechanical workshop, the dimensions being 18 mm internal diameter, 38 mm external diameter, and 40 mm in height. To prevent the liquid araldite from sticking (when hardened) to the inside of the mould, this was coated with a thick layer of Teflon spray (Fluolion spray-dry lubricant from Walker Brothers Limited, Liverpool, England). When set the araldite plug was removed from the mould. The all araldite end was then carefully ground down to flatness, ensuring that the pellets were not placed at an angle to the horizontal, and this was then glued onto a home-built stainless steel rotating

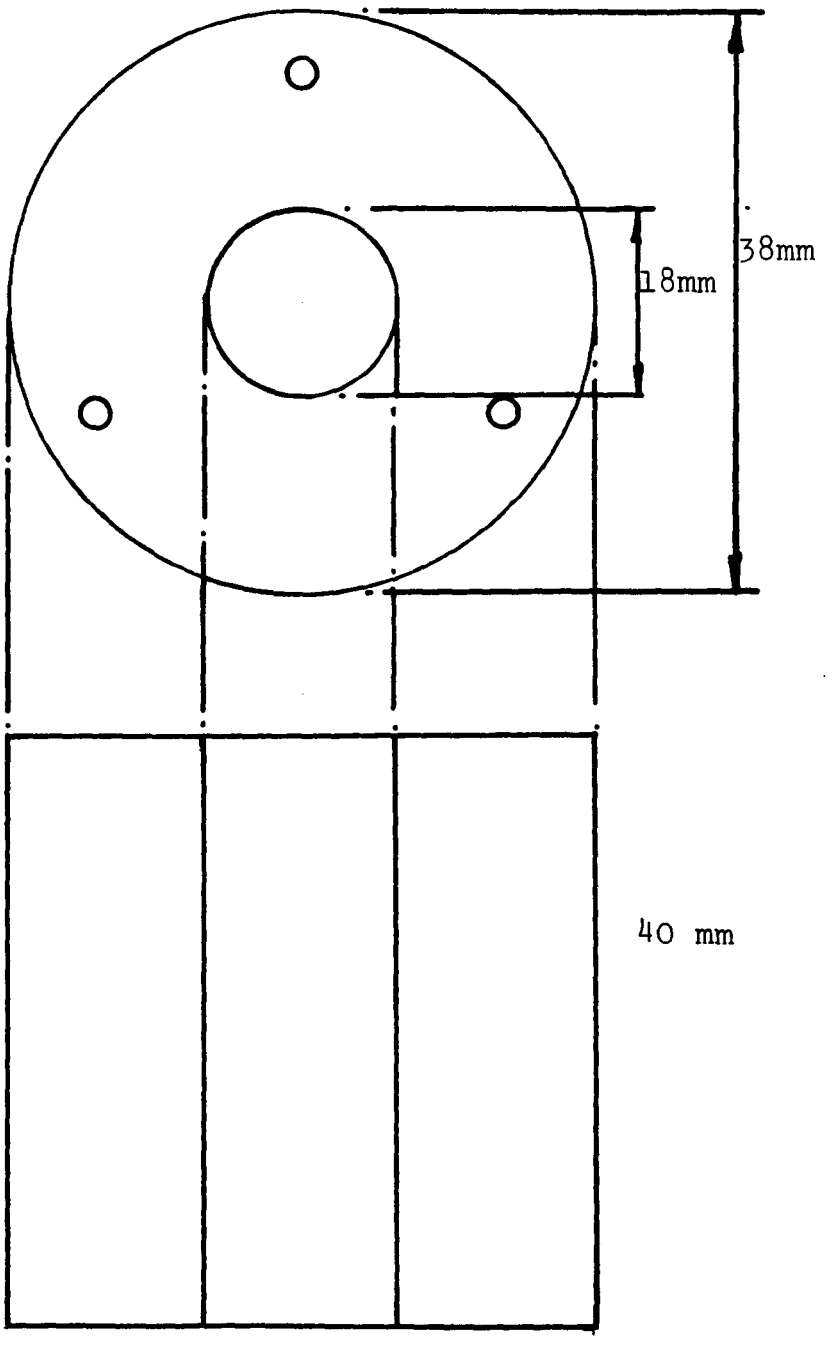

FIGURE 4.1 The Casting Mould.

shaft of dimensions 8 cm x 2.54 cm^2. This consitituted the calcite rotating disc, but before it could be used experimentally, it was necessary to grind down the calcite surface to flatness. This was achieved using a succession of 180, 320 and 600 (corresponding to a roughness of 60, 45 and 30 micron respectively) Brammet Pads (Engis, Maidstone, Kent). Final polishing required the use of diamond sprays (Hyprez Diamond Lapping Compounds, Engis) to produce a smooth flowless finish. The crystal was polished using a series of finer diamond sprays, 25, 8, 6, 3, 1, $^1/_4$ micron for 20 min. each, lubricating the polishing surface with Hyprez lubricating spray (Engis) when required. Before changing from one spray to another the calcite surface was carefully washed to remove any remaining diamond grit of the previous size.

4.1.1.2 SINGLE CRYSTAL ICELAND SPAR ROTATING DISCS

Rotating discs were also formed using single crystals of calcite. Iceland spar was the form of calcite chosen because of its easy availability, its unflawed crystals, and its ease of cleaving. The crystals (supplied by Richard Taylor Minerals, Cobham, Surrey) were from Chihuahua, Mexico. They were cleaved to the appropriate size, approximately 1 cm^3 ~~cubed~~, and were cast in araldite and ground down to $^1/_4$ micron smoothness, as for the pellets. Since each face exposed is the (100) plane[1] it was of no importance how the faces were orientated.

The finished surface was then finally washed with distilled water to remove any remaining lapping compound, and the surface was allowed to dry. Once dry the surface of the rotating disc was painted using a solution of polystyrene in carbon-tetrachloride (0.5g in 20 cm^3), so that only a small circular area of the crystal typically (0.657 cm^2) was left exposed, the rest being covered with a thin layer of polymer. In the dissolution solutions used this layer proved to be chemically inactive, and providing care was taken not to physically tear the layer and thus expose a new calcite surface underneath, the layer lasted as long as the crystal was used before repolishing.

4.1.1.3 ANGLED SINGLE CRYSTAL ROTATING DISCS

Iceland spar rotating discs were also fabricated with the crystal faces set at an angle to the horizontal before casting. The apparatus shown in Figure 4.2 was used for this purpose. Angled mounts were built in the workshop from Teflon, and were cast to 5, 10, 20° ± 10%; the mounts having the same cross-sectional area as the stainless steel mould. These moulds were placed in the holder and the brass cross-piece adjusted so that when the iceland spar crystal was snug against the 'V', then the C_3 axis of the crystal was held at a constant angle with respect to the horizontal. The crystal was cleaved to size (approximately 1 cm^3) and was glued to the mount in its predetermined position. When set the mount was removed from the gig and was placed in the casting mould, where it was cast into a disc. This, when set, was taken

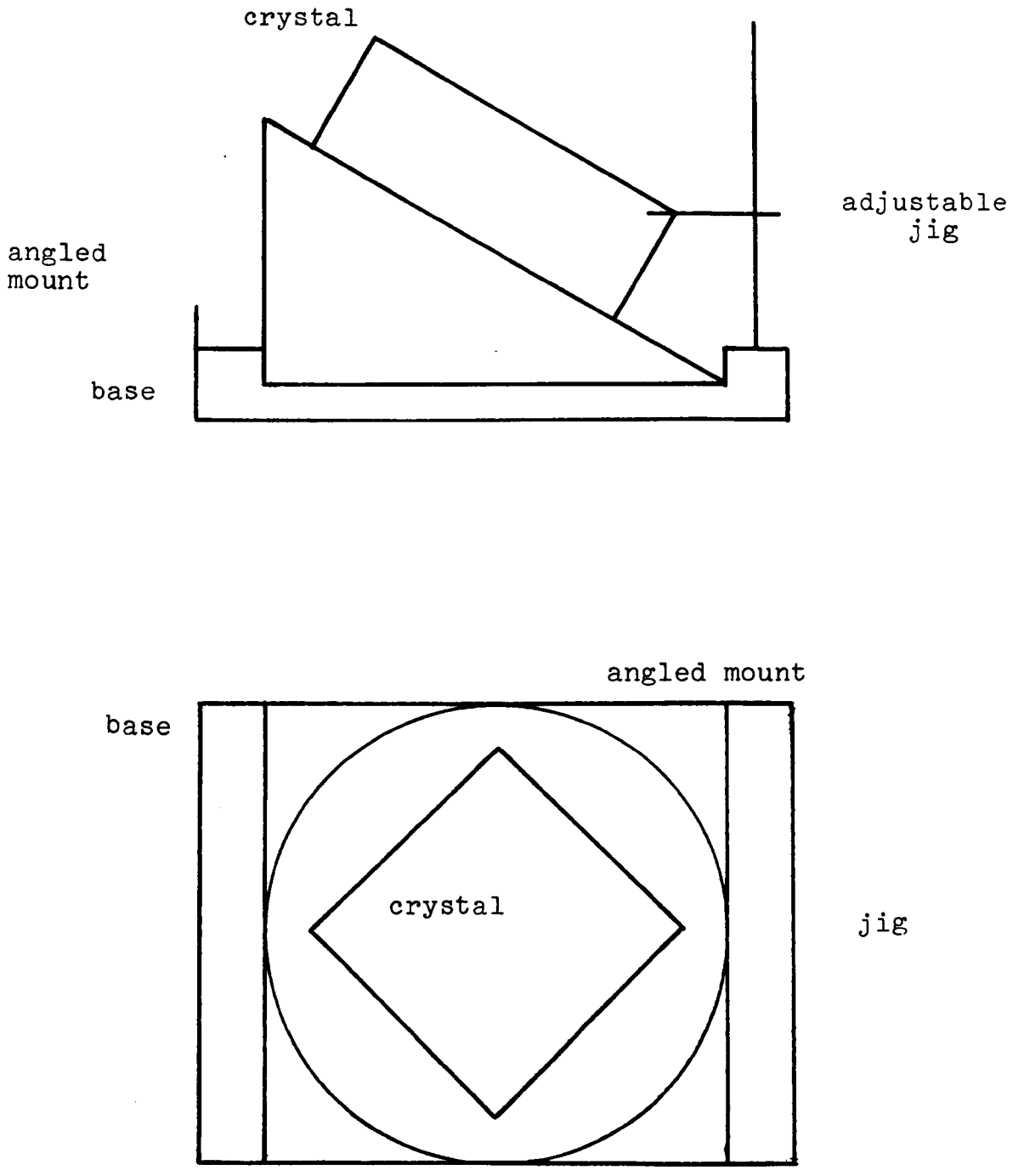

FIGURE 4.2 Apparatus used for casting angled crystals.

out and polished as before, the only difference being that preliminary grinding (to level off the angle to approximate flatness) was achieved using 150 Brammet Pads (100 micron).

4.1.1.4 CLEAVED BUT UNPOLISHED ROTATING DISCS

Rotating discs were also fabricated from unpolished cleaved Iceland Spar. To produce these the apparatus shown in Figure 4.3 was used. A mould of heat shrink, of diameter equal to that of the stainless steel mould, was formed using a cylinder of Teflon of similar diameter. This was covered with vacuum grease and the heat shrink moulded to it. The Teflon cylinder was then removed. A single crystal of Iceland Spar was glued onto the base and liquid araldite carefully added until the top surface of the crystal was just lapped by the araldite. This was then allowed to set. Once set the outer casing of heat shrink was cut away, leaving the araldite plug which was glued onto the stainless steel shaft and all the surface apart from a circular central area, was painted out.

4.1.1.5 CHALK ROTATING DISCS

The chalk samples used were collected fron an outcrop at Lulworth Cove, Dorset. Two kinds of chalk discs were made and used. The first kind, as with the unpolished, cleaved Iceland Spar, was fabricated using a heat shrink mould. The second kind was made as for the polished Iceland Spar, in that the chalk was cut into the approximate size, placed in the stainless steel mould,

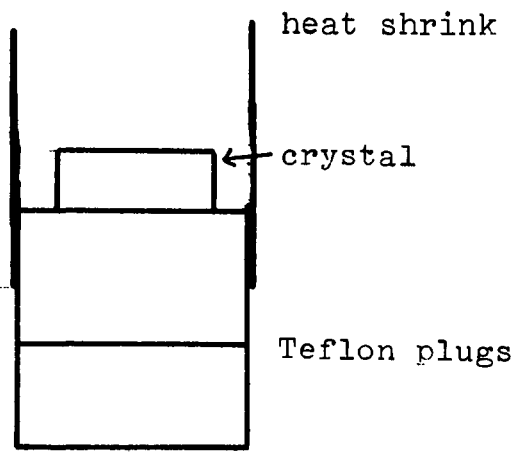

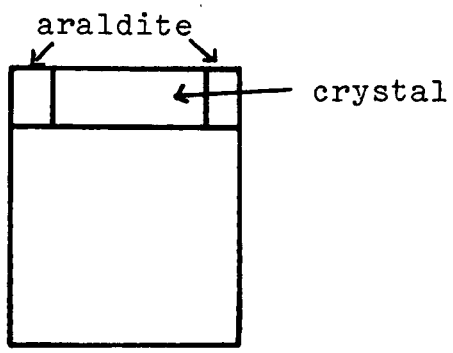

FIGURE 4 3 The apparatus used for casting cleaved Iceland Spar crystals.

and a rotating disc made by pouring in liquid araldite. This was polished as previously, but this time the finest polishing pad used was the 600 Brammet Pad.

4.1.2 THE ROTATING DISC ASSEMBLY AND APPARATUS

The rotation of the calcium rotating disc was controlled using an Oxford Electrode (Oxford, England) Rotating Disc Assembly and Proportional feedback Rotation Speed Controller, with digital display, with a range of 0 - 50 Hz.

All experimental work was carried out in a glass reaction vessel of approximately 150 cc capacity, blown by the departmental glass blower. This vessel (Figure 4.4) had a water jacket built into it for thermostatic control, the water being kept at a temperature of 25 $\pm$ 0.2°C by a Grant SU6 thermostat control (Grant Instruments Limited, Cambridge, England). A gas inlet was built into the vessel to allow a stream of gas to be bubbled into the reaction vessel, the gas being a mix of white spot nitrogen and carbon dioxide (both from British Oxygen) of selected composition. The gases were taken from their gas cylinders, and the flow rates were roughly controlled using needle valves. The gases flowed into 'Flostats' (G.A.Platton, Basingstoke, Hantshire) where the flow rates were accurately adjusted and controlled. The flowstats consisted of a gap meter and a flow meter joined together using a double bango connector. The CO_2 gap meter (M/N BSF) was connected to a 100 - 250 $cm^3\ min^{-1}$ flow meter, and the nitrogen gap meter (M/N BC) was

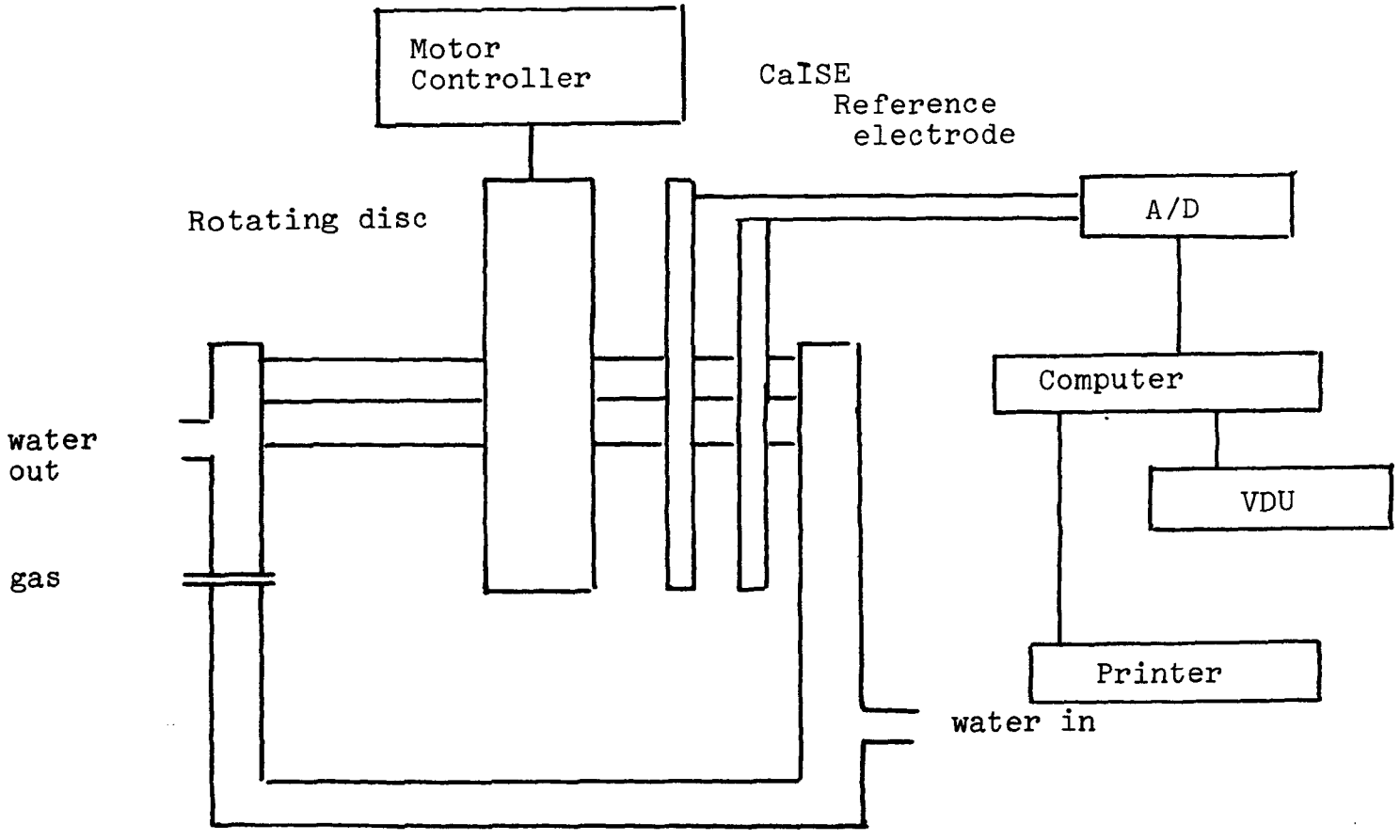

FIGURE 4.4 Experimental set-up for the use of rotating discs.

connected to a 500 - 5000 $cm^3 min^{-1}$ flow meter. Using these flow meters it was possible to cover a large range of partial pressures of carbon dioxide. The two flow lines were then joined and the mixture bubbled into the reaction vessel. With mixed gas streams it was necessary to construct a bleed into the flow line to reduce the pressure of gas glowing into the reaction mixture, and thus reduce the turbulence.

4.1.3 THE DETECTION OF CALCIUM

In this section the various methods used to detect calcium and their mode of operation will be given.

4.1.3.1 FLUORIMETRIC

This method involved the removal of reaction solution at known time intervals and the addition of these samples to calcein (disodiumfluorescein iminodiacetate) to which the calcium chelates, and the fluorescence spectrum of the complex could then be measured and the concentration of calcium found. Before measurements could be taken the fluorimetric spectrometer (Perkin Elmer Fluorimetric Spectrometer 204 , Perkin Elmer) had first to be calibrated. The procedure followed was as described by Vogel.[2]

The calibration was achieved by firstly making up calcium standards in the range 0 - 4 μg of calcium ions per 25 cm^3, by adding sufficient stock calcium solution to a 25 cm^3 volumetric flask, to which 5 cm^3 of 0.4M

potassium hydroxide had already been added, and making up to the mark with doubly distilled water. (Details for the preparation of these solutions are given in Section 4.1.5.2.)

The fluorescence of the calcium standards was then determined at 540 nm with excitation at 330 nm, and a calibration curve was produced. The samples withdrawn from the reaction solution were diluted down to the same concentration range as the calibration curve, and they were then prepared as above, before having their fluorescence measured.

It was found that because of background Ca^{2+} present either in the KOH (BDH analar 0.001% impurity), the distilled water, or in the calcein, it was impossible to achieve full scale reading on the spectrometer, and the scale which could be used was of insufficient accuracy to be of quantitative use. Other workers who have used this method to detect calcium, have experienced similar problems.[3]

Considering these problems, associated with determining calcium concentrating using fluorimetry, the low sensitivity, the need for pre-titration, the fact that reaction solution was consumed, and because of the extra time needed to find the concentration of calcium, it was decided not to use this method for the determination of calcium.

4.1.3.2 CALCIUM ION-SELECTIVE ELECTRODE

Calcium ion-selective electrodes, as discussed in Chapter 2, were chosen for their quick response time, ease of operation, the fact that the calcium concentration could be found instantaneously, and because they consumed no reaction solution. Two different types of calcium ion-selective electrodes (Ca.I.S.E.) were used, the Radiometer (F2112) calcium ion-selective electrode (V.A. Howe England) and the Action (310) calcium ion selective electrode (Spectronic Services, Garforth, Leeds). The reason for the change being primarily price - the Action being approximately half the price of the Radiometer. It, however, suffered from being far bulkier and thus less easy to use, and it also had a far lower tolerance to impurities such as copper ions present in solution.

To activate both electrodes the membrane was filled with the supplied internal filling solution and the membrane was screwed onto the main portion of the electrode. For the Action there was then the simple matter of soaking the electrode in approximately 10^{-2} $mol.dm^{-3}$ calcium chloride solution, in order to achieve the Nernstian calibration slope of approximately 28 mV/ decade. However, the radiometer had first to be soaked in concentrated ammonia solution, in order to have the correct slope. To calibrate the electrodes the response in mV was measured when the electrodes were inserted into varying calcium solutions of differing strengths, with respect ot a standard saturated calomel

electrode ($E^{\ominus}$ = + 0.2415V). In all quoted potential values the values are quoted with respect to this standard calomel electrode. The preparation of the stock calcium solutions and all other solutions used is given in Section 4.1.5. The figures given in Table 4.1 are for a typical calibration experiment (at 25 ± 0.2°C), and the graph Figure 4.5 is typical calibration curve giving rise to a calibration slope of -27.9 mV/decade.

TABLE 4.1 Typical calibration slope at 25 ± 0.2°C

$[Ca^{2+}]$ /mol dm^{-3}	log $[Ca^{2+}]$	Potential/mV
9.1274×10^{-3}	-2.040	-23.7
4.781×10^{-3}	-2.320	-19.2
1.9672×10^{-3}	-2.706	- 8.4
9.9401×10^{-4}	-3.003	- 1.7
1.003×10^{-4}	-3.999	28.4
5.017×10^{-5}	-4.300	34.3
1.004×10^{-5}	-4.999	58.7

The response time of a Ca.I.S.E., is the time taken for 95% of the total change to have occurred. To measure this the electrodes, calomel and Ca.I.S.E., were rapidly transferred from solutions of differing calcium concentrations, making sure that the electrodes were carefully cleaned and dried, using distilled water, and cotton wool, before insertion, to prevent any contamination of solution, and recording the response on a Y, T recorder.

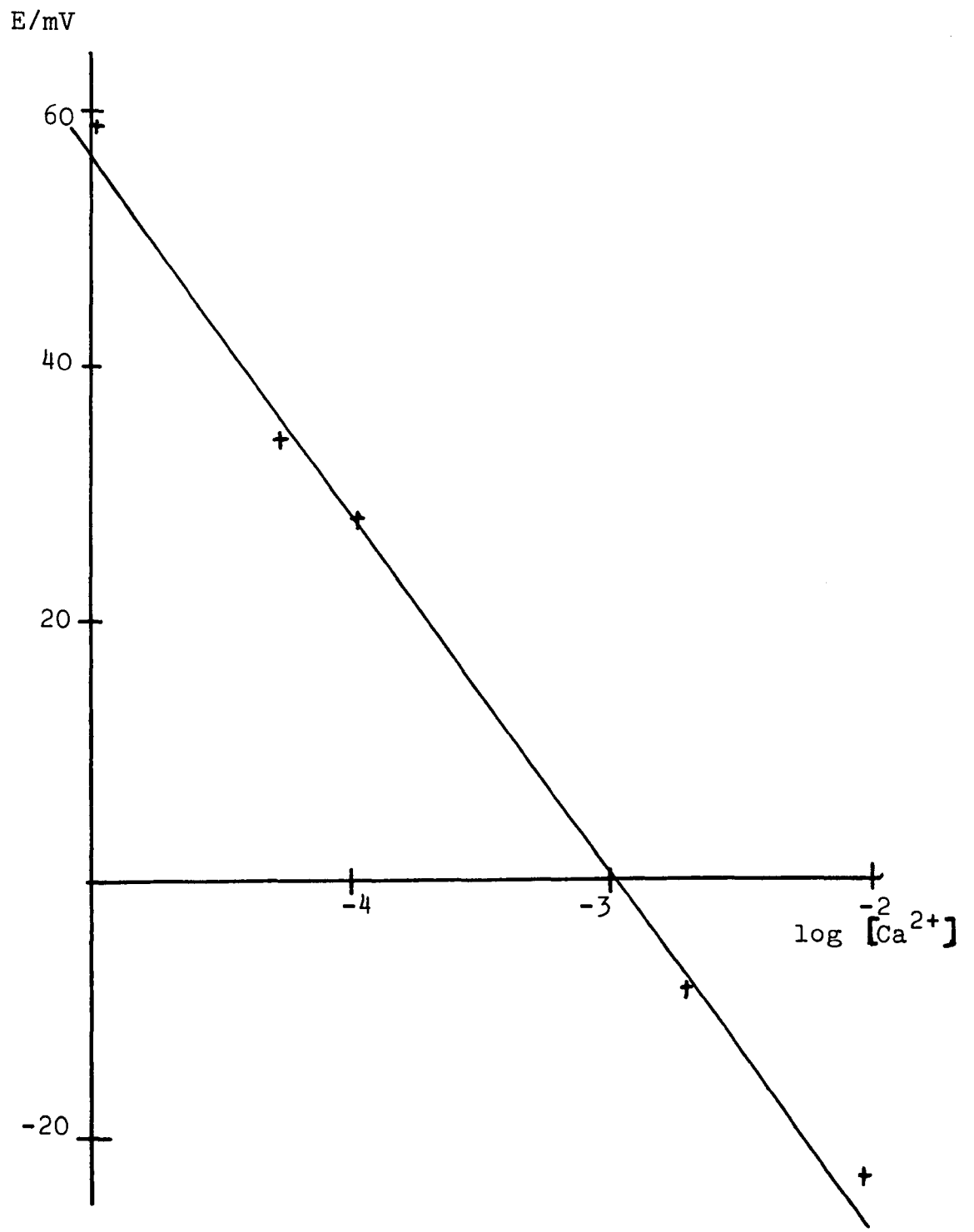

FIGURE 4.5 Typical calibration curve for Ca.I.S.E.

To eliminate systematic error these 'dunking' experiments were performed in a random order.

The resulting transcients (Figure 4.6) show a typical result (recorded on a Servoscribe 1s YT recorder) and were analysed using the equation:[4,5]

$$E_t = E_f + (E_i - E_f) \exp\left(\frac{-t}{\tau}\right)$$

E_f = final mV reading
E_i = initial mV reading
E_t = mV reading at time t
t = time/seconds
τ = response time/seconds.

By plotting graphs of $\log\left(\frac{E_t - E_f}{E_i - E_f}\right)$ versus t then the response time could be found. It was found that the response time was far quicker when going from low concentrations to high concentrations by a factor of approximately two for the same concentrations (see Section 2.3). For the change from 10^{-5} mol dm^{-3} Ca^{2+} to 10^{-4} mol dm^{-3} Ca^{2+}, the range of typical experiments, then the response time was found to be 3.3 seconds (Figure 4.7).

4.1.4 EXPERIMENTAL PROCEDURE

In this section the experimental procedure for the measurement of the dissolution of calcite, and the computer control of the experiment will be given.

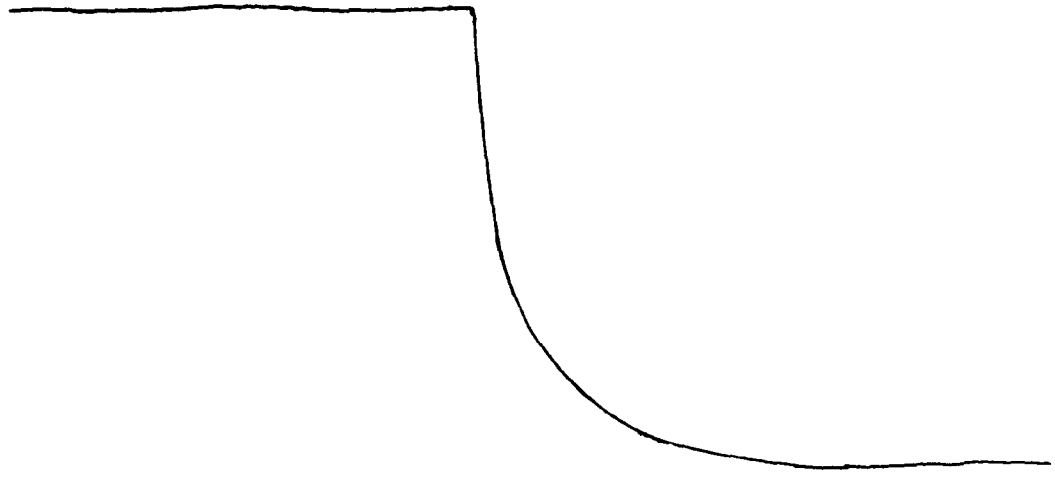

FIGURE 4.6 Transient resulting from a concentration change of 10^{-4} to 10^{-5} mol.dm^{-3} Ca^{2+}

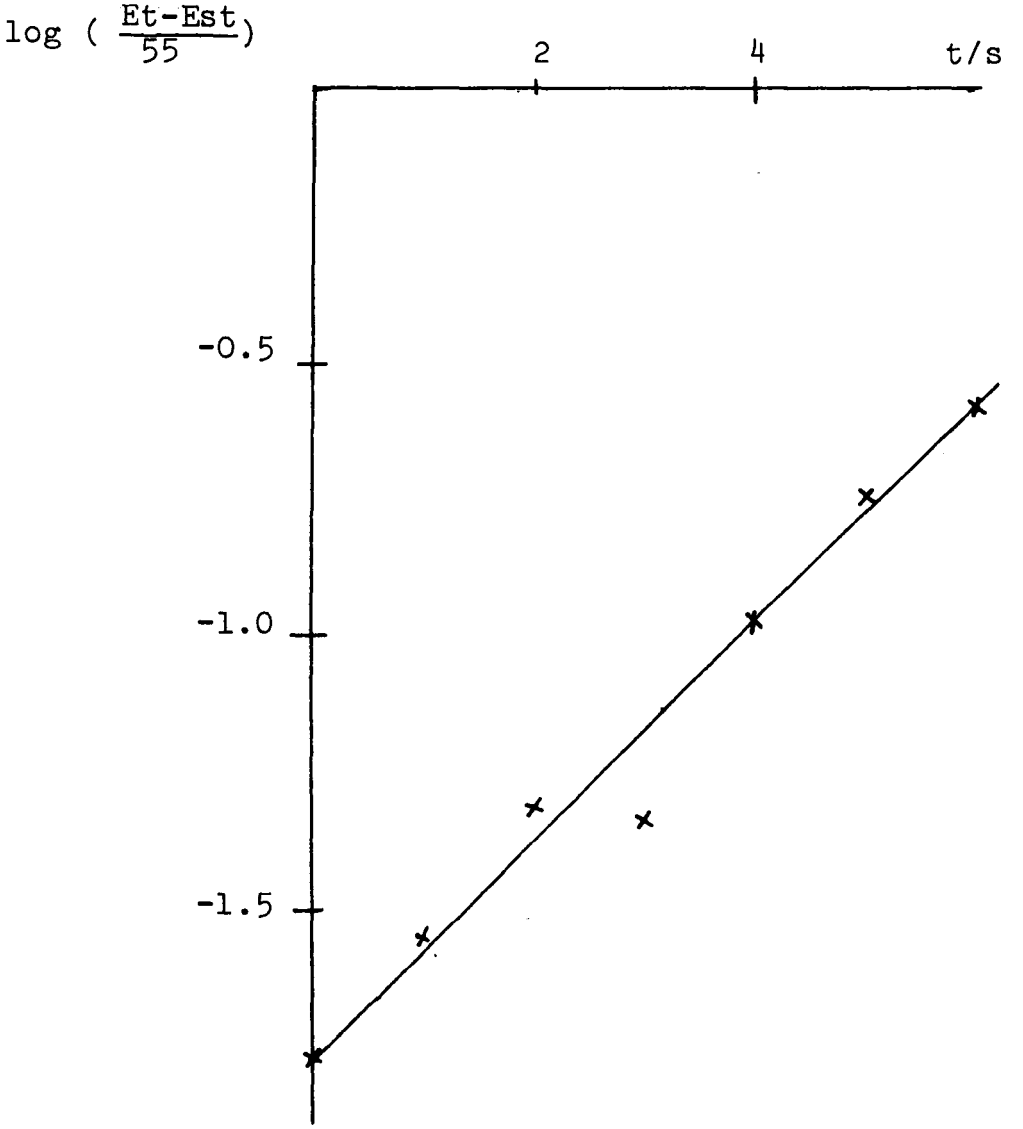

FIGURE 4.7 Calibration of I.S.E.'s response time.

To begin experimentation the Ca.I.S.E. was calibrated, and after the slope was found it was entered into the 'PADDYSCAN2' programme. 100 cm^3 Of the reaction solution, made up to be 1 x 10^{-5} mol dm^{-3} in calcium, was added into the thermostated reaction vessel. This background calcium was necessary to have a starting point for the Ca.I.S.E., and was also used as a reference concentration. The perspex lid was then placed on top of the vessel, and the desired gas mixture was chosen and the gas allowed to bubble through the solution for approximately 10 min., to equilibrate. The two electrodes, calomel and Ca.I.S.E. were then inserted into the lid and they were connected up to the Radiometer pH meter. An inert titanium rotating disc electrode was then placed in solution and rotated at the chosen rotation speed, to establish the stirring conditions for the experiment. This was important as the Ca.I.S.E. reading is highly dependent on the stirring patterns. This was then left to come to thermal equilibrium, as indicated by a steady mV reading ($\pm$ 0.1 mV).

Once this had been achieved the titanium disc was replaced by the single crystal calcite rotating disc, which had previously been carefully washed and dried. The intercept (as indicated by the m.V. reading was entered into the Apple as were the time delay and the number of points. The programme then ran to completion, the potential was measured at set time intervals, the graph was displayed and the data was stored, from which the dissolution rate was later found.

4.1.4.1 PRELIMINARY WORK

Initially the dissolution was followed by recording the output from the Ca.I.S.E. on the Servoscribe, YT recorder, via a Radiometer PHM 64 Research pH meter (V.A.Howe). This trace was then converted manually into millivolts and this data typed into the computer programme 'PADDY CORRECT'. This turned the mV readings into concentrations of calcium using a calibration subroutine of which the parameter had already been entered. This method proved extremely laborious and prone to error and uncertainty, both in the conversion into mV and in the entering of data via the keyboard.

4.1.4.2 THE COMPUTER LINK-UP

To improve the speed, ease of use, and accuracy of operation it was decided to interface the experiment to an Apple II micro-computer. This being done via an Analab interface card (Hayden Data Systems, London, England) which possessed a twelve bit A/D converter capable of taking up to twenty readings per second.

The A/D was calibrated by sending a known voltage, (supplied by a D.C. potentiometer, Time Electronics Limited, Tonbridge, Kent), through the A/D into the Apple, and noting the binary number which this corresponded to (the binary number appearing on the V.D.U.). The supplied voltage was altered and the binary number changed, the change was noted and the calibration curve (Table 4.2, Figure 4.8) was drawn up, the slope being

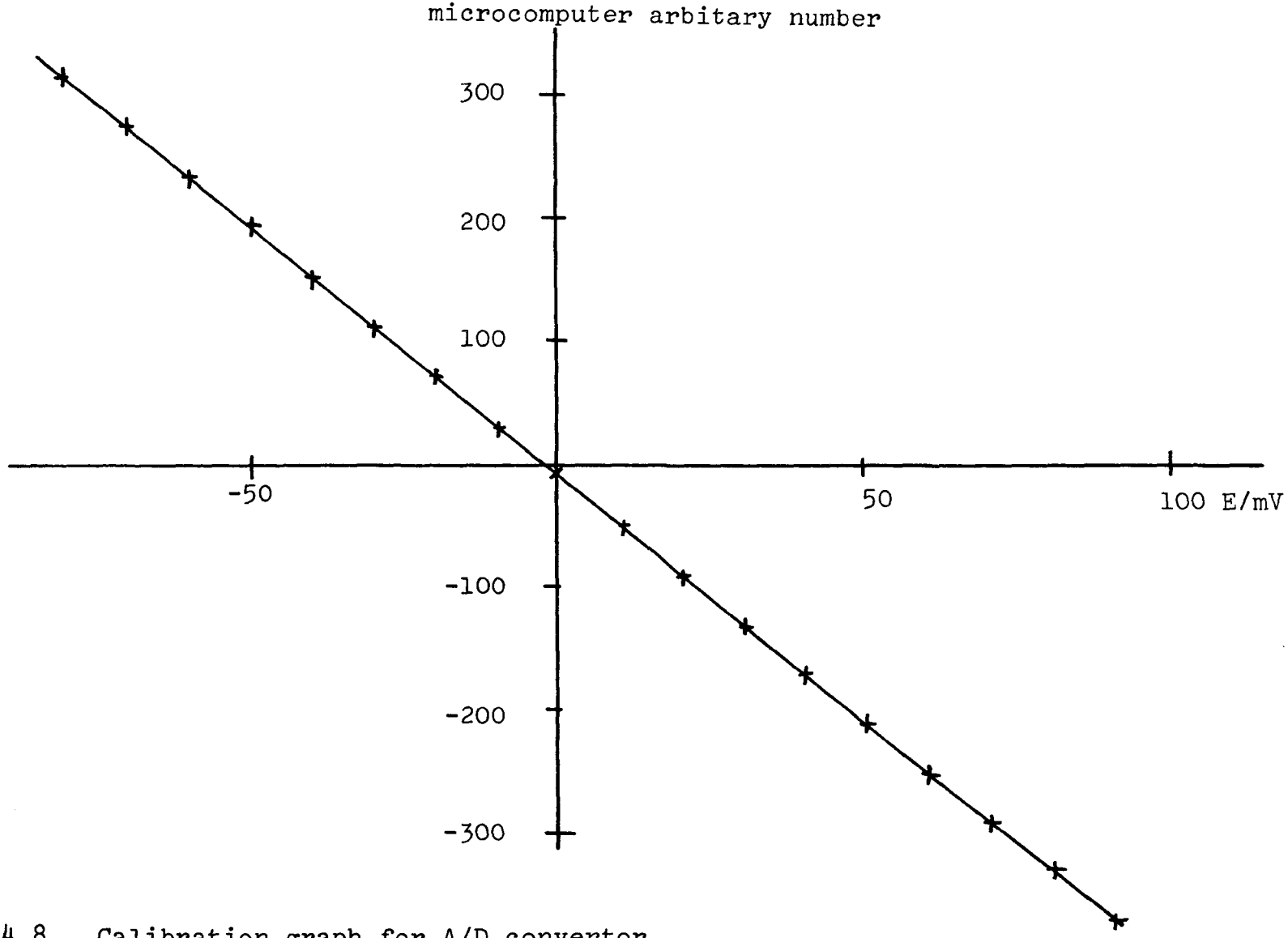

FIGURE 4.8 Calibration graph for A/D convertor

TABLE 4.2 Calibration of A/D convertor

mV	APPLE READING
90	-376
80	-336
70	-295
60	-255
50	-214
40	-174
30	-133
20	-92
10	-52
0	-11
-10	30
-20	71
-30	111
-40	152
-50	192
-60	233
-70	273
-80	314
-90	354

found using a least square fit programme. This calibration curve was written into the computer programme 'PADDYSCAN2' which when running displayed any voltage passing through the A/D on the screen of the V.D.U. as m.V.'s. All computer software programmes were written in Apple soft Basic.

Heyden Data Systems also supplied the 'Quick I/O' software programme, which was used to control the collection of data in 'PADDYSCAN2'. When running,this programme first asked for the calibration slope of the Ca.I.S.E., (Sl) the millivolt reading that appeared on the V.D.U. (It), the number of points to be collected (No), and the time interval between the points (DY). Once this data had been entered the potential of the system (in millivolts) was recorded at the set time interval until the total number of data points had been collected. A graph was then drawn up of calcium concentration versus time, the millivolt readings having been converted to concentrations via a sub-routine. The programme then presented the option of either abandoning the collected data or storing it in a data file on floppy discs. Further software programmes were written which allowed the editing of the collected data. To analyse the data the 'CURFIT' programme written by Paul K. Warme (Interactive Microware) was used. This took in the data file, either as time and concentration data points, or else as concentration values at set time intervals, plotted out the data as concentration versus time, and then allowed the dissolution rate to be found at any point on the curve. The graph and equation of any straight line drawn, could be printed out on a Silent Type Printer. Listings of all programmes used are given in the Appendix.

Using the interface it was possible to carry out work which would have been impossible if the chart recorder method had been used, it also allowed far more experimental work to be carried out because of the great saving of time involved in the analysis of each experiment.

4.1.5 CHEMICALS USED IN THE PREPARATION OF SOLUTIONS AND THE DISSOLUTION EXPERIMENTS CARRIED OUT.

This section is concerned with the preparation of the solutions used for experimentation, and the use to which these solutions were put.

4.1.5.1 PREPARATION OF THE STOCK CALCIUM SOLUTION

In all the experimental preparations discussed, unless otherwise stated, all chemicals used are Analar grade from B.D.H. (Poole, Dorset) and the water used to prepare the solutions is 'Nanopure' water supplied by the University of Liverpool's Oceanography Department. This water is doubly distilled and is then deionised to give a resistivity of more than 10^7 ohm cm.

To make up the stock calcium solution approximately 2.5g of calcium carbonate was dissolved in as little concentration hydrochloric acid as possible (in a 250 cc volumetric flask) and this solution was made up to the mark with water. This stock standard solution, of approximately 0.1 mol dm^{-3}, was then diluted down to the required strengths for the calibration of the Ca.I.S.E.

The required range was from 1 x 10^{-5} to 1 x 10^{-2} mol dm^{-3}, and when these calibrating solutions were made up sufficient potassium chloride was added to make up the ionic strength to 0.3 mol dm^{-3}. This was the ionic strength used for all measurements with the Ca.I.S.E.

4.1.5.2 PREPARATION OF SOLUTIONS USED IN THE FLUOROMETRIC DETERMINATION OF CALCIUM

The stock calcium solution was made up as described in Section 4.1.5.1. The 0.4 mol dm^{-3} potassium hydroxide solution was prepared by disolving 22.464g of KOH in a one litre flask, and making up to the mark with distilled water. The calcein solution was prepared by dissolving approximately 0.060g of calcein in as little of the 0.4 mol dm^{-3} KOH as possible in a 1 dm^3 volumetric flask, and then making this up to the mark using distilled water.

4.1.5.3 DISSOLUTION REACTION AT pH 3.0

Initial experiments were carried out using 10^{-3} mol dm^{-3} hydrochloric acid, which was made up by diluting down concentrated HCl. The concentration was checked against weighed amounts of sodium carbonate. The diluted HCl was made up in batches of one litre and 22.365g of potassium chloride was added to increase the ionic strength to approximately 0.3 mol dm^{-3}. The pH of this solution was checked using the Radiometer PHM 64 pH meter and a Radiometer combination pH electrode, the electrode being previously calibrated using buffer solutions.

Using the 0.3 mol dm^{-3} HCl as the reaction solution a series of experiments were carried out at various rotation speeds, with a steady stream of pure nitrogen being passed into the solution at all times.

4.1.5.4 DISSOLUTION EXPERIMENTS IN THE pH RANGE 4.05 - 5.42

The dissolution rate of calcite was then measured in the pH range 4.05 - 5.42, using Walpole's acetic acid sodium acetate buffer system.[6] Preliminary work was done at pH 4.05, requiring 200 ml of 0.2 mol dm^{-3} sodium acetate to be added to 800 ml of 0.2 mol dm^{-3} acetic acid (making one litre of buffer solution). The sodium acetate was made up in batches of one litre (as was the acetic acid) by dissolving 27.76g sodium acetate in one litre of water. The acetic acid was made up by diluting 11.6 ml of glacial acetic acid up to the mark in a one litre volumetric flask. The two solutions were then mixed in the correct proportions and 19.35g of potassium chloride was added to keep the ionic strength of the solution at 0.3 mol dm^{-3}. The pH of the solution was checked using the Radiometer pH meter and combination pH electrode which had previously been calibrated with B.D.H. standard pH solutions at pH 4 and pH 7. As previously the dissolution rate was measured as a function of rotation speed, with a steady stream of pure nitrogen being passed into the solution.

To study the dissolution rate at higher pH's the

concentration of acetic acid was changed, while that of the sodium acetate was kept constant, the two solutions then being mixed in the same proportions. Table 4.3 lists the pH values for the various concentrations of acetic acid, the pH again being checked using the calibrated pH electrode. Dissolution rates were again measured as a function of rotation speed with a constant supply of nitrogen being bubbled through.

4.1.5.5 DISSOLUTION USING SØRENSEN'S CITRATE BUFFER

To study the rotation speed dependence of the dissolution at higher pH's it was decided to use Sørensen's citrate buffer.[7] This buffering system being chosen as it contained no phosphate, which would interfere with the

TABLE 4.3 pH as a function of Acetic acid .

[Acetic acid] /mol dm^{-3}	pH
1.6	2.93
0.16	4.05
0.12	4.21
0.08	4.52
0.016	5.21
0.008	5.42

Ca.I.S.E. membrane's performance. The buffer consisted of 570 cc 0.1M disodium hydrogen citrate mixed with 430 cc 0.1M sodium hydroxide. These stock solutions were made up in batches of one litre (in volumetric flasks). The disodium hydrogen citrate was made up by reacting citric acid with sodium hydroxide. 8g Of sodium hydroxide was dissolved in 200 cm^3 of water, in a one litre volumetric flask, 21.0g of citric acid was added, and when dissolved the solution was made up to the mark. The 0.1M NaOH was prepared by dissolving 4g of sodium hydroxide in one litre of water. The two solutions were then mixed in the correct proportions and 6.4142g of potassium chloride was added to make the ionic strength of the solution 0.3 mol dm^{-3}. The pH of this solution was checked using the pH meter calibrated using standard buffer solutions, and was found to be 6.11.

Using this solution the rotation speed dependance of the dissolution was measured for a constant supply of nitrogen being passed through and also with various partial pressures of carbon dioxide bubbling through the solution.

4.1.5.6 DISSOLUTION USING ANGLED CRYSTALS

For this work crystals which had been set at an angle (0°, 5°, 10° and 20°) were ground down to flatness. The rate of dissolution was then measured in 0.3 mol.dm^{-3} potassium chloride solution. For this work there is no rotation speed effect, and all the experiments were carried

out at 10 Hz, with a stream of pure nitrogen being passed through the solution. Before each experiment the crystal had to be reground, but after the initial grinding it was sufficient to begin the polishing using the 6 μ diamond spray, because of the small depth of calcite being dissolved during a typical run.

4.1.5.7 DISSOLUTION IN THE PRESENCE OF COPPER

Experiments were carried out to study what effect the presence of inhibitors would have on the dissolution rate. The inhibitors chosen were scandium and copper. It was found that the scandium could not be used because when introduced into the reaction solution it caused the Ca.I.S.E. to drift continuously and thus it was impossible to measure the dissolution rate. The experiments on copper were carried out in 0.3mol.dm^{-3} potassium chloride. At first the copper (as copper II chloride) was added during the progress of an experiment via a syringe. This, however, proved unsatisfactory as the injection of the copper caused a sudden jump in the potential of the Ca.I.S.E., and therefore the concentration of calcium as displayed on the V.D.U. became false. Experiments were then carried out with the copper already present in the reaction solution before the experiments began, the membrane having been calibrated in the presence of this quantity of copper ions.

The copper solution was approximately 0.1 mol.dm^{-3} copper (II) chloride, and the dissolution rate was measured

with copper in the concentration rate of 10^{-6} to 10^{-3} mol dm^{-3}.

4.2 ELECTRON MICROSCOPY

To check on the smoothness of the polished rotating calcite discs, and to try and characterise the surface after reaction, it was decided to use a Scanning Electron Microscope (S.E.M.) to examine the calcite surface.

4.2.1 INSTRUMENTAL

For the study of the calcite surfaces a Philips 501 Scanning Electron Microscope was used which had a maximum magnification of X 40,000. The camera used to photograph the image was a Nikon using Ilford FP4 black and white, 35 mm film.

4.2.2 METHOD OF USE FOR THE S.E.M.

In this section the preparation of samples for use in the S.E.M. and the use of the S.E.M. will be given.

4.2.2.1 PREPARATION OF SAMPLES

The required samples, either after grinding or after reaction, were carefully washed and dried, and the top 0.5 cm of the rotating discs were carefully laithed off using an electric laith in the workshop. The samples were again carefully washed and dried (to remove any dust from laithing) and were then glued to an aluminium

mount of the S.E.M. Because of the non-conducting nature of the disc surface all the samples had first to be coated with a thin layer of gold, using an Edwards gold splutterer (S150 Edwards Splutterer Coater), to avoid the build-up of charge when the electron beam struck the sample surface.

The gold spluttering was achieved by inserting the samples into the Edwards S150 and then evacuating the chamber. Argon gas (British Oxygen) was briefly passed into the chamber to flusk out any impurities, and after this was turned off and the pressure was reduced to 10^{-1} Torr. With the High Tension switch at 8.5 the samples were spluttered ten times for approximately fifteen seconds a time, at intervals of twenty seconds. The pressure was then released and the samples withdrawn. Finally, to ensure good electrical contact between the surface and the aluminium mount, a strip of silver loaded resin was painted down a side of the sample, connecting the surface to the aluminium mount. The samples were then ready for insertion into the S.E.M.

4.2.2.2 USE OF THE S.E.M.

To use the Philips 501 S.E.M. the chamber was first depressurised, the sample inserted, and the chamber pressurised; once the chamber had reached a pressure of 1×10^{-4} Torr, then the microscope could be used to obtain an image of the crystal's surface. This consisted of:- switching on the High Tension switch;

changing the S.E.D. control from Ø to 1; and saturating the filament so that the sharpest possible image was obtained at the least setting, which involved tilting the sample through approximately 2Ø - 3Ø°, since the surface was so flat. The picture could then be brought into focus using the course, medium, and fine focus controls, and by means of the black and gain controls. Once a suitable image had been obtained on the vidiscreen, then this could be photographed on the oscilloscope. This was achieved by adjusting the black control level to the required contrast and adjusting the gain control so that the signal level on the videoscope's grey scale range was set to just below the centre (Figure 4.9).

This done the 'Scan Mode" was changed from '250 lines' to 'photo' and the 'line time' was changed from 'S.T.V.' to '16 msec' (in order to allow the image to be captured). The completed, the '1X' mode was pressed, the shutter on the camera opened and 'Expose' on the S.E.M. pressed. Once the 'expose' light had extinguished the photograph had been taken and the shutter on the camera was closed, and the film wound on. The settings on the camera were as follows:- exposure time at 'B' (or manual) and the aperture was set at F.2.4.

This S.E.M. also incorporated an E.D.A.X. analyser, which analyses the sample surface by means of Energy Dispersion Analysis (E.D.A.), which analyses the top few amstrons of the surface.

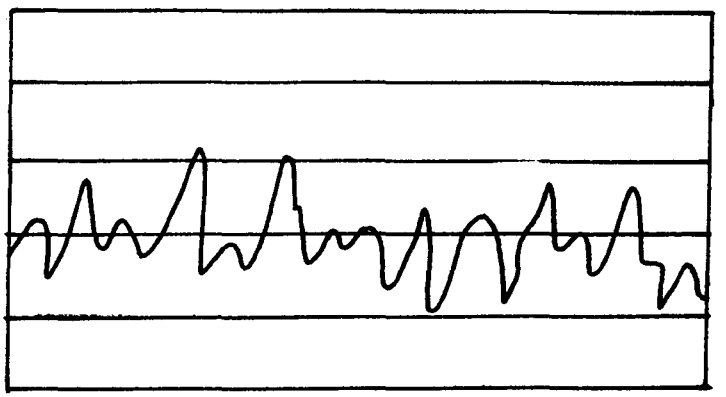

FIGURE 4.9 The setting on the videoscope before photography, i.e., the basic part of the signal is just below the centre of the screen.

4.3 EXPERIMENTS ON POWDERS

Precipitation and dissolution studies on powdered calcite were carried out at the Freshwater Biological Association (F.B.A.) at Wareham, Dorset. Instead of using a Ca.I.S.E. to detect calcium, calcium was determined using an iterative procedure from pH and conductivity measurements. From these measurements, at fixed time intervals, together with a knowledge of the equilibria established in the calcium bicarbonate system, the concentration of calcium could be calculated. To interpret the conductivity data the Onsager and Fuoss equation[8] was used. The computer programmes are listed in the Appendix. The powder used for all experiments was Analar Calcium carbonate (B.D.H.) in its calcite form. The specific surface area was calculated to be 0.22 m^2 g^{-1} using B.E.T. nitrogen absorption analysis, assuming the molecular cross-sectional area to be 0.162 nm^2.

4.3.1 APPARATUS USED FOR EXPERIMENTATION

In this section the apparatus used to measure the dissolution and precipitation rates of powdered calcite, at the F.B.A., will be described in detail.

4.3.1.1 PRECIPITATION WORK

All the glassware used in Dorset was soaked overnight in chromic acid to remove any impurities which could have induced precipitation. The glassware was then carefully washed out approximately six times with distilled water to remove the acid. For precipitation work the experimental

arrangement was as shown in Figure 4.10 and 4.11. The reaction vessel was a five necked cylindrical flask of approximately 500 cm^3 capacity, each neck ending with a screw thread to enable Teflon caps to be fitted, to stop any dust entering which could have lead to precipitation.

Because conductivity is so temperature dependant the thermostat used was stable to 0.002 ^{o}C. The tank was built in the workshops of the F.B.A. and consisted of two totally independant tanks, the outer water bath being maintained at a temperature of 0.2^{o}C below the inner transformer oil bath. For all experiments the temperature of this inner oil bath was kept at 25 $\pm$ 0.002^{o}C. The pH was measured using a radiometer PHM 64 Research pH meter and a radiometer combination pH electrode. The conductivity was measured with a standard platinum-black conductivity cell of cell constant 1.404. The flow of nitrogen (British Oxygen) was controlled by means of needle valves and a flowstat supplyed by G.A. Platton. This entered the reaction solution *via* a glass frit ending in an S3 sinter. This was to ensure a more rapid outgassing of carbon dioxide because of the much smaller bubble size and thus considerably increased surface area.

4.3.1.2 DISSOLUTION WORK

A slightly different experimental arrangement was needed to study the dissolution of powder, and this is shown in Figure 4.12. The reaction vessel used in this

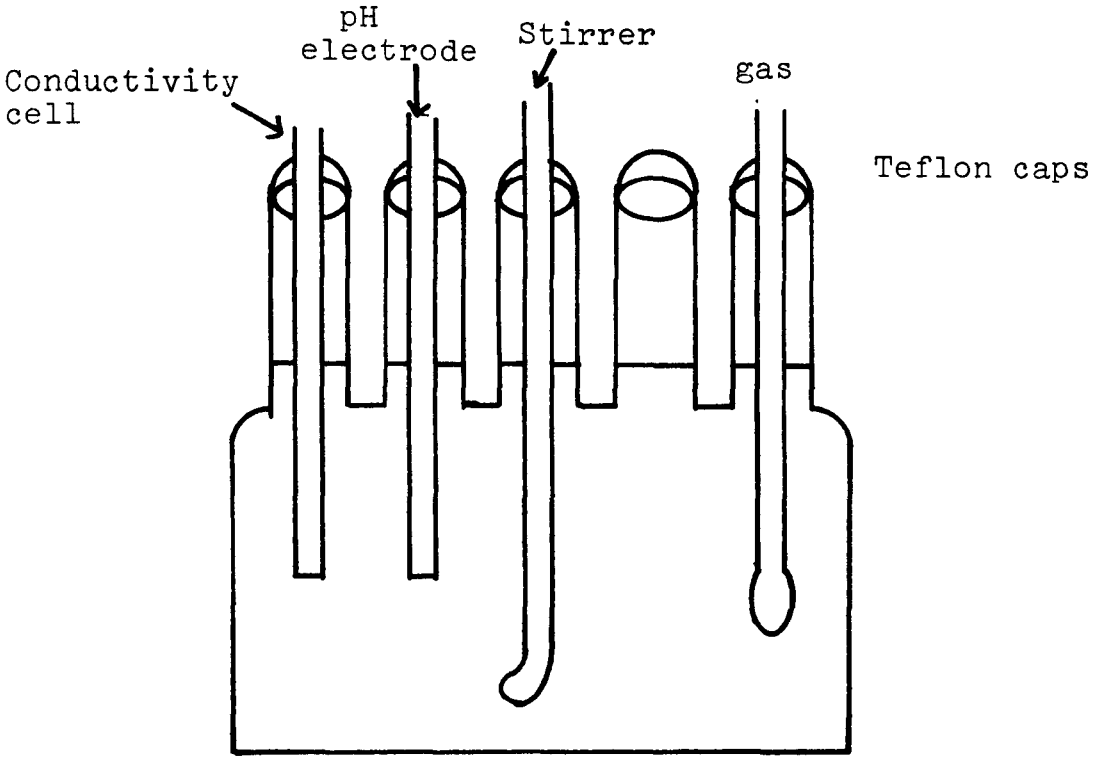

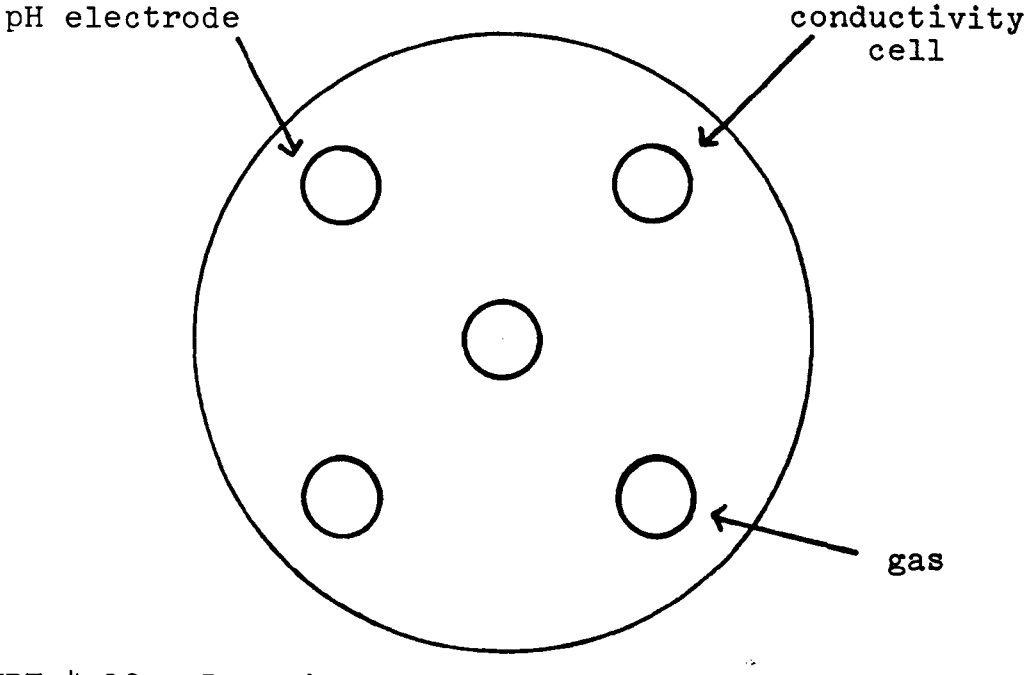

FIGURE 4.10 Reaction vessel used for the precipitation of powders.

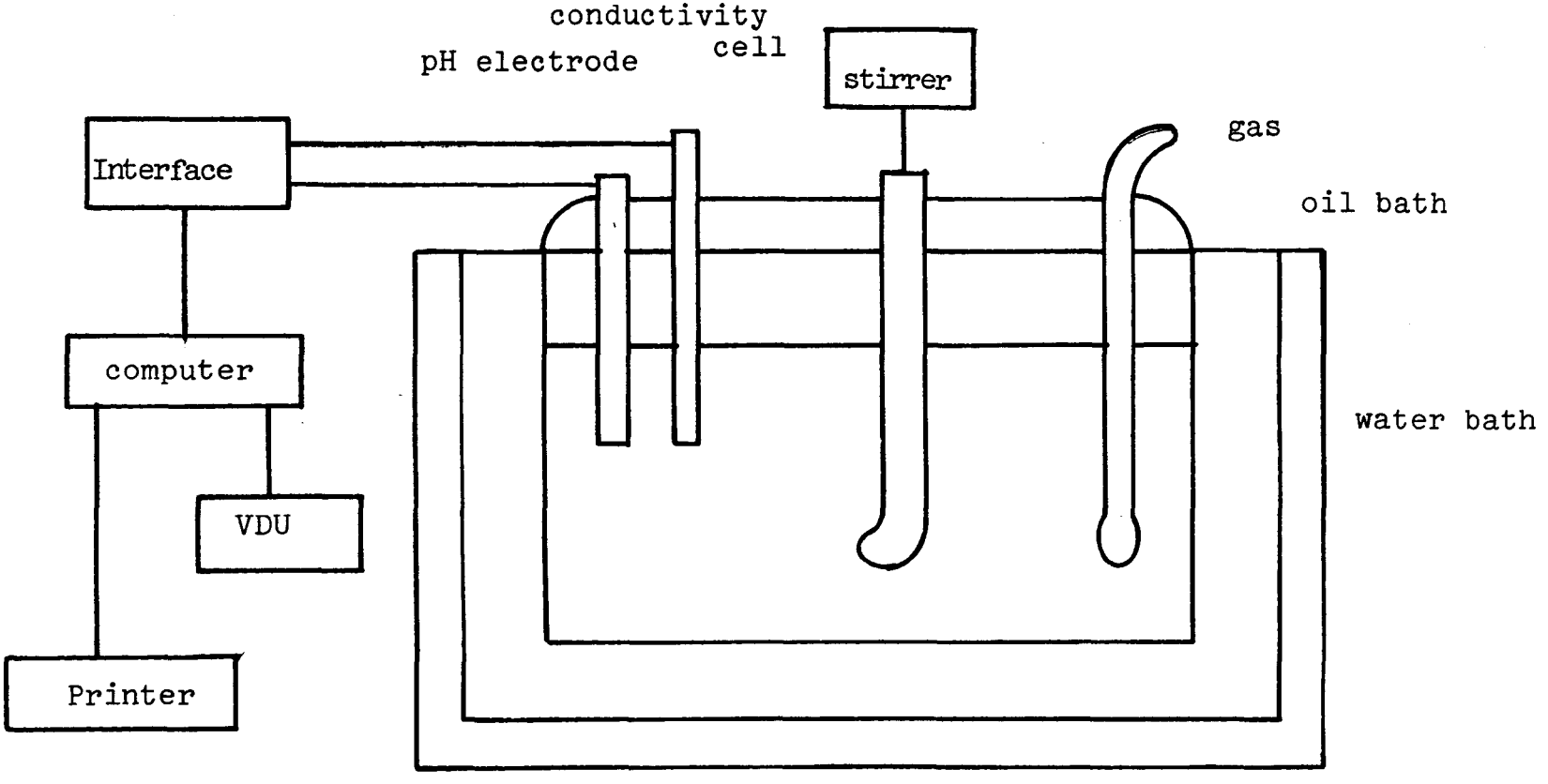

FIGURE 4.11 Experimental set-up as used for studying the precipitation of powders.

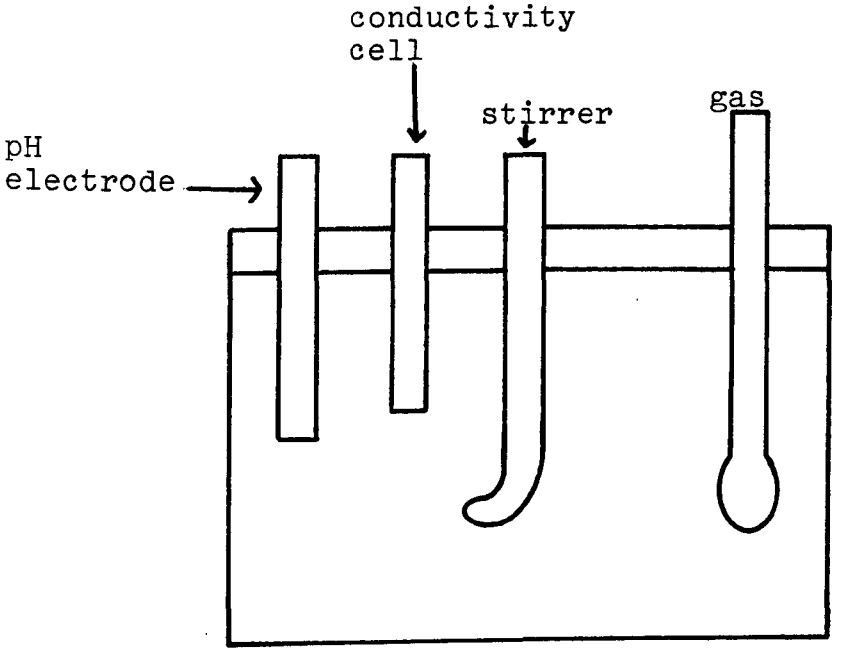

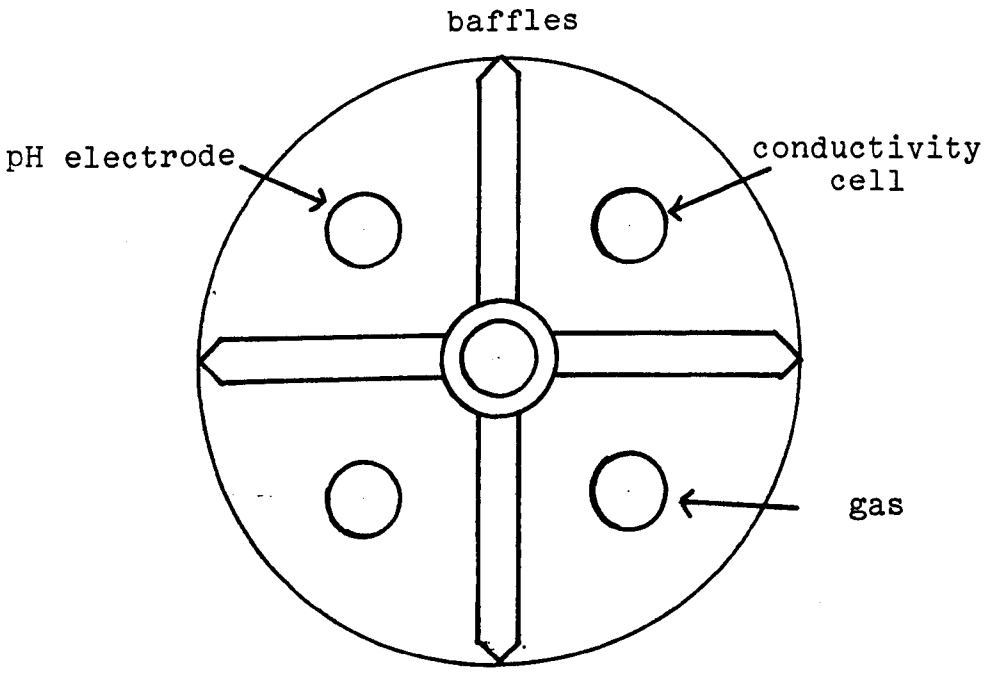

FIGURE 4.12 Apparatus used for studying the dissolution of powders.

case was a one litre polypropylene beaker, covered by a perspex lid with holes cut out for the stirrer, electrodes and gas lines. As this work involved the study of the dissolution at various partial pressures of carbon dioxide a mixed carbon dioxide-nitrogen gas stream was needed, and therefore a gas mixing system was used. The flows of both gases were controlled using needle valves and flow-stats, the two flows were then mixed, passed through water at 25°C, to presaturate the mixture, and then introduced to the reaction solution via an S3 sinter.

4.3.2 SOLUTION PREPARATION

The water used to make up all solutions was triply distilled, made by passing singly distilled water though activated charcoal, to remove any organic impurities, and this was subsequently distilled a further two times. All chemicals used were of Analar Grade (B.D.H.) unless otherwise stated.

The precipitation work used a solution of calcium bicarbonate and a suspension of calcium carbonate in water. The calcite suspension was prepared by taking approximately 6g of the calcite powder and adding this to 100 cm^3 of water. The calcite powder had previously been dried in an oven and was stored in a vacuum desiccator until use. This suspension was used for all experiments. The solution of calcium bicarbonate was made up by dissolving 0.5g of the dried calcite in approximately one litre of water. The calcite was added to the water in a

one litre round bottomed flask, and this was stirred overnight, using a magnetic Teflon stirrer, with a constant supply of carbon dioxide bubbling through the solution. The carbon dioxide (British Oxygen) was passed through at approximately 50 ml min^{-1}, the bleed being kept below water, to eliminate the possibility of dust entering the system, forming sites for the spontaneous heterogeneous nucleation of calcite. During the course of the overnight stirring the white suspension disappeared leaving a clear colourless solution.

This stock solution was approximately 5 mmol dm^{-3}. For experimental work a solution of 350 μ siemen was required corresponding to a total calcium concentration of 2.5 mmol dm^{-3}. This was achieved by diluting the stock solution with distilled water. The stock solution was first divided into two parts, and just under 500 cm^3 of the distilled water was added to both parts, and these solutions were placed in a thermostat for thirty minutes to achieve thermal equilibrium. Final adjustment of the conductivity was achieved using the conductivity cell and a Wayne Kerr B642 A.C. bridge. Thermostated distilled water was added until the desired conductivity was achieved.

To calibrate the pH electrode two buffer solutions were needed. For the precipitation experiments the buffers used were at pH 7.413 and pH 9.186, while for dissolution work pH 7.413 and pH 4.008 were used (all buffers being thermostated at 25°C). The buffer at pH 9.180 was the

borax buffer system made up by dissolving 3.8g of borax in one litre of water at 25°C. [9] The buffer at 7.413 was Sørensen's hydrogen phosphate/bihydrogen phosphate buffer system.[10] This was made up by dissolving 1.179g, potassium bihydrogen phosphate and 4.302g bisodium hydrogen phosphate in one litre of water at 25°C. The buffer used for pH 4.008 was the potassium hydrogen phthalate buffer,[11] made up by dissolving 10.120g of potassium hydrogen phthalate ($C_6H_5CO_2HCO_2K$) in one litre of water at 25°C.

4.3.3 COMPUTER CONTROL OF THE EXPERIMENTS

In all the work done on powders, the instrumental control, timing, data collection and subsequent numerical analysis was performed using an Apple II micro-computer. The interface to the Wayne Kerr B642 bridge, and PHM 64 pH meter was incorporated into a rack system built in the electronic workshops of the F.B.A. This incorporated a relay system which permitted the isolation of the combination electrode from the conductivity cell while readings were being taken, as required, because otherwise they interfered with each other. In this Section all of the computer programmes will be given and their use explained.

All of the software programmes were written in Applesoft BASIC by Dr. W.A.House, although some alterations were needed for the dissolution experiments.

4.3.3.1 COLLECTION OF DATA

The data collection was initated using the programme 'STARTUP'. This began by the calibration of the pH electrode using the appropriate buffers. The pH electrode and the conductivity cell were then entered into the reaction solution, and a stopwatch started, in order to allow for the increase in conductivity due to the leakage of KCl from the combination pH electrode into the solution. One minute before the addition of the calcite suspension the programme 'STARTUP' was terminated by entering the time elapsed since the insertion of the electrodes. This initialised a machine code programme already stored in the memory of the Apple and was protected from the Applesoft interupter and DOS. The design of the instrumental control and data retrieval programmes permitted the Apple to run BASIC programmes at the same time that data was being collected, and they were only interrupted when readings from the instruments were being taken. The interupts were generated by the interface system. The procedure allowed the collected data to be stored in a safe buffer from where it could later be collected.

After this minute a reading was taken of the conductivity and pH values by the Apple and the suspension was added within a further minute. After this time interval further readings of pH and conductivity were taken at set time intervals. The intervals were initially one minute apart, but because of the decreasing reaction rate

the time interval was doubled after the first ten readings, and also after each subsequent ten readings.

Data files could be collected at any time during the course of the reaction, using the programme 'ANALY'. This retrieved the stored data from the safe buffer and transferred it to floppy discs. This created data files containing time, pH, and conductivity.

4.3.3.2 ANALYSIS OF DATA

To analyse the data stored on floppy discs, the computer programmes, 'COMPOST', 'TNCAL', and 'SMOOTH' were used. The pH, conductivity, and time values stored by means of 'ANALY' were used to evaluate the solution composition of the reaction solution, giving the concentration of dissolved calcium in terms of calcium bicarbonate, using the 'COMPOST' programme, which also calculated the growth affinity β. Where:

$$\beta = \sum_i \Delta \mu_i / RT^{12}$$

$\Delta\mu$ = change in chemical potential

$$= \ln \left(a_{Ca^{2+}} a_{CO_3^{2-}}\right) / K_{sp}$$

K_{sp} = solubility product of calcite.

'COMPOST' employed an iterative method which involved a knowledge of the chemical equilibria for the calcium bicarbonate system together with the measured pH and conductivity values to work out the concentrations. The programme iterated on β and calculated the corresponding solution composition and the specific conductance using the Fuoss and Onsager theory. This involved lengthy

calculations and was, therefore, very time consuming, typically taking three minutes for each data point to be analysed. This could, however, be speeded up by compiling the BASIC programme 'COMPOST' into machine code. However, it was not possible to run this compiled programme 'COMPOST.OBJ' at the same time as the machine code data retrieval programe, as both programmes used the same portion of the Apple's 'Highmem' and therefore interfered with each other. The compiled programme speeded up the analysis to approximately one minute per data point.

From the new data files created using either 'COMPOST' or 'COMPOST.OBJ' the number of moles of calcium deposited per unit mass of seed material at each time interval was computed using 'TNCAL'. The precipitation rate was expressed as:

$$\frac{dNCa/dt}{W} \quad \left(\frac{\text{rate of change in the number of moles of calcium per unit time}}{\text{Mass of speed crystal}} \right)$$

Where $dNCa/dt$ = rate of change in the number of moles of calcium per unit time (mmol s^{-1})

W = weight of seed crystal added (g).

Lastly, the experimental precipitation rate data was smoothed using the computer programme 'SMOOTH' enabling the precipitation rates to be evaluated. This used an n point quadratic smoothing function[13] to

produce a smooth curve. n was variable between 5 and 13 and for this work a five point smoothing was employed.

To quantify the effect of copper on the rate of precipitation the FORTRAN programme 'RATECON' was used. This compared the precipitation rate with no copper present to that measured in the presence of copper.

4.3.4 EXPERIMENTAL PROCEDURE

In this section the experimental procedure used in the dissolution and precipitation measurements, and the work carried out to study the effect of the presence of copper on the precipitation rate will be described.

4.3.4.1 PRECIPITATION WORK

It was decided to use the 'free-drift' method rather than the 'pH stat' method to follow the course of the experiment. As described in Section 1.1 this consists of following the reaction and measuring the pH and conductivity as a function of time.

To start experiments 300 ml of the calcium bicarbonate solution was added to the five necked cylindrical flask, and this was placed in the thermostat together with the appropriate buffer solutions to achieve thermal equilibrium. Once this had been reached the programme 'STARTUP' was run. This commenced by asking for the pH of the first buffer solution (9.180) to be used in the calibration of the combination pH electrode. The pH electrode was placed in the first buffer solution, which

was constantly stirred using a magnetic stirrer. Once the valve had stabilised (as indicated by a steady valve on the Radiometer pH meter) the pH value was entered and the computer automatically measured the corresponding voltage value from the pH meter. The programme then asked for the next buffer value (7.413). The pH electrode was carefully washed and dried and placed in the buffer solution. Once stabilised the pH value was entered. The pH electrode was then removed, washed and dried and together with the conductivity cell was placed in the reaction solution, and a stopclock started. The nitrogen was then turned on and as the gas bubbled through the solution the carbon dioxide was slowly outgassed, leading to the solution becoming saturated with respect to calcite as the pH value increased. After approximately thirty minutes the pH had risen from approximately 5 to $\sim$ 7.8, indicating that the desired degree of supersaturation had been obtained. The gas was then disconnected and the solution left for a further thirty minutes to regain its thermal equilibrium.

Once this had been achieved, as indicated by a steady pH and conductivity reading, the calcite seed could be added. This seed in suspension had been allowed to arrive at thermal equilibrium in the thermostat, and 1 cm^3 of it was removed, after vigorous shaking, placed in a small vial which was then placed in the thermostat. The time since the insertion of the electrodes into the reaction solution was entered into the Apple, to allow the

conductivity data to be corrected for the leakage of KCl from the combination pH electrode. This leakage rate had previously been measured for this experimental configuration, and had been found to be 0.03352 $\mu S\,min.^{-1}$ at 25°C. Once this time had been entered a reading was taken of pH and conductivity by the Apple.

Within the next minute the 1 cm^3 of calcite suspension was added to the reaction solution, using a Pasteur pipette. The sample vial being carefully washed out with reaction solution to ensure that all of the suspension had been transferred. After one minute further pH and conductivity values were measured and readings were then taken at the time intervals described in Section 4.3.3.1. The length of an experiment was typically 292 minutes at which time readings were taken every sixteen minutes.

4.3.4.2 PRECIPITATION IN THE PRESENCE OF COPPER

To study the effect of copper ion concentration on the rate of precipitation a solution of approximately 3×10^{-2} mol dm^{-3} Copper (II) chloride was made up by dissolving 1.2786g of Analar Copper (II) chloride (B.D.H.) in 250 cm^3 of triply distilled water. 0.01 cm^3 Of this solution was added to the reaction solution using a graduated micropipette dispenser, before the addition of the suspension and the experiment continued as described in the last section.

TABLE 4.4 Calibration curve for the leakage rate of KCl from the combination pH electrode.

TIME/min.	CONDUCTIVITY/μS	TIME/min.	CONDUCTIVITY/μS
0	420.71	0	425.34
2	420.75	5	425.47
5	420.92	10	425.55
10	421.07	15	423.67
15	421.25	20	425.72.
22	421.32	25	425.85
25	421.43	30	426.02
31	421.52	35	426.16
35	421.70	40	426.19
40	421.80	45	426.26
45	421.89	50	426.34
50	421.95	55	426.66
55	422.07	60	426.70
60	422.20	65	426.77
65	422.40	70	426.93
70	422.43	75	426.95
75	422.51	80	427.18
80	422.59	85	427.25
85	422.80	90	427.43
95	423.01	95	427.48
100	423.06	100	427.61
no gas		gassing	

4.3.4.3 DISSOLUTION WORK ON POWDERS

A slightly different experimental arrangement was needed to study the dissolution rate of powders. It was decided to use 800 ml of reaction solution for these experiments, but first it was necessary to measure the leakage rate of the combination pH electrode in this new configuration. This consisted of monitoring the change in conductivity (using the Wayne Kerr Bridge) as a function of time, with the electrode in its experimental configuration, both with and without gas passing through the solution. From these results (Table 4.4) a calibation curve (Figure 4.13) was constructed and the leakage rate was found to be 0.02198 $\mu S\ min^{-1}$.

Preliminary work was done without the baffles but this proved to be unsatisfactory because gas bubbles were drawn into the cavity of the conductivity cell and produced eratic readings. The pH electrode also suffered from similar problems. With the baffles in place the gas stream was diverted and the problem was greatly reduced giving a far steadier reading.

For the experiments, 800 cm^3 of triply distilled water was placed in the reaction vessel which, together with the pH buffer solutions, was emersed in the thermostat and allowed to obtain thermal equilibrium. Once this had been obtained the programme 'STARTUP' was run and the pH combination electrode calibrated using the 4.008 and 7.431 pH buffer solutions. Gas of the required partial

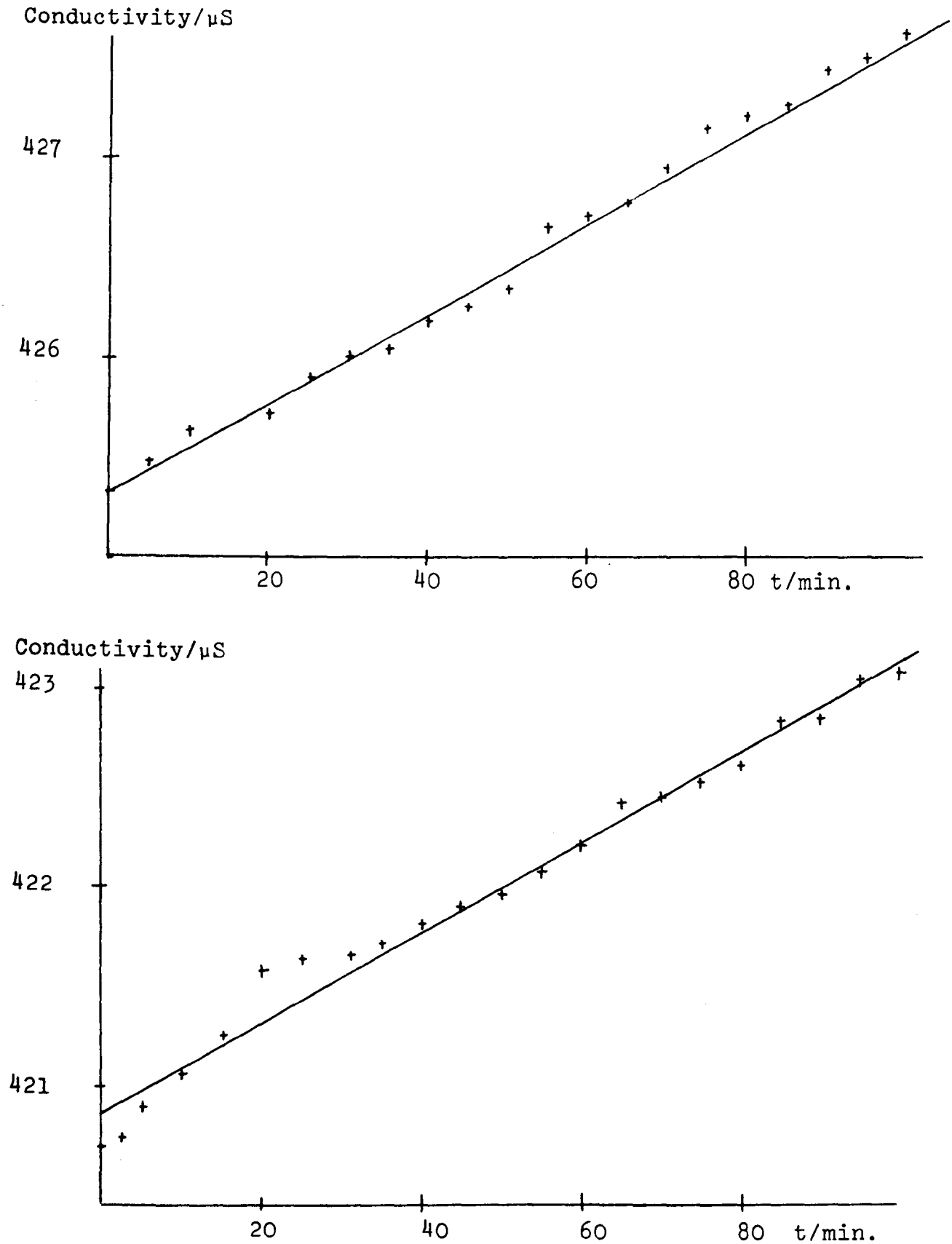

FIGURE 4.13 Calibration of leakage rate

pressure of carbon dioxide was passed into the reaction solution, the pH electrode and conductivity cell inserted into the reaction vessel, and the stop clock started. The change in the pH value of the reaction solution was noted until a steady pH value was achieved, i.e., when the solution was in equilibrium with the gas phase.

Meanwhile the amount of dried calcite to be used in the experiment was calculated. This was achieved using the computer programme 'CAHCO3'. This allowed the composition of a $Ca(HCO_3)_2$ solution to be determined from a knowledge of the partial pressure of CO_2 in equilibrium with the solution with the condition that the solution was in equilibria with the calcite, i.e., $\beta = \emptyset$. This allows the calculation of the total mass of calcium carbonate dissolved at equilibrium.At least 1Ø times this amount was then carefully weighed out, ready for its addition to the reaction solution. This large excess was needed because as discussed in Section 1.1 in dissolution work on powders, the assumption is made that there is no significant area change during the course of the experiment, and the only way in which this is a valid assumption is if less than 10% of the powder initially added is dissolved, otherwise the change in surface area can become significant and therefore the assumptions are invalidated.

Upon attainment of a steady pH value, the Wayne Kerr A.C. bridge was trimmed; however, due to the lack of any background electrolyte it was necessary to use a very

sensitive scale, i.e., 0 - 100 μS, which led to problems which are discussed later. The time elapsed since the insertion of the electrodes into the reaction solution was entered, and pH and conductivity values were measured by the computer. Within the next minute the weighed amount of calcite was added and the weighing boat was carefully washed out with the reaction solution. The experiment then proceeded as described for the precipitation work (Section 4.3.4.1).

The Wayne Kerr B642 bridge had decade conductivity ranges covering 0 - 10, 0 - 100, 0 - 1000 and 0 - 10,000 μS. Because of the low conductivity of the reaction solution at the start of the reaction, it was necessary to use a very low conductance scale to balance the bridge. However, as the reaction proceeded the conductance rapidly increased causing the meter to come off scale, requiring the bridge to be rebalanced. This involves breaking into 'STARTUP'. Firstly, the data already collected was stored on floppy discs using 'ANALY'. Then 'STARTUP' was rerun. This had to be modified to enable the pH calibration parameters to be typed in rather than performing the calibration each time the bridge was rebalanced. The changes made are shown in the Appendix.

All of the data files collected during any one run by 'ANALY' were analysed as described previously in Section 4.3.2.2 by using 'COMPOST', or 'COMPOST.OBJ'. For the final analysis, using 'TNCAL', and 'SMOOTH', slight alterations were needed in the programmes.

'TNCAL' was altered to express the rate of dissolution as mol $cm^{-2}s^{-1}$, and the printout format was changed so that the term $[Ca^{2+}]x[HCO_3^-]$ was printed. 'SMOOTH' was adjusted so that instead of giving the rate, the term (rate $-k_1[H^+]$) was outputed (where k_1 is the transport constant for H^+ as defined and measured by Plummer et al.,[14]).

Experiments were then carried out over a wide range of partial pressures of carbon dioxide (ρ = 0.048 → 0.248 atm).

It was then decided to study the rate of calcite dissolution with a finer powder to see if any differences in behaviour could be detected. The powder chosen was Calopake F (from Sturge Chemicals) having a specific surface area of 5.65 m^2g^{-1} (from nitrogen B.E.T. adsorption analysis). However, this powder was so finely divided that upon introducing it into the reaction solution the reaction occurred so fast that it could not easily be followed, with 90% of the reaction occurring in the first five minutes. With this speed of reaction the concentration of CO_2 in solution could not be controlled using the N_2/CO_2 mixing system. For the first few minutes the partial pressure of CO_2, as calculated by the computer was far greater than the partial pressure flowing through the gas mixing system (as CO_2 was released by the reaction of calcite). This occurred in all the dissolution experiments which meant that the first points in the experiment had to be discarded until ρCO_2 returned to the level set. However in the case of

Calopake F, by the time this had occurred, the reaction was virtually completed.

4.4 PRECIPITATION USING THE ROTATING DISC

Experiments were carried out to try and characterise the back reaction in dissolution (i.e., precipitation) by monitering the flux of disolving calcium when the product ($[Ca^{2+}] \times [CO_3^{2-}]$) was near to Ksp, the solubility product for calcite.

The apparatus used was the same as that for monitering dissolution, but instead of starting at $[Ca^{2+}]_{initial}$ = $\sim 1 \times 10^{-5}$ mol dm^{-3} of calcium chloride in 0.3 mol dm^{-3} KCl $[Ca^{2+}]_{initial}$ used was 3.5×10^{-4} mol dm^{-3}, in order to allow the experiment to come to completion in a reasonable amount of time. Originally the stock calcium solution, as described in Section 4.1.5.1, was used, but the pH was found to be 3.4 when measured using the Radiometer pH meter.

Therefore a new stock solution of calcium was made up using calcium nitrate ($CaNO_3 \cdot 4H_2O$). 5.9059g Was dissolved in 250 cm^3 of distilled water in a volumetric flask giving a stock solution of 0.1000 mol dm^{-3}. When a reaction solution was made up of 3.5×10^{-4} mol dm^{-3} Ca^{2+} in 0.3 molar KCl and this was degassed the pH was measured and was found to be 6.78.

Once the mV reading had steadied (to $\pm$ 0.15 mV), with nitrogen bubbling through the solution and the titanium disc spinning at 10 Hz,then the ground, etched, single

crystal calcite disc was inserted and the change in concentration of Ca^{2+} was monitored. The reaction was allowed to continue until the solubility product of calcite was exceeded, as indicated by the calcium concentration remaining constant for over one hour. At this stage the rate of the forward and backward reactions are equal. A typical experiment would last for approximately seven hours.

1. L.Bragg, In: "The Crystalline State, Vol. IV, Crystal Structure of Minerals", p.128, G.Bell and Sons, London, 1953.
2. A.I.Vogel, In: "Textbook of Quantitative Inorganic Chemistry", Forth Ed., Longman, New York.
3. B.L.Kepner, D.M.Hercules, *Anal.Chem.*, 35, 1238 (1962).
4. J.Koryta, In: "Ion Selective Electrodes", Cambridge University Press, Cambridge (1975).
5. K.Toth, I.Cavaller, E.Pungor, *Anal.Chim.Acta*, 57, 131 (1971).
6. J.Walpole, *J.Chem.Soc.*, 105, 2501 (1914).
7. O.Sørensen, *Ergebn Physiori.*, 12, 393 (1912).
8. L.Onsager, R.M.Fuoss, *J.Phy.Chem.*, 36, 625 (1967).
9. M.Kulthoff, *J.Biol.Chem.*, 63, 135 (1925).
10. O.Sørensen, *Biochem.Z.*, 22, 352 (1909).
11. L.Clark, B.Lubs, *J.Bacteriol.*, 2, 1 (1917).
12. G.E.Cassford, W.A.House, A.D.Pethybridge, *J.Chem. Soc., Faraday Trans. I*, 79, 1617 (1983).
13. R.W.Hamming, In: "Numerical Methods for Scientists and Engineers", 2nd Ed., McGraw Hill, New York, (1978).
14. L.N.Plummer, T.M.Wigley, D.L.Parkhurst, *Am.J.Sci.*, 278, 179 (1978).

CHAPTER 5

RESULTS AND DISCUSSION

This chapter is concerned with the analysis and discussion of the results obtained from the experimental work described in Chapter 4. For single crystal rotating discs it will be shown that reproducible, well-defined hydrodynamics are set up, which allow the dissolution reaction to be characterised. This reaction occurs through three processes, two being transport controlled, the third being a surface controlled reaction. The role of surface preparation will be explained and the extent to which this affects the number of kinks and terraces, and thus the rate of reaction, will be given, as will the extent to which copper(II) ions act as inhibitors on the rate.

It will be shown that the surface rate constant measured for the dissolution of powders is consistant with that obtained for the rotating disc, despite the lack of well-defined hydrodynamics, and the vast difference in area. The effect of copper (II) ions on the precipitation rate will also be examined.

5.1 RESULTS OBTAINED FROM THE DISSOLUTION OF ROTATING CALCITE DISCS

This section will describe the results obtained using rotating calcite discs, made from both powdered pellets and single crystals.

5.1.1 POWDERED PELLETS

Rotating discs incorporating powdered pellets (made as described in Section 4.1.1.1) displayed several problems

TABLE 5.1 Flux of dissolution of powdered calcite pellets at pH 3.0

FLUX OF DISSOLUTION x 10^9 / mol $cm^{-2}s^{-1}$	ROTATION SPEED / Hz
3.905	9
2.336	9
2.449	9
2.237	9
1.967	9
	16
1.977	16
4.739	16
4.504	16
2.285	16
4.140	25
2.087	25
2.285	25
4.119	25
4.489	25
6.805	36
5.605	36
5.211	36
2.004	36
2.202	36

experimentally. Firstly, when the pellets were polished, using diamond lapping compound, cracks often became apparent, into which the lapping compound absorbed, and at which it was seen that dissolution occurred preferably. Pellets which had absorbed the lapping compound could not be used for various obvious reasons. Firstly, it was impossible to be sure that all of the diamond grit had been removed before changing sprays, thus leading to uncertainty in the degree of smoothness after polishing. Secondly, absorbed lapping compound might contaminate the reaction solution, and lastly, dissolution occurred preferably at the cracks thus not all of the exposed surface reacted at the same rate. To overcome these problems, pellets were polished using calcium carbonate powder. The powder being placed on a cloth mat and this was lubricated using hexane. This overcame the problem of absorption, but still left the problem of cracks appearing, and also led to uncertainty in the degree of surface reproducibility. The measured flux of dissolution as measured for powdered pellets, at various rotation speeds, are tabulated in Table 5.1 and are shown in Figure 5.1. As can be seen the measured fluxes are erratic and unreproducible, though they indicate that dissolution increases with rotation speed.

To overcome the problems associated with the stress in grinding these pellets, the pellet size was changed from 7.5 to 2.5 mm radius, as described in Section 4.1.1.1. Pellets formed using these pellets were easier to polish

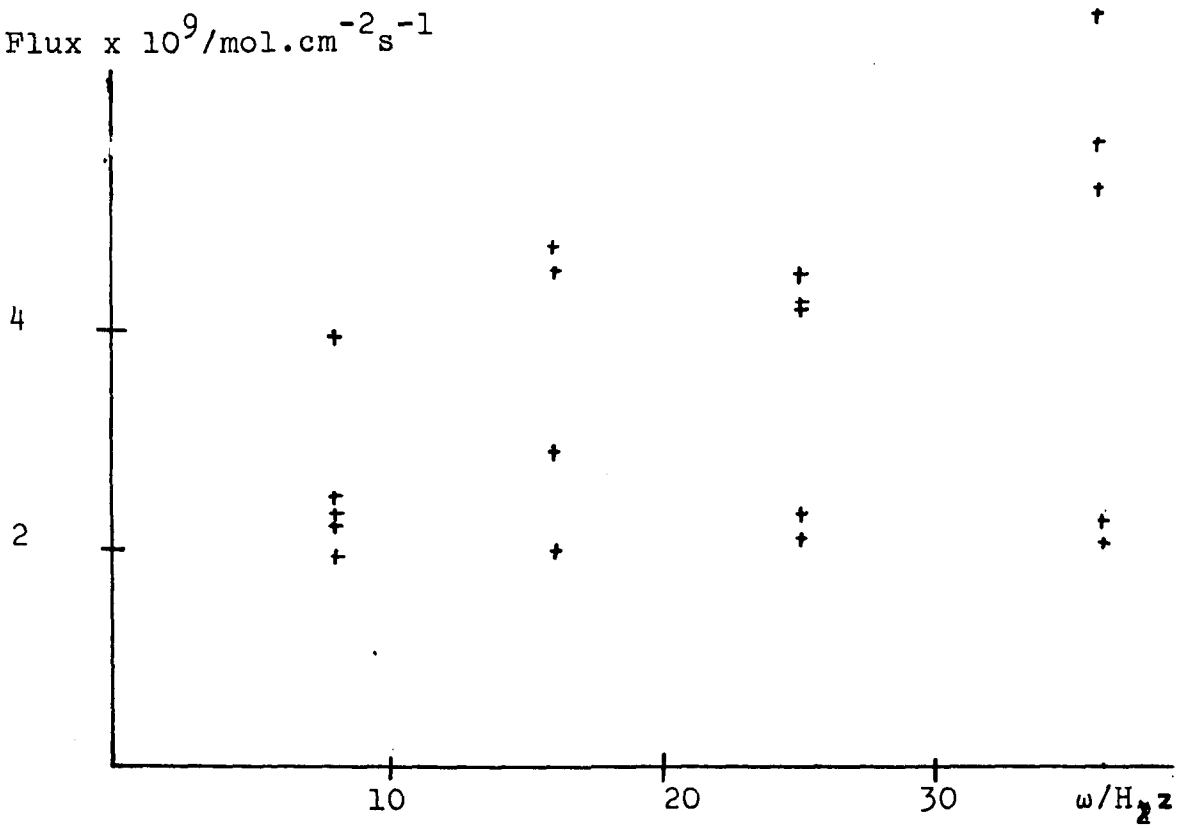

FIGURE 5.1 Plot of J vs. ω

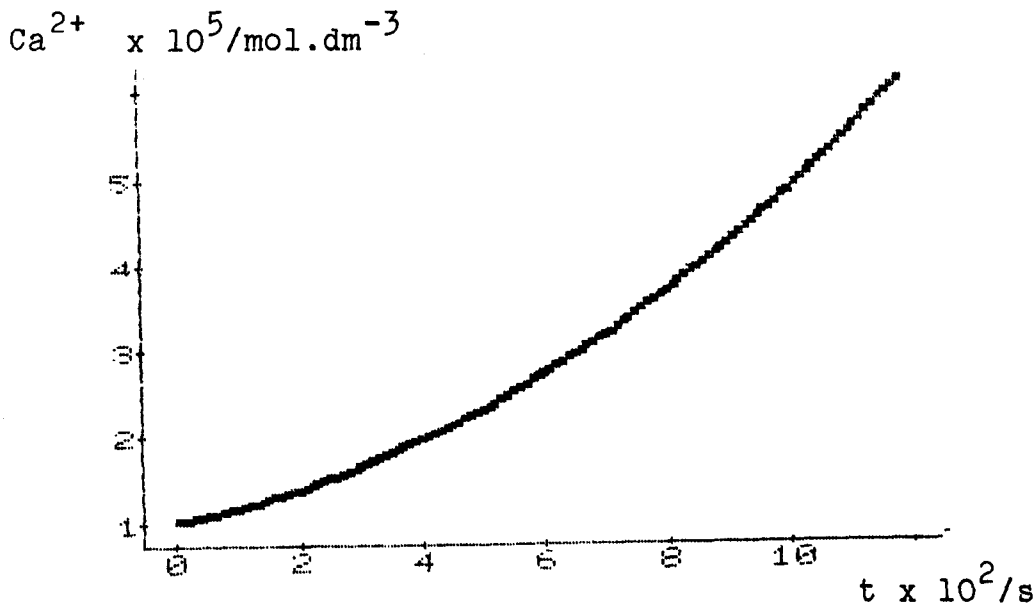

FIGURE 5.2 Plot of Ca^{2+} vs. time during the etching process.

without causing flaws in the pellet surface, but an additional problem arose in that it was difficult to centrally place these pellets before casting. This central placing was essential if edge effects were not to be encountered, and for the calcite disc to behave as a rotating disc as opposed to a rotating cylinder (see Section 3.3).

A further possible problem with forming pellets from powders using a press may arise in the observation of Burns and Bredig[1] and Dachille and Roy,[2] that grinding calcite powders at room temperature was sufficient to produce a small amount of aragonite, and that the percentage of arogonite increased with the grinding time. Thus, the morphology of the pellets may not be pure calcite and analysis would, therefore, be required to check on the composition of each crystal.

In conclusion the use of pellets in forming calcite rotating discs proved unsatisfactory. It was impossible to polish the crystals in such a way as to form reproducible surfaces, the surfaces formed being liable to produce cracks upon dissolution, and there was the possibility of a morphology change in the calcium carbonate upon the formation of the pellets.

5.1.2 DISSOLUTION OF SINGLE CRYSTAL ROTATING DISCS

To enable direct comparison to be made between experiments carried out on different discs, it was decided to use single crystal, as opposed to powdered calcite. Single crystals, which cleaved easily, would have

the advantage of producing reproducible surfaces, and would not suffer from the absorption problems experienced when using pellets.

The crystal chosen was Iceland Spar. This had two main advantages; firstly, it cleaved very easily, enabling crystals to be cut to size, and secondly, the crystals cleaved in such a fashion that each face exposed was the (100) plane, presenting no problem in orientating the crystal before mounting.

5.1.2.1 PRELIMINARY PREPARATION OF THE CALCITE DISC

Before the single crystal rotating disc could be used for dissolution experiments, it was found that the calcite surface had first to be "run in". This was necessary because, as shown in Figure 5.2, without this treatment the dissolution rate continuously increased up to a point at which a final steady rate was achieved. Once this rate had been obtained then the dissolution occurred at a constant rate. Therefore, to ensure that all the experimentally determined data could be directly compared it was necessary to make sure that the crystal had reached this maximum dissolution rate before beginning experimentation.

The procedure adopted consisted of rotating the calcite disc at 25 Hz, for 20 min., in 10^{-3} mol.dm^{-3} HCl. Figure 5.2 shows the effect of such treatment. After this time had elapsed, the crystal was carefully washed with distilled water, dried, and was then considered ready

for use. The rationale for this break in period will be given later. This treatment with HCl also served to clean the surface of any organic impurities absorbed during polishing.

5.1.2.2 DISSOLUTION IN 10^{-3} mol.dm^{-3} HYDROCHLORIC ACID

Experiments were carried out using a solution of 10^{-3} mol.dm^{-3} hydrochloric acid, with sufficient potassium chloride added to increase the ionic strength of the reaction solution to 0.3 mol.dm^{-3}. The solution was prepared as described in Section 4.1.5.3., and a stream of pure nitrogen bubbled through the reaction solution at all times. Data consisting of calcium concentrations, at set time intervals, was stored on floppy discs and this was later analysed using the 'CURFIT' programme as outlined in Section 4.1.4.2. Figure 5.3 shows plots of $[Ca^{2+}]$ versus time for various rotation speeds. As can be seen the $[Ca^{2+}]$ increases linearly with time, and the rate of dissolution is increased by an increase in rotation speed.

The measured dissolution rates (mol.dm^{-3}s^{-1}) were transformed into fluxes (J), (mol.cm^{-2}s^{-1}) by considering the area of calcite exposed and the volume of reaction solution (Table 5.2). Using these figures a Levich plot of flux vs. $\omega^{1/2}$ was obtained. As can be seen from Figure 5.4, an excellent Levich plot was obtained (i.e., a straight line passing through the origin) with a gradient of 1.970×10^{-8} mol.cm^{-2}s$^{-3/2}$.

The points shown in Figure 5.4 and tabulated in Table 5.2 are an average of many runs for each rotation speed.

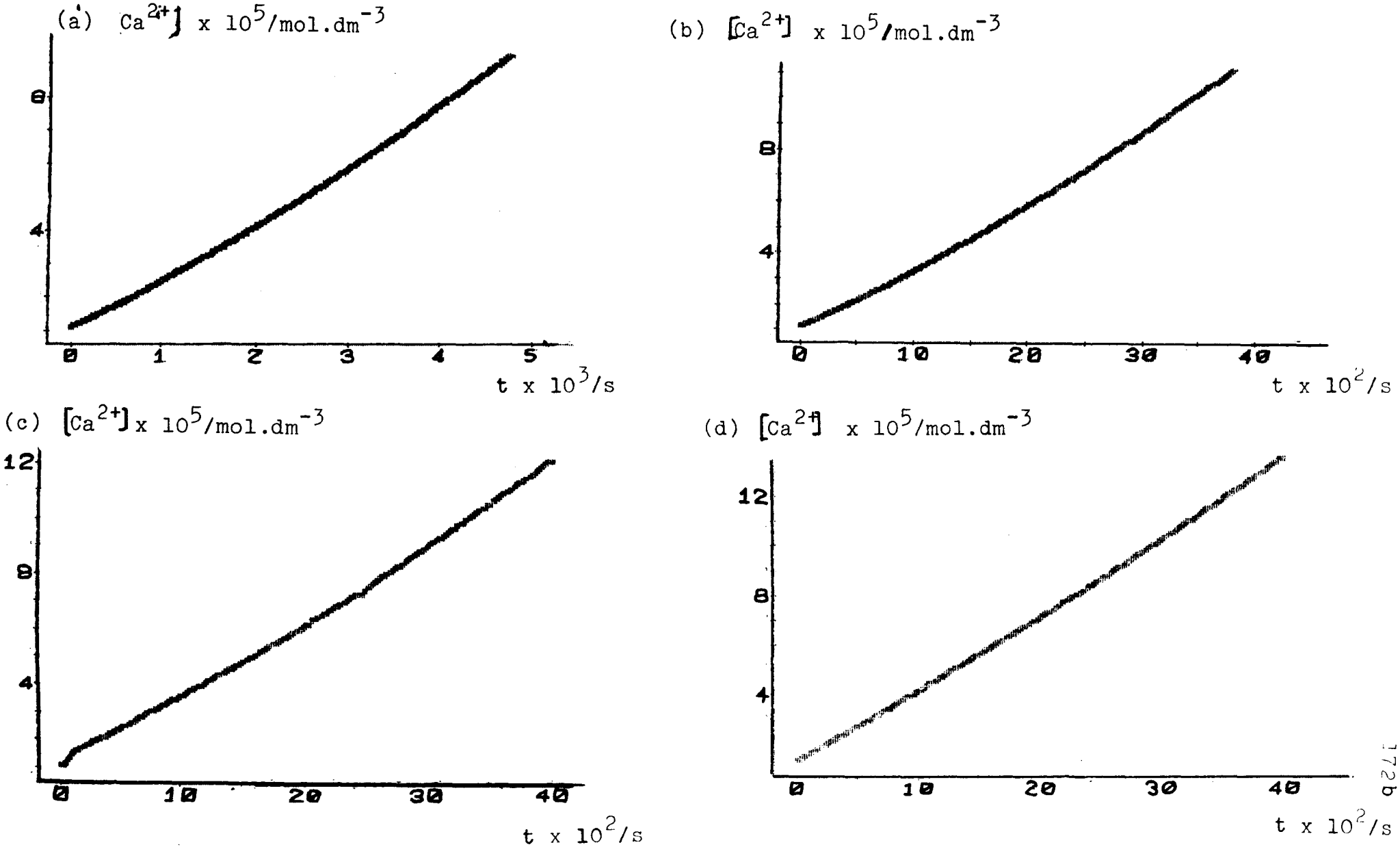

FIGURE 5.3 Plots of concentration vs. time for pH 3.0 (a) 10 Hz, (b) 20 Hz, (c) 25 Hz, (d) 30 Hz.

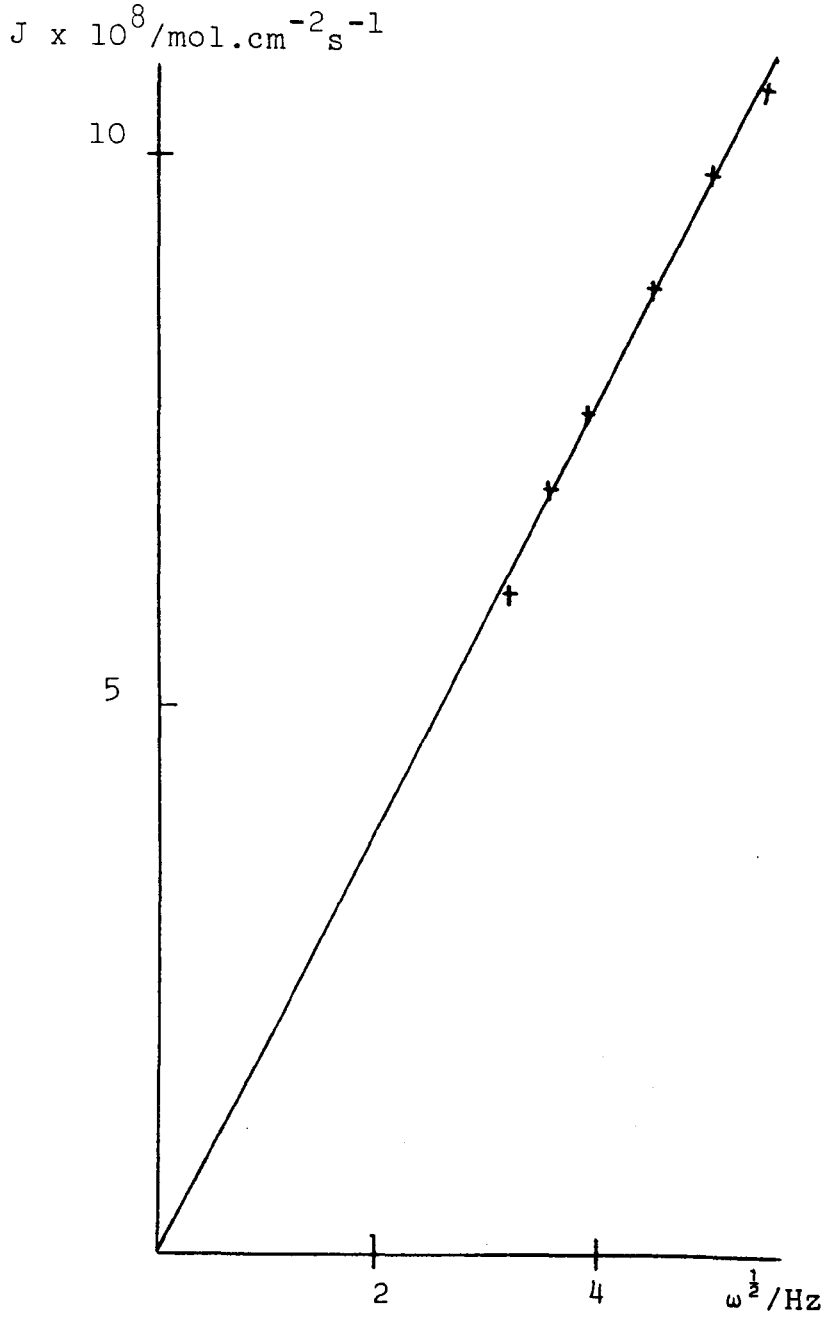

FIGURE 5.4 Levich plot for 10^{-3}M HCl.

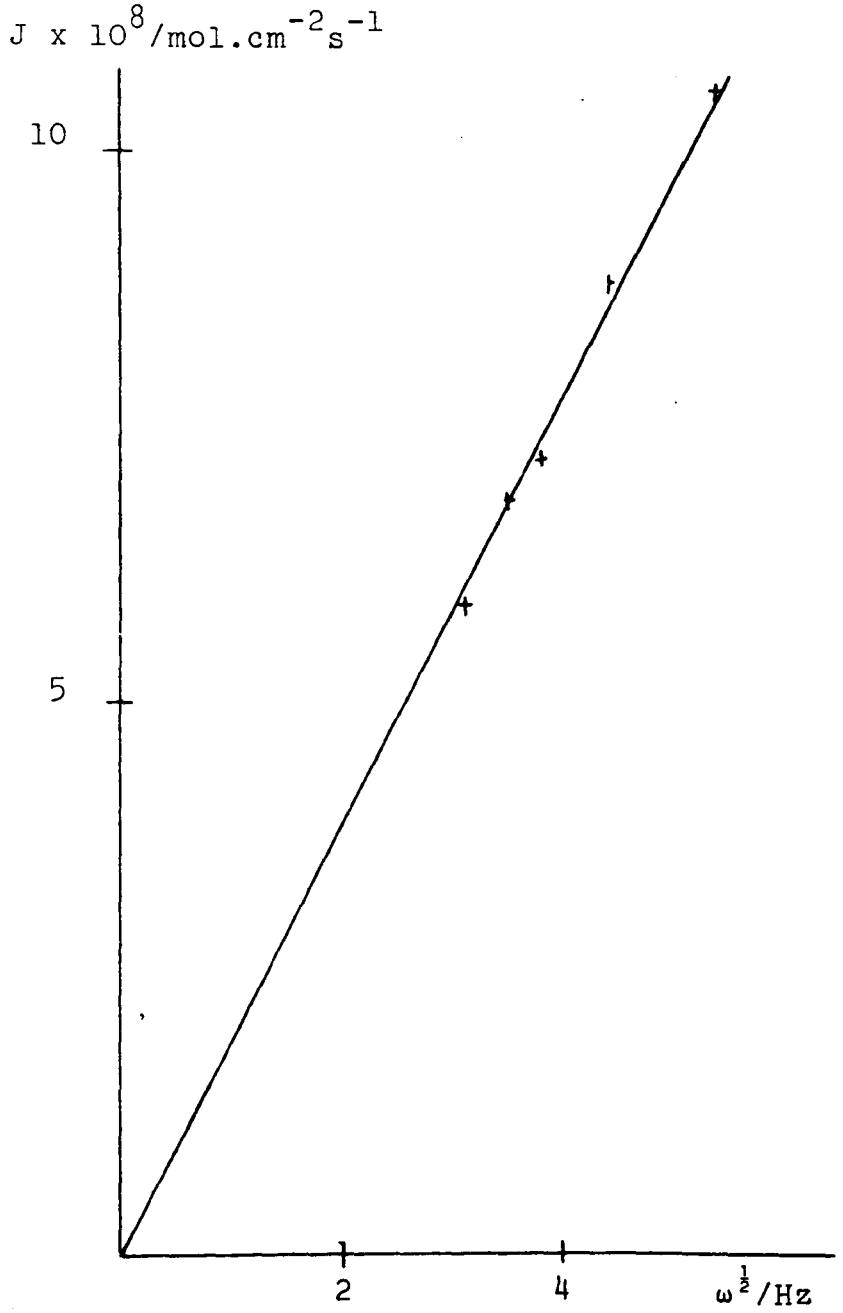

FIGURE 5.5 Levich plot for 10^{-3}M HCl.

TABLE 5.2 Flux as a function of $\omega^{1/2}$ for pH 3.0

$\omega^{1/2}$/Hz	FLUX/mol.cm^{-2}s^{-1}
3.16	6.06×10^{-8}
3.53	7.02×10^{-8}
3.87	7.67×10^{-7}
4.47	8.83×10^{-8}
5.00	9.84×10^{-8}
5.48	1.061×10^{-7}

TABLE 5.2b Flux as a function of $\omega^{1/2}$ for pH 3.0

$\omega^{\frac{1}{2}}$/Hz	FLUX/mol.cm^{-2}s^{-1}
3.16	5.86×10^{-8}
3.53	6.80×10^{-8}
3.87	7.15×10^{-8}
4.47	8.76×10^{-8}
5.00	9.52×10^{-8}
5.48	1.048×10^{-8}

Table 5.2b show fluxes obtained using a different crystal and Figure 5.5 shows the corresponding Levich plot, giving a slope of 1.931×10^{-8} mol.cm^{-2}s$^{-3/2}$. These values are within 2% of each other and thus show the reproducibility of the crystal surfaces.

If the reaction occurring at the calcite surface is:

$$2H^+ + CaCO_3 \rightarrow 2HCO_3^- + Ca^{2+} \qquad 5.1$$

with the rate determining step being H^+ transfer across the diffusion layer, then using the Levich equation (3.28), the flux of dissolving calcium will be given by:

$$2.0\ J\ Ca^{2+} = 1.554\ D_{H^+}^{2/3}\ \nu^{-1/6}\ [H^+]_\infty\ \omega^{1/2} \qquad 5.2$$

(the factor of 2 appearing as 2 protons are needed to release 1 calcium ion). The diffusion coefficient for the proton can be calculated from the slopes of Figures 5.4 and 5.5. This was found to yield an average value of $7.46 \times 10^{-5} cm^{-2} s^{-1}$, in excellent agreement with the literature value of $7.64 \times 10^{-5} cm^2 s^{-1}$ as found by Gostisa-Michele et al.[3], using a high precision mechanical rotating disc electrode in $3 \times 10^{-3} mol.dm^{-3}$ HCl with 1 $mol.dm^{-3}$ potassium chloride added as background electrolyte. This shows that:-

1. The surface satisfies the conditions for correct hydrodynamic flow to the rotating disc surface.
2. The rate determining step in the dissolution of calcium carbonate at this pH is the transport of protons to the disc surface.

In these experiments, using $10^{-3} mol.dm^{-3}$ HCl no buffer was used as the very small quantity of calcium dissolved was insignificant to alter the pH to any significant extent. In a typical experiment the concentration

of calcium rose from 1 x 10^{-5} to approximately 7 x 10^{-5} $mol.dm^{-3}$, corresponding to a pH change of 0.06 units.

5.1.2.3 DISSOLUTION IN THE pH RANGE 4.21 TO 5.62 USING SODIUM ACETATE/ACETIC ACID BUFFERS

The solutions for these experiments were made up as described in Section 4.1.5.4, and using these solutions the dissolution rate was measured at various rotation speeds with a constant supply of nitrogen being passed through the solution.

The dissolution rates were converted into fluxes and Tables 5.3 to 5.5 show the fluxes for various rotation speeds, at [HA] = 0.016, 0.008 and 0.08 $mol.dm^{-3}$ respectively.

TABLE 5.3 [HA] : 0.016 $mol.dm^{-3}$

$\omega^{1/2}/Hz^{1/2}$	FLUX/$mol.cm^{-2}s^{-1}$	$1/\omega^{1/2}/Hz^{-1/2}$	$1/FLUX/mol^{-1}cm^{2}s$
2	2.389×10^{-8}	0.5	4.187×10^{7}
2	2.679×10^{-8}	0.5	3.733×10^{7}
3	4.197×10^{-8}	0.333	2.382×10^{7}
3	4.392×10^{-8}	0.333	2.277×10^{7}
4	5.203×10^{-8}	0.25	1.922×10^{7}
4	5.487×10^{-8}	0.25	1.822×10^{7}
5	6.662×10^{-8}	0.2	1.501×10^{7}
5	6.422×10^{-8}	0.2	1.537×10^{7}

TABLE 5.4 $[HA] = 0.008\ mol.dm^{-3}$

$\omega^{1/2}/Hz^{1/2}$	FLUX/mol. $cm^{-2}s^{-1}$	$1/\omega^{1/2}/Hz^{-1/2}$	$1/FLUX/mol^{-1}cm^{2}s^{1}$
2	1.061×10^{-8}	0.5	9.431×10^{7}
3	1.618×10^{-8}	0.333	6.179×10^{7}
4	2.343×10^{-8}	0.25	4.274×10^{7}
5	2.969×10^{-8}	0.2	3.372×10^{7}

TABLE 5.5 $[HA] = 0.08\ mol.dm^{-3}$

$\omega^{1/2}/Hz^{1/2}$	FLUX/mol. $cm^{-2}s^{-1}$	$1/\omega^{1/2}/Hz^{-1/2}$	$1/FLUX/Mol.^{-1}cm^{2}s$
2	7.122×10^{-8}	0.5	1.404×10^{7}
3	1.052×10^{-7}	0.333	9.504×10^{6}
4	1.353×10^{-7}	0.25	7.389×10^{6}
5	1.882×10^{-7}	0.2	5.314×10^{6}

Figures 5.6 - 5.8 show the fluxes as a function of $\omega^{1/2}$, and as can be seen excellent Levich plots are obtained for each concentration. The values in Tables 5.3 to 5.5 represent the average values for many measurements.

The question arises as to whether the reaction occurring is the attack of acetic acid with the calcite surface i.e.,:

$$2CH_3CO_2H + CaCO_3 \rightarrow H_2CO_3 + Ca^{2+} + 2CH_3CO_2^- \qquad 5.3$$

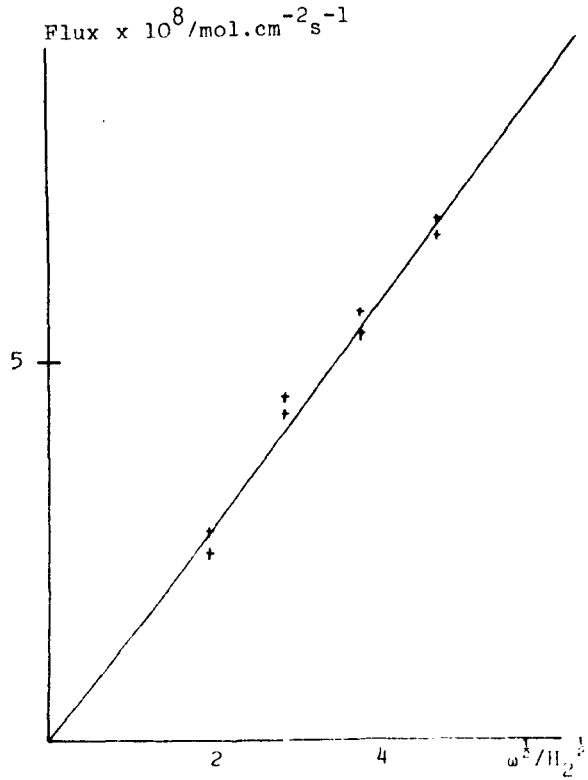

FIGURE 5.6 Levich Plot for $[HA]$ = 0.016mol.dm^{-3}

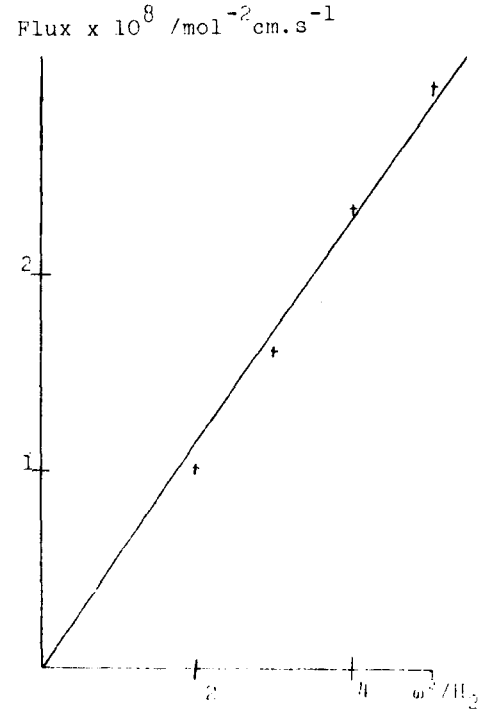

FIGURE 5.7 Levich Plot for $[HA]$ = 0.008 mol.dm^{-3}

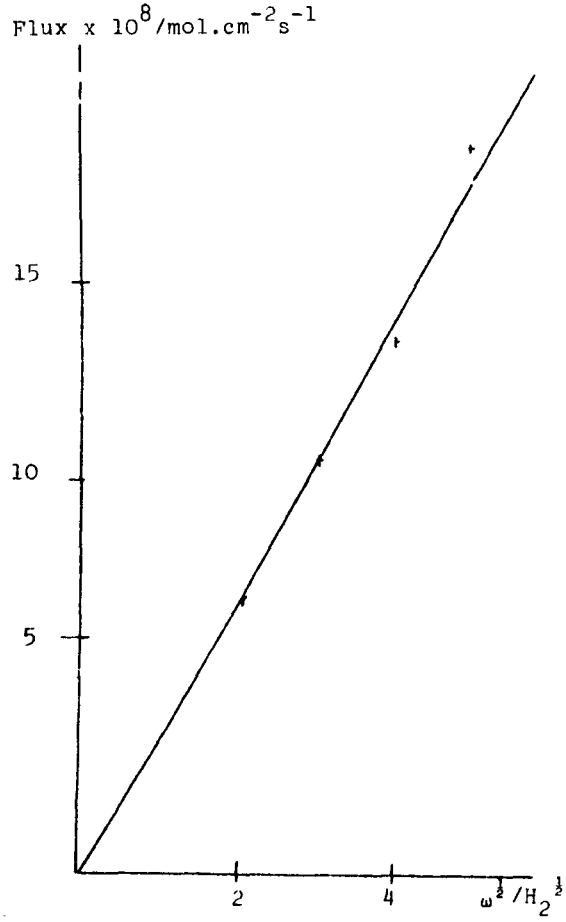

FIGURE 5.8 Levich Plot for [HA] = 0.08 mol.dm^{-3}

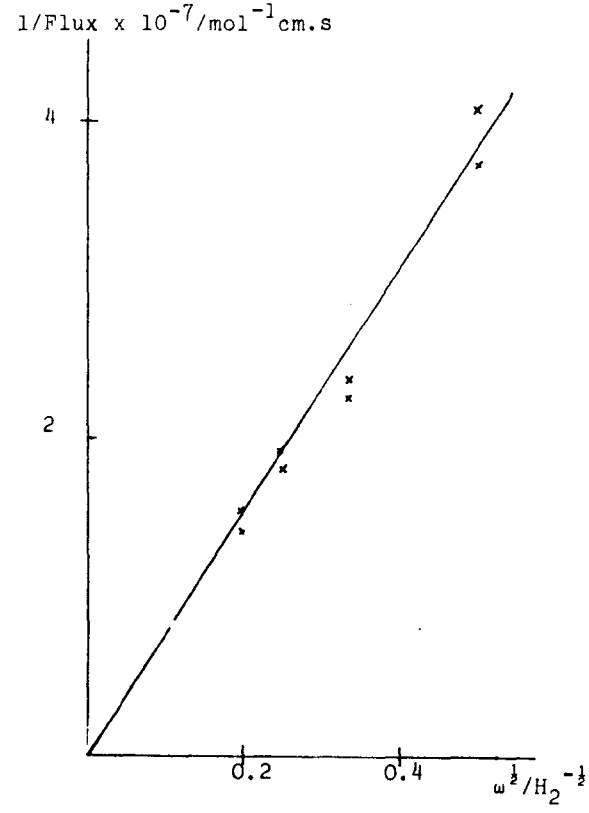

FIGURE 5.9 Koutecky Levich plot for [HA] = 0.016 mol.dm^{-1}

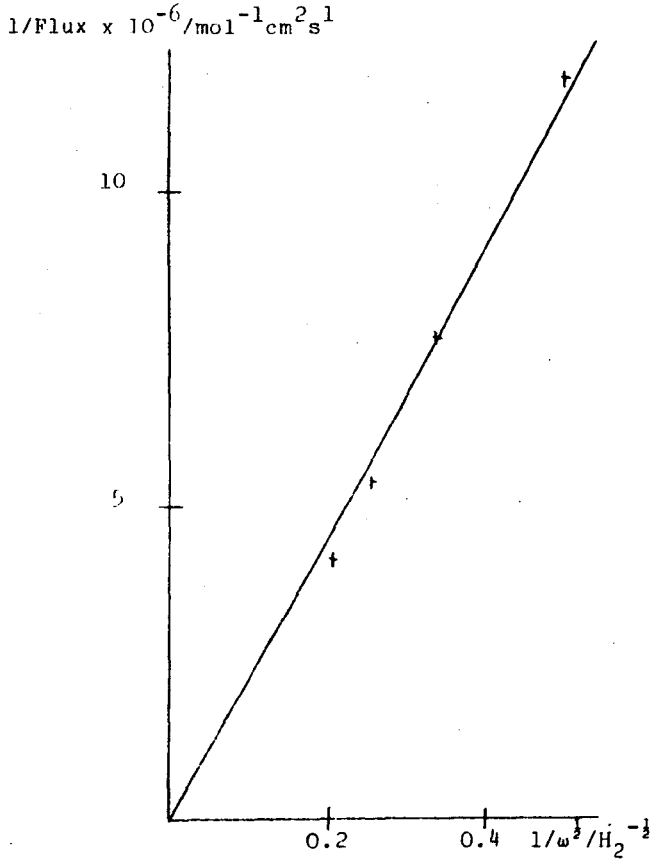

FIGURE 5.10 Koutecky Levich Plot for [HA] = 0.08 mol.dm^{-3}

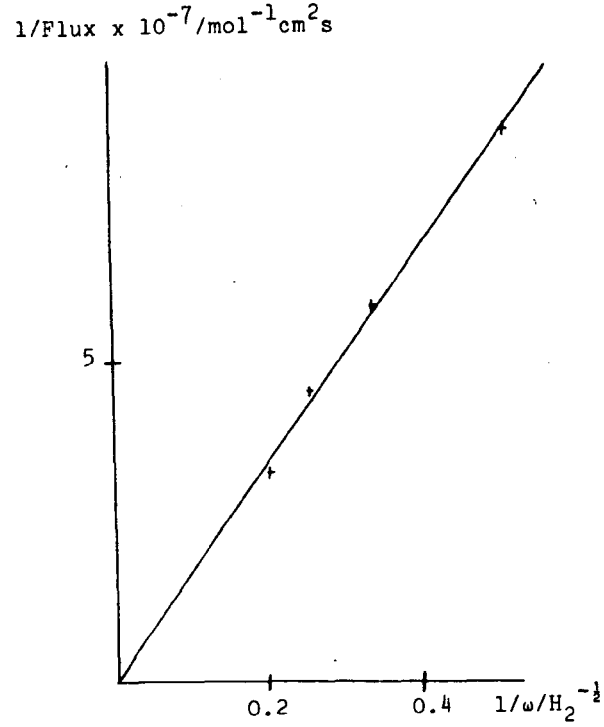

FIGURE 5.11 Koutecky Levich Plot for [HA] = 0.008 mol.dm^{-3}

or whether the acetic acid first dissociates and the chemical step is the attack of protons on the surface:

$$2CH_3CO_2H \rightleftharpoons 2H^+ + 2CH_3CO_2^- \xrightarrow{CaCO_3} Ca^{2+} + H_2CO_3 + 2CH_3CO_2^- \qquad 5.4$$

If the latter case occurs then as described in Section 3.4, the behaviour can be described by the Koutecky-Levich equation (3.44) i.e.,:

$$\frac{1}{J} = \frac{1}{HA}\left[\frac{0.64\,\nu^{-1/6}}{D_{HA}^{2/3}\sqrt{\omega}} + \left(\frac{[A^-]}{k'_1 K_A D_{H^+}}\right)^{\frac{1}{2}}\right] \qquad 5.5$$

Where the symbols have been defined in Chapter 3.

If the value $9.1 \times 10^5 s^{-1}$ [4,5] is used for k_1 and that of 1.75×10^{-8} mol.cm^{-2} [6] for K_A, then equation 5.5 becomes:

$$\frac{1}{J} = \frac{2}{CH_3CO_2H}\,\frac{639}{\sqrt{\omega}} + 5.74 \qquad 5.6$$

as the sodium acetate concentration was kept constant throughout the experiment.

From equation 5.6,since the maximum rotation speed employed was 25 Hz, then this second term is negligible, i.e., the kinetics of dissolution for acetic acid are sufficiently rapid that the reaction may be described by pure Levich behaviour. Figures 5.9 - 5.11 show

Koutecky-Levich plots for the three acetic acid concentrations.

If the slopes of Levich plots ($J_{Ca^{2+}}/\omega^{\frac{1}{2}}$) are plotted as a function of acetic acid concentration a straight line is expected from the Levich equation (3.28). Figure 5.12 shows such a plot using the values listed in Table 5.6. As can be seen such behaviour is followed

TABLE 5.6 Slopes from Levich plots as a function of HA

[HA] /mol.dm^{-3}	LEVICH PLOT SLOPES / 10^{9}mol.cm^{-2}s$^{-3/2}$
0.008	5.778
0.016	13.341
0.032	22.503
0.04	29.354
0.064	33.748
0.08	36.053
0.12	31.746
0.16	31.919

when the concentration of acetic acid is less than 0.043 mol.dm^{-3}, showing that the rate determining step is acetic acid transport across the diffusion layer. Thus, the kinetics of calcite dissolution at this pH can be described by the Levich equation, with D and C_{∞} relating to the acetic acid. From the slope of Figure 5.12 the diffusion coefficient of acetic acid can be calculated and was found to be 8.60 x 10^{-6}cm^{2}.s^{-1}, in reasonable agreement

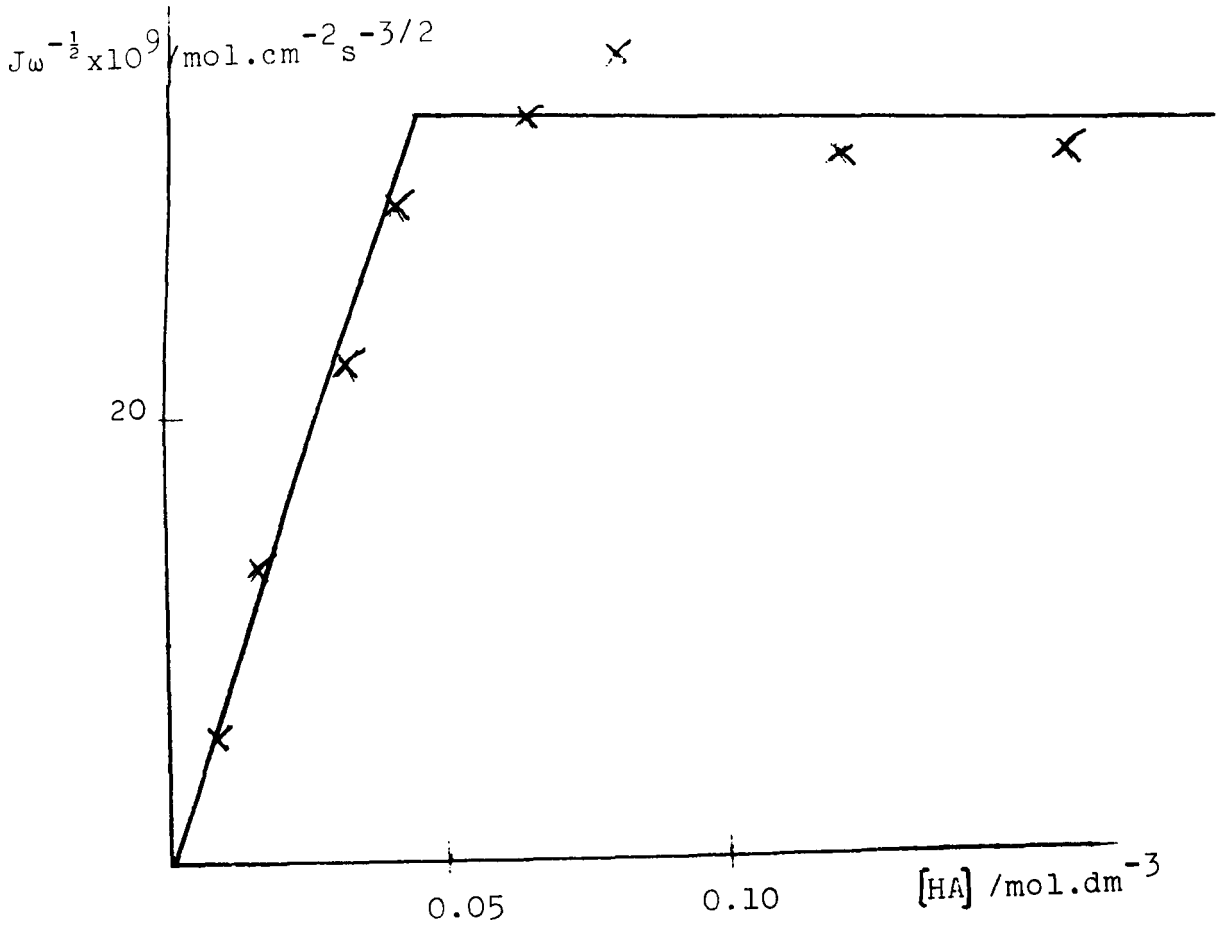

FIGURE 5.12 Slopes from Levich plots as a function of HA .

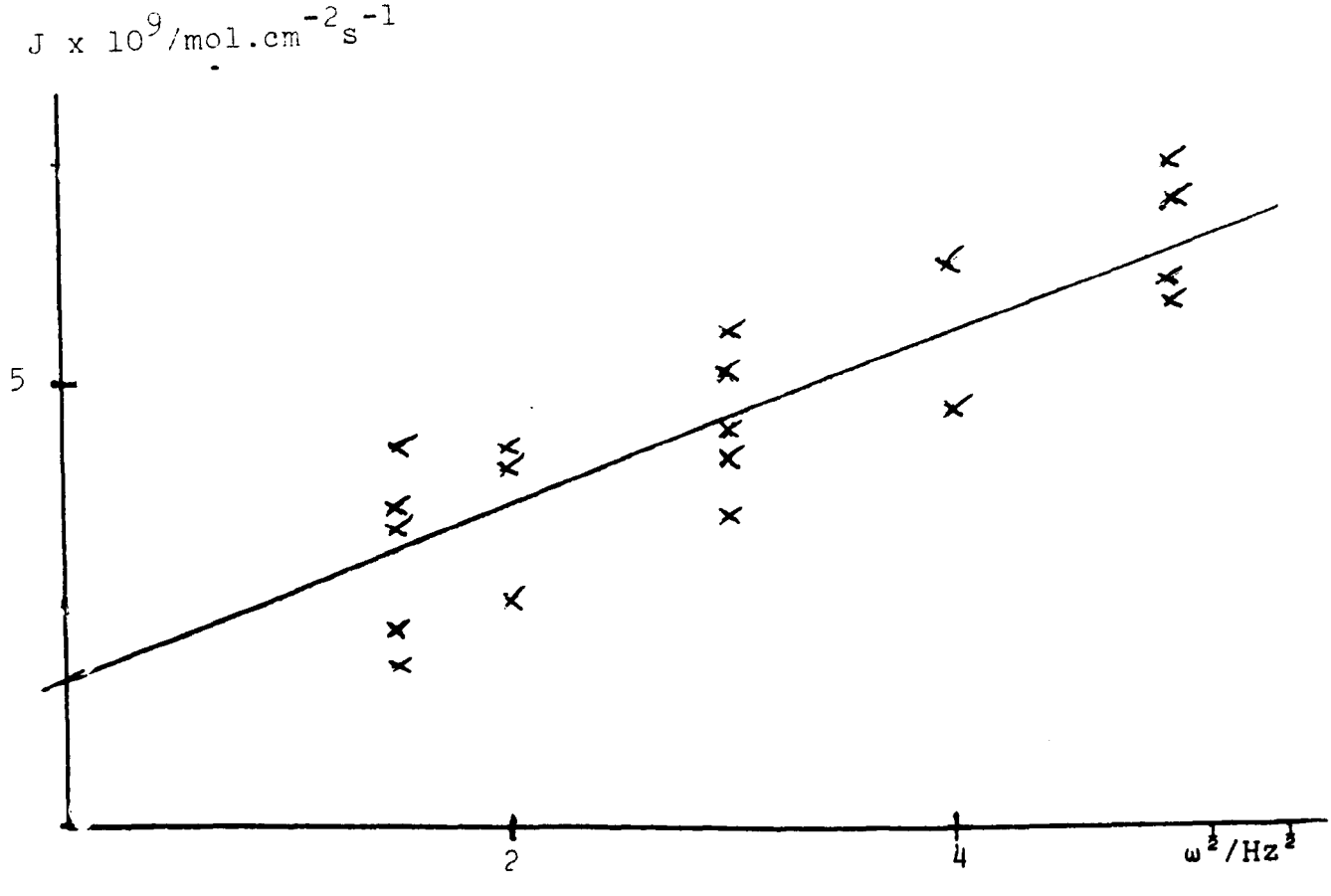

FIGURE 5.13 Levich plot for dissolution at pH 6.11.

with the value of 1.01×10^{-5} $cm^2.s^{-1}$ as calculated by Bidstrup and Geankoplis[7] using their version of the Wilke-Chang approximation.

However, when [HA] exceeds 0.043 $mol.dm^{-3}$ then the graph levels off, indicating that the rate of dissolution becomes independant of the acetic acid concentration. This may be attributable to the onset of CO_2 bubble formation at the surface of the disc, i.e., when the concentration of CO_2 builds up to the level at which the solubility is exceeded, then the rate determining step becomes the transport of CO_2 away from the rotating disc's surface. This was verified by the observation of bubbles at the disc's surface.

The onset point of this condition may be calculated by considering Henry's law, i.e.,;

$$[CO_2]_{aq.} = K_H \, \rho CO_2 \qquad 5.7$$

ρCO_2 = partial pressure of carbon dioxide/atm.

K_H = Henry's law constant.

Bubbles will form when ρCO_2 becomes greater than 1 atmosphere. Using a value of 0.032 $mol.dm^{-3}atm.$ for K_H[8] and considering that two molecules of acid are required to liberate one molecule of CO_2, then from equation 5.7 the onset of gaseous CO_2 evolution would be expected at approximately $2 \times K_H = 0.064$ $mol.dm^{-3}$, since the rate of reaction at the disc surface is fast enough to consume all

TABLE 5.7 Dissolution at pH 6.11 with pure N_2 being passed through the solution.

$\sqrt{\omega}/Hz^{1/2}$	FLUX/10^{-9}mol.cm^{-2}s^{-1}	BUFFER RATIO	CRYSTAL NUMBER
1.5	4.462	1	1
1.5	4.077	½	1
1.5	5.132	1	2
1.5	2.748	2	2
1.5	2.210	½	2
2.0	5.101	1	1
2.0	3.048	1	1
2.0	5.368	2	2
3.0	4.177	1	1
3.0	5.372	1	1
3.0	6.685	1	2
3.0	4.954	½	2
3.0	5.965	2	2
4.0	7.528	1	1
4.0	5.539	1	1
5.0	7.223	1	1
5.0	7.029	1	1
5.0	8.902	½	2
5.0	7.321	½	2
5.0	8.429	2	2

the protons at the surface. The experimental value (found from Figure 5.12) gives a value of 0.043 mol.dm^{-3} in approximate agreement with the calculated value.

5.1.2.4 DISSOLUTION AT pH 6.11 USING SØRENSEN'S CITRATE BUFFER

The solutions used for experiments carried out in this section were made up as described in Section 4.1.5.5. At first experiments were carried out at various rotation speeds, with a constant supply of pure N_2 being bubbled through the reaction solution (to prevent the build-up of CO_2).

Further experiments were carried out altering the concentration of the buffer components. Table 5.7 lists the fluxes as a function of rotation speed and also indicates the concentration of buffer used, as well as the different crystals used.

Figure 5.13 shows the fluxes plotted as a function of $\omega^{\frac{1}{2}}$. As can be seen there is a non-zero intercept and a linear dependence upon $\omega^{\frac{1}{2}}$. This suggests a surface controlled reaction is occurring as well as a transport controlled reaction.

A question arises as to the identity of the species in the rate determining step. Is it the transport of protonated citrate (CH) or of H^+ across the diffusion layer? The Levich equation (3.28) can be employed to calculate the expected slope of Figure 5.13 for both cases. For H^+ transfer:

$$J/\sqrt{\omega} = 1.554\ \nu^{-1/6}\ D_{H}^{2/3}\ [H^+]_\infty \qquad 5.8$$

$$= 4.678 \times 10^{-12}\ \text{mol.cm}^{-2}\text{s}^{-3/2}$$

while for the case of protonated citrate:

$$J/\sqrt{\omega} = 1.554\ \nu^{-1/6}\ D_{CH}^{2/3}\ [CH]_\infty \qquad 5.9$$

D_{HC} can be estimated using the formula of Bidstrup and Geankoplis[7] (equation 3.45):

$$D_{HC} = \frac{6.6 \times 10^{-8}\ (\chi M)^{\frac{1}{2}} T}{V^{0.6}}$$

The symbols being as previously defined,

$$D_{HC} \approx 5.901 \times 10^{-6}\text{cm}^2\text{s}^{-1}$$

substituting this value into equation 5.9 gives:

$$J/\sqrt{\omega} = 2.22 \times 10^{-9}\ \text{mol.cm}^{-2}\text{s}^{-3/2} \qquad 5.10$$

in agreement with the measured slope. Thus the rate determining step at this pH is the transport of protonated citrate to the calcite surface. Thus the overall rate of dissolution can be given by:

$$J = k_1[H^+] + k_2 \qquad 5.11$$

k_2 = surface controlled reaction

k_1 = rate constant for H^+ transfer.

In the presence of weak acids which dissociate then $[H^+]$ should be replaced by [weak acid] and the diffusion coefficient used in k_1 should be replaced accordingly.

The reaction giving rise to the surface controlled rate constant is attributable to the reaction of water with the calcite surface i.e.,

$$CaCO_3 + H_2O \rightarrow Ca^{2+} + HCO_3^- + OH^- \qquad 5.12$$

The reason for this reaction being non-transport controlled, is the large quantity of water present. The OH^- produced is rapidly protonated by the buffer system forming H_2O.

The dissolution rate was then measured with a mixture of N_2/CO_2 passing through the reaction solution, using the gas mixing system described in Section 4.1.2. An air bleed had to be constructed to reduce the pressure of the gas before bubbling it into the reaction solution. The partial pressures of carbon dioxide used were 0.091 and 0.167 atm. Table 5.8 shows the flux as a function of $\omega^{\frac{1}{2}}$ and ρCO_2, also indicating where a new crystal was used.

As can be seen from Figure 5.14, the rate of dissolution increases with ρCO_2 and shows a linear dependance

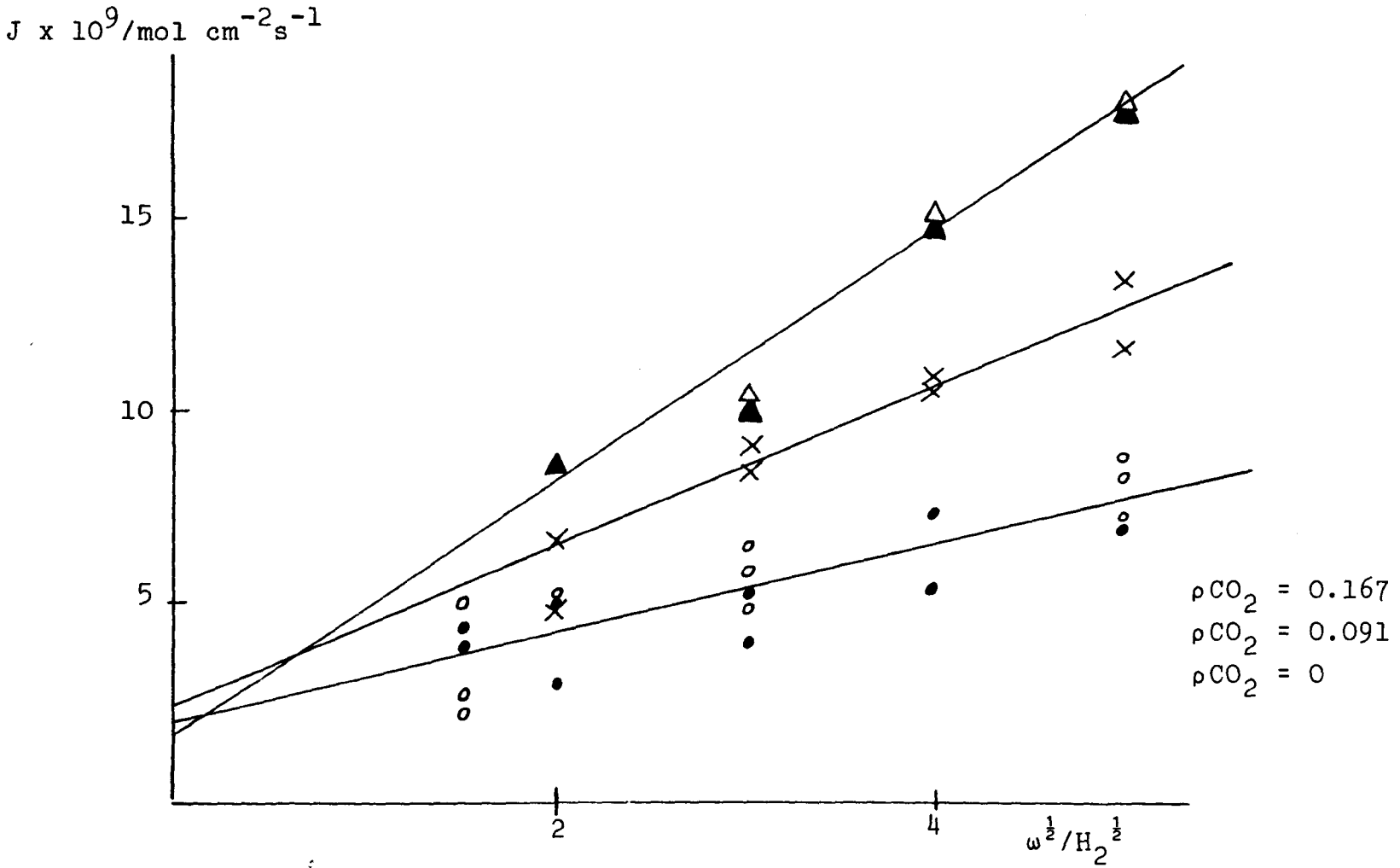

FIGURE 5.14 Plot of J vs. $\omega^{\frac{1}{2}}$ at pH = 6.11

TABLE 5.8 Dissolution at pH 6.11 at various values of ω and ρCO_2.

$\omega^{\frac{1}{2}}/H_2^{\frac{1}{2}}$	FLUX x 10^9/mol.cm^{-2}s^{-1}	ρCO_2/atm.	CRYSTAL NUMBER
2	6.761	0.091	2
2	5.966	0.091	3
3	8.512	0.091	2
3	9.235	0.091	2
4	10.583	0.091	2
4	11.006	0.091	3
5	11.663	0.091	3
5	13.457	0.091	2
2	7.911	0.167	2
2	8.640	0.167	3
3	11.540	0.167	2
3	11.139	0.167	3
4	15.223	0.167	3
4	14.733	0.167	3
5	18.192	0.167	3
5	17.939	0.167	2

on $\omega^{\frac{1}{2}}$. The slopes from Figure 5.14 were measured and they are plotted as a function of ρCO_2 in Figure 5.15 showing that the slopes vary linearly with ρCO_2.

This suggests that the transport controlled reaction could be caused by the reaction of carbonic acid with the calcite surface i.e.,

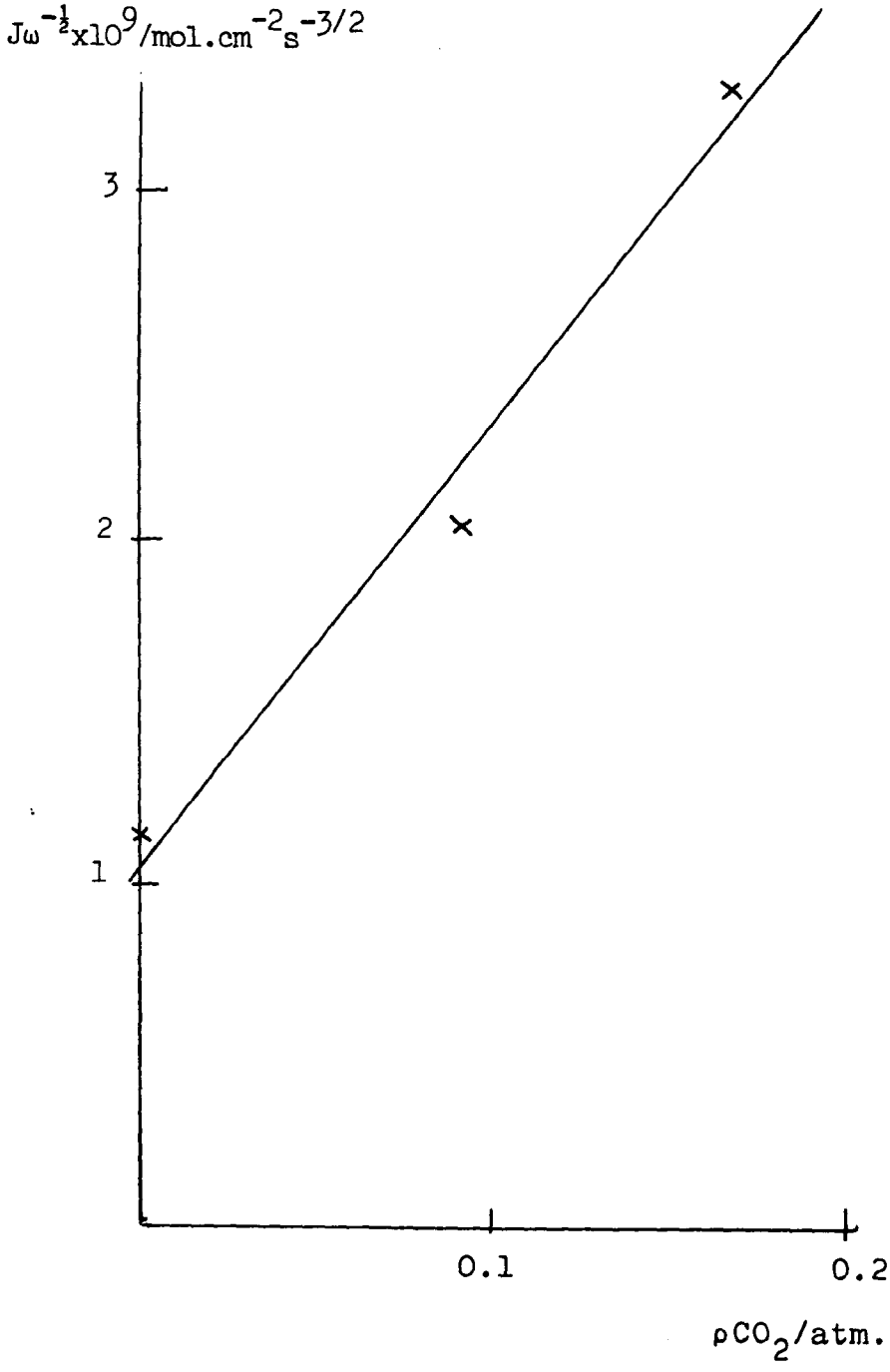

FIGURE 5.15 Plot of $J/\omega^{\frac{1}{2}}$ vs. ρCO_2.

$$CO_2 + H_2O \rightleftharpoons H_2CO_3 \qquad 5.13$$

$$H_2CO_3 + CaCO_3 \rightarrow Ca^{2+} + 2HCO_3^- \qquad 5.14$$

Thus, the rate of dissolution is being controlled by three processes, two transport controlled, H^+ and H_2CO_3, and the H_2O surface controlled reaction. Thus the overall rate of dissolution can be given by:

$$J = k_2 + k_1[H^+] + k_3[H_2CO_3] \qquad 5.15$$

$$= k_2 + 1.554\ \nu^{-1/6}\{D_{H^+}^{2/3}[H^+] + D_{H_2CO_3}^{2/3}[H_2CO_3]\}\sqrt{\omega} \qquad 5.16$$

This assumes that the equilibrium

$$H_2O + CO_2 \overset{k_{hyd}}{\rightleftharpoons} H_2CO_3 \qquad K_{H_2CO_3} = \frac{[H_2CO_3]}{[CO_2]}$$

is so slow that there is no supplementation of reacting H_2CO_3 in the vicinity of the rotating disc through the hydration of dissolved CO_2. This assumption is supported by literature values of 0.025 to 0.04 s^{-1} [9] for the hydration rate constant ($k_{hyd.}$). These values are "slow" on the rotating disc time scale[10] suggesting that we may confidently use equation 5.16 which may be written in

terms of the Henry's law constant K_H for the solubility of CO_2 in water. Thus equation 5.16 becomes:

$$J = k_2 + 1.554\ \nu^{-1/6}\{D_{H^+}^{2/3}[H^+] + D_{H_2CO_3}^{2/3} K_{H_2CO_3} K_H \rho CO_2\}\sqrt{\omega} \qquad 5.17$$

Thus, using the gradient of Figure 5.15 and, equation 5.7, i.e:

$$[CO_2]_{aq} = K_H \rho CO_2$$

then

$$D_{H_2CO_3}^{2/3} K_{H_2CO_3} = 5.3 \times 10^{-7} cm^{4/3} s^{-2/3}$$

The diffusion coefficient can be estimated using equation 3.45 yielding a value of $1.31 \times 10^{-5} cm^2 s^{-1}$. This thus gives a value for $K_{H_2CO_3}$ of 9.597×10^{-4}. This value is compared with other literature values in Table 5.9 , and as can be seen satisfactory agreement is obtained. This may be taken to vindicate the form of equation 5.17 and the kinetic model on which it is based.

It should be noted that all three lines shown in Figure 5.14 have a similar intercept. The average value is:

$$k_2 = 2.1 \pm 0.3 \times 10^{-9}\ mol.cm^{-2} s^{-1}$$

TABLE 5.9 Comparison of values for $K_{H_2CO_3}$ at 25°C

AUTHOR	$K_{H_2CO_3}$	REFERENCE
Bolin[11]	9.091×10^{-4}	12
Barth[12]	2.591×10^{-3}	13
Skirrow[13]	2.00×10^{-3}	14
This work	9.579×10^{-4}	

It should be stressed that the points shown in this figure were obtained using a number of different crystals, and that where a crystal was used more than once, it was freshly prepared before each run. This shows the reproducibility of the surfaces used and also allows comparisons to be made with confidence between data obtained using different experimental conditions.

5.1.2.5 DISSOLUTION OF GROUND BUT UNETCHED CRYSTALS

It has been shown in the previous section that the overall rate of dissolution of Iceland Spar is described by equation 5.15:

$$J = k_1[H^+] + k_3[H_2CO_3] + k_2$$

This value of k_2 is, however, an order of magnitude greater than the values quoted by Plummer *et al.*,[14] who found $k_2 = 1.2 \times 10^{-10}$ mol.cm^{-2}s^{-1} using crushed Iceland Spar. This discrepancy may be attributable to the different surface treatments. Plummer *et al.*, crushed

their Iceland Spar, wet sieved it, and then washed it in 10^{-3}M HCl for 10 seconds, compared to the prolonged treatment used to pretreat the rotating calcite disc in this work.

Figure 5.16 shows electron micrographs of the surface of the rotating disc after polishing, and after polishing and etching. The surface before etching is smooth down to the resolution of the S.E.M.. After etching, however, the surface has become roughened and pits can be seen.

Experiments were, therefore, carried out in which Iceland Spar rotating discs were polished but not etched. The crystals were polished to different degrees of smoothness (as defined by the smallest diamond spray used in the polishing). As described in Section 4.1.5.6 the dissolution of these discs was measured in 0.3M KCl for 7000 seconds with a stream of pure N_2 bubbling through the solution at all times. Table 5.10 lists the measured fluxes as a function of grit size ($\sim$ roughness) and Figure 5.17 shows the plot of flux versus grit size.

The intercept of this graph gives the rate of dissolution for a "smooth polished crystal". From Figure 5.17 this gives a value of 1.4×10^{-10} mol.cm^{-2}s^{-1} in good agreement with the value of Plummer et al.

From Figure 5.16 the average dimension of the etch pits of the treated surfaces are $\sim$ 150 μm. Extrapolation of Figure 5.17 to 150 μ gives a dissolution rate of 1.9×10^{-9} mol.cm^{-2}s^{-1}, in excellent agreement with the measured value.

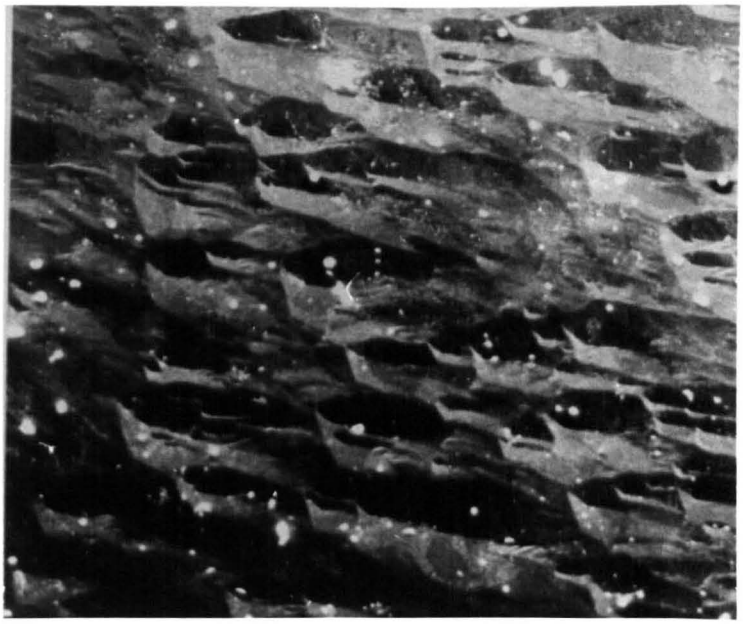

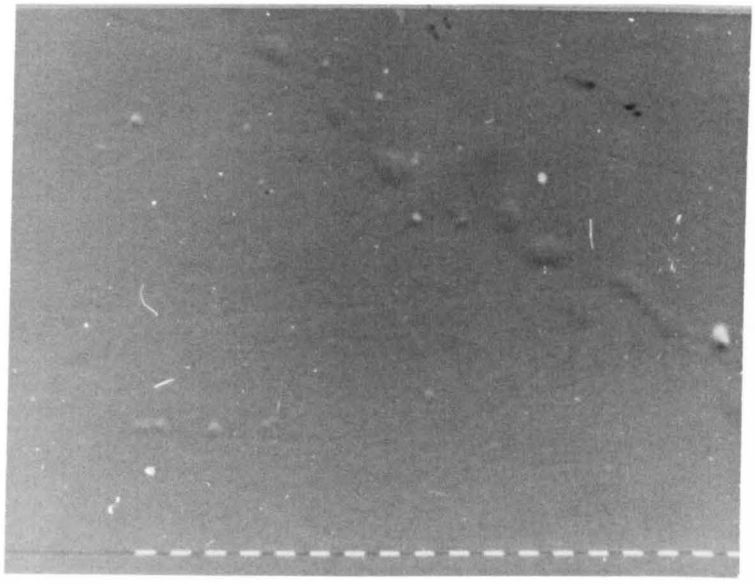

FIGURE 5.16 S.E.M. of etched calcite surface and polished surface

6.85 cm = 100 μ

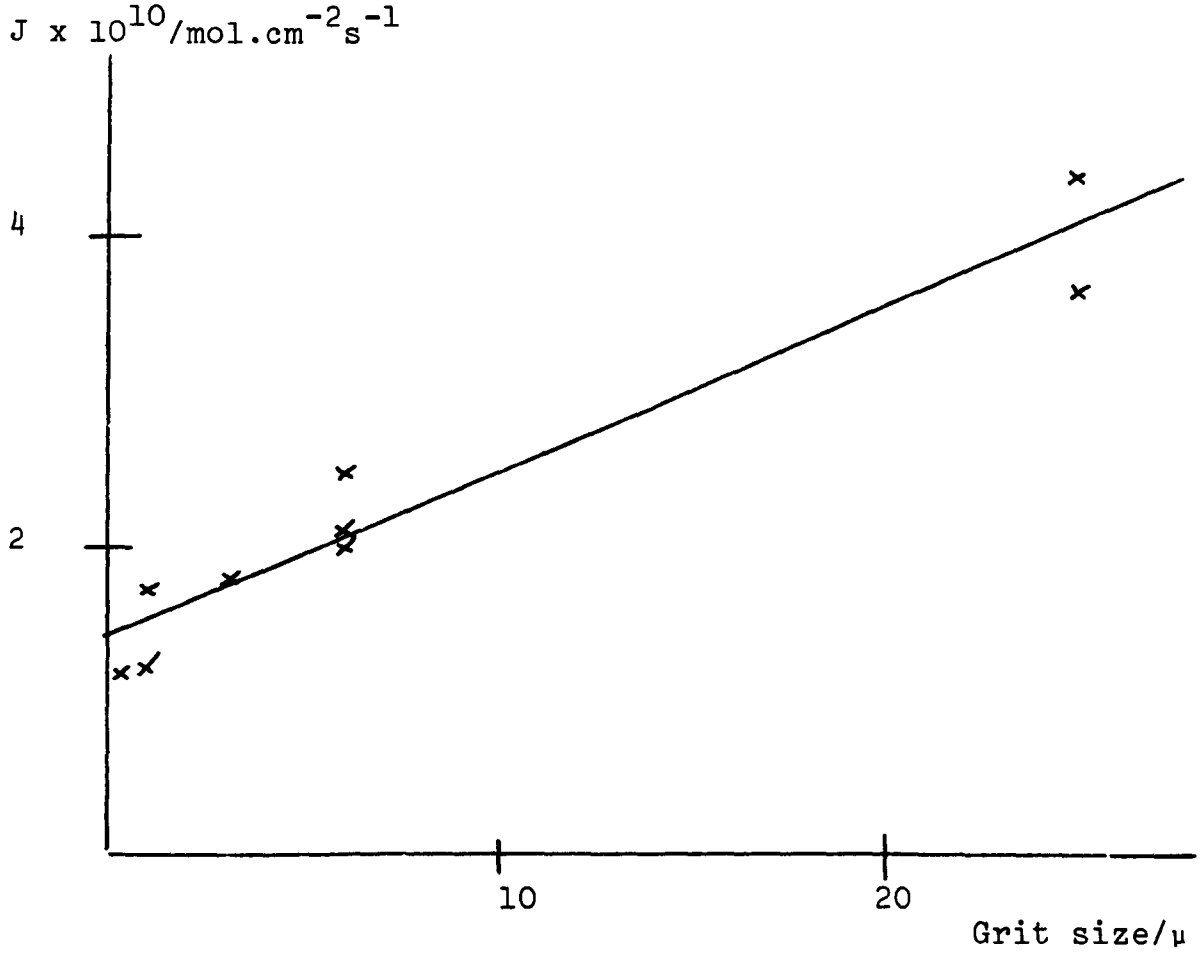

FIGURE 5.17 Plot of J vs. grit size.

TABLE 5.10 Flux of dissolving calcium as a function of grit size.

GRIT SIZE/μ	FLUX x 10^{10}/mol.cm^{-2}s^{-1}
¼	1.201
1	1.1743
1	1.242
6	2.446
6	2.029
6	2.062
25	4.370
25	3.637

To return to the work of Sjöberg and Rickard, mentioned in Section 1.1; their values obtained using the rotating disc were far different to both the work of Plummer et al., and with that obtained during the course of this work. However, their discs were only polished down to 30μ, and from extrapolating Figure 5.17 their values lie quite close to the expected line of flux vs. grit size.

Another reason for disagreement is that Sjöberg and Rickard used the initial rate of the reaction to find the flux while this work, and that of Plummer et al., have used the final rates.

5.1.2.6 DISSOLUTION OF CLEAVED CRYSTALS

Clearly, surface roughness plays an important role in governing the rate of dissolution. Implicit in this is the notion that the history of the calcite will effect the dissolution rate: the more the sample has been dissolved, the rougher the surface will become, and thus the

dissolution rate will increase.

Figure 5.18 shows a dissolution experiment carried out in 10^{-3}M HCl on a freshly cleaved Iceland Spar surface subjected to no polishing or etching (Section 4.1.1.4) As is apparent, at first there is no dissolution, but as the reaction progresses the rate steadily increases up to the expected value.

This transition corresponds to the surface changing from being essentially flawless, with no sites available for dissolution to occur - to being fully roughened (as shown in Figure 5.16).

It has already been shown that the rate of dissolution, at this pH, for fully roughened surfaces is governed by the rate of H^+ transfer to the rotating disc's surface. However, from Figure 5.18 it is apparent that this does not apply to a flawless surface, i.e., the rate of reaction is only controlled by H^+ transport when the surface has been roughened, creating kink sites for the dissolution to occur at.

The theory of three dimensional nucleation has been developed by Harrison and Thirsk[15] and it predicts that for instantaneous nucleation, with the slow step being the dissolution at the edges of nucleii, the rate is given by:

$$J = J^{\infty}\left(1 - [\exp - (\alpha t^2)]\right) \qquad 5.18$$

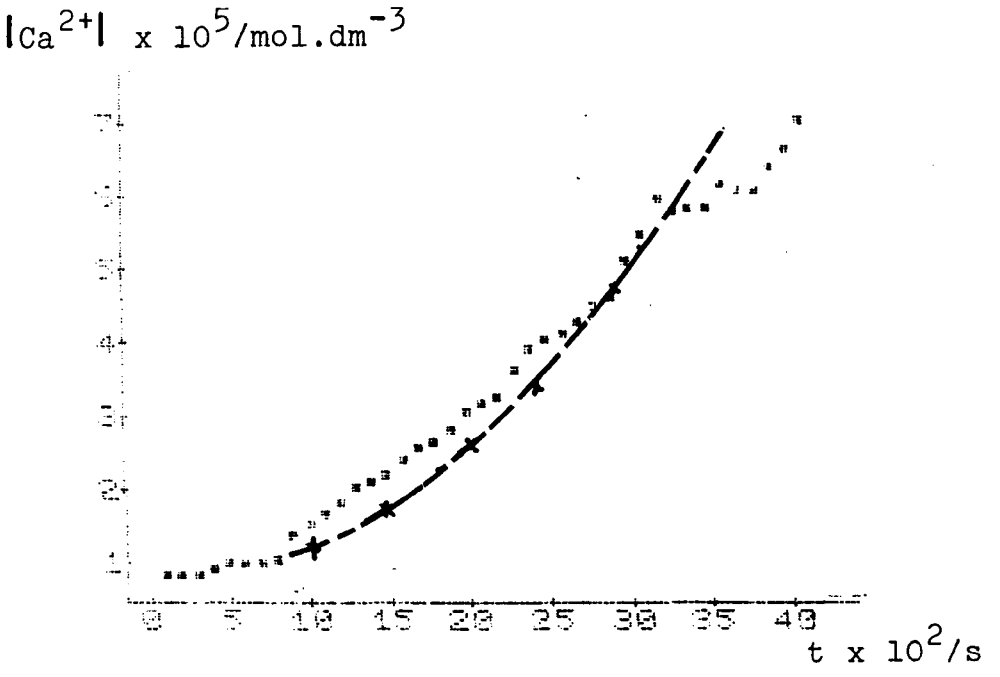

FIGURE 5.18 Plot of $[Ca^{2+}]$ vs. time for a cleaved Iceland Spar crystal at pH 3.

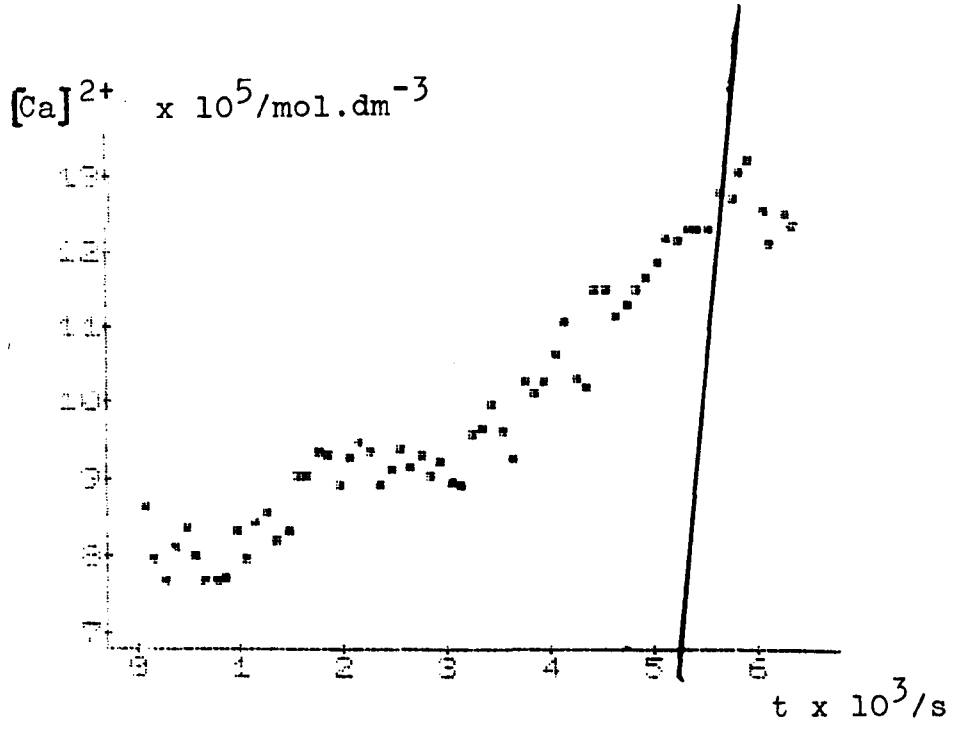

FIGURE 5.19 Plot of $[Ca^{2+}]$ vs. time for a cleaved Iceland Spar crystal at pH 6.11.

J^{∞} = steady state dissolution rate

α = constant, dependant upon the number of nucleation sites and the rate constant for the dissolution at the edge of the nucleus.

The dashed line in Figure 5.18 is the integrated form of equation 5.18 i.e:

$$[Ca^{2+}]-[Ca^{2+}]_o = J^{\infty}\left(t-\tfrac{1}{2}\sqrt{\pi}/\alpha \ \mathrm{erf}(\sqrt{\alpha}t)\right) \qquad 5.19$$

showing that satisfactory agreement is seen between theory and experiment.

Further experiments were carried out in 6.11 buffer using these unpolished unetched crystals, and Figure 5.19 shows the dissolution for a typical experiment. The solid line is the rate expected from equation 5.11 for a fully roughened surface. Even after 6000s. the rate of dissolution is still an order of magnitude less than the expected value.

If equation 5.18 applies, then it would be expected that:

$$[Ca^{2+}] - [Ca^{2+}] \propto J^{\infty} \ \frac{\alpha t^3}{3} \qquad 5.20$$

TABLE 5.11 Comparison of the k_2 values obtained using different calcite samples.

AUTHOR	SAMPLE	k_2/mol.cm^{-2}s^{-1}
Plummer et al.,[14]	Crushed Iceland Spar	1.10×10^{-10}
This work	Rotating disc	1.4×10^{-10}
This work	Powder BDH	1.34×10^{-10}
House et al.,[16]	Powder BDH	1.35×10^{-10}
House et al.,[16]	Powder Calopake F	3.61×10^{-11}

Figure 5.20 shows such a plot, the slope drawn in having the expected value of 3, showing reasonable agreement with the theory.

These results would seem to indicate that the measured rate of dissolution will be dependant on the history of the calcium carbonate sample. However, there exists an agreement between the value obtained using polished, but unetched, rotating discs, with that of Plummer. To establish whether this agreement is coincidental, work was carried out repating Plummer's work on dissolution, using BDH powder, shown to consist of small rhombahedral particles <5μm in diameter;[16] details of this work will be given later. The rate constant measured was 1.34×10^{-10} $mol.cm^{-2}s^{-1}$, showing good agreement. These values are listed in Table 5.11. Also shown in Table 5.11 are the values measured by House et al.,[16] for the precipitation of calcium carbonate using the same BDH powder and also for Calopake F, a commercially prepared calcite of large specific area 5.65 m^2g^{-1}. Agreement is seen for the BDH sample, but not for the Calopake F.

This agreement may be understood if the following assumptions are made:

1. The exposed calcite surfaces are the cleaved (100) planes of Iceland Spar and
2. The surface has not been subjected to prolonged dissolution in aqueous media.

The first point is obviously true for the rotating disc

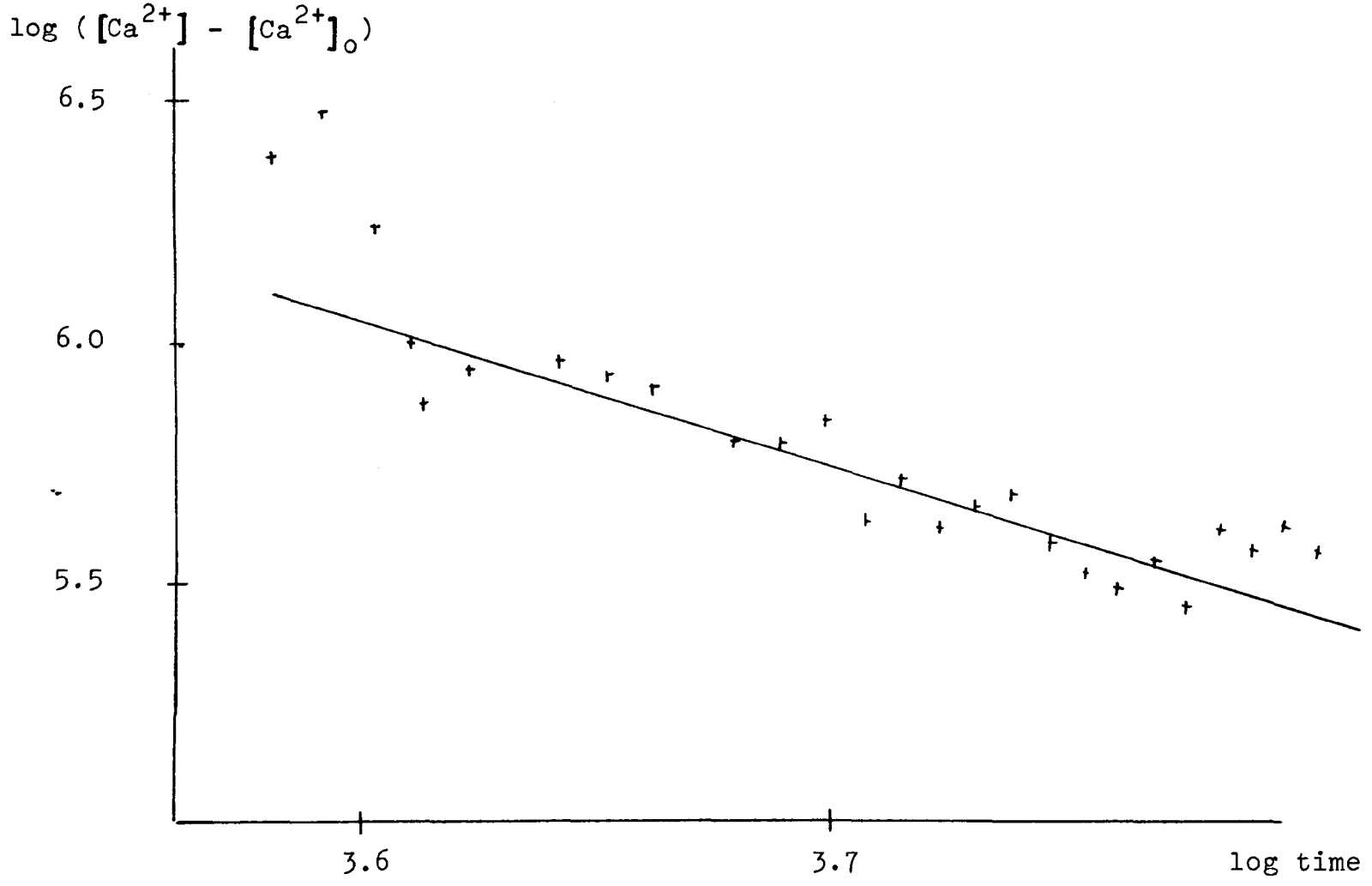

FIGURE 5.20 Plot of log ($[Ca^{2+}] - [Ca^{2+}]_o$) vs. log time.

as the Iceland Spar crystal is positionedto expose this face. It is also likely to be the case for Plummer's samples as in crushing his sample the Iceland Spar will cleave preferentially along the (100) plane. The second point is true for all of the experiments. Thus, flawless Iceland Spar, either cleaved or ground, (either by polishing or in the form of powders), which has suffered no previous dissolution will dissolve at a rate of 1.3×10^{-10} $mol.cm^{-2}s^{-1}$.

However, this value will increase as the surface is subjected to dissolution and surface roughening. It will also be different if the exposed crystal faces are different from the (100) cleavage plane, and this is probably the reason why Calopake F shows a different rate constant to the other samples. In the formation of the large surface area the normal cleavage rhombs are destroyed.

5.1.2.6 DISSOLUTION OF ANGLED CRYSTALS

To study the effect of changing the exposed crystal face the dissolution rate was measured in a set of rotating disc experiments in which the crystals had deliberately been set at an angle, θ, to the normal cleavage plane, using the apparatus described in Section 4.1.1.3. The dissolution of these crystals was measured in 0.3M KCl for 7000s. and the fluxes were found. Table 5.12 lists the measured flux as a function of θ and the dependance of flux on θ is shown in Figure 5.21.

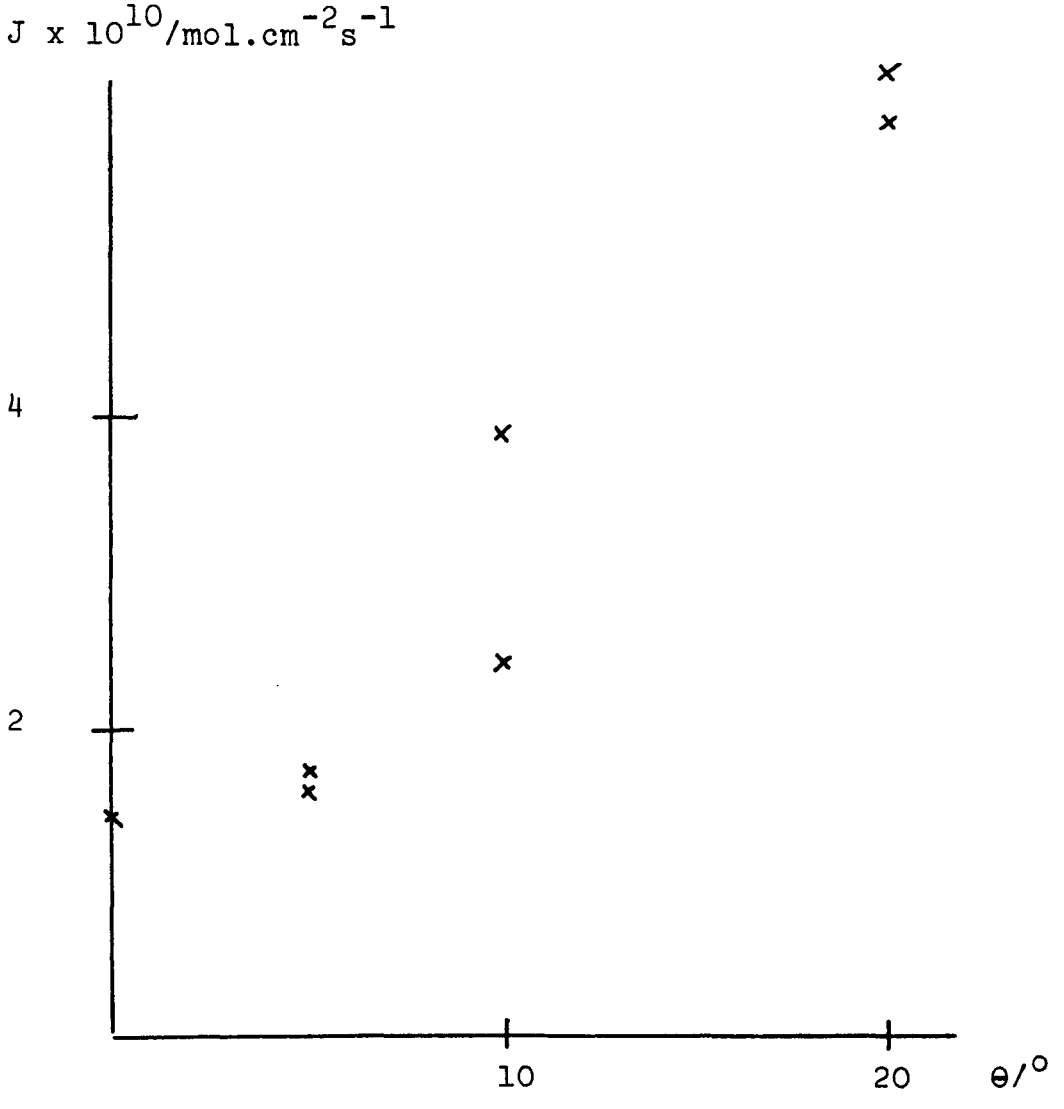

FIGURE 5.21 Plot of J vs. θ

TABLE 5.12 Flux of dissolving calcium as a function of θ

$\theta/^{o}$	FLUX x 10^{10}/mol.cm^{-2}s^{-1}
0	1.41
5	1.634
5	1.712
10	2.431
10	3.980
20	6.209
20	5.903

This linear dependance can be understood if it is assumed that the increased dissolution rate is due to there being an increase in the number of dissolution sites available because of the terraces introduced into the crystal surface by polishing the disc at an angle to the crystal plane (Figure 5.22).

Dissolution is thought to take place more readily at terraces because of the presence of kinks on the terraces (Figure 5.23). Dissolution will preferably occur at kinks because these sites have less nearest neighbour interactions.

Simple geometry shows that the number of terraces N_T is given by:

$$N_T \propto \tan\theta \propto \theta \quad \text{(for small } \theta\text{)}$$

and if the number of kinks is assumed to be α the number of terraces, then this is in agreement with the data shown in Figure 5.21.

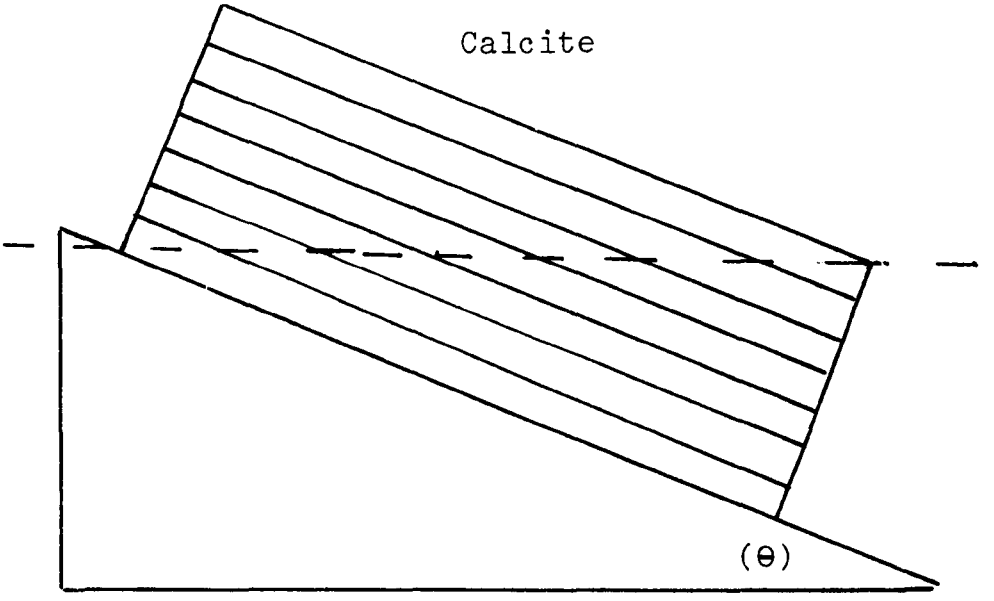

FIGURE 5.22 A crystal cast at an angle (θ) when ground horizontal to the surface exposed cuts across the (100) planes.

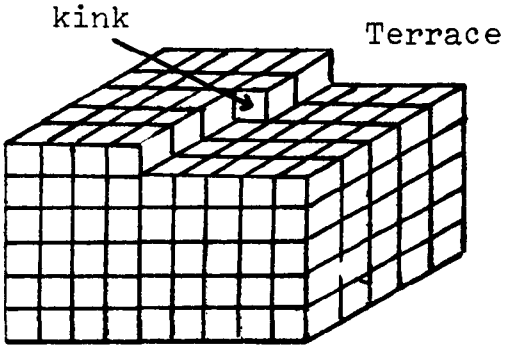

FIGURE 5.23 The surface of a crystal showing kink and terraces

Support for the idea that the increased rate observed with increasing θ comes from S.E.M.'s taken off the samples after dissolution (Figure 5.24). Macroscopic terraces are clearly visible and the number increases with θ. It may be assumed that the number of macroscopic terraces observed are α to the number of terraces initially formed. Hence the observed increase in flux may be concluded as being due to the increase in the number of terraces formed on the surface.

In conclusion it has been shown that the dissolution of Iceland Spar is strongly influenced by the surface morphology of the sample. In particular:

1. Freshly cleaved flawless surfaces are essentially unreactive, even in 10^{-3}M HCl. As dissolution proceeds, however, the surface becomes roughened and the rate increases, until eventually a steady state is obtained. This transition can be described in terms of an equation derived assuming three dimensional instantaneous nucleation, i.e.,

$$J = J^{\infty} \left(1 - [\exp -(\alpha t^2)]\right)$$

2. Good agreement is found between different samples and different experimental methods in the case of cleaved or polished Iceland Spar which has not previously been subjected to dissolution. In this case $k_2 = 1.30 \times 10^{-10}$ mol.cm^{-2}s^{-1}.
3. Surfaces obtained by misorientating the crystal dissolve faster that the (100) cleavage plane becomes more terraces, and thus more kinks are produced at which dissolution can occur.

a

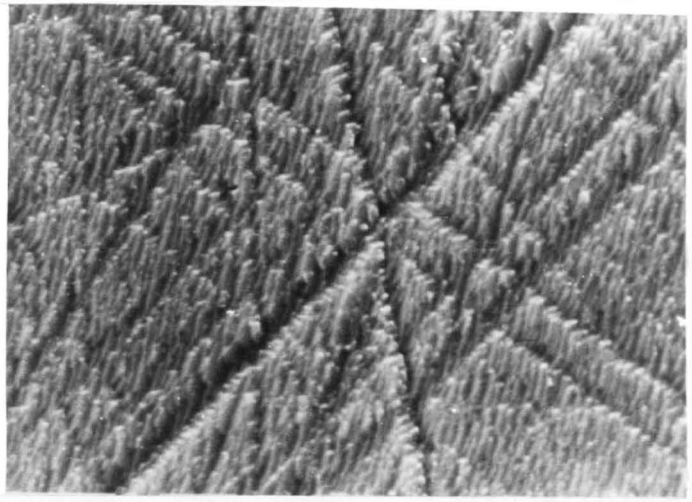

b

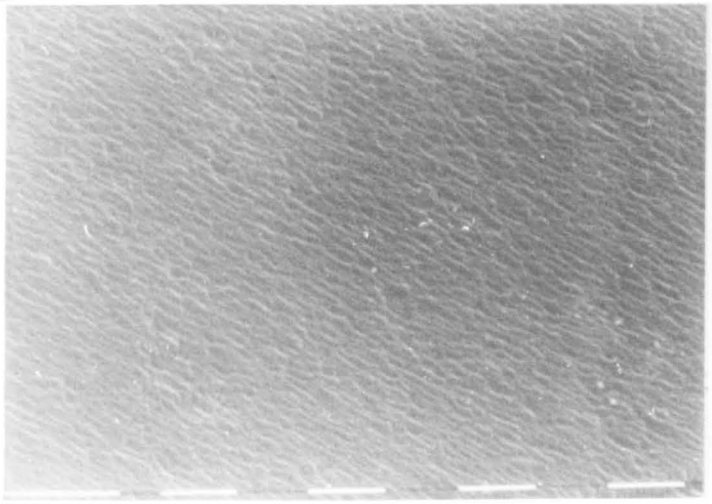

c

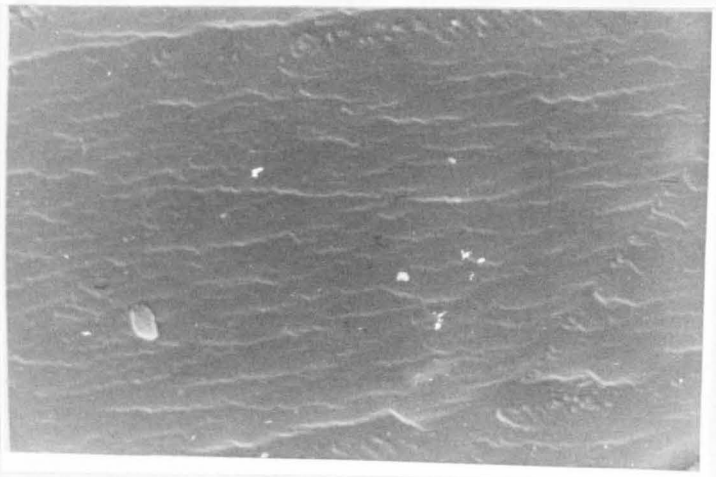

d

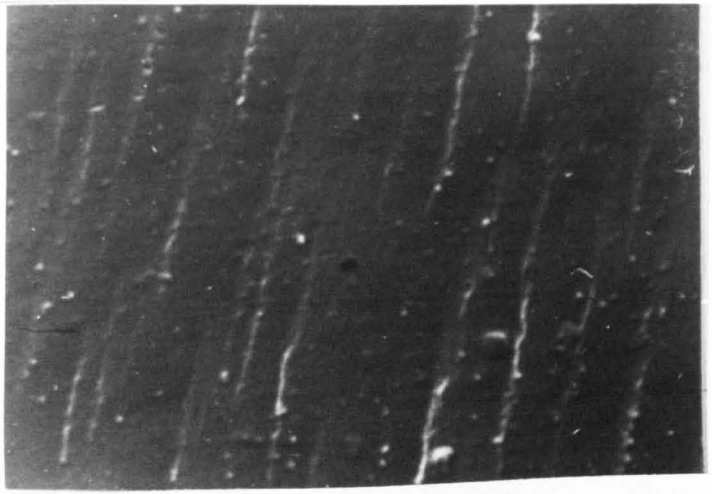

FIGURE 5. S.E.M. of calcite crystals cast at an angle (a) 20°, (b) 10°, (c) 5° and d 0° 1.26 cm = 10 μ

5.1.2.7 DISSOLUTION IN THE PRESENCE OF COPPER(II) IONS

As described in Section 4.1.5.7. dissolution experiments were carried out on flat single crystals in 0.3 $mol.dm^{-3}$ KCl with copper(II) chloride present in the reaction solution. The concentration range of copper(II) ions used was from 10^{-6} to 10^{-3} $mol.dm^{-3}$. The dissolution rate was measured, and the flux of dissolving calcium calculated. These fluxes are listed as a function of copper ion concentration in Table 5.13 and are shown in Figures 5.25 - 5.27. In all cases (10^{-6}, 10^{-5}, 10^{-4} $mol.dm^{-3}$ Cu^{2+}), the flux is far less than the standard run showing the inhibiting effect of copper(II) ions on the dissolution rate. A further point of interest is that instead of dissolution reaching a steady rate and then continuing, the rate of dissolution slows down with time in the presence of copper (see especially Figure 5.26, the dissolution in the presence of 10^{-5} $mol.dm^{-3}$ Cu^{2+}). This effect is far less apparent in the presence of 10^{-4} $mol.dm^{-3}$ Cu^{2+}.

The dissolution was also measured in the presence of 10^{-3} $mol.dm^{-3}$ Cu^{2+}. However, no measurable increase of calcium could be detected, even after 10,000 seconds of rotation in the reaction solution.

Thus, as can be seen, the presence of 10^{-3} $mol.dm^{-3}$ Cu^{2+} is sufficient to totally inhibit the dissolution of calcite while the presence of 10^{-6} $mol.dm^{-3}$ Cu^{2+} reduces the rate by approximately half by sticking onto the available kink sites. Once these sites are occuped by copper ions

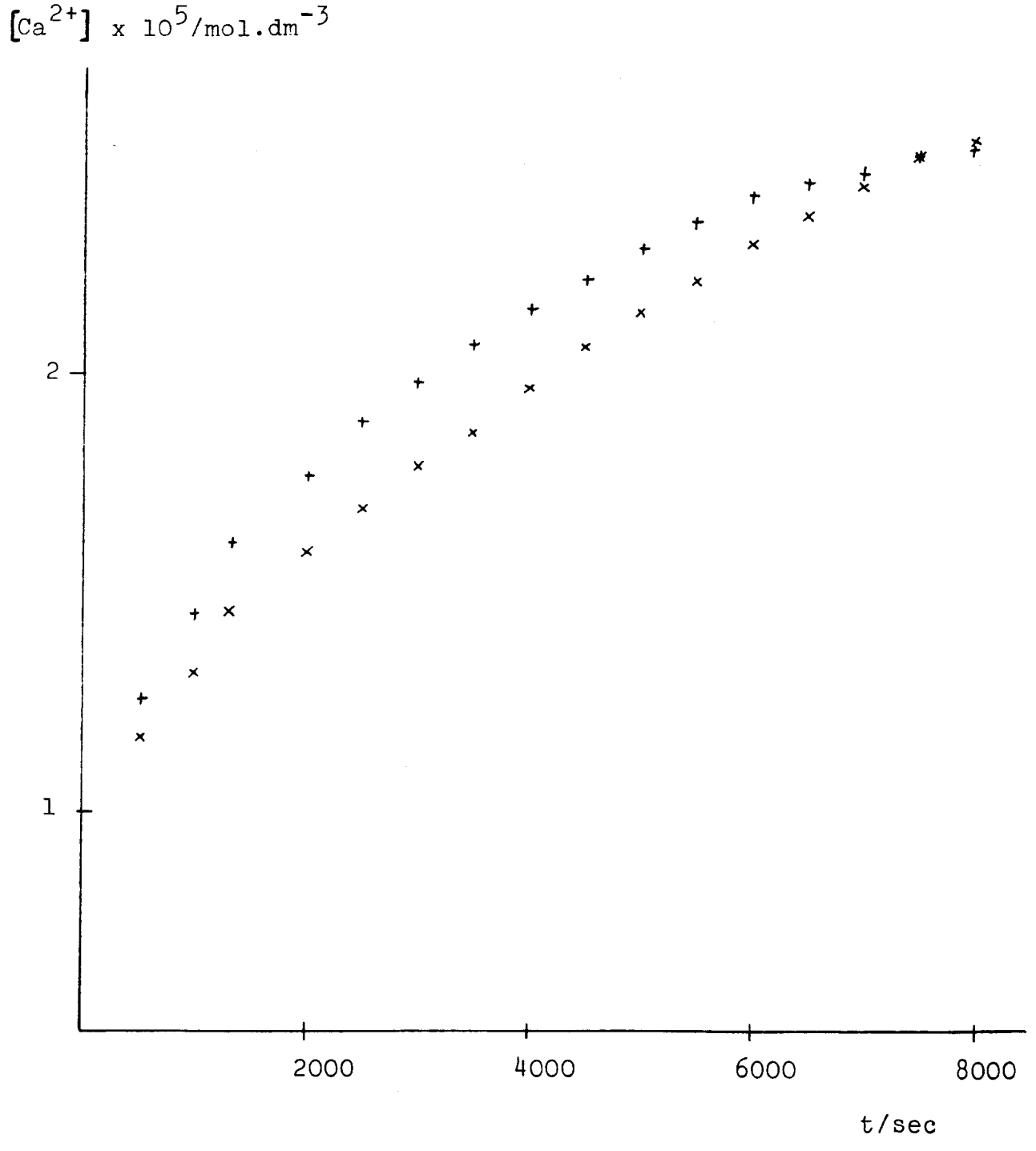

FIGURE 5.25 Dissolution of Ca^{2+} in the presence of 10^{-6}M Cu^{2+}

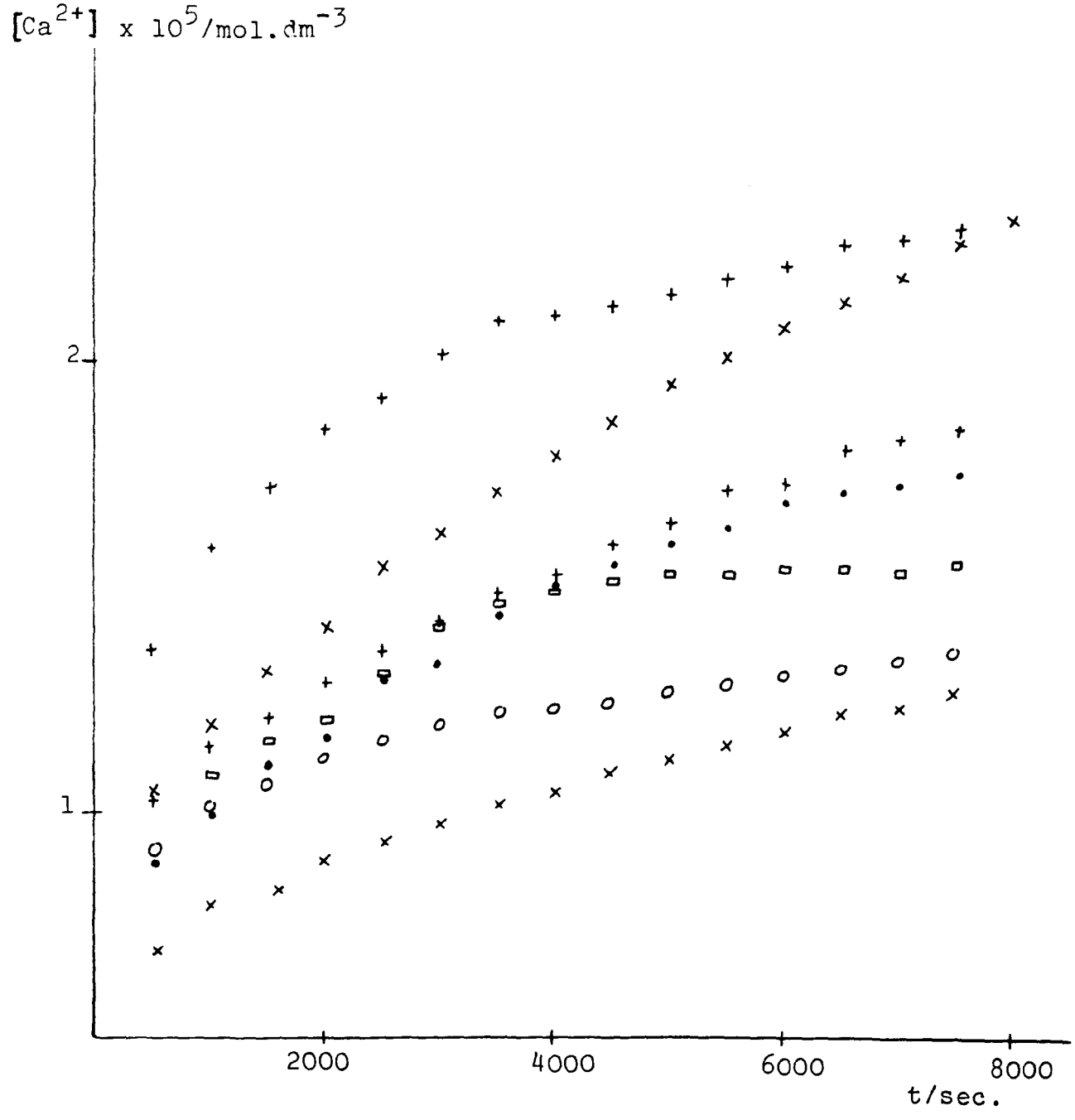

FIGURE 5.26 Plot of Ca^{2+} vs. time in the presence of 10^{-5}M Cu^{2+}

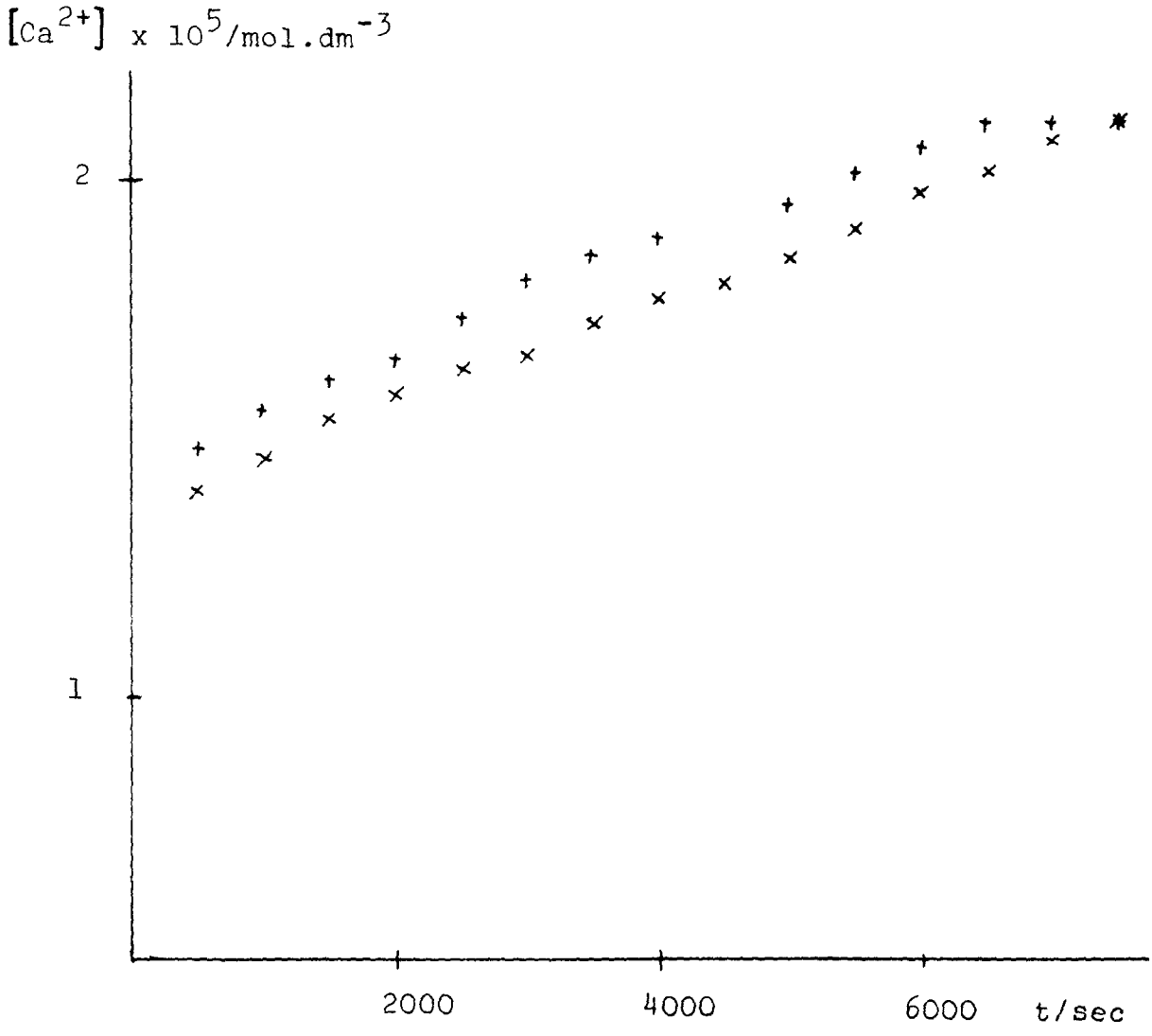

FIGURE 5.27 Dissolution of Ca^{2+} in the presence of 10^{-4}M Cu^{2+}

TABLE 5.13 Flux of dissolving calcium as a function of $[Cu^{2+}]$

$[Cu^{2+}]$/mol.dm^{-3}	FLUX x 10^{10}/mol.cm^{-2}s^{-1}
1 x 10^{-6}	4.65
1 x 10^{-6}	4.99
1 x 10^{-5}	7.64
1 x 10^{-5}	3.91
1 x 10^{-5}	5.69
1 x 10^{-5}	3.61
1 x 10^{-5}	5.97
1 x 10^{-5}	6.04
1 x 10^{-5}	4.53
1 x 10^{-4}	9.27
1 x 10^{-4}	8.47

then they can no longer act as sites for dissolution, and thus the rate falls. 10^{-6} mol.dm^{-3} copper solution exhibits such a large effect because only mono kink coverage is required. This is the reason why increasing the copper concentration up to 10^{-4} mol.dm^{-3} shows no additional inhibition. In fact, increasing the copper concentration actually reduces the inhibitory effect. This anomaly can be understood by considering the copper(II) ion in solution.

It exists in its hydrated form $Cu(H_2O)_6^{2+}$ which exhibits slightly acidic behaviour, i.e.,

$$Cu(H_2O)_6^{2+} \rightleftharpoons Cu(H_2O)_5 OH^+ + H^+ \qquad 5.20$$

The equilibrium constant for this has been reported in the literature as between $10^{-6.8}$ - $10^{-7.4}$ and the measured change in pH at different $[Cu^{2+}]$ corresponds well with the value of K. Thus, it is this decrease in pH, caused by increasing the concentration of Cu^{2+} which reduces the inhibitory effects measured. Total inhibition is shown when $[Cu^{2+}]$ reaches 10^{-3} mol.dm^{-3} as this concentration leads to the formation of a layer of copper carbonate on the crystal surface, as can be seen from Figure 5.27. This shows an electronmicrograph taken of a calcite crystal after dissolution in the presence of 10^{-3}mol.dm^{-3} Cu^{2+}. Instead of the steps which are normally observed, the surface has a porous structure as a thin layer of copper carbonate is formed.

5.1.2.8 CHALK ROTATING DISCS

Chalk rotating discs were formed as described in Section 4.1.1.5. The surface could not be polished with the diamond sprays, as the porous nature of the sample absorbed the lapping fluid. The surface was, therefore, only polished down to 30μ using the 600 Brammet pads. The dissolution of these discs was then measured in 0.3M KCl, and the flux was found to be 1.39 x 10^{-9} mol.cm^{-2}s^{-1}.

Cleaved chalk samples were also prepared and when the dissolution was measured for these the flux found was 1.25 x 10^{-9} mol.cm^{-2}s^{-1}. Both of these values are

FIGURE 5.27 S.E.M. of a calcite disc dissolved in the presence of 10^{-3}M Cu^{2+}

1.41 cm = 10 μ

higher than the values for polished Iceland Spar, even when the roughness factor is taken into account. This is probably due to the fact that chalk does not cleave along set cleavage planes, and thus the surface exposed is already rough and does not need dissolution to create kink sites. This can be seen from Figure 5.29 which shows S.E.M.'s of the chalk samples illustrating the flawed nature of the exposed surface.

5.2 ANALYSIS USING POWDERED CALCITE

This section will discuss the results obtained from precipitation and dissolution experiments performed on powdered calcite with a specific surface area of 0.22 m^2g^{-1},

5.2.1 PRECIPITATION WORK

As described in Section 4.3.6.1 these experiments consisted of adding a weighed amount of calcite seed suspension, to a calcium bicarbonate solution, and following the course of the reaction by measuring pH and conductivity values at set time intervals. These values were then analysed using the computer programmes described in Section 4.3.2.1 and 4.3.2.2, outputting values of the growth affinity (β) and the precipitation rate.

Table 5.14 lists the output from a typical precipitation experiment and Figure 5.30 shows how the precipitation rate varies as a function of time, the rate decreasing exponentialy with time. This is illustrated more usefully in Figure 5.31, where precipitation rate is

a

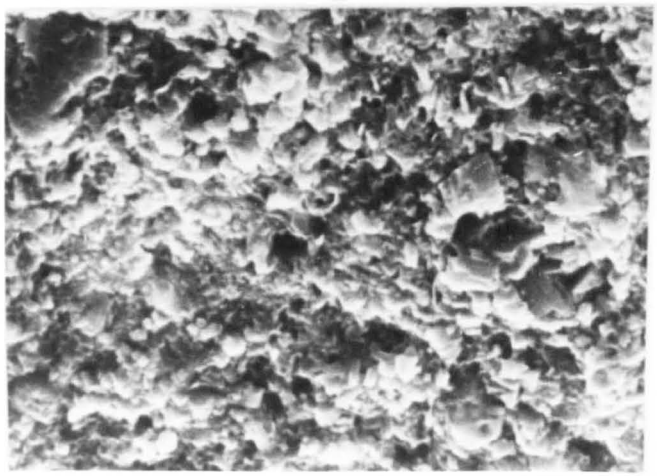

b

c

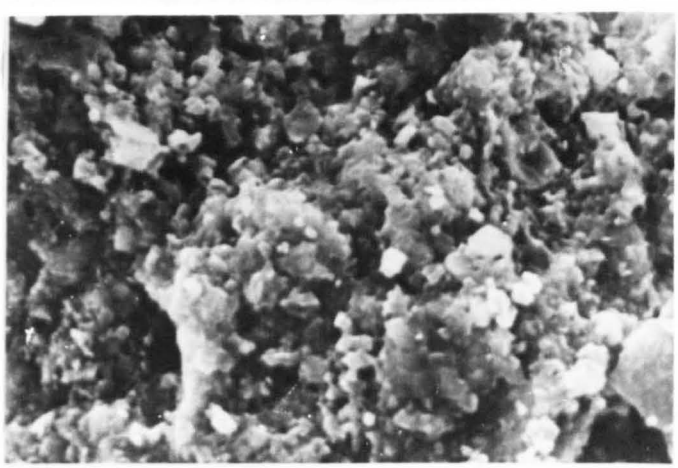

FIGURE 5.29 S.E.M. of chalk rotating discs (a) ground, (b) ground and dissolved (c) cleaved and dissolved, 1.17 cm 10 μ

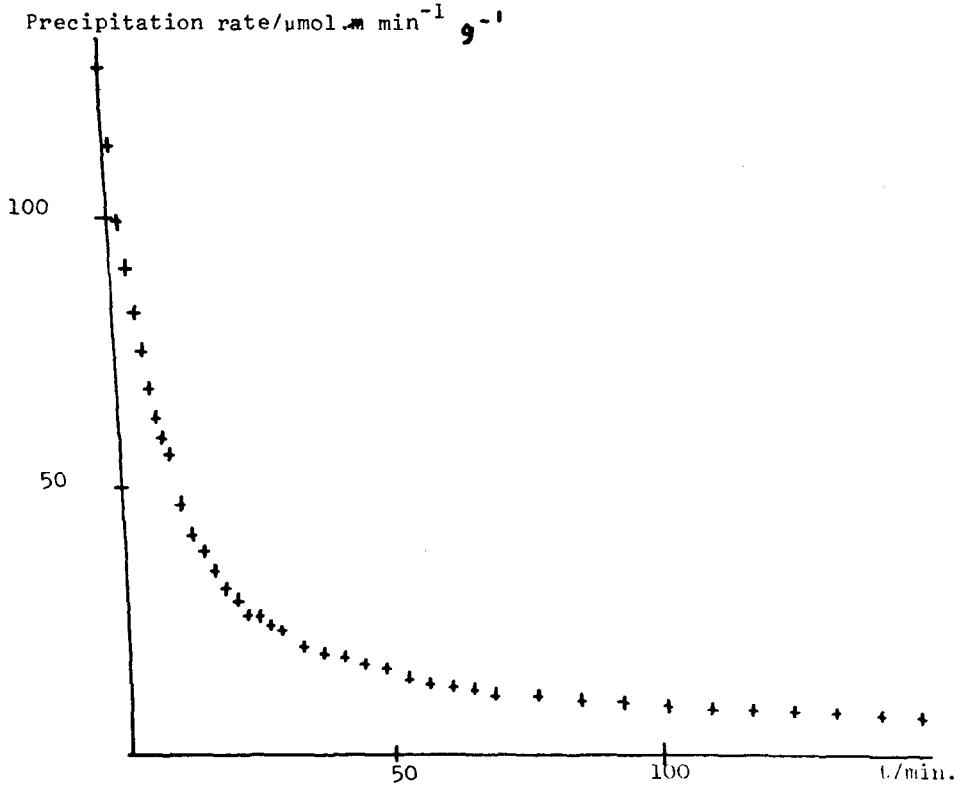

FIGURE 5.30 Graph of precipitation rate vs. time for a typical precipitation experiment.

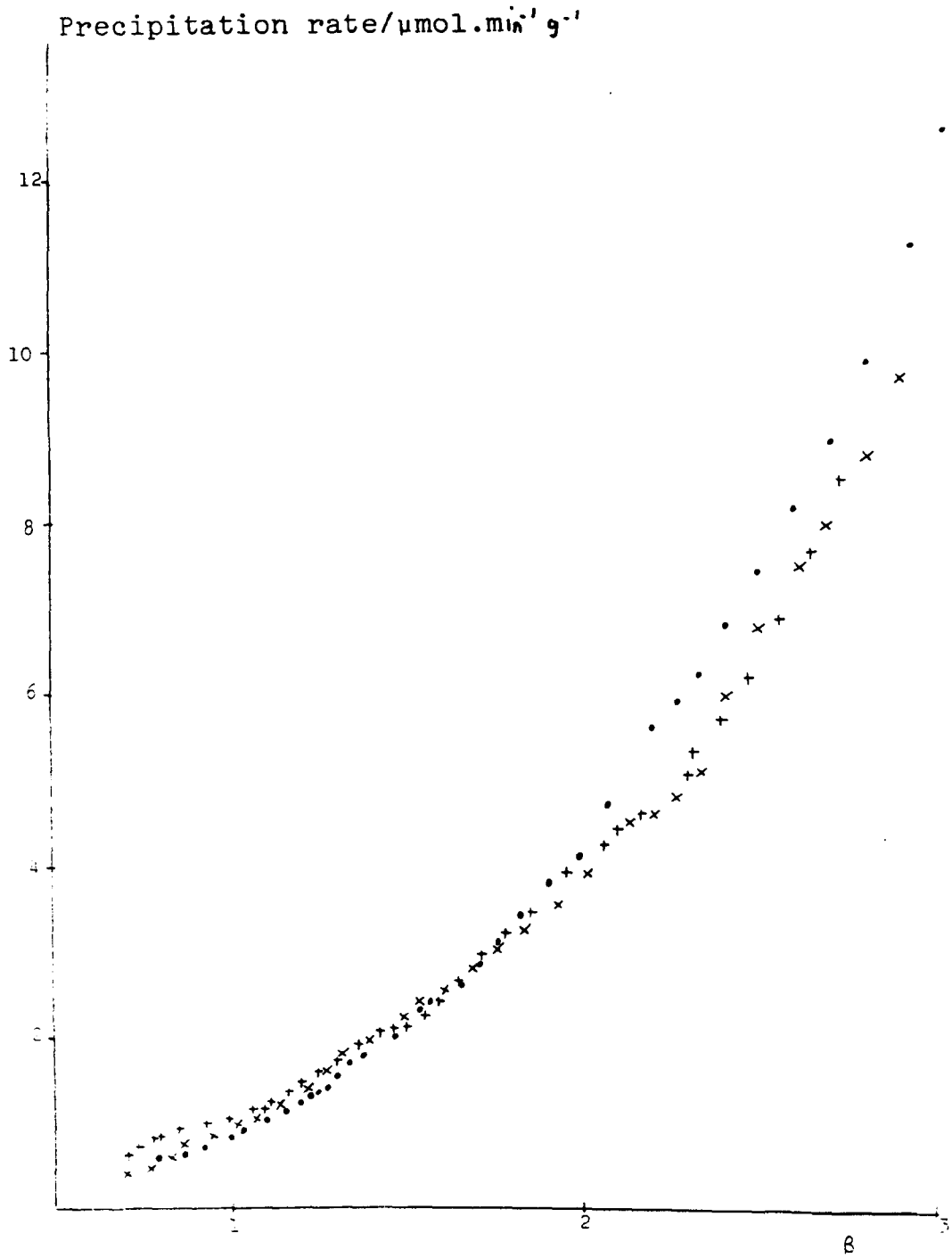

FIGURE 5.31 Precipitation experiments carried out on powders.

TABLE 5.14 Output for a typical precipitation experiment.

T/MIN.	PRECIPITATION RATE/ $\mu mol.min^{-1} g^{-1}$	β
0	12.75	2.999
2	9.96	2.789
4	8.25	2.572
6	6.88	2.397
8	5.97	2.252
11	4.71	2.066
15	3.83	1.893
19	3.15	1.753
23	2.65	1.647
27	2.46	1.566
33	2.09	1.462
41	1.82	1.368
49	1.56	1.299
57	1.39	1.237
65	1.28	1.191
77	1.14	1.108
93	1.02	1.059
109	0.88	1.027
125	0.83	0.999
141	0.79	0.983

plotted as a function of β (growth affinity), and as expected[16] the precipitation rate decreases with decreasing growth affinity. Figure 5.31 also shows two additional experiments illustrating the reproducibility of the results.

5.2.1.1 PRECIPITATION IN THE PRESENCE OF COPPER(II) IONS

As described in Section 4.3.4.2 the precipitation reaction was studied in the presence of 10^{-5}M Cu^{2+}, to see

if the copper would inhibit the crystal growth. The data from these experiments was analysed as previously. Figure 5.32 shows the plot of precipitation rate vs. β for two such experiments. These, when contrasted with Figure 5.31, illustrate the difference in the precipitation rate; β falls far less steeply in the presence of copper.

To quantify the effect of copper on the rate the FORTRAN computer programme 'RATECON' was employed, which calculated the precipitation rate constant both with, and without, the added copper. Before this programme could be used, the data created using 'COMPOST' (see Section 4.3.2.2) were reprocessed. The range of the β function was divided into twenty equidistance portions and the corresponding values of pH, pCO_2 and HCO_3^- were found using the BASIC programme 'INTERPOLATE'. These values were then entered into the 'RATECOM' programme, which calculated the rate constants for the reaction using the carbonate site model of House et al.[16]

Table 5.15 lists these rate constants and as shown the presence of 10^{-5}M Cu^{2+} in the reaction solution reduces the rate constant by a factor of one half.

The plots shown in Figure 5.32 are not identical due to the saturation indices of the solutions being different at the start of the reaction, that with the higher saturation index showing less inhibition. This effect has also been observed by House[17] who investigated the reduction of calcite growth in the presence of phosphate,

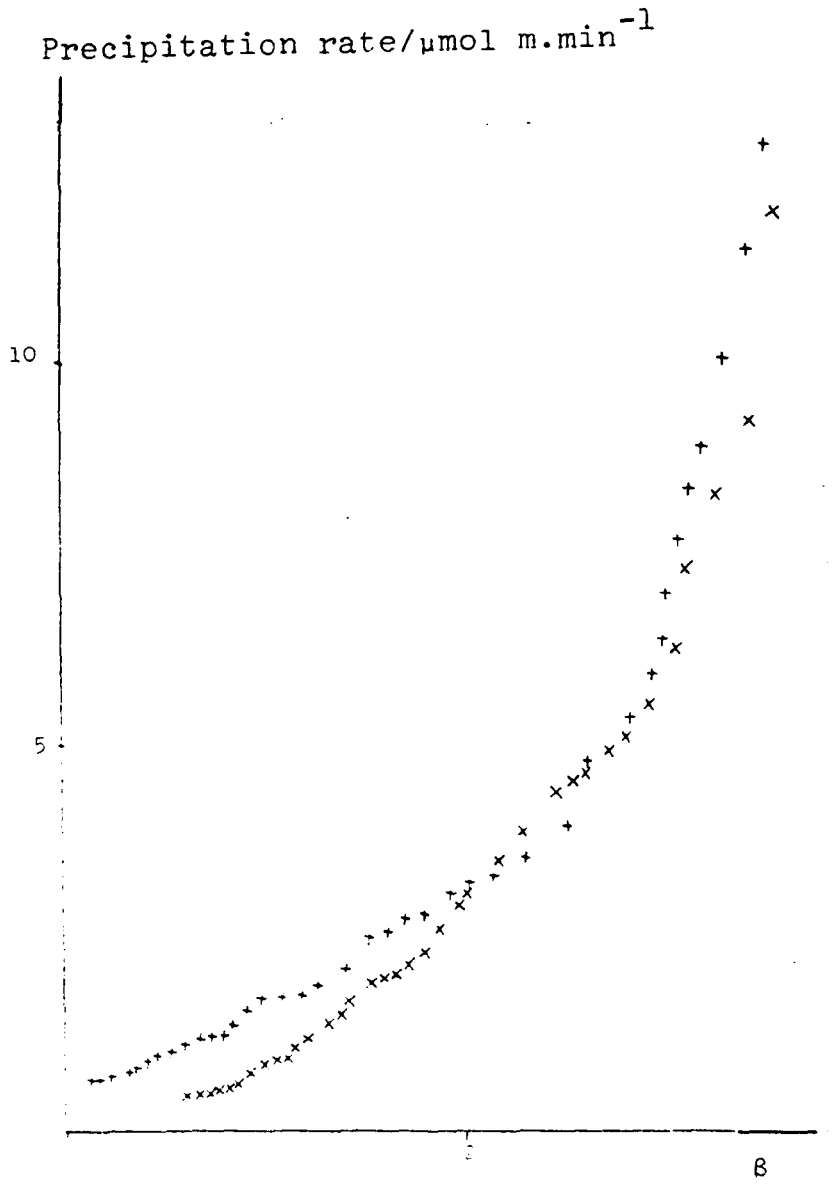

FIGURE 5.32 Precipitation experiments on calcite powder in the presence of Cu^{2+}

TABLE 5.15 Rate constants for precipitation

$k/dm^3min.^{-1}g^{-1}$	$[Cu^{2+}]/mol.dm^{-3}$
0.09457	0
0.1077	0
0.1075	0
0.05516	1×10^{-5}
0.05900	1×10^{-5}

finding that the effectiveness of phosphate as an inhibitor was reduced by increasing the initial saturation index.

5.2.2 DISSOLUTION EXPERIMENTS

To investigate the dissolution of powdered calcite, experiments as described in Section 4.3.4.3 were undertaken, i.e., the dissolution of a weighed amount of powdered calcite was measured as a function of pCO_2, (in the range 0.048 - 0.248 atm.). The data collected was again analysed using the iterative method, described in Section 4.3.2.2., though the output format was slightly altered, as described in Section 4.3.4.3, for reasons which will be given later.

Table 5.16 lists the output from a typical dissolution experiment, in this case pCO_2 was 0.077 atm. Figure 5.33 shows (Rate - $k_1[H^+]$) plotted as a function of ($[Ca^{2+}].[HCO_3^-]$). As shown all of the points, apart from the first few, lie on a straight line, giving an intercept of 1.743×10^{-10} $mol.cm^{-2}s^{-1}$, and a gradient

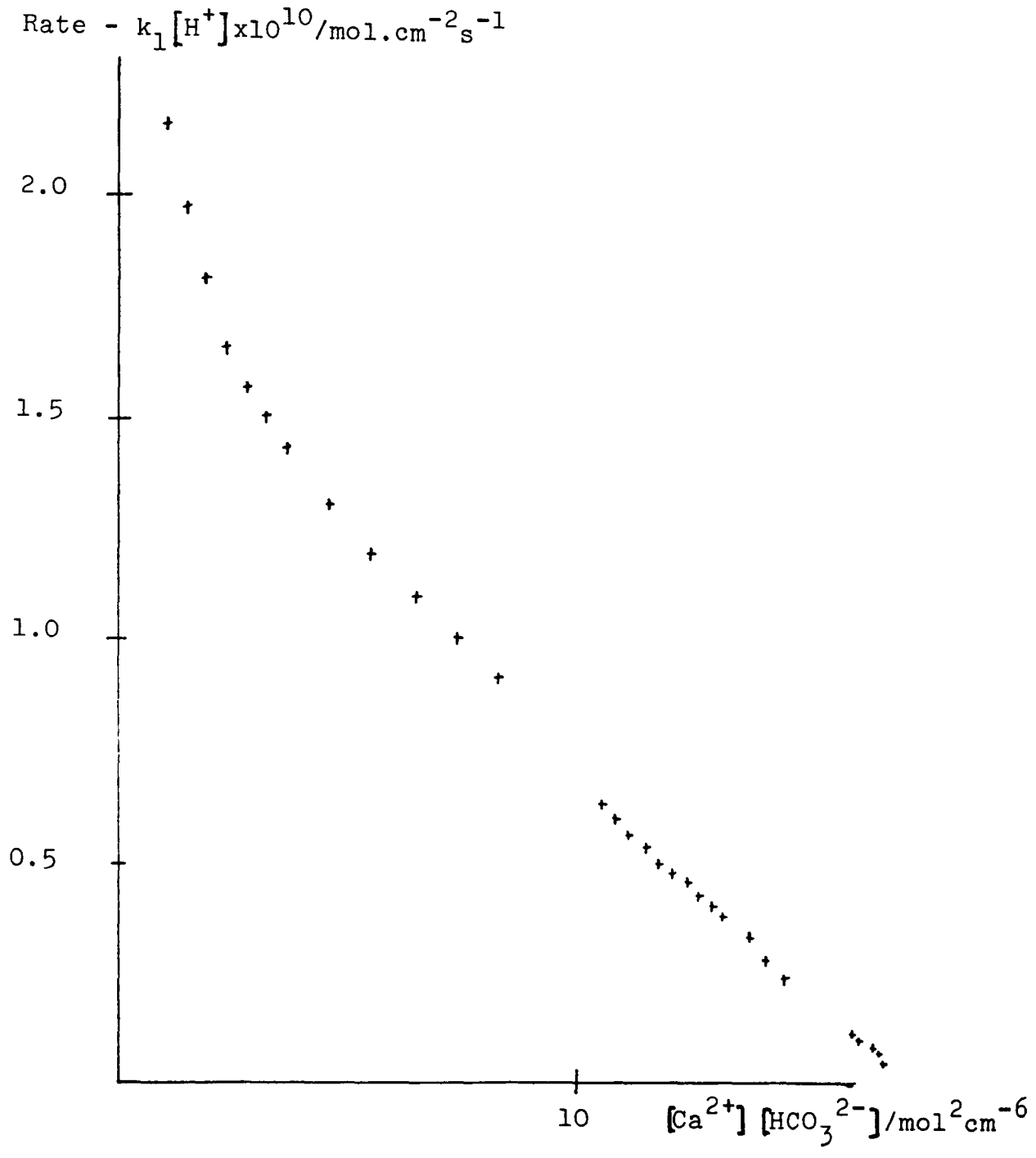

FIGURE 5.33 Typical dissolution experiment on powders

TABLE 5.16 Output from a typical dissolution experiment

T/min.	ρCO_2/atm.	$[Ca^{2+}][CO_3^{2-}]$/ mol^2dm^{-6}	RATE $k_1[H^+] \times 10^{10}$/ $mol.cm^{-2}s^{-1}$
0	168.9	0.146	-
2	103.5	0.761	2.33
4	81.9	1.53	1.97
6	77.5	2.41	1.66
8	74.4	3.29	1.50
11	73.2	4.67	1.30
15	71.0	6.51	1.09
19	74.3	8.31	0.905
27	76.9	10.86	0.593
29	77.0	11.51	0.531
31	76.8	12.12	0.473
33	76.5	12.68	0.422
35	76.0	13.21	0.375
39	76.8	14.10	0.278
50	77.1	15.96	0.103
52	77.3	16.20	0.093
54	76.9	16.42	0.089
56	77.0	16.64	0.070
58	77.1	16.84	0.051
61	77.2	17.11	0.029

of $-0.1022 \times 10^{-11} mol.cm^{-2}s^{-1}atm^{-1}$ (calculated using a linear regression analysis).

The reason for the points at the beginning of the experiment not falling on the line can be understood by considering ρCO_2 of the system. Upon the addition of the powder the rate of reaction is so fast that the level of CO_2 becomes unstable as can be seen in Figure 5.34. Therefore, the concentrations calculated by the programme 'COMPOST' become unreliable and data could only be taken after the ρCO_2 value has settled. The gaps

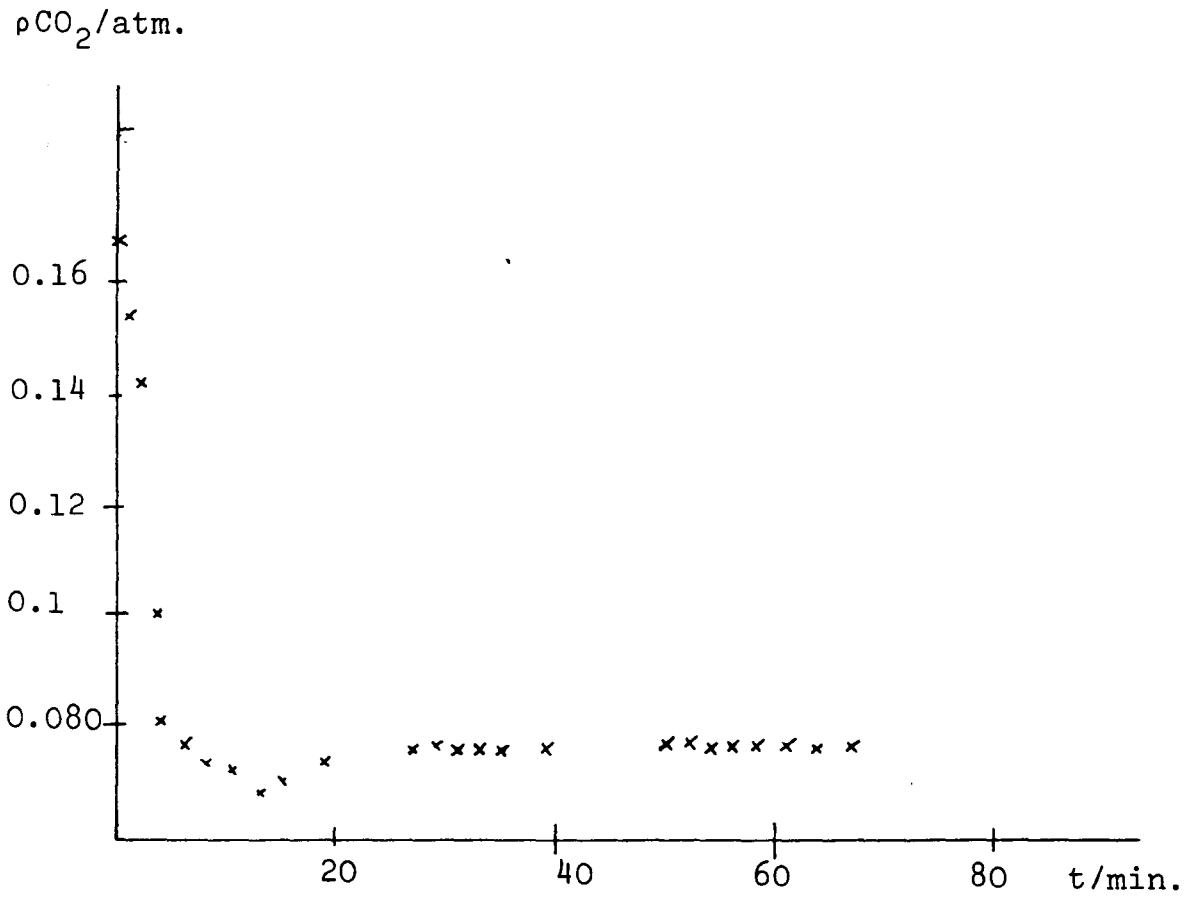

FIGURE 5.34 Plot of pCO_2 vs. time.

which appear in the data correspond to the occasions when the Wayne-Kerr B604 A.C. Bridge needed to be rebalanced, for reasons already described in Section 4.3.4.3.

The dissolution reaction was then measured for differing values of ρCO_2, in each case discounting the data measured before a steady ρCO_2 value had been obtained. The reaction occurred faster at higher ρCO_2 as $[H_2CO_3]$ increased. Table 5.17 lists the gradients and intercepts

TABLE 5.17

ρCO_2/atm.	INTERCEPT x 10^{10}/ $mol.cm^{-2}s^{-1}$	SLOPE x 10^{10}/ $mol.cm^{-2}s^{-1}atm^{-1}$
0.048	1.680	-0.1246
0.0527	1.541	-0.1242
0.077	1.743	-0.1022
0.101	2.224	-0.0957
0.167	2.520	-0.0795
0.177	2.498	-0.0786
0.205	2.771	-0.0761
0.248	2.793	-0.0698

for plots of (rate $-k_1[H^+]$) *vs.* ($[Ca^{2+}].[HCO_3^-]$) for various ρCO_2, and Figure 5.35 shows these intercepts as a function of ρCO_2 giving a gradient of $6.412 \times 10^{-10} mol.cm^{-2}s^{-1}atm^{-1}$ and an intercept of $1.344 \times 10^{-10} mol.cm^{-2}s^{-2}atm^{-1}$.

In order to compare these results obtained from measuring the dissolution of calcite powder, with those obtained using the rotating disc, as well as those measured

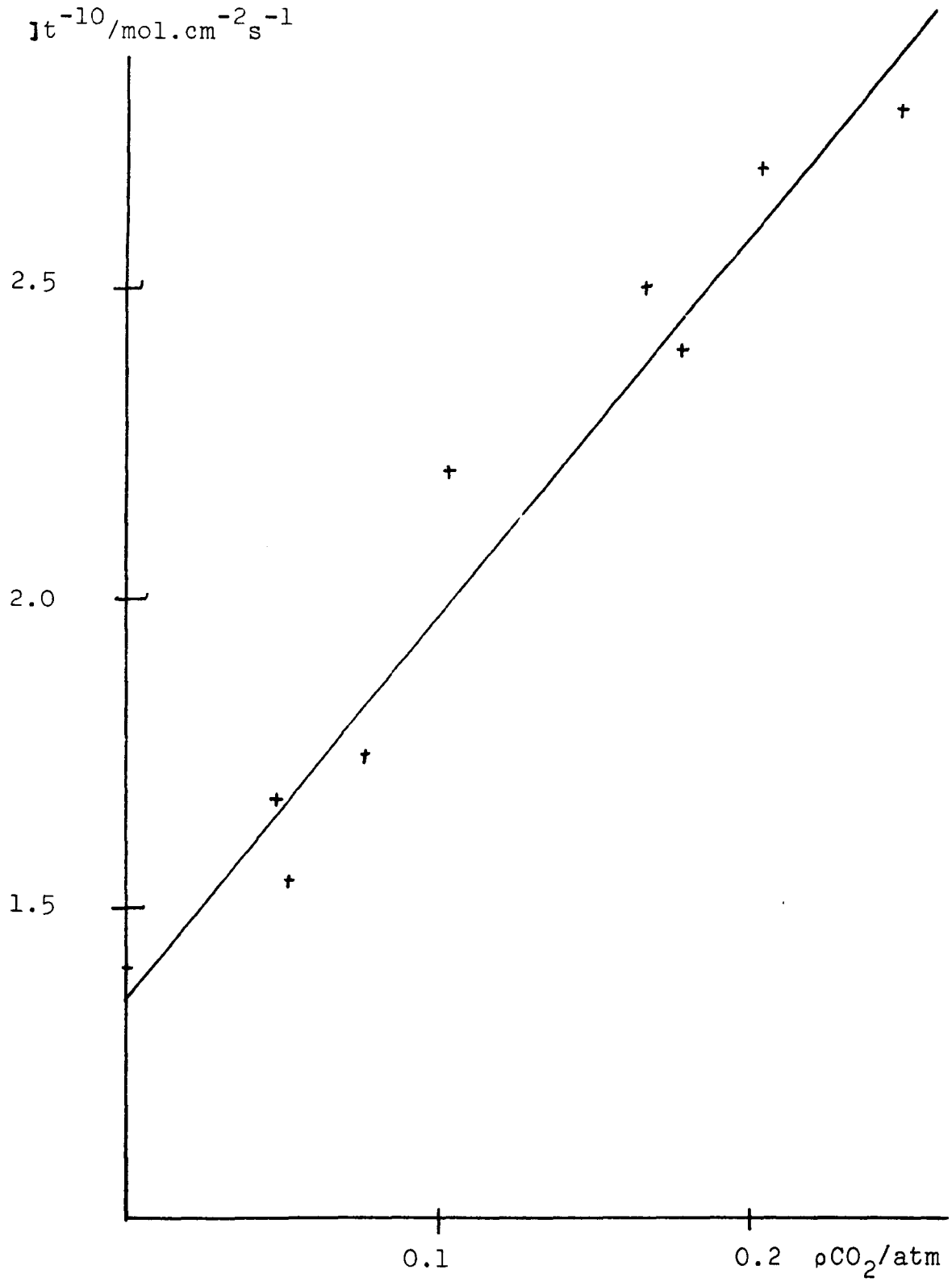

FIGURE 5.35 Plot of 1t vs. pCO_2 for dissolution experiments on powders.

by Plummer *et al.*,[14] and House *et al.*,[16] then, as described earlier, the output format of 'COMPOST', and 'TNCAL', was altered giving the dissolution rate in terms of $mol.cm^{-2}s^{-1}$, and outputting the terms ($[Ca^{2+}].[HCO_3^-]$) and (rate - $k_1[H^+]$). (k_1 being the rate constant for the reaction of protons with calcite, as defined and measured by Plummer *et al.*)

They described the overall rate of dissolution for crushed Iceland Spar to be:

$$R = k_1[H^+] + k_3[H_2CO_3] + k_2 - k_4[Ca^{2+}][HCO_3^-]$$

The terms being as defined previously.

This equation may be compared to equation 5.15 which describes the rate of dissolution measured using the rotating disc.

Thus, if a graph is drawn of (rate - $k_1[H^+]$) *vs.* ($[Ca^{2+}].[HCO_3^-]$), Figure 5.33,then the gradient corresponds to k_4 and the intercept to ($k_3[H_2CO_3] + k_2$). If the intercepts are measured over a range of pCO_2, and a plot is drawn of intercept *vs.* pCO_2 (Figure 5.35), then the intercept of this line corresponds to where $[H_2CO_3] = 0$, and this gives the k_2 value.

From Figure 5.35, $k_2 = 1.34 \times 10^{-10}$ $mol.cm^{-2}s^{-1}$. The value has already been compared with other values in Section 5.1.2.6 and good agreement was shown with all the other samples used apart from Calopake F. It was, therefore, decided to study the dissolution of this powder

to investigate whether the measured rate constant would differ from that obtained with the BDH powder, and, if so to compare it to the value measured by House.

However, as described previously in Section 4.3.4.3, the powder was so finely divided that the ensuing reaction occurred too fast for it to be monitored successfully with the apparatus available, and therefore no useful information could be obtained.

5.3 PRECIPITATION USING THE ROTATING DISC

5.3.1 INTRODUCTION

The aim of this set of experiments was to study the kinetics of calcite precipitation, by means of monitering the dissolution reaction in the region where the product $[Ca^{2+}][CO_3^{2-}]$ is close to k_{sp}, the solubility product of calcite.

In this region the rate of dissolution will be reduced due to the occurrance of the back reaction, precipitation. Eventually the concentration of dissolved calcium will remain constant when the rates of dissolution ar precipitation are equal, i.e., when the solubility product is equalled by the product $[Ca^{2+}][CO_3^{2-}]$.

Several empirical models have been derived to describe the kinetics of precipitation, and of dissolution, based on experiments carried out on powders, and the aim of this section was to find if the experimental data, obtained using the rotating disc, could be fitted to any of the empirical models.

Dorange and Guetchidjian,[18] who studied the dissolution of marble chips as a function of pCO_2 and initial calcium concentration considered the chemical reaction to be the attack of water on the marble surface i.e:

$$CaCO_3 + H_2O + CO_2 \rightarrow Ca(HCO_3)_2 \qquad 5.22$$

and found that the rate of reaction was governed by the degree of undersaturation in the system.

$$R = k([Ca^{2+}]_{eq.} - |Ca|_b) \qquad 5.23$$

$[Ca^{2+}]_{eq.}$ = equilibrium concentration of Ca^{2+} in solution

$[Ca^{2+}]_b$ = bulk calcium concentration.

Sjöberg[19,20] studied the dissolution of powdered calcite at various pH's and from his values he derived the following empirical equation, again governed by the degree of undersaturation:

$$R = Ak(k_{sp}^{\frac{1}{2}} - [Ca^{2+}]^{\frac{1}{2}}[CO_3^{2-}]^{\frac{1}{2}}) \qquad 5.24$$

A = area of calcite.

Later work by Sjöberg and Rickard[21] showed that, under the experimental conditions used, equations 5.23 and 5.24

were indistinguishable. They also showed that the chemical reaction above pH 6 was the attack of water on the calcite surface.

Davies and Jones[22] studied the precipitation of silver chloride from supersaturated solutions and derived the following equation:

$$R = ks\ (\ [Ag^+]^{\frac{1}{2}}[Cl^-]^{\frac{1}{2}} - K_{sp}^{\frac{1}{2}})^2 \qquad 5.25$$

S = surface area

i.e., the rate of growth is proportional to the square of the supersaturation, with the rate determining step being the simultaneous dehydration and crystallisation of Ag^+ and Cl^- ions, from an absorbed monolayer, onto the crystal surface.

Equation 5.25 can be redefined to apply to the dissolution of calcite:

$$R = Ks\ (K_{sp}^{\frac{1}{2}} - [Ca^{2+}]^{\frac{1}{2}}[CO_3^{2-}]^{\frac{1}{2}})^2 \qquad 5.26$$

Thus, three kinetic models exist to describe the rate of dissolution of calcite and they are listed in Table 5.18, the terms being as previous defined.

5.3.2 NUMERICAL CALCULATIONS

In order to fit these models to the experimental data, $[Ca^{2+}]$ and $[CO_3^{2-}]$ have to be known. $[Ca^{2+}]$ is measured by

TABLE 5.18 Various kinetic models for the dissolution of calcite.

EQUATION	AUTHOR
$R = k([Ca^{2+}]_{eq.} - [Ca^{2+}]_b)$	Dorange and Guetchidjian[18]
$R = Ak(k_{sp}^{\frac{1}{2}} - [Ca^{2+}]^{\frac{1}{2}}[CO_3^{2-}]^{\frac{1}{2}})$	Sjöberg[19]
$R = sk(k_{sp}^{\frac{1}{2}} - [Ca^{2+}]^{\frac{1}{2}}[CO_3^{2-}]^{\frac{1}{2}})^2$	Davies and Jones[22]

the Ca.I.S.E., but $[CO_3^{2-}]$ has to be calculated knowing the equilibria set up in the bicarbonate-water system.

$$CaCO_3 + H_2O \rightleftharpoons Ca^{2+} + HCO_3^- + OH^- \rightleftharpoons H_2O + CO_3^{2-} \qquad 5.27$$

$$\frac{[H^+][CO_3^{2-}]}{[HCO_3^-]} = k_2 = 7.94 \times 10^{-10} \text{ mol.dm}^{-3} \text{ 23} \qquad 5.28$$

$$[H^+][OH^-] = k_w = 1.400 \times 10^{-14} \text{ mol.dm}^{-3} \text{ 6} \qquad 5.29$$

Considering the mass balance in equation 5.27, then:

$$[Ca^{2+}]_{dis.} = [HCO_3^-] + [CO_3^{2-}] \qquad 5.30$$

$[Ca^{2+}]_{dis.}$ = concentration of dissolved calcium

since one CO_3^{2-} dissolves for every Ca^{2+}. We assume that the pH is high enough for the loss of CO_2 in the equation:

$$HCO_3^- + H^+ \rightleftharpoons H_2CO_3 \rightleftharpoons H_2O + CO_2\uparrow \qquad 5.31$$

is negligible.

Redefining equation 5.30 gives:

$$[Ca^{2+}]_{dis.} = x + y \qquad 5.32$$

x and y are the concentrations of HCO_3^- and CO_3^{2-} respectively.

Considering the charge balance in equation 5.27, gives:

$$[H^+] + 2[Ca^{2+}]_{dis.} = 2[CO_3^{2-}] + [HCO_3^-] + [OH^-] \qquad 5.33$$

therefore,

$$[H^+] + 2[Ca^{2+}]_{dis.} = 2y + x + [OH^-] \qquad 5.34$$

substituting for $[OH^-]$ and $[H^+]$ (equations 5.28, 5.29) and rearranging gives:

$$2k_2x(y[Ca^{2+}]_{dis.} - y^2) - k_w y^2 + k_2^2x^2 - k_s x^2 y = 0 \qquad 5.35$$

and finally substituting for x (equation 5.32) yields:

$$y^3k_2 + y^2(k_2^2 - 2[Ca^{2+}]_{dis.}k_2 - k_w) + y(k_2[Ca^{2+}]^2_{dis.} -$$

$$2[Ca^{2+}]_{dis.}k_2^2) + k_2^2[Ca^{2+}]^2_{dis.} = 0 \qquad 5.36$$

The cubic equation (5.36) can be solved approximately using Newton's method. This gives three roots as the solution, but two can be discarded as they give values of y (= $[CO_3^{2-}]$) greater than the amount of calcium dissolved.

5.3.3 EXPERIMENTAL

As described fully in Section 4.4 experiments were carried out in 100 cm^3 0.3M KCl with a background calcium concentration of 3.5×10^{-4} $mol.dm^{-3}$. The calcite disc was inserted into the reaction solution and the calcium concentration was monitored until it had remained constant for over one hour. When this had occurred the rate of the forward and backward reaction were equal.

In order to plot the various models it was necessary to find the solubility product of calcite and the concentration of CO_3^{2-}. The solubility product was determined experimentally, it was considered that when the concentration of calcium remained constant, then the solubility product had been reached, i.e:

$$K_{sp} = [Ca^{2+}]_{Total}\ [CO_3^{2-}]$$

TABLE 5.18 The predicted values of $[Ca^{2+}]$ as a function of time predicted by (a) Sjöberg and (b) Davies-Jones.

	$[Ca^{2+}] \times 10^{4}$/mol.dm^{-3}	t/s
(a)	3.500	0
	3.626	1000
	3.720	2000
	3.877	4000
	4.103	5000
	4.252	12000
	4.311	16000
	4.346	20000
	3.671	24000
(b)	3.500	0
	3.626	1000
	3.696	2000
	3.803	4000
	3.945	8000
	4.019	12000
	4.069	16000
	4.101	20000
	4.131	24000
	4.155	28000

TABLE 5.19 Change of $[Ca^{2+}]$ with time as measured using the rotating disc.

t/s	$[Ca^{2+}] \times 10^{4}$/mol.dm^{-3}
0	3.50
500	3.56
1000	3.62
2000	3.74
3000	3.76
5000	3.80
6000	3.87
7000	3.95
8000	4.02
9000	4.07
10000	4.11
12000	4.18
15000	4.23
17000	4.27
19000	4.36
21000	4.35
23000	4.33
25000	4.32

$$= \left([Ca^{2+}]_{initial} + [Ca^{2+}]_{dis.} \right) y$$

$[Ca^{2+}]_{dis.}$ can be found from the Ca.I.S.E. and y can be found from equation 5.36. The calcium profiles were drawn up for both the Sjoberg and Davies-Jones models. These are listed in Table 5.19 and shown in Figure 5.36.

5.3.4 RESULTS

Table 5.20 lists the measured change in $[Ca^{2+}]$ with time for a typical experiment, and as can be seen after approximately 24,000 seconds the concentration reaches a steady value. The fluctuations are due to background noise being picked up.

This experimental data (together with the results from a second experiment) is displayed in Figure 5.36 and as can be seen good agreement is shown with the model of Sjöberg. This shows that the rate of reaction is given by equation 5.24 i.e:

$$R = k(K_{sp}^{\frac{1}{2}} - [Ca^{2+}]^{\frac{1}{2}} [CO_3^{2-}]^{\frac{1}{2}})$$

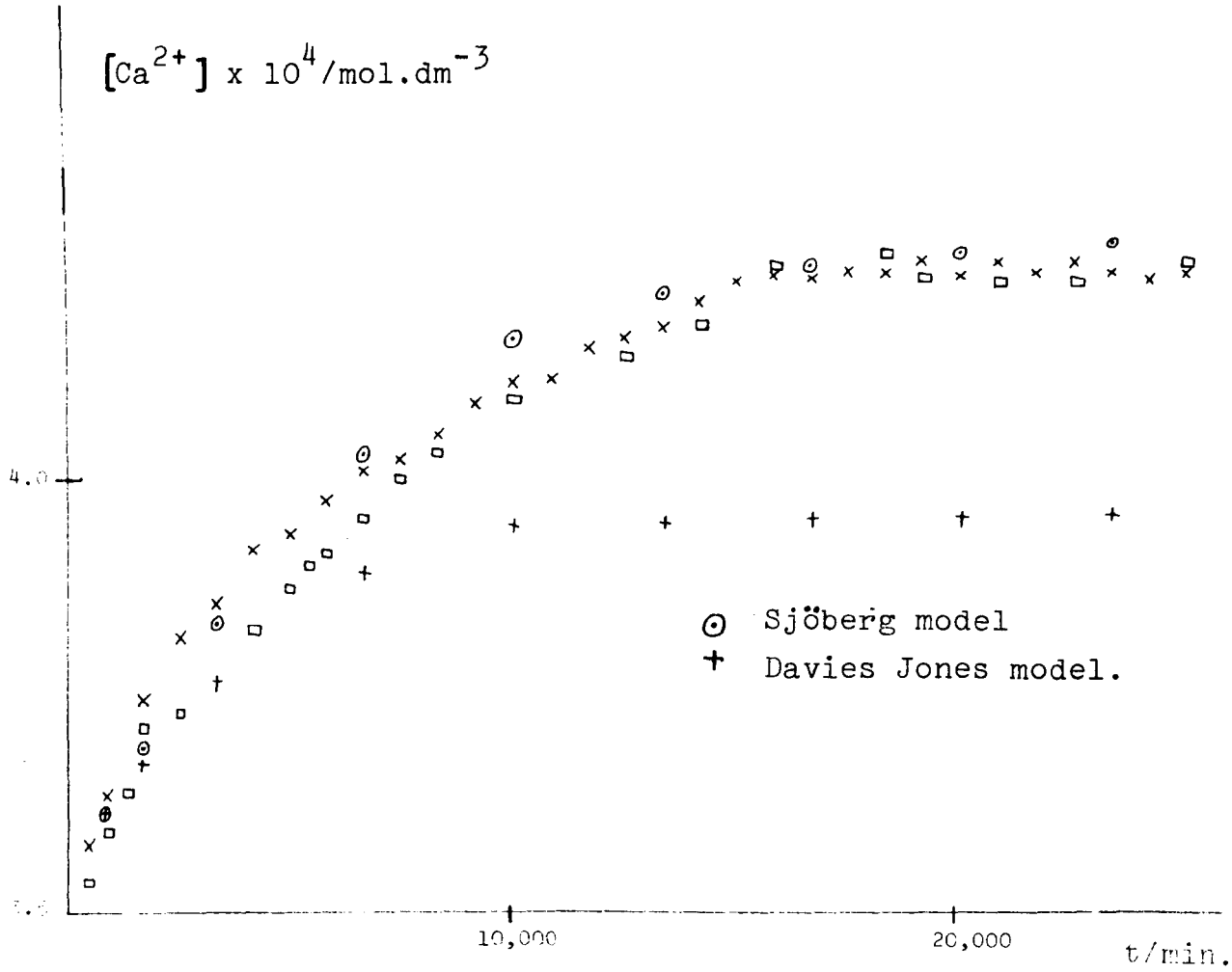

FIGURE 5.36 Plot of $[Ca^{2+}]$ vs. time.

1. J.H.Burns, M.A. Bredig, *J.Chem.Phys.*, 25, 1281, 1956.

2. F.Dachille, R.Roy, *Nature*, 186, 34, 1960.

3. V.B.Gostisa-Michelcic, W.Vielstich, A.Heindrichs, *Ber Bansenges*, 76, 19 (1972).

4. W.J.Albery, R.P.Bell, *Proc.Chem.Soc.*, 163 (1963).

5. M.Eigen, E.M.Eyring, *J.Am.Chem.Soc.*, 84, 3254 (1962).

6. R.C.West, In: "CRC Handbook of Chemistry and Physics", 59th Ed., CRC Press, Boca Raton Fl, 1978.

7. D.E.Bidstrup, C.J.Geankoplis, *J.Chem.Eng.Data*, 8, 170 (1963).

8. J.M.Edmond, J.M.Gieskes, *Geochim et Cosmochim Acta*, 34, 1261 (1970).

9. W.Stumm, J.J.Morgan, In: "Aquatic Chemistry", Second Ed., p.211, Wiley New York, 1981.

10. A.J.Band, L.R.Faulkner, In: "Electrochemical Methods", p.434, Wiley, New York, 1980.

11. B.Bolin, *Tellus*, 12, 274 (1960).

12. D.Barth, C.Tondre, G.Lappai, J.J.Delpuech, *J.Phys. Chem.*, 85, 3660 (1981).

13. G.Skirrow, In: "Chemical Oceanography", (G.Skirrow, J.P.Riley Eds.,), Vol. 2, p.37, Academic Press, New York, 1975.

14. L.N.Plummer, T.M.Wigley, D.L.Parkhurst, *Am.J.Sci.*, 278, 179 (1978).

15. J.A.Harrison, H.K.Thirsk, In: "Electroanalytical Chemistry", Vol. 5, p.98, Ed., A.J.Band, Marcel Dekker, New York, 1971.

16. G.E.Cassford, W.A.House, A.D.Pethybridge, *J.Chem.Soc., Faraday Trans. I*, 79, 1617 (1983).

17. W.A.House, unpublished work.

18. G.Dorange, A.Guetchidjian, *CK Acad.Sci.Paris Ser.C.*, 286, 159 (1978).

19. E.L.Sjöberg, *Geochim.et Cosmochim.Acta*, 40, 441 (1976).

20. E.L.Sjöberg, *Stockholm Contrib.Geol.*, 32, 1 (1978).

21. D.Rickard, E.L.Sjöberg, *Am.J.Sci.*, 283, 815 (1983).

22. C.W.Davies, A.L.Jones, *Trans.Faraday Soc.*, 51, 812 (1955).

23. See page 278 of reference 9.

CHAPTER 6

CHANNEL ELECTRODES

6.1 INTRODUCTION

The rotating disc, with its well defined hydrodynamics, has proved useful in differentiating between the chemically controlled and transport controlled reactions occurring in the dissolution of calcite, and these rate constants have been measured as a function of pH and pCO_2.

However, use of a rotating disc has certain problems associated with it. The system has a poor transient time, as substances have to be transported from the rotating disc surface to the detection system. Also, in the study of the effect on inhibitors on the rate it is difficult to add the inhibitor during the course of the reaction, because of the time needed to thoroughly mix the solution. The measurement of inhibitor absorbed onto the surface is also difficult.

Another system which has used defined hydrodynamics and which can overcome the problems outlined above is the channel electrode, and the closely related tubular electrode. In these systems instead of the electrode moving and causing the solution to flow (as in the rotating disc), the electrode is stationary and the solution is forced to flow over the electrode surface, thus continuously replenishing the reactive species of interest.

To overcome the problems associated with inhibitors the apparatus shown in Figure 1 could be used. As shown, one face of the channel electrode is formed by a single crystal of calcite which has two copper electrodes attached to the surface. All of the crystal apart from the area

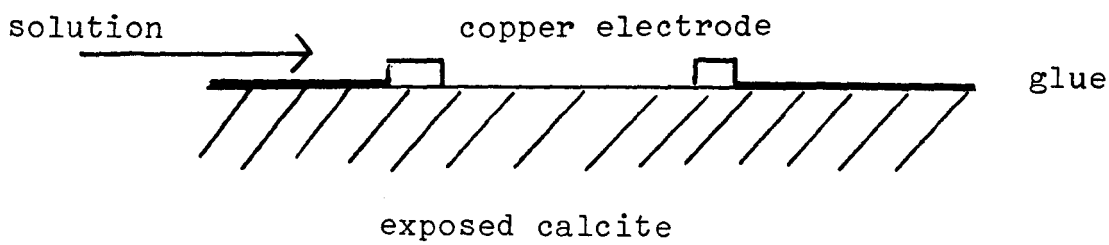

FIGURE 6.1 Flow of solution over a calcite channel electrode

between these two electrodes is covered with a non-reacting glue. As the solution flows over the first electrode copper is dissolved. This solution then flows over the exposed calcite surface and some of the copper is absorbed onto kink sites. The second electrode is set at such a potential that any copper in solution is reduced.

$$Cu^{2+} + 2e \rightarrow Cu$$

Thus from a knowledge of the amount of copper dissolved and the amount left in solution after flowing over the calcite surface. The amount of copper absorbed can be found.

To add the inhibitor during the course of the reaction an injection system could be used, and the solution would be well mixed before passing over the calcite surface.

Such a system would show a faster response time as the detector can be placed directly on the calcite surface, and it would be more sensitive than an I.S.E., as it would respond to the actual concentration and not to log (concentration).

Another point of interest is that measurement of the current transients resulting from a potential step at the channel electrode, allow the measurement of the diffusion coefficient without a knowledge of the concentration of the reactive species. In the case of a channel electrode incorporating a single crystal of Iceland Spar, measurement of the current transient resulting from a sudden change of flow rate over the crystal would allow the diffusion coefficient

of the reacting species to be found. This would enable the mechanism to be defined with more confidence, and it would enable $K_{H_2CO_3}$ to be calculated more exactly. As shown in Table 5.9, the literature values for $K_{H_2CO_3}$ cover a wide range, and the value found from the work described in this thesis is dependant upon the Wilke Chang value for $D_{H_2CO_3}$, which is only an approximation to within 15%. If this value could be found, then the value for $K_{H_2CO_3}$ could be quoted with far more confidence. As an initial step, the electrochemistry of a well documented system was studied to characterise the cell and to ensure that experiments agreed with theory.

6.2 THE DEVELOPMENT OF CHANNEL ELECTRODES

Blaedel and Klatt[1] used a platinum tubular electrode and measured the current voltage curve for the ferri-ferro cyanide system. The tubular electrode was formed of plexiglas which was moulded round seamless platinum tubing. The flow rate was controlled by a stopcock and was measured using a calibrated rotameter over the range 2 - 10 $\mu l\ min^{-1}$. They rigorously derived the theory for convective diffusion in the tubular electrode, and found that theory and experiment were in good agreement.

Blaedel and Boyer[2] then proceeded to use the tubular electrode in a stop-flow experiment. They found that this produced reproducible results, and great sensitivity. They were able to detect concentrations down to 0.01 μM. Later work[3] involved the use of glossy carbon and gold tubular electrodes.

The first use of a channel electrode was described by Meyer *et al.*,[4] who used it to measure the chloride concentration in a flowing solution, by a mixture of chronopotentiometric and voltammetric analysis. Their cell was machined from blocks of lucite, the internal dimensions being 7 x 1.27 x 0.476 cm. The electrode used was a strip of silver foil, with dimensions 0.5 x 0.5 cm, cemented to the base of the cell. This was polished, after setting, to ensure non-turbulent flow. They found that this cell gave excellent reproducibility, and was extremely accurate when calibrated immediately before analysis. The use of channel electrodes for use in chronopotiometric analysis has also been reported by Posey and Meyer,[5] and by Aoki and Matsuda.[6]

Compton and Coles[7] reported the use of a channel electrode for use in Electrochemical E.S.R. They constructed a flow system with the channel electrode located at the centre of the cavity, and thus upon reaction, radicals were generated *in situ*. They used a demountable flow cell made of silica glass, having internal dimensions of 0.4 x 6 x 30 mm. The electrode used was a platinum strip, typically 0.5 x 0.5 cm, glued onto the cover plate. The platinum strip was then polished, using diamond sprays, for streamline flow, and the cover plate was connected to the rest of the cell. The flow rate was gravity controlled, the solutions flowing through capillary tubes. They were able to demonstrate the plug flow of solution through their cell.

Further electrochemical E.S.R. research by Compton et al., have used similar cells to investigate E.C.,[8] E.C.E.,[9] reactions, and, in conjunction with rotating disc, and rotating ring disc experiments, they were able to differentiate between the E.C.E. and D.I.S.P.1. mechanism.[10]

The usefullness of channel electrodes has been extended by the development of the double channel electrode.[11-13] These can be used in an analogous way to rotating ring disc electrodes to investigate the mechanisms of reactions. Species are formed on the up-stream electrode and are subsequently destroyed on the lower. The amount of material regenerated on the lower electrode is a function of cell geometry, and the kinetics of reaction.

6.3 THEORY FOR CHANNEL ELECTRODES

This section will outline the theory of channel electrodes, and of the potential step experiment. This was obtained using a FORTRAN programme based upon the theory derived by Dr. R.G.Compton.

Consider the following reaction:

$$A \pm ne \rightarrow B$$

If it is assumed that A is the only electroactive species present in the bulk of the solution, then the convective - diffusive equation, describing the concentration of A (c) is given by

$$\frac{\partial c}{\partial t} = D\frac{\partial^2 c}{\partial y^2} - \frac{3}{2}\bar{U}\left(1 - (b^2 - y^2/b^2)\right)\frac{\partial c}{\partial x} \qquad 6.1$$

D = diffusion coefficient of A

b = half-height of channel

$\bar{U}$ = mean solution velocity

x = distance from upstream edge of electrode

y = distance normal to electrode, from electrode surface.

The terms in equation 6.1 are illustrated in Figure 6.2. It has been shown,[14] that if:

$$\frac{x_E D}{\bar{U}b^2} \ll 1, \qquad x_E = \text{length of electrode,}$$

equation 6.1 can be rewritten in terms of normalised variables i.e.,

$$\frac{\partial u}{\partial \tau} = \frac{\partial^2 u}{\partial \varepsilon^2} - \varepsilon\frac{\partial u}{\partial x} \qquad 6.2$$

$$\tau = \left(\frac{9\bar{U}^2 D}{x_E^2 b^2}\right)^{1/3} t$$

$$x = x/x_E$$

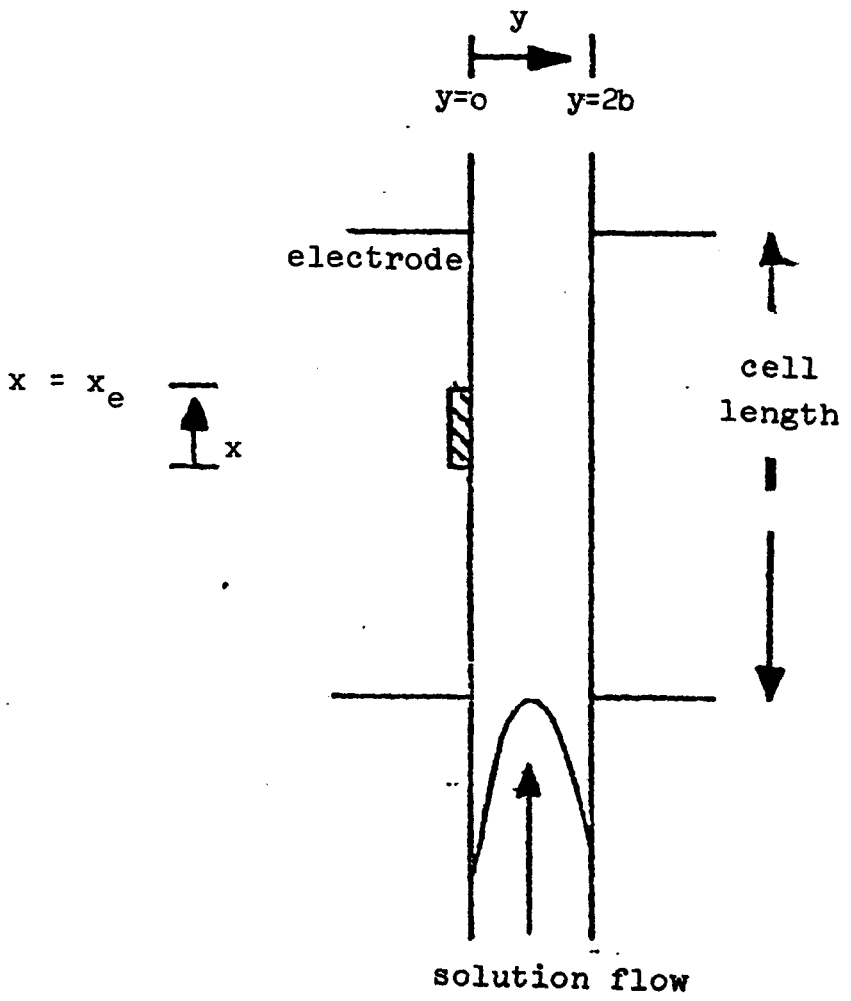

FIGURE 6.2 The geometry for the flow cell.

$$\varepsilon = \left(\frac{3\,\bar{U}}{b\,Dx_E}\right)^{1/3} y$$

and $u = c - c_\infty$

To solve the above equations requires the setting of boundary conditions, which for the case of the potential step are as follows:-

at $\tau < 0$, no current flows through the electrode,

but

at $\tau > 0$, when the potential is stepped, the surface concentration changes from c_∞ and u becomes u'. u' is independant of χ, i.e., the concentration, c, is assumed to be constant along the electrode. This will be a valid assumption for reversible voltammetric waves, but will only be true for currents close to the transport limited value for irreversible waves.

TABLE 6.1 The boundary conditions for the potential step experiment.

$\tau = 0$	$\varepsilon \geqslant 0$	$u = 0$
$\tau > 0$	$\varepsilon \to \infty$	$u \to 0$
$\tau > 0$	$\varepsilon = 0$	$u = u'$

The boundary conditions are listed in Table 6.1. The solution of equation 6.2 involves the use of double Laplace transformations,[15] first with respect to τ

(variable s) and then with respect to χ (variable p). This gives:

$$s\bar{\bar{u}} = \frac{\partial^2 \bar{\bar{u}}}{\partial \varepsilon^2} - p\varepsilon\bar{\bar{u}} \qquad 6.3$$

$\bar{\bar{u}}$ = double Laplace transform of u.

The solution of equation 6.3 involves use of the Airy function,[16] details of which are given by Compton and Coles.[8]

The current, I, due to the reaction of A is given by:

$$I \alpha \int_0^{1.0} \left.\frac{\partial c}{\partial \varepsilon}\right|_{\varepsilon=0} d\chi \qquad 6.4$$

The solution of equation 6.4 requires the use of inverse Laplace transformations and the Airy function, and gives the following series solution:

$$\frac{I(\tau)}{I(\tau \to \infty)} = 1 + \int_s^{-1} \frac{\Gamma(5/3)}{Ai'(0)} \sum_{n=1}^{\infty} \frac{c_n s^{(n-1)}}{\Gamma(5/3 + 2n/3)} \qquad 6.5$$

Ai'(0) = Airy function

Γ = Gamma function

c_n = coefficient readily compiled from the definition of the Airy function.

The series in equation 6.5 cannot be simply inverted, to solve it, use is made of the Levin transformation,[17] which approximates the series, by a series of rational functions which can then be individually inverted. This finally gives:

$$\frac{I(\tau)}{I(\tau\to\infty)} = 1-3.844 \lim_{n\to\infty} \sum_{m=1}^{n} \frac{g_n\ (q_m)\exp(q_m\tau)}{h'_n\ (q_m)} \qquad 6.6$$

h_n and g_n are Levin coefficients

q_m = complex roots of the following equation

$$h_n(S) = 0, \quad h'_n(S) = \frac{dh_n(S)}{ds}$$

The sum in equation 6.6 was solved using the FORTRAN programme " PADDY " which is listed in the Appendix.

For values of $\tau > 0.2$, the series was found to converge satisfactorily by considering $n < 10$ (Table 6.2). This curve is shown in Figure 6.3. As can also be seen from this Figure, for $\tau < 0.2$ the convergence was less good, (Table 6.2), even when n values as large as 20 were taken, and in this region it was only possible to give a range of values (hence the error bars in Figure 6.2).

Soliman and Chambre,[18] in their study of heat transfer showed that the flux at a point χ along the electrode was given by the approximation:

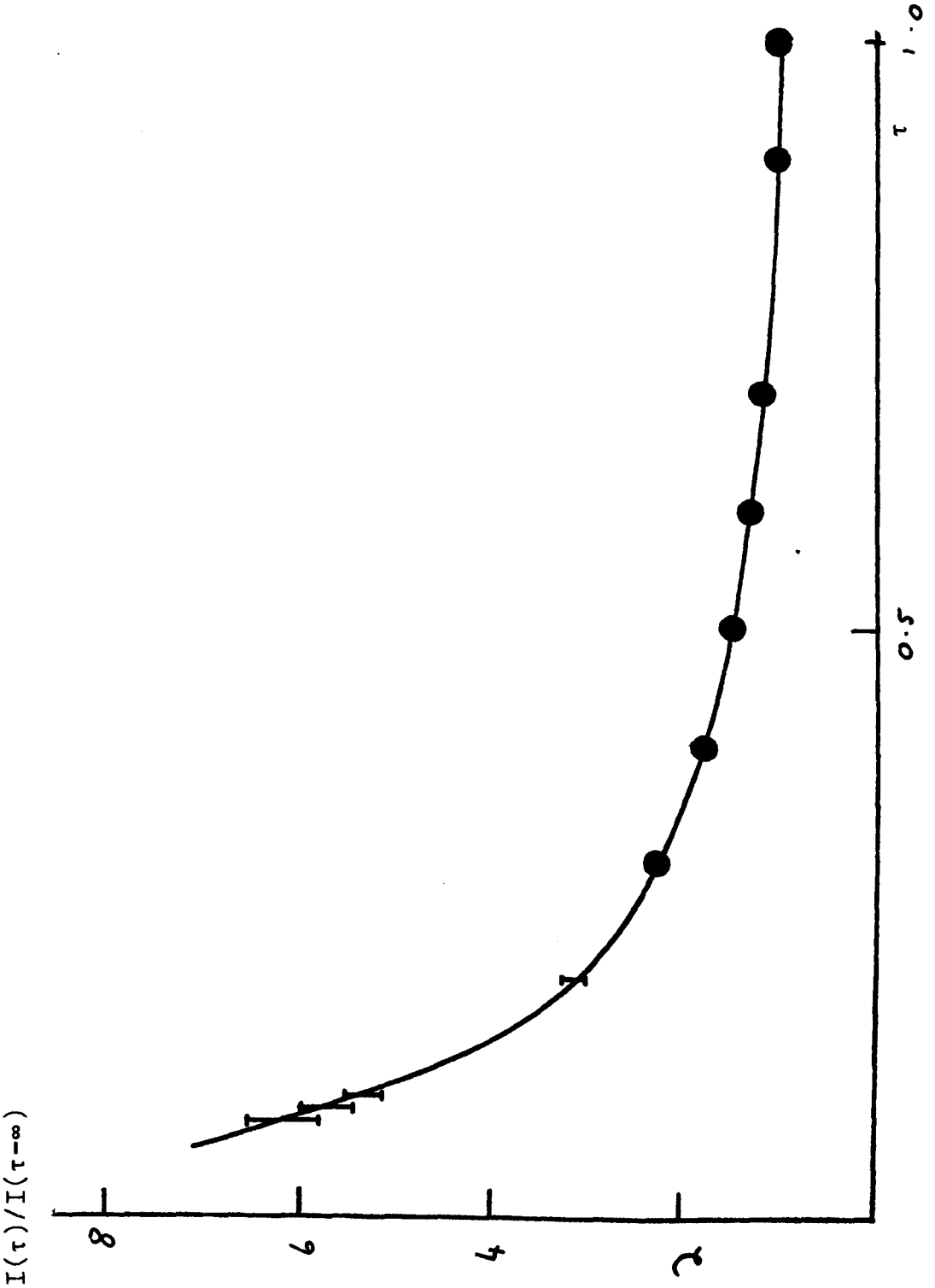

FIGURE 6.3 Theoretical current transients.

TABLE 6.2 Converged values for Levin Transformation

τ	n = 9	n = 10	n = 11
1.0	1.02392	1.02403	1.02408
0.9	1.05149	1.05157	1.05139
0.8	1.1007	1.09998	1.09986
0.7	1.1806	1.1797	1.1802
0.6	1.3037	1.3043	1.3071
0.5	1.4953	1.5008	1.4967
0.4	1.8042	1.7891	1.7881
0.3	2.2620	2.2620	2.2804
0.2	3.1257	3.2322	3.0660
0.1	5.5148	5.1260	5.1204
0.09	5.9200	5.4045	5.7270
0.08	6.3624	5.7663	6.5454

$$\frac{(u/\varepsilon)_{\chi,\tau}}{(u/\varepsilon)_{\chi,\tau\to\infty}} = \frac{1.048}{\sqrt{\tau'}} \qquad 6.7$$

$$\tau' = \tau/\chi^{2/3}$$

which is valid for $\tau' < 1.0$.

6.3 EXPERIMENTAL

The cell used for these experiments (shown in Figure 6.4) was a demountable channel electrode having dimensions of 0.4 x 6 x 30 mm, when assembled. The platinum working

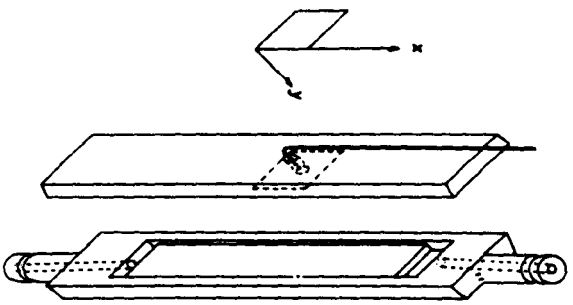

FIGURE 6.4 The flow cell

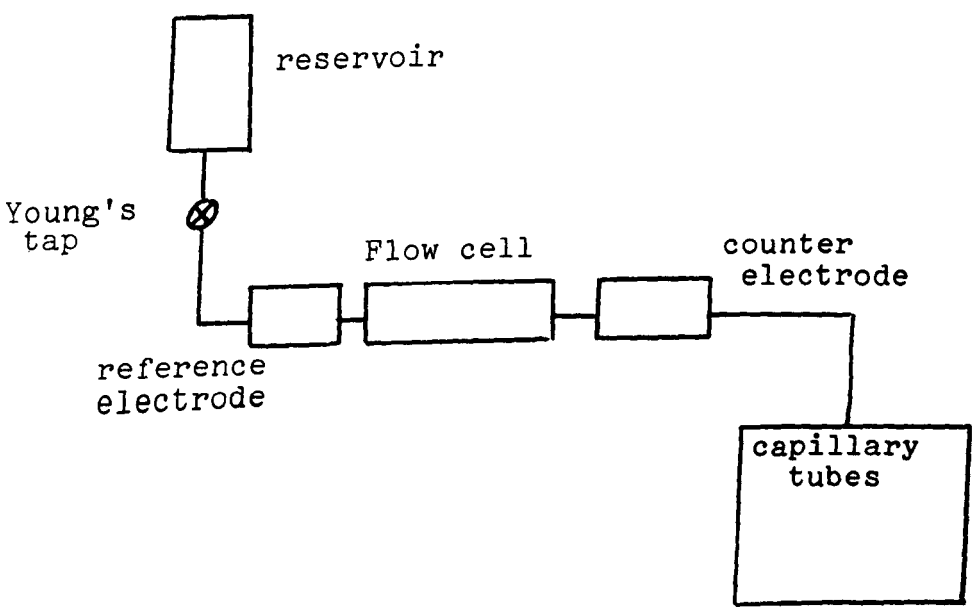

FIGURE 6.5 The experimental set-up for the flow cell experiment.

electrode, of typical dimensions 0.5 x 0.5 cm, was glued to the cover plate and electrical contact was made via a hole in the cover plate. The electrode was square shaped, with a strip protruding, and it was this protruding strip which emerged on the far side of the cover plate and allowed electrical contact to be made.

When the platinum electrode had set, it was polished using diamond lapping sprays, and the cell was assembled using a low temperature melting cosmetic depilatory wax (Boots, p.l.c.). To equalise the pressure across the full width of the cell and establish laminar flow, deeper box sections were constructed at the entrance to the channel. It has been shown[2] that once steady state conditions are set up in such a cell, the velocity profile across the width of the channel is plug flow.

This cell was connected to a flow system constructed of P.V.C. tubing (altex tubing) and silicon rubber. At the head of the system was a reservoir of 250 ml capacity and the solution was gravity fed from this to a collection of capillary tubes of various sizes, which controlled the flow rate of the system. A schematic representation of the complete flow system is shown in Figure 6.4. The platinum gauze counter electrode was placed downstream of the cell while the reference electrode (Ag/AgCl) was placed upstream. Before all experiments the solution in the reservoir was purged of O_2 by bubbling through white spot nitrogen (BOC), which had been purified by passing over a B.T.S. catalyst.

6.3.2 SOLUTION PREPARATION

All chemicals used were Analar grade from B.D.H. The solution used for the experimental work consisted of 3×10^{-3}M potassium ferricyanide, with a background electrolyte of 0.1M potassium chloride. 1.0082g $K_3Fe(CN)_6$ and 7.435g KCl were dissolved in 1 l. nanopure water (Section 4.9).

6.3.3 EXPERIMENTAL TECHNIQUE

The solution was placed in the reservoir and degassed for twenty minutes. The Young's tap was then opened and the solution was allowed to flow through the flow system.

In order to verify the hydrodynamics of the system, voltammagrams were measured at various flow rates, changed by altering Δh, the height difference between the level of the base of the capillary and the level of liquid in the reservoir, and/or changing the capillary tube. The potentiostat used was built in the department, and the potentials were measured using a Thornton D.V.M. The current voltage curves were recorded on a Bryans XY recorder (6 000 series).

Current time curves were then obtained at various flow rates, using a Bryans X, Y, T recorder, by stepping the applied potential from a value where no electrochemical reaction was occurring to one where the current was diffusion limited. This potential jump was achieved using a pulse generator built in the departmental electronic workshop. The time base was started, the potential was changed and the subsequent transcient was analysed.

6.4 RESULTS

The flow of solution through the capillary tubes controlled the overall rate of flow through the system, and so the different capillaries had to be calibrated.

For each capillary tube the flow rate was measured as a function of Δh. It was assumed that the level of the liquid remained unchanged during the calibration, due to the small volume of liquid flowing.

The reservoir was filled with nanopure water and for various Δh values the Young's tap was opened and the solution was allowed to flow, for a measured time, into a pre-weighed weighing bottle. The top of the bottle was covered with aluminium foil, to prevent evaporation. After several hours the bottle was reweighed and thus the weight of water and thus the volume, flowing per second was found. This experiment was performed at different Δh's for each capillary tube, and graphs of flow rate *vs.* Δh were drawn up - calibrating the capillary tubes. Table 6.3 lists the calibration parameters for a particular capillary d = 0.2 mm, and the calibration curve is shown in Figure 6.6. The capillary tubes were found to give flow rates in the range 1×10^{-1} to $5 \times 10^{-3} cm^3 s^{-1}$.

For the various flow rates, current voltage plots were taken and the limiting currents (I_{lim}) were measured. These are listed in Table 6.4. From the Levich equation, as rewritten for channel electrodes by Matsada,[19]:

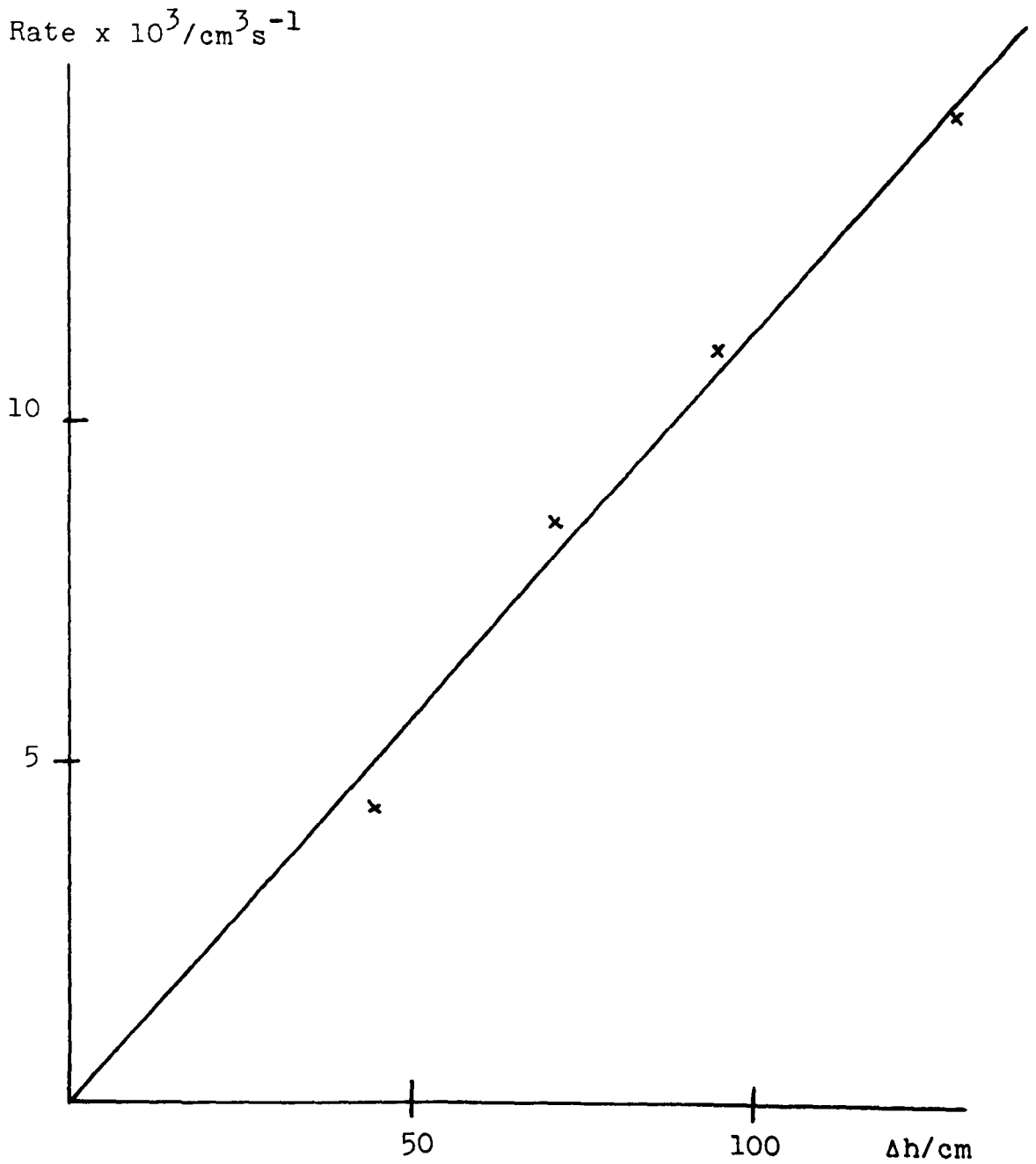

FIGURE 6.6 Calibration curve for 0.2 mm capillary tube.

$$i_{lim} = 1.165\ nFcD^{2/3}\ \bar{U}^{-1/3}\ b^{-1/3}\ Wx_e^{2/3} \qquad 6.8$$

W = width of channel

V_f = fluid flow = $2.\bar{U}$ w.b.

Thus, a plot of log i_{lim} vs. log V_f should show a slope of 1/3. Figure 6.7 shows such a plot with the expected slope of 1/3 drawn in, as can be seen good agreement is shown.

The intercept of this graph allows the diffusion coefficient of $Fe(CN)_6^{3-}$ to be calculated. A value of $7.5 \times 10^{-6} cm^2 s^{-1}$ was found in excellent agreement with the literature value of $7.63 \times 10^{-6} cm^{-2} s^{-1}$, as found by von Stackleberg et al.,[20] using a polarographic technique.

For the current time transients the potential was switched from + 600 mV to 0 mV and the current was measured as a function of time. Figure 6.8 shows a typical result using the capillary tube (calibrated as $8.696 \times 10^{-3} cm^3 s^{-1}$). From these transients the time t_2 (the time taken for the current to fall from its very large initial value to twice the final steady state value) were found.

From Figure 6.3 this corresponds to a τ value of 0.35, thus from the definition of τ,

$$\tau = \left(\frac{9\ \bar{U}^2\ D^{1/3}}{x_E^2\ b^2} \right) t_2 = 0.35 \quad .$$

Table 6.4 lists the experimentally determined values of t_2, at various volume flow rates (V_f), and Figure 6.9

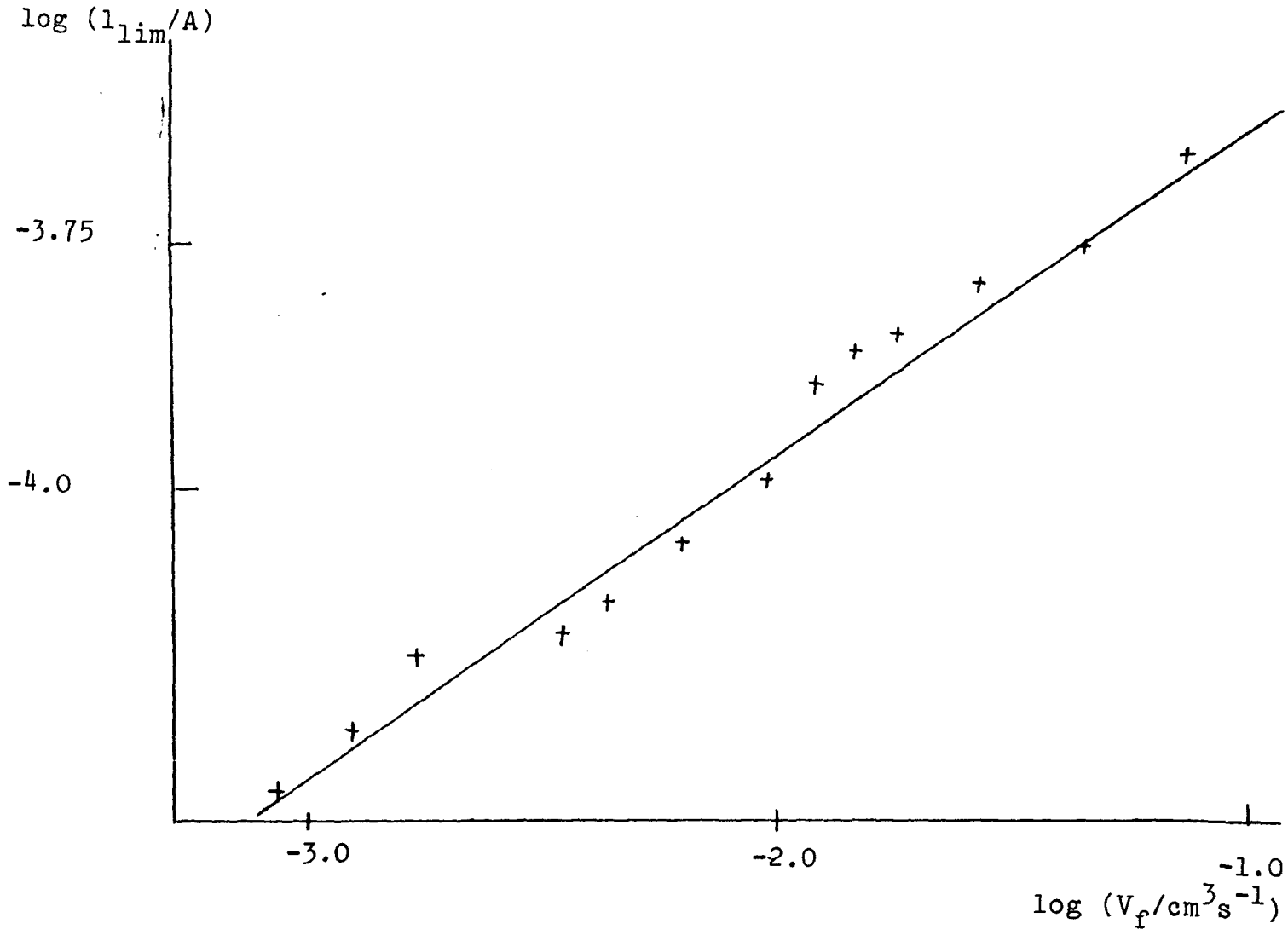

FIGURE 6.7 Levich plot for the channel electrode.

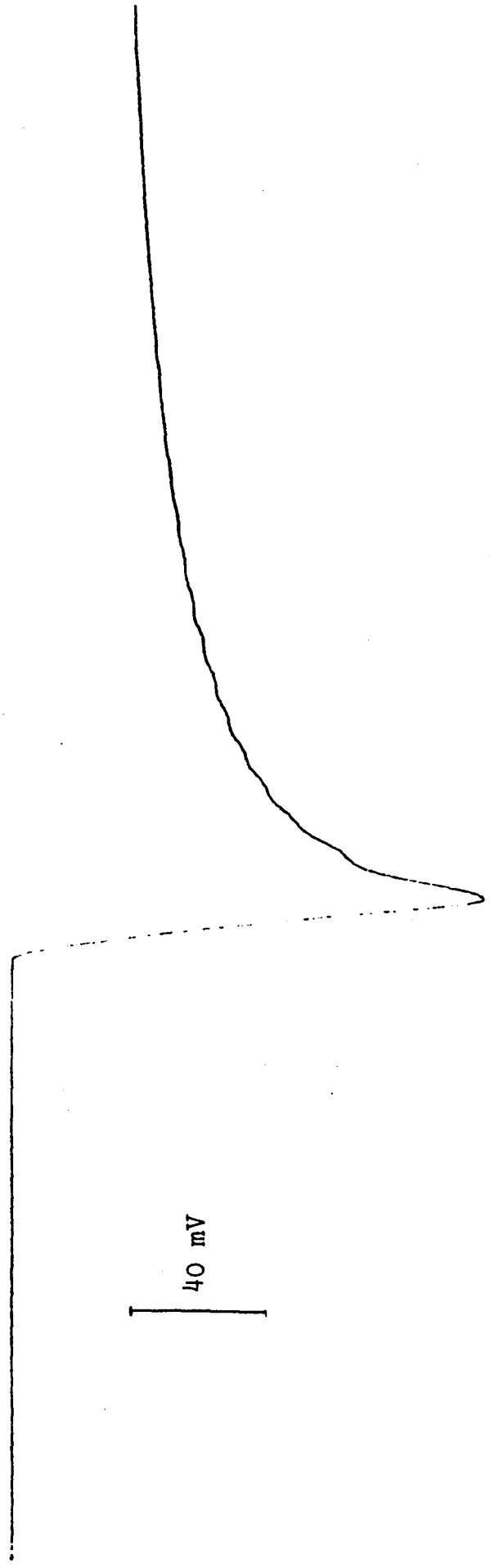

FIGURE 6.8 Typical current transcient

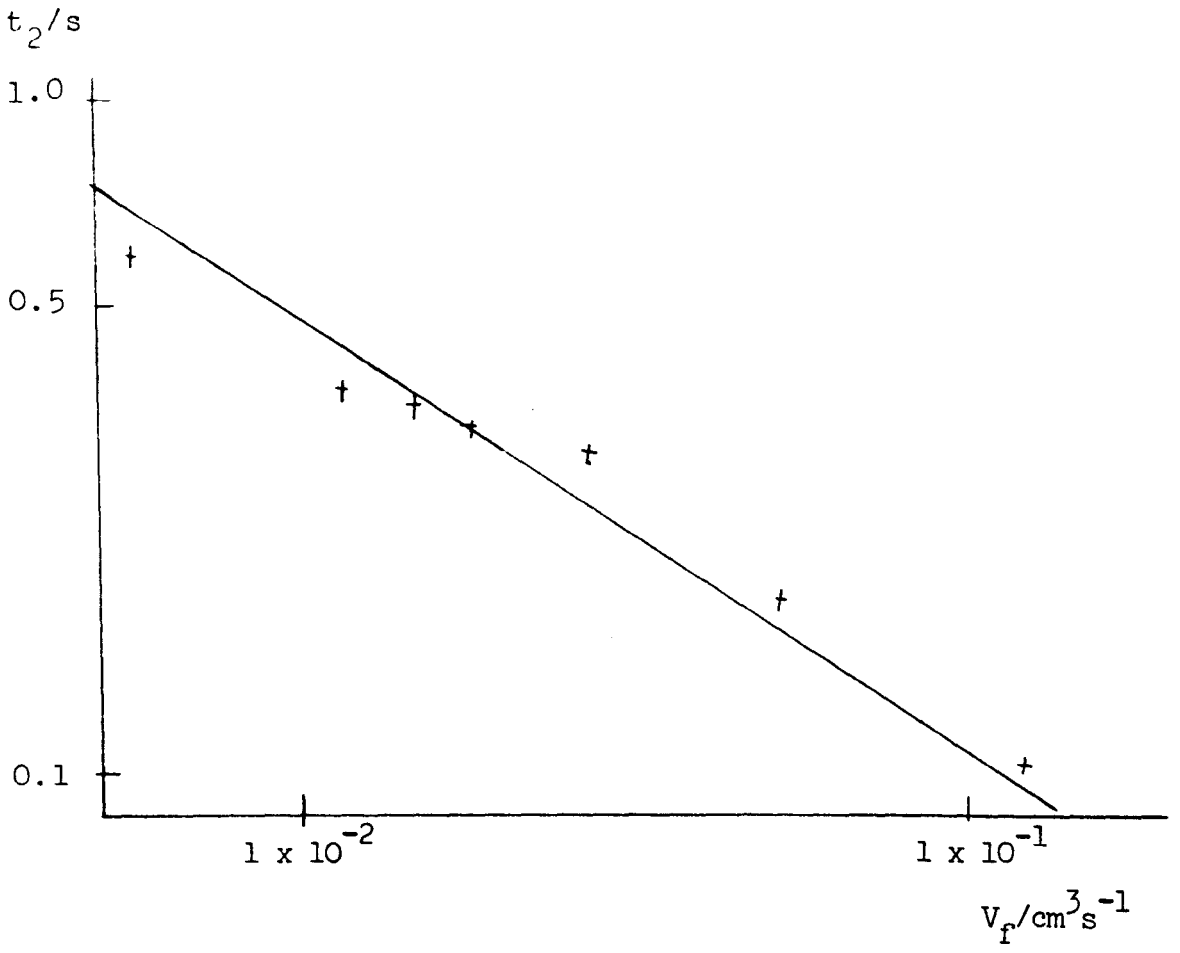

FIGURE 6.9 Plot of t_2 as a function of V_f.

TABLE 6.3 Calibration parameters for calibration of the 0.2 mm capillary.

Δh/cm	VOLUME OF WATER/cm^3	TIME/s	RATE x $10^3/cm^3s^{-1}$
38	3.1463	7 300	0.431
70.4	6.4197	7 500	0.856
94.9	8.6377	7 800	1.107
127.6	7.5370	5 160	1.461

TABLE 6.4 I_{lim} values as a function of flow rate

log Vf	log I_{lim}
-1.121	-3.654
-1.3421	-3.765
-1.569	-3.790
-1.741	-3.846
-1.829	-3.827
-1.916	-3.873
-2.024	-4.001
-2.209	-4.062
-2.373	-4.122
-2.460	-4.155
-2.778	-4.160
-2.9016	-4.251
-3.154	-4.319

shows the log-lot plot, giving a slope of -0.627, in close agreement with the theoretical slope of -2/3.

The line drawn in Figure 6.8 is that calculated using the experimentally determined value for D and the measured values for the geometry of the system.

So, as can be seen, the theory for the transients produced by a potential step at a channel electrode, is in close agreement with the experimental results.

TABLE 6.4 Experimentally determined values of t_2 as a function of flow rate.

V_f/cm^3s^{-1}	t_2/s
1.021×10^{-1}	0.096
4.549×10^{-2}	0.223
2.697×10^{-2}	0.321
1.814×10^{-8}	0.354
1.481×10^{-2}	0.376
1.213×10^{-2}	0.394
9.462×10^{-3}	0.671

Unfortunately in the time available it was not possible to complete the second half of the aims of this section, i.e., the construction of a flow cell incorporating a crystal of Iceland Spar.

1. W.J.Blaedel, L.N.Klatt, *Anal.Chem.*, 38, 879 (1966).
2. W.J.Blaedel, C.W.Boyer, *ibid.*, 43, 1538 (1971).
3. W.J.Blaedel, C.W.Boyer, *ibid.*, 49, (49), 1977.
4. R.E.Meyer, M.C.Banta, P.M.Lantz, F.A.Posey, *J.Electroanal.Chem.*, 30, 345 (1971).
5. F.A.Posey, R.E.Meyer, *J.Electroanal.Chem.*, 30, 359 (1971).
6. K.Aoki, H.Matsuda, *ibid.*, 90, 333 (1978).
7. R.G.Compton, B.A.Coles, *ibid.*, 144, 87 (1983).
8. R.G.Compton, B.A.Coles, *ibid.*, 127, 37 (1981).
9. R.G.Compton, D.J.Page, G.R.Sealy, *ibid.*, 161, 129 (1984).
10. R.G.Compton, P.J.Daly, P.R.Unwin, A.M.Waller, *ibid.*, 191, 15 (1985).
11. K.Aoki, H.Matsuda, *ibid.*, 77, 49 (1979).
12. K.Aoki, H.Matsuda, *ibid.*, 94, 157 (1978).
13. T.Tsuru, T.Nishimura, K.Akoi, S.Haruyama, *Denki Kagaku*, 50, 712 (1982).
14. R.G.Compton, G.R.Searly, *J.Electroanal.Chem.*, 145, 35 (1983).
15. M.L.Boas, In: "Mathematical Methods in the Physical Sciences", p.592, J. Wiley & Sons, Inc., New York, 1966.
16. M.Abramowitz and I.A.Stegun, In: "Handbook of Mathematical Functions", p.446, Dover, New York, 1970.
17. D.Levin, *Internat.J.Comput.Math.*, 371 (1973).
18. M.Soliman, P.L.Chambre, *Int.J.Heat Mass Transfer*, 10, 342 (1953).

19. H.Matsuda, *J.Electroanal.Chem.*, 15, 325 (1967).

20. M.von Stackleberg, M.Pilgram, V.Tooms, *Z.Elektrochem.*, 57, 342 (1953).

APPENDIX

This section will test the computer programmes used during the course of this work.

```
5  DIM MV(2000)
10  HIMEM: 36095:D% = 0
20  IF  PEEK (36096) +  PEEK (382
     52) <  > 172 THEN  PRINT  CHR$
     (4)"BLOAD QUICKI/O"
30  CALL 36096
35  INPUT "SLOPE =";SL
38  INPUT "INTERCEPT =";IT
40  INPUT "DELAY BETWEEN POINTS (
     SECS)";DY
50 DY% =  INT (DY * 10)
60  INPUT "NO OF POINTS ";NO
65  & TI1:T = D%
67  & AI0: & AI0
68 MX =  - 10000000000:MN =  - MX

70  FOR I = 1 TO NO
75 T = T - DY%: IF T <  - 32768 THEN
     T = T + 65536
80  & AI0:M = M + D%:K = K + 1: &
     TI1: IF D% > T THEN  GOTO 80

90 MV(I) = M / K:M = 0:K = 0
93 TM = (I - 1) * DY
95  PRINT TM;: HTAB 5: GOSUB 1000

100  IF MV(I) > MX THEN MX = MV(I
     )
110  IF MV(I) < MN THEN MN = MV(I
     )
120  NEXT I
130  HGR2 : HCOLOR= 3
135 SC = 170 / (MX - MN)
140  FOR I = 1 TO NO:X = I * 250
     NO:Y = SC * (MV(I) - MN): HPLOT
     X,Y: NEXT I
145  GET A$: TEXT
150  INPUT "JUNK OR DISC (J,D)";A
     $
160  IF A$ = "J" THEN  END
170  IF A$ = "D" THEN  GOTO 200
180  PRINT "": GOTO 150
200 D$ =  CHR$ (4)
210  INPUT "FILENAME = ";FF$
220  PRINT D$"OPEN ";FF$
230  PRINT D$"WRITE ";FF$
240  PRINT 2 * NO
250  FOR I = 1 TO NO:TM = (I - 1)
     * DY: PRINT TM: PRINT MV(I)
     : NEXT I
260  PRINT D$"CLOSE ";FF$
270  END
1000 MV(I) = (MV(I) + 8.4426) / 4
     .0971
1005 MV(I) = MV(I) + 204:MV(I) =
     MV(I) / 10
1007  PRINT MV(I)," ";
1010 MV(I) = (MV(I) - IT) / SL
1020 MV(I) = 10 ^ MV(I)
1025  PRINT MV(I)
1030  RETURN
```

COMPOST

```
5  HOME :RT = 0:D$ =  CHR$ (4):ENABLE = 768:DISABLE = 770: POKE 768,88: POKE 769
,96: POKE 770,120: POKE 771,96
6  INPUT "DESTINATION FILENAME FOR COMPOSITION DATA (NOTE THIS FILE SHOULD ALREA
DY EXIST :RUN 1000 IF NEEDED ? ";G$
7  CALL DISABLE
8  PRINT : PRINT D$:"PR£1": PRINT  CHR$ (15)
9  CALL ENABLE
10  DIM P(5),K(5),W(5),M(4),L(4),U(4),D(4,4),R(6,4),H(4,4),C(6),V(4),Z(4),T(4),F
(4,4),N(4),Q(51),B(51),X(51),O(51,9)
52 A = 0.5085:R1 = 0.9970:P7 = 14.004
53 D3 = 78.54:N1 = 0.008909:JC = 1
54 L(1) = 59.5:L(2) = 69.3:L(3) = 44.5:L(4) = 44.5
55  INPUT "IS THE TEMP. 25 C ?(Y/N)";A$
60  IF A$ = "Y" THEN T = 25 + 273.16:T1 = T: GOTO 130
65  INPUT "TEMPERATURE ? ";T:T = T + 273.16:T1 = T
70  INPUT "DEBYE-HUCKEL CONSTANT ? ";A
72  INPUT "DENSITY OF WATER ?";R1
74  INPUT "PKW FOR WATER ?";P7
75  INPUT "DIELECTRIC CONSTANT =";D3
80  INPUT "VISCOSITY OF WATER =";N1
85  PRINT "PLEASE INPUT LIMITING CONDUCTANCE VALUES ?"
90  INPUT "CA ?";L(1): INPUT "CO3 ?";L(2): INPUT "HCO3 ?";L(3): INPUT "CAHCO3+ ?
";L(4)
95  GOTO 130
122  HOME
125  INPUT "TEMP(C) ?";T:T1 = T + 273.16:T = T1
130 P(1) = 14.8435 - 3404.71 / T - 0.03279 * T
132 P(2) = 6.498 - 2902.39 / T - 0.02379 * T
134 P(3) = 2.95 - 0.0133 * T
136 P(4) = 27.393 - 4114 / T - 0.05617 * T
138 P(5) =  - 1.4
140 P8 =  - 13.417 + 2299.6 / T + 0.01422 * T
142 P6 = 13.543 - 3000 / T - 0.0401 * T
155  REM  CONSTANTS ARE GROUPED HERE
157 I1 = 0.001:E = 4.8032E - 10:C1 = 299.79 / (96487.0 * E)
160  HOME
162  PRINT  TAB( 4);"TEMPERATURE="; INT ((T - 273.16) * 100) / 100;"C"; TAB( 21)
;"DH CONS.=";A
165  PRINT  TAB( 4);"DENSITY=";R1; TAB( 21);"DI/CON=";D3
168  PRINT  TAB( 4);"VISCOSITY OF WATER =";N1
170  PRINT  TAB( 4);"PK1="; INT ( - P(1) * 1E4) / 1E4; TAB( 21);"PK2="; INT ( -
P(2) * 1E4) / 1E4
175  PRINT  TAB( 4);"PK3="; INT ( - P(3) * 1E4) / 1E4; TAB( 21);"PK4="; INT ( -
P(4) * 1E4) / 1E4
180  PRINT  TAB( 4);"PKH"; INT ( - P8 * 1E4) / 1E4; TAB( 21);"PKW=";P7
185  PRINT  TAB( 4);"PKSO="; INT ( - P6 * 1E4) / 1E4
190  PRINT : PRINT  TAB( 4);"LIMITING CONDUCTANCE VALUES :"
195  PRINT  TAB( 4);"CA : ";L(1); TAB( 21);"CO3 : ";L(2)
200  PRINT  TAB( 4);"HCO3 : ";L(3); TAB( 21);"CAHCO3+ : ";L(4)
220 I2 = I1
230 K(1) = 10 ^ (P(1))
240 K(2) = 10 ^ (P(2))
250 K(3) = 10 ^ (P(3))
260 K(4) = 10 ^ (P(4))
270 K(5) = 10 ^ (P(5))
280 K7 = 10.0 ^ ( - P7)
290 K8 = 10 ^ (P8)
300 K6 = 10 ^ (P6)
305  CALL DISABLE
310  PRINT D$;"PR£0"
315  CALL ENABLE
320 E = 4.80324E - 10:C1 = 299.79 / (96487 * E):ND = 0
325  INPUT "FILENAME OF T,PH CONDUCTIVITY DATA ? ";F$
327  CALL DISABLE
330  PRINT : PRINT D$;"OPEN" + F$
335  PRINT D$;"READ" + F$
340  FOR J = 1 TO 51
345  INPUT Q(J): INPUT B(J): INPUT X(J)
350  IF Q(J) = 9999.9 THEN  GOTO 365
355 ND = ND + 1
360  NEXT J
365  PRINT D$;"CLOSE" + F$
367  CALL ENABLE
370  INPUT "PROCESS DATA FROM TIME ? ( MIN ) ";TZ
372  FOR J = 1 TO 51
374  IF Q(J) >  = TZ THEN NZ = J: GOTO 378
376  NEXT J: REM USE DATA FROM NZ TO ND
378 P9 = B(NZ):C6 = X(NZ)
380 NZ = NZ + 1
```

```
[illegible]  GOTO [illegible]
[illegible]  REM ******************************
400  REM  DETERMINES S AND IONIC COMPOSITION
401  PRINT "POINT £ ";NZ - 1;" PH = ";P9;" TIME =";Q(NZ - 1)
405  REM ******************************
407 I4 = 0:S = 0:D9 = 3:I1 = I2
440 I5 = P6 * 10.0 ^ S
450 A9 = 1.0 / 10.0 ^ P9
460 I3 =  SQR (I1)
470 F1 = I3 / (1 + I3) - 0.3 * I1
480 A8 =  - A * F1:G = 10.0 ^ A8
500 C7 = G * A9
510  GOSUB 800
520  GOSUB 1500
530 P5 = ( - X2 +  SQR (X2 * X2 - 4.0 * X1 * X3)) / (2.0 * X1)
540  GOSUB 2500
550  IF I4 = 0 THEN 460
560  GOSUB 3500
570 V9 = (C6 - C5) / C5
575  REM  C5 IS THE CALCULATED CONDUCTIVITY IN MICROSEMONS
580  IF  ABS (V9) < 0.0001 THEN 670
590  IF V9 > 0 THEN 640
600  IF V9 < 0 THEN 620
610  PRINT "ERROR IN 610,V9=0?"
620 S = S - D9
630  GOTO 650
640 S = S + D9
650 D9 = D9 / 2
660  GOTO 440
670 C8 = Q1 + Q2 + Q3 + Q4
680 I2 = I1
690  RETURN
700  REM ********************************
705  REM  DETERMINES APP. DISSOCIATION CONSTANTS USING DH THEORY
710  REM ********************************
800 Y = 10 ^ (A * F1)
810 Y4 = Y * Y * Y * Y
820 Y8 = Y4 * Y4
830 W(1) = K(1) * Y
840 W(2) = K(2) * Y * Y * Y
850 W(3) = K(3) * Y4
860 W(4) = K(4) * Y8
870 W(5) = K(5) * Y4
880 W1 = K7 * Y
890 W2 = K5 * Y8
900  RETURN
1000  HOME : INPUT "ARE YOU SURE YOU NEED A NEW FILE(Y/N) ? ";A$
1010  IF A$ = "N" THEN  STOP
1020  INPUT "FILENAME FOR COMPOSITION DATA (S£) ? ";G$
1030  PRINT : PRINT  CHR$ (4);"OPEN" + G$
1040  PRINT  CHR$ (4);"DELETE" + G$
1042  PRINT  CHR$ (4);"OPEN";G$
1045  PRINT  CHR$ (4);"WRITE";G$
1048  PRINT "T,PH,CAT,PCO2,CA,CO3,HCO3,SI,I DATA"
1050  PRINT  CHR$ (4);"CLOSE" + G$
1060  PRINT "FILE ";G$;"CREATED & CLEAR"
1070  STOP
1500 W3 = W(1) * K8:W4 = W(2) * W(3)
1520 W5 = A9 * A9:X1 = W3 * A9 + 2 * W(2) * W3
1540 X1 = X1 / W5
1550 X2 = W1 * W4 - A9 * C7 * W4 - W2 * W5
1560 X2 = X2 / (A9 * W4)
1570 X3 = W2 * W1 * A9 + 2 * W2 * W5 * W(5)
1580 X3 =  - X3 / (W(1) * W(2) * K8 * W(5))
1590  RETURN
1600  REM *********************************
1610  REM  DETERMINES CONC. OF IONS:Q1:CA    Q2:CAHCO3;  Q3:CAOH   Q4:CACO3  Q5:
CARB  Q6:HCO3  Q7:OH
1620  REM  ********************************
2500 W5 = A9 * A9:W6 = W2 * A9:W7 = W(1) * W(2)
2530 W9 = K8 * P5:Q1 = W6 * A9 / (W7 * W9):Q2 = W6 / (W(2) * W(3))
2560 Q3 = W6 * W1 / (W7 * W9 * W(5))
2570 Q5 = W7 * W9 / W5
2580 Q6 = W(1) * W9 / A9:Q7 = W1 / A9
2600 I2 = C7 + Q7 + Q6 + 4 * Q5 + 4 * Q1 + Q3 + Q2:I2 = 0.5 * I2 / R1
2620  IF  ABS (I1 - I2) / I2 < 0.001 THEN 2660
2630 I4 = 0
2640 I1 = I2
2650  RETURN
```

```
3000  REM  *********************************
3010  REM  DETERMINES SPECIFIC CONDUCTANCE,C7, FROM CA,CO3,HCO3,CAHCO3 CONS.
3020  REM *********************************
3500 M(1) = U1
3510 M(2) = 05
3520 M(3) = 06
3530 M(4) = 02
3540 Z(1) = 2
3550 Z(2) =  - 2
3560 Z(3) =  - 1:Z(4) = 1
3580  FOR J = 1 TO 4:V(J) = 0: NEXT J
3581  FOR J = 1 TO 6
3582  FOR J1 = 1 TO 4
3583 R(J,J1) = 0
3584  NEXT J1: NEXT J
3590  FOR J = 1 TO 4
3600  FOR J1 = 1 TO 4
3610 H(J,J1) = 0
3620 F(J,J1) = 0
3630  NEXT J1: NEXT J
3650 T3 = 0
3660  FOR J = 1 TO 4
3670 T(J) = M(J) * Z(J) * Z(J)
3680 T3 = T3 + T(J)
3690  NEXT J
3700  FOR J = 1 TO 4
3710 N(J) = T(J) / T3
3720 U(J) = C1 * L(J) /  ABS (Z(J))
3730  NEXT J
3740  FOR J1 = 1 TO 4
3750  FOR J = 1 TO 4
3760 D(J,J1) = 0
3770  IF J = J1 THEN 3790
3780  GOTO 3800
3790 D(J,J1) = 1
3800  NEXT J: NEXT J1
3820  FOR J = 1 TO 4
3830  FOR J1 = 1 TO 4
3840 C2 = 0
3850  FOR J2 = 1 TO 4
3860 C2 = C2 + N(J2) * U(J2) / (U(J) + U(J2))
3870  NEXT J2
3880 H(J,J1) = D(J,J1) * C2 + N(J1) * U(J1) / (U(J) + U(J1))
3890 F(J,J1) = 2 * H(J,J1) - D(J,J1)
3900  NEXT J1
3910  NEXT J
3920  FOR J = 1 TO 4
3930 C3 = 0:C4 = 0
3950  FOR J1 = 1 TO 4
3960 C2 = Z(J1) * N(J1)
3970 C3 = C3 + C2:C4 = C4 + C2 / L(J1)
3990  NEXT J1
4000 R(1,J) = Z(J) - Z(J) * C3 / (L(J) * C4)
4010  NEXT J
4020  FOR J = 2 TO 6
4030 J9 = J - 1
4040  FOR J1 = 1 TO 4
4050 C3 = 0
4060  FOR J2 = 1 TO 4
4070 C3 = C3 + F(J1,J2) * R(J9,J2)
4080  NEXT J2
4090 R(J,J1) = C3
4100  NEXT J1: NEXT J
4120 C(1) = 0.2929:C(2) =  - 0.3536:C(3) = 0.0884
4150 C(4) =  - 0.0442:C(5) = 0.0276:C(6) =  - 0.0193
4180 C2 = 29.165 / (N1 *  SQR (D3 * T1))
4190 C3 = 1.9807E + 6 /  SQR ((D3 * T1) ^ 3)
4200 T4 =  SQR (T3):C5 = 0
4220  FOR J = 1 TO 4
4230 C4 = 0
4240  FOR J1 = 1 TO 6:C4 = C4 + C(J1) * R(J1,J)
4260  NEXT J1
4270 A1 = C3 * Z(J) * C4:A2 = C2 *  ABS (Z(J)):A3 = A1 * T4
4300 A1 = (A1 * L(J) + A2) * T4:V(J) = L(J) - A1:C5 = C5 + M(J) *  ABS (Z(J)) *
V(J)
4330  NEXT J
4340 C5 = C5 * 1000
4350  RETURN
4360  STOP
```

```
6005 C5 =  INT (C5 * 100) / 100:C8 =  INT (C8 * 1E6) / 1E3:01 =  INT (01 * 1E6)
 / 1E3:06 =  INT (06 * 1E6) / 1E3:I1 =  INT (I1 * 1E6) / 1E3:S =  INT (S * 1E3) /
 1E3:P5 =  INT (P5 * 1E6) / 1E3:05 =  INT (05 * 1E8) / 1E3
6010 O(JC,1) = Q(NZ - 1):O(JC,2) = P9:O(JC,3) = C8:O(JC,4) = P5:O(JC,5) = 01:O(J
C,6) = 05:O(JC,7) = 06:O(JC,8) = S:O(JC,9) = I1
6015 JC = JC + 1:
6020  IF RT = 0 THEN  PRINT " T    PH   COND  CALC   CAT  PCO2  CA    CO3 HCO3
SI   I": PRINT  TAB( 10);"US"; TAB( 18);"US"; TAB( 23);"MM"; TAB( 28);"MM"; TAB(
 34);"MM"; TAB( 39);"1E-5"; TAB( 45);"MM"; TAB( 55);"MM"
6040  PRINT Q(NZ - 1);"  ";P9;"  ";C6;"  ";C5;"  ";C8;"  ";P5;"  ";01;"  ";05;"
 ";06;"  ";S;"  ";I1
6050  PRINT D$;"PR£0"
6052  CALL ENABLE
6055 RT = 1
6060  RETURN
7000  CALL DISABLE: PRINT : PRINT D$;"APPEND" + G$
7010  PRINT D$;"WRITE" + G$
7020  FOR J1 = 1 TO JC
7030  FOR J = 1 TO 9
7040  PRINT O(J1,J)
7050  NEXT J
7060  NEXT J1
7070  PRINT D$;"CLOSE" + G$
7080  CALL ENABLE
7090  RETURN
10000  STOP
```

```
      COMMON AL(60,60),BE(60,60)
      REAL IMZ(60)
      EXTERNAL X02AAF,C02AEF
      DIMENSION A(60),B(60),C(60),GM(60),CC(60),
     1BB(60),REZ(60),T(60),POP(60,60)
      AIO=0.35502805388781?
       AIPO=-0.25881940379280?
      AO =AIO
      DO 2 J=1,20
      JJ=3*J-1
2     A(JJ)=0.0
      A(1)=AIPO
      DO 3 M=1,19
      JJ=3*M+1
      JM=3*M-2
      ZIO=1./(FLOAT(3*M+1))/(FLOAT(3*M))/(FLOAT(3*M-1))
3     A(JJ)=A(JM)*(FLOAT(3*M-1))*ZIO
      A(3)=AIO/6.0
      DO 4 M=2,20
      JJ=3*M
      JM=3*M-3
      ZIO=1./(FLOAT(3*M))/(FLOAT(3*M-1))/(FLOAT(3*M-2))
4     A(JJ)=A(JM)*(FLOAT(3*M-2))*ZIO
      CO=A(1)
       C(1)=(2.0*A(2))-((CO*A(1))/AO)
       DO 8 J =2,59
       JH =J-1
       SUM =0.0
       DO 9 K =1,JH
       KK=J-K
       H= (C(KK)*A(K))/AO
9      SUM =SUM+H
      HH=(CO*A(J))/AO
       SUM = SUM + HH
8      C(J)= ((FLOAT(J+1)*A(J+1))-SUM)
      TTH=(3.0**(-2./3.))/AIO
      OTH =-(3.0**(-1./3.))/AIPO
      GMO=TTH*2./3.
      GM(1)=4.*OTH/9.
      GM(2)=2.
      DO 10 J=1,19
      AJ=FLOAT(J)
      JJ=3*J+2
      JK=3*J-1
      AK=FLOAT(JK)
10    GM(JJ)=GM(JK)*((5./3.)*(2.*AK/3.))*((8./3.)
     1*(2.*AK/3.))
      DO 11 J=1,19
      JJ=3*J+1
      JK=3*J-2
      AK=FLOAT(JK)
11    GM(JJ)=GM(JK)*((5./3.)*(2.*AK/3.))*((8./3.)
     1*(2.*AK/3.))
       GM(3)=GMO*40./9.
      DO 12 J=2,20
```

```
      JJ=3*J
      JK=3*J-3
      AK=FLOAT(JK)
 12    GM(JJ)=GM(JK)*((5./3.)+(2.*AK/3.))*((8./3.)
     1+(2.*AK/3.))
C      WORK OUT CC(J)
      DO 19 J=1,40
 19   CC(J)=C(J)/GM(J)
      DO92 JJ=1,25
      WRITE(6,93)CC(JJ)
 92   CONTINUE
 93   FORMAT(1X,'CC(JJ) =',F16.14)
 25   WRITE(6,98)
 98   FORMAT(1X,24HENTER T,NEGATIVE TO STOP)
      READ(5,*) TT
      IF(TT)21,21,22
 22    WRITE(6,23)TT
 23   FORMAT(1X,3HT= ,F6.3)
      WRITE(6,31)
 31   FORMAT(1X,29HENTER TINT THE TIME INTERVALS)
      READ(5,*) TINT
      WRITE(6,24)
 24   FORMAT(1X,19HENTER N NO OF TERMS)
      READ(5,*) N
      NW=N+1
       CALL RAPP(CC,AL,BE,NW)
       DO 95 IK =3,N
        DO 95 I =1,IK
        WRITE(6,91)AL(IK,I)
 95      CONTINUE
 91     FORMAT(1X,'AL(N) =',F16.8)
      DO 82 IL = 3,N
       IZ=IL+1
      DO 82 I=1,IZ
       WRITE(6,83)BE(IZ,I)
 82   CONTINUE
 83   FORMAT(1X,'BE(N)=',F16.6)
       DO 26 K =3,N
       IFAIL = 0
       TOL=X02AAF(X)
       KW=K+1
      DO 32 L=1,KW
      LC=K+2-L
 32   BB(LC)=BE(K,L)
      CALL C02AEF(BB,KW,REZ,IMZ,TOL,IFAIL)
      DO85 I=1,K
      WRITE(6,86)REZ(I),IMZ(I)
 85   CONTINUE
 86   FORMAT(1X,'REZ(I) =',F16.11,1X,'IMZ(I)=',F16.11)
      WRITE(6,97)IFAIL
 97   FORMAT(1X,'IFAIL =',F6.4)
      LLL=IFIX(TT/TINT)
 80    DO 36 L=1,LLL
      T(L)=FLOAT(L)*TINT
      SUM=0.0
```

```
      SUMIM=0.0
      DO 35 J=1,K
      IF(REZ(J).LT.-174.0) GO TO 202
      RA=REZ(J)*T(L)
      RB=IMZ(J)*T(L)
      RS=SIN(RB)
      RC=COS(RB)
      RE=EXP(RA)
      RR=(RE*RC)
      RP=(RE*RS)
      TERMR =RR
      GO TO 201
202   TERMR =0.0
201    IF(REZ(J).LT.-174.0) GO TO 203
       TERMI =RP
       GO TO 204
203    TERMI =0.0
204    CALL GPN(REZ(J),IMZ(J),K,GR,GI)
       CALL HPPN(REZ(J),IMZ(J),K,HR,HI)
       GDHR=((GR*HR)+(GI*HI))/CMODU(HR,HI)
       GDHI=((HR*GI)-(HI*GR))/CMODU(HR,HI)
       TERM1=(TERMR*GDHR)-(TERMI*GDHI)
       TERM2 =(TERMR*GDHI)+(TERMI*GDHR)
       SUMIM =SUMIM+TERM2
35    SUM= SUM + TERM1
36     POP(K,L) =(SUM*GM0)/A(1)
       IF(K.GT.3) GO TO 311
       WRITE(6,37) (T(LK),LK=1,LLL)
37     FORMAT(1X,3HT= ,(3X,F9.5))
311    WRITE(6,38)K,(POP(K,LA),LA=1,LLL)
38     FORMAT(1X,3HN= ,I3,(3X,F20.6))
25     CONTINUE
       GO TO 25
21     CONTINUE
       STOP
       END
       SUBROUTINE RAPP(CC,AL,BE,N)
       DIMENSION CC(61),AL(60,60),BE(60,60),D(60)
       NM1=N-1
       DO 40 K=2,NM1
       KP1=K+1
       DO 10 J=1,KP1
10    D(J)=(-1.0)**(J-1)*GAMA(K)/GAMA(J-1)/GAMA(K-J+1)*
     1((J-1.)/(K+1.))**(K-2)
       DO 20 I=1,K
       AL(K,I)=0.0
       DO 20 L =1,I
20     AL(K,I)=AL(K,I)+CC(L)*D(K-I+L+1)/CC(K-I+L+1)
       DO 30 I=1,KP1
30     BE(K,I)=D(K-I+2)/CC(K-I+2)
40     CONTINUE
       RETURN
       END
       FUNCTION CMODU(FC,FD)
       CMODU=(FC*FC)+(FD*FD)
```

```
      RETURN
      END
      FUNCTION GAMA(J)
      G=1
      DO 3 I=1,J
    3 G=G*I
      GAMA=G
      RETURN
      END
      SUBROUTINE CMULT(AX,BX,S,T,Y,Z)
      Y=(AX*S)-(BX*T)
      Z=(BX*S)+(AX*T)
      RETURN
      END
       SUBROUTINE GPN(AY,BY,K,GR,GI)
      COMMON  AL(60,60),BE(60,60)
      SUMR=AL(K,1)
      TERMR=AL(K,1)
      SUMI=0.0
      TERMI=0.0
      JC=K
      DO 99 JP=2,JC
      JG=JP-1
      CALL CMULT(TERMR,TERMI,AY,BY,Y,Z)
      TERMR=AL(K,JP)*Y/AL(K,JG)
      TERMI=Z*AL(K,JP)/AL(K,JG)
      SUMI=SUMI+TERMI
   99 SUMR=SUMR+TERMR
      GR=SUMR
      GI=SUMI
      RETURN
      END
      SUBROUTINE HPPN(AZ,BZ,K,HR,HI)
      COMMON AL(60,60),BE(60,60)
      SUMI=0.0
      SUMR=BE(K,2)
      TERMI=0.0
      TERMR=BE(K,2)
      DO 61 JP=2,K
      JG=JP+1
      CALL CMULT(TERMR,TERMI,AZ,BZ,Y,Z)
      TERMR=Y*BE(K,JG)*(FLOAT(JP))/BE(K,JP)/(FLOAT(JP-1))
      TERMI=Z*BE(K,JG)*(FLOAT(JP))/BE(K,JP)/(FLOAT(JP-1))
      SUMI=SUMI+TERMI
   61 SUMR=SUMR+TERMR
      HR=SUMR
      HI=SUMI
      RETURN
      END
```

The Dissolution Kinetics of Iceland Spar Single Crystals

RICHARD G. COMPTON AND PADRAIG J. DALY

Department of Inorganic, Physical and Industrial Chemistry, The University of Liverpool, P.O. Box 147, Liverpool L69 3BX, England

Received November 19, 1983; accepted February 22, 1984

The dissolution of Iceland spar has been studied using a rotating disk method. This allows measurements to be made under conditions of well-defined mass transport and with single crystals prepared with surfaces having reproducible characteristics. The dissolution reaction was studied in the pH range 3.0–6.2 and with varying partial pressures of carbon dioxide. In general the flux of dissolving Ca^{2+} is given by the equation $j_{Ca^{2+}}$/mole cm^{-2} sec^{-1} = $k_1[H^+] + k_2 + k_3[H_2CO_3]$, where we find k_2 to be 2.1×10^{-9} mole cm^{-2} sec^{-1} at 25°C (in citrate buffers) and k_1 and k_3 are given by the rate of transport of H^+ and H_2CO_3, respectively, to the disk surface. In the presence of weak acids such as acetic acid which can rapidly dissociate on the rotating disk time scale then $[H^+]$ should be replaced by [weak acid] in the above equation and the diffusion coefficient used in calculating k_1 should be that of the weak acid.

INTRODUCTION

The dissolution (and precipitation) of calcium carbonate is of considerable importance in the understanding of natural hard-water systems (1) and accordingly has received a considerable amount of attention (2–12). Previous kinetic studies, made upon suspensions of powdered calcium carbonate, have shown that the dissolution rate is increased by the presence of both H^+ and dissolved CO_2 and attempts have been made to separate surface chemical kinetic effects from mass transport effects (usually by varying the speed of a magnetic stirrer). Inevitably this approach is hampered by the ill-defined hydrodynamic conditions prevailing in such suspensions. We have thus undertaken what we believe is the first study of calcium carbonate dissolution using a rotating disk method (although the calcite precipitation reaction has been studied in this way (13)). The rotating disk offers the advantage of well-defined mass transport, the rate of which can be altered by changing the disk rotation speed (14). The pattern of flow near a rotating disk has been solved approximately by Von Karman (15) and the solution improved by Cochran (16) and this description of the hydrodynamics allows the calculation of the rate of transport to the surface of the disk (17).

The use of a rotating disk allows us to make measurements of dissolution kinetics using single crystals of Iceland spar. This offers the additional advantage over studies using powdered material, in that the crystals can be polished so as to produce reproducible surfaces allowing comparisons between different experimental conditions to be made with confidence.

In this work we have examined the effects of altering the pH of the solution and the partial pressure of CO_2 over the solution under conditions where the concentration of calcium ions and carbonate or bicarbonate ions is sufficiently low that the back reaction (i.e., precipitation) may be neglected. The precipitation reaction will be considered in a subsequent paper.

EXPERIMENTAL

A. Materials. Solutions were made up using triply distilled deionized water (resistivity $> 10^7$ ohm cm). BDH Analar grade reagents (citric acid, potassium chloride, sodium ace-

0021-9797/84 $3.00

tate, acetic acid, hydrochloric acid, sodium hydroxide) were used throughout. Iceland spar crystals were obtained from Richard Taylor Minerals (Cobham, Surrey, England) and these originated from Chihuahua, Mexico. British Oxygen supplied carbon dioxide and "white spot" nitrogen.

B. Techniques. Rotating disks were fabricated by setting a single crystal of Iceland spar (typical approximate dimensions $10 \times 10 \times 3$ mm) in a cylinder of Araldite epoxy resin (cast using Resin MY753 with hardener HY951, from Ciba-Geigy, Cambridge, England). Cylindrically shaped electrodes have been shown to give satisfactory hydrodynamic behavior (14, 18, 19) under a wide variety of conditions despite early reservations by Riddiford (20). The rotating disk was then polished using a succession of finer diamond-lapping compounds (Engis, Maidstone, England) either by hand or in conjunction with a Kent Mark II polishing machine. The smallest diamond grit used was 0.25 μm. Where necessary preliminary polishes of particularly rough surfaces were carried out using 45- and 30-μm Bramet abrasive pads (Engis). The finished surface was then rinsed with dilute acid to remove any possible impurities (9) and painted with a solution of polystyrene in carbon tetrachloride so that only a central disk-shaped portion of the crystal was exposed, the remainder being covered by a film of polymer after the solvent had evaporated. This procedure is essential since the calculations by Levich for convective-diffusion to the rotating surface assume that it has cylindrical symmetry about the axis of rotation (17). The area of exposed calcite was obtained through measurements of the diameter of the central disk using a traveling microscope. Rotation of the electrode was achieved using an Oxford Electrodes (Oxford, England) rotating disk assembly and motor-controller. The disk was rotated in a glass reaction vessel of capacity 100 cm^3 which was water-jacketted to allow thermostatting at 25 $\pm$ 0.5°C. A constant stream of a N_2/CO_2 gas mixture of chosen composition was bubbled into the solution throughout a run.

The rate of calcium carbonate dissolution was monitored using a Radiometer (F2112) Calcium Ion Selective Electrode (CaISE) located immediately adjacent to the rotating disk. Readings from the CaISE were taken relative to a saturated calomel electrode using a Radiometer PHM 64 meter (which was also used for pH measurements). The meter was interfaced to an Apple II microcomputer using an Adalab interface card (Heyden Data Systems, London, England) which possesses a 12-bit A/D converter capable of taking up to 20 readings per second. This allowed software to be written which recorded millivolt readings from the CaISE at chosen time intervals and converted these readings into calcium ion concentrations. Calcium ion concentration–time profiles were then displayed graphically at the Apple monitor and a least-square fit used to determine the dissolution rate.

The conversion required to change millivolt readings from the CaISE into calcium concentrations was found daily by calibration. Generally responses were close to the 27.5-mV/decade value expected theoretically. At high pH (>4) the response was nearly constant day by day although at lower pH (<4) some drift was found but this was not sufficient to prevent quantitative measurements being made provided that either the total $[Ca^{2+}]$ change during the reaction was much less than the total $[H^+]$ change or that the system was buffered against pH change.

The response time of the CaISE was determined by rapidly transferring the electrode between solutions of differing $[Ca^{2+}]$. The transients were found to obey the expected (21, 22) exponential form

$$E(t) = E_f + (E_i - E_f) \exp(-t/\tau), \quad [1]$$

where E_i and E_f are the initial and final potentials of the CaISE. The "response time," τ, of the electrode was found to be 3.3 sec. This time scale is substantially faster than that of any of our dissolution experiments, even at the highest acid concentration used.

Consideration was given to the likely transit time between the rotating disk and the CaISE,

a distance of ca. 1 cm. Experiments in which the green dye fluorescein was injected into the reaction vessel indicated that mixing took place throughout the vessel on a time scale of less than 15 sec even at the slowest rotation speed employed. Thus the transit time was thought to be comparable to the response time of the electrode.

THEORY

The rate of transport of a species by convection and diffusion to the surface of a rotating disk has been described by Levich (17). Under the condition that the species reacts sufficiently fast at the disk surface that its surface concentration is effectively zero, the flux j of material to the disk is given by

$$j/\text{mole cm}^{-2}\ \text{sec}^{-1} = 1.554 D^{2/3} \nu^{-1/6} C_\infty \sqrt{\omega}, \quad [2]$$

where D is the diffusion coefficient ($\text{cm}^2\ \text{sec}^{-1}$) of the species, ν is the kinetic viscosity ($\text{cm}^2\ \text{sec}^{-1}$) of the solvent, C_∞ (mole cm^{-3}) is the bulk concentration of the species, and ω (Hz) is the rotation speed of the electrode.

The derivation of Eq. [2] assumes that the diffusing species is not involved in any homogeneous chemical reactions. This is not the case when we are considering the transport to the disk of protons formed from a buffer solution that contains a weak acid which does not itself react at the disk:

$$\text{Solution HA} \underset{k'_{-1}}{\overset{k'_1}{\rightleftharpoons}} \text{H}^+ + \text{A}^- \quad K_a = k'_1/k'_{-1}$$

$$\text{Disk H}^+ \longrightarrow \text{products.}$$

In this situation the flux is less than would be calculated on the basis of the total concentration of HA because of the finite value of k'_1. The problem has been described mathematically by Koutecky and Levich (23) who showed that

$$\frac{1}{j} = \frac{1}{[\text{HA}]}\left[\frac{0.64\upsilon^{1/6}}{D_{\text{HA}}^{2/3}\sqrt{\omega}} + \left(\frac{[\text{A}^-]}{k'_1 K_a D_{\text{H}^+}}\right)^{1/2}\right], \quad [3]$$

where D_{HA} and D_{H^+} are the diffusion coefficients of HA and H^+, respectively.

For species for which experimental data is not available it has been shown that diffusion coefficients of uncharged species may be estimated to within ~10% by the following empirical equation due to Wilke and Chang (24, 25)

$$D \simeq 6.6 \times 10^{-8} \frac{(xM)^{1/2} T}{\eta V^{0.6}} \quad [4]$$

where η is the solvent viscosity (cP), T the absolute temperature, M is the molecular weight of the solvent, x is an association parameter characteristic of the solvent, 2.6 for water, and V($\text{cm}^3\ \text{mole}^{-1}$) is the molar volume of the diffusing species and estimated using the method of Le Bas (26).

RESULTS AND DISCUSSION

Experiments were performed throughout the pH range 3–6.2 using solutions containing either unbuffered HCl, acetic acid/sodium acetate buffer, or citric acid/sodium hydroxide buffer (Sørensen's buffer). In all experiments the total ionic strength of the solution was brought up to 0.3 mole dm^{-3} by the addition of KCl.

We consider first the results obtained at high pH. Figure 1 shows typical plots of $[\text{Ca}^{2+}]$ with time for a solution of Sørensen's buffer at pH 6.11. The data in Fig. 1 was obtained with pure nitrogen being bubbled through the reaction vessel so as to prevent CO_2 from

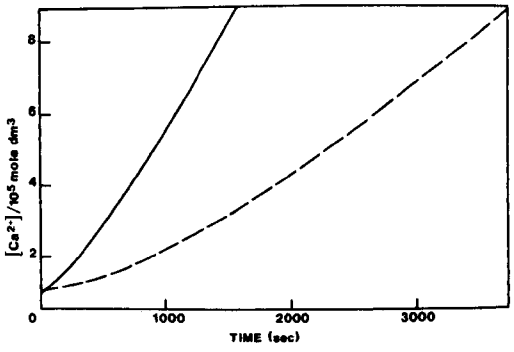

FIG. 1. Typical $[\text{Ca}^{2+}]$ vs time plots for the dissolution of Iceland spar with a pH 6.11 Sørensen's buffer solution for $p_{CO_2} = 0$. The two lines relate to ω = 2.25 Hz (– – –) and 25 Hz (——).

building up. The calcium ion concentration is seen to increase linearly with time. As is apparent from Fig. 1 the rate of dissolution is increased by an increase in the rotation speed of the electrode. If the reaction

$$H^+ + CaCO_3 \rightarrow HCO_3^- + Ca^{2+}$$

is fast enough to reduce the concentration of H^+ at the disk surface to zero we would expect the flux $j_{Ca^{2+}}$ of dissolving Ca^{2+} to be given by Eq. [2] with D and C_∞ relating to H^+. Figure 2 shows fluxes obtained from a number of runs, such as are shown in Fig. 1, plotted against the square root of the rotation speed. It is clear that there is a linear dependence of $j_{Ca^{2+}}$ upon $\sqrt{\omega}$ as predicted by Eq. [2] but there is a nonzero intercept. This behavior is most easily reconciled with a kinetic scheme in which dissolution occurs as a result of two processes only one of which is transport-controlled. If the transport-controlled reaction is that of H^+ diffusion then we can write

$$j_{Ca^{2+}} = k_1[H^+] + k_2, \qquad [5]$$

where from Eq. [2], $k_1 = 1.554 D_{H^+}^{2/3} \nu^{-1/6} \sqrt{\omega}$. Also shown in Fig. 2 is a line whose slope has been calculated theoretically from the known concentration of H^+ and the value of 7.64×10^{-5} cm^2 sec^{-1} (27) for D_{H^+} using Eq. [2]. Good agreement is seen between the theoretical behavior and the least-mean-square fit shown in Fig. 2 for the data for $p_{CO_2} = 0$. In view of this good agreement we conclude that augmentation of the flux of H^+ by dissociation of the buffer is, for this buffer, negligible. The reaction giving rise to the intercept in Fig. 2 may be attributed to

$$CaCO_3 + H_2O \rightarrow Ca^{2+} + HCO_3^- + OH^-,$$

which would not be expected to be transport-controlled owing to the large amounts of water available. In our buffered system the OH^- would be rapidly protonated to form H_2O.

Also shown in Fig. 2 are data obtained when bubbling two different mixtures of CO_2 and N_2 through the solution as dissolution proceeds. The rate of dissolution is seen to increase as p_{CO_2} increases. Figure 3 shows the slope of the Levich plots in Fig. 2 as a function of p_{CO_2}. The linear dependence suggests that the rate of dissolution is being increased by the reaction

$$H_2CO_3 + CaCO_3 \rightarrow Ca^{2+} + 2HCO_3^-,$$

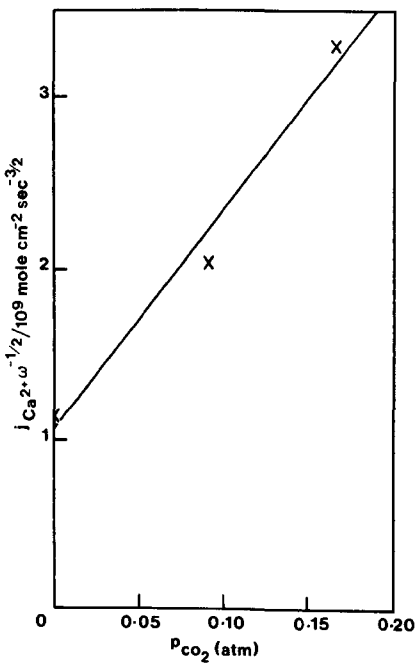

FIG. 3. The dependence of the least-mean-square slopes of the lines in Fig. 2 as function of p_{CO_2}.

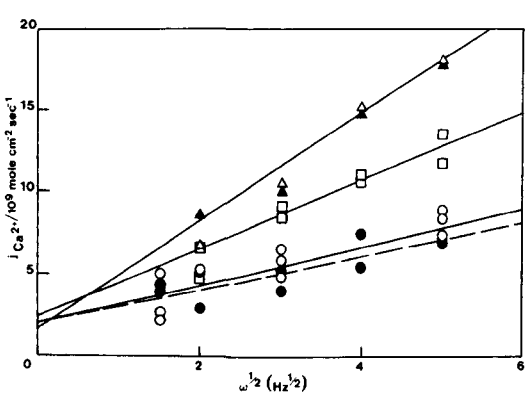

FIG. 2. Levich plots for dissolution with pH 6.11 Sørensen's buffer obtained for $p_{CO_2} = 0$ (○, ●), 0.091 (□), and 0.167 (△, ▲). Different symbols relate to different crystals. The dashed line shows the theoretical slope calculated using Eq. [2] for the case of $p_{CO_2} = 0$.

which by extension of Eq. [2] would lead to the expression for the dissolution rate

$$j_{Ca^{2+}} = k_2 + 1.554\nu^{-1/6}\{D_{H^+}^{2/3}[H^+] + D_{H_2CO_3}^{2/3}[H_2CO_3]\}\sqrt{\omega}, \quad [6]$$

where we have assumed the equilibrium

$$H_2O + CO_2 \overset{k_{hyd}}{\rightleftharpoons} H_2CO_3 \quad K_{H_2CO_3} = \frac{[H_2CO_3]}{[CO_2]}$$

to be slow so that there is no supplementation of the reacting H_2CO_3 in the vicinity of the disk through hydration of dissolved CO_2. This assumption is supported by published values of 0.025 to 0.04 sec^{-1} (28) for the hydration rate constant k_{hyd}. These values are "slow" on the rotating disk timescale (29) suggesting that we may confidently use Eq. [6] which may be rewritten in terms of the Henry Law constant, K_H, for the solubility of CO_2 in water:

$$j_{Ca^{2+}} = k_2 + 1.554\nu^{-1/6}\{D_{H^+}^{2/3}[H^+] + D_{H_2CO_3}^{2/3} \cdot K_{H_2CO_3} \cdot K_H \cdot p_{CO_2}\}\sqrt{\omega}, \quad [7]$$

where p_{CO_2} is the partial pressure (atm) of CO_2 and,

$$[CO_2(aq)] = K_H\, p_{CO_2}. \quad [8]$$

From Fig. 3, and assuming a value of 0.032 mole dm^{-3} atm^{-1} for K_H (30) we find that

$$D_{H_2CO_3}^{2/3} K_{H_2CO_3} = 5.3 \times 10^{-7}\ cm^{4/3}\ sec^{-2/3}.$$

The diffusion coefficient of H_2CO_3 may be estimated to be 1.3×10^{-5} cm^2 sec^{-1} by using Eq. [4]. This gives a value for $K_{H_2CO_3}$ of 9.6 $\times 10^{-4}$. In Table I we compare this value with other published values for the equilibrium

TABLE I

Comparison of Values for $K_{H_2CO_3}$ at 25°C

Author	$(K_{H_2CO_3})^{-1}$	Reference
Bolin	1100	(31)
Barth	386	(32)
Skirrow	500	(33)
This work (assuming $D_{H_2CO_3}$ $= 1.3 \times 10^{-5}$ sec^{-1})	1042	

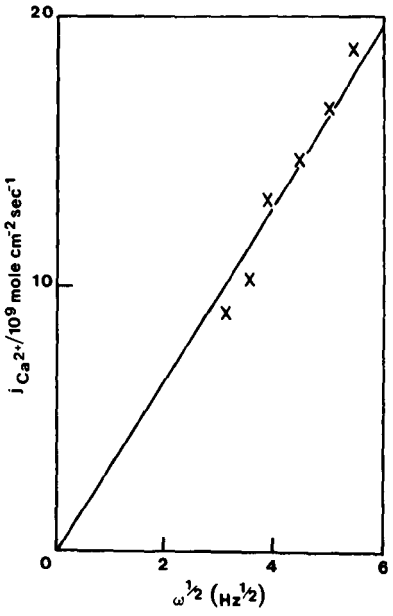

FIG. 4. A Levich plot for Iceland spar dissolution in 10^{-3} mole dm^{-3} HCl.

constant for CO_2 hydration. The value obtained by us is comparable with the other values and so, particularly given the approximation inherent in applying the empirical rule of Eq. [5], may be considered sufficiently good agreement to vindicate Eq. [7] and the kinetic model on which it is based.

It is satisfying that all the lines in Fig. 2 have the same intercept. We obtain an average value for k_2 of 2.1 $\pm$ 0.3 $\times$ 10^{-9} mole cm^{-2} sec^{-1}. It should be stressed that the points shown in Fig. 2 are composed of points obtained from several different crystals and that where one crystal has been used for more than one run it will typically, between runs, have been polished and treated as described above. We are therefore confident that our surface pretreatment leads to a reproducible surface and this enables us to confidently make comparisons between data obtained under different experimental conditions.

We now consider our results obtained from a 10^{-3} mole dm^{-3} solution of HCl (total ionic strength 0.3 mole dm^{-3}) in the absence of carbon dioxide. Fig. 4 shows a Levich plot obtained for this system. We again find agree-

ment with Eq. [5] except that now $[H_2CO_3] = 0$ and since $[H^+]$ ($=10^{-3}$ mole dm^{-3}) is so high, the k_2 term contributes negligibly to the rate.

Further, at this pH we write

$$2.0j_{Ca^{2+}} = k_2 + 1.554\nu^{-1/6}\{D_{H^+}^{2/3}[H^+] + D_{H_2CO_3}^{2/3}[H_2CO_3]\}\sqrt{\omega}. \quad [9]$$

The factor 2.0 appears since at this pH the equilibrium

$$H_2CO_3 \rightleftharpoons H^+ + HCO_3^-$$

lies in favor of H_2CO_3 and thus two molecules of hydrochloric acid are required to release one Ca^{2+} ion. The diffusion coefficient of H^+ calculated from the line shown in Fig. 4 is 7.46×10^{-5} cm^2 sec^{-1} in excellent agreement with the literature value of 7.64×10^{-5} cm^2 sec^{-1} (27). The agreement between theory and experiment again shows that the reaction between H^+ and $CaCO_3$ is very rapid leading to a zero surface concentration of H^+. It should be noted that in all the experiments with 10^{-3} mole dm^{-3} HCl, the quantity of $CaCO_3$ dissolved was insufficient to significantly perturb the pH.

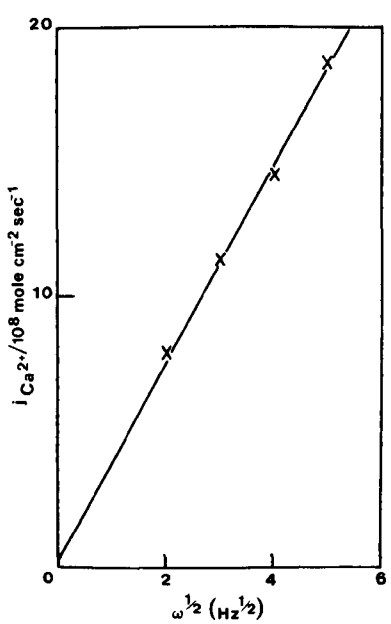

FIG. 5. A typical Levich plot for Iceland spar dissolution in an acetic acid (0.08 mole dm^{-3}) and sodium acetate (0.04 mole dm^{-3}) buffer.

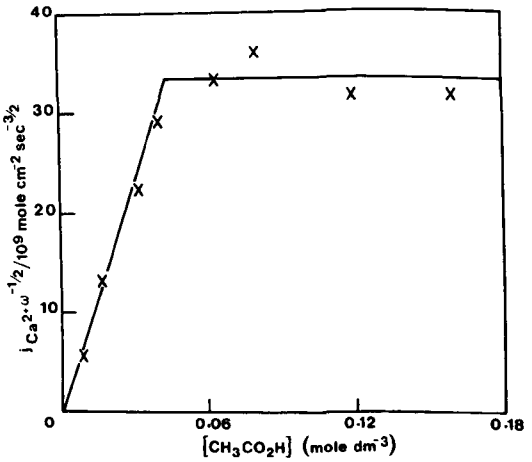

FIG. 6. Slopes from Levich plots (such as Fig. 5) plotted as a function of acetic acid concentration.

Experiments in the pH range 4.21–5.42 were carried out using acetic acid/sodium acetate buffer (total ionic strength 0.3 mole dm^{-3}). Experiments were carried out over a range of concentrations of acetic acid. Excellent Levich plots (such as Fig. 5) of $j_{Ca^{2+}}$ against $\sqrt{\omega}$ were obtained at each concentration allowing average values of $j_{Ca^{2+}}/\sqrt{\omega}$ to be found from the slope of the Levich plot at each concentration of acetic acid. These values are plotted in Fig. 6 as a function of acetic acid concentration. It is clear from Figs. 5 and 6 that the behavior in this pH range for $[CH_3CO_2H] < 0.043$ mole dm^{-3} is best described by Eq. [2] with D and C_∞ relating to acetic acid. From the slope of Fig. 6 in the low $[CH_3CO_2H]$ region we calculate a value for the diffusion coefficient of acetic acid of 8.6×10^{-6} cm^2 sec^{-1}. This is in reasonable agreement with the literature value of 1.01×10^{-5} cm^2 sec^{-1} (25).

It is interesting to consider whether the results in Fig. 6 imply that acetic acid is reacting directly with $CaCO_3$,

$$2CH_3CO_2H + CaCO_3 \rightarrow H_2CO_3 + Ca^{2+} + 2CH_3CO_2^-$$

or whether it dissociates to form H^+ which then reacts,

$$2CH_3CO_2H \rightleftharpoons 2H^+ + 2CH_3CO_2^- \xrightarrow{CaCO_3} Ca^{2+} + H_2CO_3 + 2CH_3CO_2^-.$$

The latter scheme is described by Koutecky–Levich theory (vide supra) as in Eq. [3]. If we use the values of 9.1×10^5 sec^{-1} (34, 35) for k'_1 and 1.75×10^{-8} mole cm^{-3} (36) for K_A we find that Eq. [3] reduces to

$$\frac{1}{j_{Ca^{2+}}} = \frac{2}{[CH_3CO_2H]}\left[\frac{639}{\sqrt{\omega}} + 5.74\right] \quad [10]$$

since the acetate concentration was kept constant at 0.04 mole dm^{-3} in all experiments. From Eq. [10] we see that the kinetics of acetic acid dissociation are sufficiently rapid that the second term in square brackets is negligible and that the reaction of acetate buffer at the disk will be described by the Levich equation (Eq. [2]) both when reaction proceeds indirectly via dissociation into protons and when acetic acid reacts directly with $CaCO_3$. Our results in Fig. 6 do not therefore allow us to distinguish between the two mechanisms. Again in this case the rate is too fast for the k_2 term in Eq. [7] to contribute significantly although it can be seen that the intercept in Fig. 5 is above zero.

Returning to Fig. 6 we see that at higher concentrations of acetic acid (>0.043 mole dm^{-3}) the dissolution rate becomes independent of the acetic acid concentration. We attribute this to the onset of sufficient concentrations of CO_2 at the surface of the disk so that the solubility of carbon dioxide in water is exceeded causing the formation of bubbles, as was verified by observation. Under this condition the dissolution rate is governed by transport of CO_2 away from the disk. The onset point of this condition may be calculated using Eq. [8] where $p_{CO_2} > 1$ for bubble formation. Using the values previously given for K_H, together with the requirement that two molecules of acid are required to release one molecule of CO_2 from $CaCO_3$ the onset of gaseous CO_2 evolution is expected to be at approximately $2K_H = 0.064$ mole dm^{-3} since the rate of reaction at the disk surface is fast enough to consume all the protons at the surface. From Fig. 6 we find that this occurs at 0.043 mole dm^{-3} in approximate agreement with the calculated value.

In conclusion we can see that in general the rate of dissolution of Iceland spar is given by the equation

$$j_{Ca^{2+}}/\text{mole cm}^{-2}\ \text{sec}^{-1} = k_1[H^+] + k_2 + k_3[H_2CO_3],$$

where k_1 and k_3 are given by the rate of transport to the disk surface. In the presence of a proton source, HA (e.g., acetic acid) capable of dissociating on the rotating disk time scale then $[H^+]$ is replaced by [HA] and the diffusion coefficient used in calculating k_1 should be that of HA. The value we find for k_2 is 2.1×10^{-9} mole cm^{-2} sec^{-1}. This may be compared with the value of 1.2×10^{-10} mole cm^{-2} sec^{-1} obtained by Plummer (9) from measurements on calcite powders. The value from our rotating disk measurements was found by assuming that the surface area available for the surface reaction described by k_2 is equal to the measured geometrical area. Electrochemical experiments (37) have shown that for platinum disk electrodes at least the surface roughness is unlikely to be more than twice the geometrical area provided sufficient care is taken in preparing the electrode surface. The value found by us thus represents an upper limit for the "true" rate constant but nevertheless is somewhat larger than Plummer's value which was obtained by estimating the surface area of calcite powder obtained by net sieving between either 20 and 40 mesh (mean size 0.063 cm) or 40 and 80 mesh (mean size 0.03 cm), then calculating the surface area from the weight assuming each particle to be a rhombohedron of width equal to the mean size. We believe our method to be a more reliable estimate of surface area. The reproducibility of results between different crystals shown in Fig. 2 suggests that the geometrical areas of our disks are not too far removed

from the true areas. However, the discrepancy may be more than can be understood on the basis of surface area measurements and may reflect the different buffer systems used in the two studies. Alternatively, we note that traces of metal ions such as Mg^{2+} (13), Cu^{2+} (38), Sc^{3+} (39), Pb^{2+}, Cd^{2+}, or Zn^{2+} (40), or phosphate ions (41, 42) can inhibit the dissolution process and this might be a reason for preferring the higher value.

ACKNOWLEDGMENTS

We thank Dr. W. A. House for helpful discussions and SERC and the Freshwater Biological Association for a CASE studentship for PJD.

REFERENCES

1. Stumm, W., and Morgan, J. J., "Aquatic Chemistry," 2nd ed. Wiley, New York, 1981.
2. Cassford, G. E., House, W. A., and Pethybridge, A. D., *J. Chem. Soc. Faraday Trans. I* **79,** 1617 (1983).
3. Sverdrop, H., and Bjerle, I., *Vatten* **38,** 59 (1982).
4. House, W. A., and Tutton, J. A., *J. Cryst. Growth* **56,** 699 (1982).
5. Sass, E., Morse, J. W., and Millero, F. J., *Amer. J. Sci.* **283,** 218 (1983).
6. Busenberg, E., and Plummer, L. N., *Amer. J. Sci.* **282,** 45 (1982).
7. House, W. A., *J. Chem. Soc. Faraday Trans. I* **77,** 341 (1981).
8. Ready, M. M., and Gaillard, W. D., *J. Colloid Interface Sci.* **80,** 171 (1981).
9. Plummer, L. N., Wigley, T. M., and Parkhurst, D. L., *Amer. J. Sci.* **278,** 179 (1978).
10. Sjöberg, E. L., *Geochim. Cosmochim. Acta* **40,** 441 (1976).
11. Plummer, L. N., and Wigley, T. M. L., *Geochim. Cosmochim. Acta* **40,** 191 (1976).
12. Goujon, G., and Mufaftschiev, B., *J. Colloid Interface Sci.* **57,** 148 (1976).
13. Nancollas, G. H., Kazmierizak, T. F., and Schuttringer, E., *Corrosion* **37,** 76 (1981).
14. Pleskov, Yu. V., and Filinovskii, V. Yu., "The Rotating Disc Electrode." p. 32. Plenum, New York, 1976.
15. Von Karman, T., *Z. Angew. Math. Mech.* **1,** 233 (1921).
16. Cochran, W. G., *Proc. Cambridge Philos. Soc.* **30,** 365 (1934).
17. Levich, V. G., *Acta Phys.-Chim. URSS* **17,** 257 (1942).
18. Albery, W. J., and Hitchman, M. L., "Ring-Disc Electrodes," p. 17, Oxford Univ. Press, Oxford, 1971.
19. Daly, P. J., Page, D. J., and Compton, R. G., *Anal. Chem.* **55,** 1191 (1983).
20. Riddiford, A. C., *in* "Advances in Electrochemistry and Electrochemical Engineering" (P. Delahay and C. W. Tobias, Eds.), Vol. 4, p. 47. Wiley-Interscience, New York, 1966.
21. Tóth, K., Cavaller, I., and Pungor, E., *Anal. Chim. Acta* **57,** 131 (1971).
22. Koryta, J., "Ion-selective Electrodes," p. 68. Cambridge Univ. Press, Cambridge, 1975.
23. Koutecky, J., and Levich, V. G., *Zh. Fiz. Khim.* **32,** 1565 (1956).
24. Wilke, C. R., and Chang, P., *AIChE J.* **1,** 264 (1955).
25. Bidstrup, D. E., and Geankoplis, C. J., *J. Chem. Eng. Data* **8,** 170 (1963).
26. Le Bas, G., "The Molecular Volumes of Liquid Chemical Compounds." Longmans, London, 1915.
27. Gostisa-Mihelcic, V. B., Vielstich, W., and Heindrichs, A., *Ber. Bunsenges.* **76,** 19 (1972).
28. Stumm, W., and Morgan, J. J., "Aquatic Chemistry," 2nd ed., p. 211. Wiley, New York, 1981.
29. Bard, A. J., and Faulkner, L. R., "Electrochemical Methods," p. 434. Wiley, New York, 1980.
30. Edmond, J. M., and Gieskes, J. M., *Geochim. Cosmochim. Acta* **34,** 1261 (1970).
31. Bolin, B., *Tellus* **12,** 274 (1960).
32. Barth, D., Tondre, C., Lappai, G., and Delpuech, J. J., *J. Phys. Chem.* **85,** 3660 (1981).
33. Skirrow, G., *in* "Chemical Oceanography" (G. Skirrow and J. P. Riley, Eds.), Vol. 2, p. 37. Academic Press, London, 1975.
34. Albery, W. J., and Bell, R. P., *Proc. Chem. Soc.* 163 (1963).
35. Eigen, M., and Eyring, E. M., *J. Amer. Chem. Soc.* **84,** 3254 (1962).
36. West, R. C., "CRC Handbook of Chemistry and Physics" 59th ed. CRC Press, Boca Raton, Fl., 1978.
37. Untereker, D. F., and Bruckenstein, S., *J. Electrochem. Soc.* **121,** 360 (1974).
38. Erga, O., and Terjesen, S. G., *Acta Chem. Scand.* **10,** 872 (1956).
39. Nestaas, I., and Terjessen, S. G., *Acta Chem. Scand.* **23,** 2519 (1969).
40. Terjessen, S. G., Erga, O., and Thorsen, G. V., *Chem. Eng. Sci.* **14,** 277 (1961).
41. Morse, J. W., *Amer. J. Sci.* **274,** 638 (1974).
42. Berner, R. A., and Morse, J. W., *Amer. J. Sci.* **274,** 108 (1974).

J. Electroanal. Chem., 178 (1984) 45–52
Elsevier Sequoia S.A., Lausanne – Printed in The Netherlands

CURRENT TRANSIENTS AT A CHANNEL ELECTRODE PRODUCED BY A POTENTIAL STEP

RICHARD G. COMPTON and PADRAIG J. DALY

Department of Inorganic, Physical and Industrial Chemistry, The University of Liverpool, P.O. Box 147, Liverpool L69 3BX (Great Britain)

(Received 16th April 1984; in revised form 18th June 1984)

ABSTRACT

A theory is presented which describes the transient current response to a potential step at a channel (or tubular) electrode for a reversible electrode reaction. Experimental results for a wide range of solution flow velocities are found to be in good agreement with theory.

INTRODUCTION

The channel electrode and the closely related tubular electrode are popular choices as flow-through electrodes [1] both for analytical purposes [2–4] and as well-defined hydrodynamic electrodes for the study of electrode reaction mechanisms [5,6]. In previous papers we have considered the problems of EC [7] and ECE [6] processes and of ac voltammetry [8] at such electrodes. Other workers have considered the shape of current voltage curves at such electrodes [9] and have examined both theoretically and experimentally their chronopotentiometric response [10–12]. Matsuda has solved the problems of catalytic currents [13] and kinetic currents [14] at channel electrodes. Double channel electrodes have been employed [15–17] in a similar way to ring–disc electrodes for the study of reaction mechanisms. In this paper we consider the current transient resulting from a potential step on the channel electrode at hydrodynamic equilibrium. This problem is of interest since such measurements are used to measure diffusion coefficients of electroactive species. Unlike steady-state measurements analysis of the transient provides a value for the diffusion coefficient which is not dependent on a knowledge of the number of electrons transferred in the electrode reaction, or of the concentration of the electroactive species. Furthermore, film formation or adsorption often interferes with the interpretation of steady-state limiting currents and the desired information can be obtained from the current transient before such complications interefere [18].

The mathematical solution to this problem is obtained using Laplace transformation. In this problem, as in many others of electrochemical interest, the transformed quantity of interest (in this case the current), upon solution of the appropriate

0022-0728/84/$03.00

convective–diffusion equation, is found to be represented by a power series in the Laplace transform variable. Such a series cannot usefully be inverted term-by-term. We show that the method of rational approximations [19] can be successfully used to overcome this problem and to provide accurate values for the transient current over a wide interval of time. Theory and experiment are shown to be in good agreement.

THEORY

We consider the following electrode reaction:

$$A \pm n\,e^- \rightarrow B$$

and assume only A to be present in the bulk of the solution. The convective–diffusion equation describing the concentration, c, of A is:

$$\frac{\partial c}{\partial t} = D\frac{\partial^2 c}{\partial y^2} - \frac{3}{2}\bar{U}\left[1-(b^2-y^2)/b^2\right]\frac{\partial c}{\partial x} \tag{1}$$

where D is the diffusion coefficient of A, b is the half-height of the channel, $\bar{U}$ is the mean solution velocity (cm s^{-1}), x is the distance along the channel starting from the upstream edge of the electrode and y is the distance normal to the electrode starting from the electrode surface.

We have shown previously that, providing $(x_E D/\bar{U}b^2) \ll 1$ where x_E is the length of the electrode, eqn. (1) can be simplified to:

$$\frac{\partial u}{\partial t} = \frac{\partial^2 u}{\partial \xi^2} - \xi\frac{\partial u}{\partial \chi} \tag{2}$$

where the normalised variables are defined by:

$$\tau = \left(9\bar{U}^2 D/x_E^2 b^2\right)^{1/3} t$$

$$\chi = x/x_E$$

$$\xi = \left(3\bar{U}/bDx_E\right)^{1/3} y$$

and

$$u = c - c^\infty$$

where c^∞ is the bulk concentration of A. The relevant boundary conditions for the case of a potential step are

$\tau = 0$	$\xi \geqslant 0$	$u = 0$
$\tau > 0$	$\xi \rightarrow \infty$	$u \rightarrow 0$
$\tau > 0$	$\xi = 0$	$u = u'$

It is assumed that for $\tau < 0$ no current is flowing through the electrode but that for $\tau > 0$ the surface concentration changes from c^∞ and u becomes u' ($\neq 0$). Notice that

u' is taken to be independent of χ, i.e. that the concentration c is assumed to be unchanged along the length of the electrode. This will be the case for any point on a reversible voltammetric wave but will only hold for currents close to the transport limited value for an irreversible wave. Double Laplace transformation of eqn. (2), firstly with respect to τ (transform variable s) and secondly with respect to χ (variable p) gives:

$$s\bar{\bar{u}} = \partial^2\bar{\bar{u}}/\partial\xi^2 - p\xi\bar{\bar{u}} \tag{3}$$

where $\bar{\bar{u}}$ represents the double transform of u. The solution of eqn. (3) and the application of the boundary conditions given above gives:

$$\bar{\bar{u}} = \frac{Ai\left[p^{-2/3}(s+p\xi)\right]}{Ai\left[p^{-2/3}s\right]}\bar{\bar{u}}(\xi=0) \tag{4}$$

in which $Ai[x]$ denotes the Airy function [20]. The current I due to the discharge of A is:

$$I \propto \int_0^{1.0} \left.\frac{\partial c}{\partial\xi}\right|_{\xi=0} d\chi \tag{5}$$

$$\propto \mathscr{L}_s^{-1}\left\{\mathscr{L}_p^{-1}\frac{1}{p}\left.\frac{\partial\bar{\bar{u}}}{\partial\xi}\right|_{\xi=0}\right\}_{\chi=1} \tag{6}$$

$$\propto \mathscr{L}_s^{-1}\left\{\mathscr{L}_p^{-1}\frac{1}{p^{2/3}}\frac{Ai'\left[p^{-2/3}s\right]}{Ai\left[p^{-2/3}s\right]}\bar{\bar{u}}(=0)\right\}_{\chi=1} \tag{7}$$

where for the case of interest, $\bar{\bar{u}}(\xi=0) = u'/ps$. To invert eqn. (7) we expand the logarithmic derivative of the Airy function as a power series:

$$\frac{Ai'\left[p^{-2/3}s\right]}{Ai\left[p^{-2/3}s\right]} = \frac{1}{a_0}\sum_{n=0}^{\infty} c_n s^n\left(p^{-2/3}\right)^n \tag{8}$$

where $c_0 = a_1$, $c_n = (n+1)a_{n+1} - a_0^{-1}\Sigma_{k=1}^{n} c_{n-k}a_k$ and the coefficients a_k are defined by $Ai[x] = \Sigma_{n=0}^{\infty} a_n x^n$ [20]. Substitution of eqn. (8) into the bracketed term in eqn. (7), followed by term-by-term inversion gives:

$$I \propto \mathscr{L}_s^{-1}\frac{u'}{a_0 s}\sum_{n=0}^{\infty}\frac{c_n s^n}{\Gamma\left(\frac{5}{3}+\frac{2n}{3}\right)} \tag{9}$$

The first term in the series in eqn. (9) corresponds to the steady-state current flowing when the transient effects have died away. We may therefore write:

$$\frac{I(\tau)}{I(\tau\to\infty)} = 1 + \mathscr{L}_s^{-1}\frac{\Gamma\left(\frac{5}{3}\right)}{Ai'[0]}\sum_{n=1}^{\infty}\frac{c_n s^{n-1}}{\Gamma\left(\frac{5}{3}+\frac{2n}{3}\right)} \tag{10}$$

The series in eqn. (10) cannot be simply inverted. We therefore adopt the method

of rational approximations. That is we approximate the series by a sequence of rational functions $\tilde{f}_n(s) = g_n(s)/h_n(s)$ whose members are then inverted analytically to give a sequence of functions $\{f_n(\tau)\}$ which one hopes will converge rapidly as $n \to \infty$. For a series such as in eqn. (10) one possible method of generating a suitable sequence is to calculate the Pade table [21] and then invert successive elements on the leading diagonal until convergence is achieved. However, this method, in this case, was found to generate poles in the right-hand half-plane $Re(s) > 0$ for some values of $n > 10$. This is unsatisfactory since it leads to terms of the form Ae^{at}, $a > 0$ in our approximate solution. Similar problems have emerged in the application of the Pade table to other Laplace transform inversions [21,22]. We therefore turned to the method of Levin transformation [23] to provide a suitable sequence of rational functions. Applying the Levin U_d transformation to each of the partial sums, $\tilde{f}_n(s)$ where:

$$\tilde{f}_n(s) = \sum_{k=1}^{n+1} c'_n s^{k-1} \tag{11}$$

and $c'_n = c_n/\Gamma(5/3 + 2n/3)$ we obtain the rational approximation U_n,

$$U_n = g_n(s)/h_n(s) \tag{12}$$

where:

$$g_n(s) = \sum_{i=1}^{n} \alpha_{ni} s^{i-1} \tag{13}$$

and:

$$h_n(s) = \sum_{i=1}^{n+1} \beta_{ni} s^{i-1} \tag{14}$$

The coefficients α_{ni} and β_{ni} depend on the coefficients $c_n/\Gamma(5/3 + 2n/3)$, in the series in eqn. (11) in the following way:

$$\alpha_{ni} = \sum_{j=1}^{i} \binom{n}{j-1} \frac{(n+2-j)^{n-2}}{c'_{n+2-j}} (-1)^{j+1} c'_{i-j+1} \tag{15}$$

and:

$$\beta_{ni} = (-1)^{i+1} \binom{n}{i-1} \frac{(n+2-i)^{n-2}}{c'_{n+2-i}} \tag{16}$$

Thus from eqns. (10), (11) (12) we finally obtain:

$$\frac{I(\tau)}{I(\tau \to \infty)} = 1 + \lim_{n \to \infty} \frac{\Gamma(\frac{5}{3})}{Ai'[0]} \mathscr{L}_s^{-1} g_n(s)/h_n(s) \tag{17}$$

$$= 1 - 3.488 \lim_{n \to \infty} \sum_{m=1}^{n} \frac{g_n(q_m)}{h'_n(q_m)} \exp(q_m \tau) \tag{18}$$

where q_m are the complex roots of the equations:

$$h_n(s) = 0 \tag{19}$$

and:

$$h'_n(s) = \mathrm{d}h_n(s)/\mathrm{d}s \tag{20}$$

The sum in eqn. (18) was evaluated using a Fortran computer program. For values $\tau > 0.2$ satisfactory convergence was found by considering $n < 10$. The resulting current transient is shown in Fig. 1. For $\tau < 0.2$ the convergence was less good even taking n as large as 20 and in this region it is only possible to give a range of values in which $I(\tau)$ may lie, as shown in Fig. 1.

Theoretical work on eqn. (2) has been carried out by Soliman and Chambre in the field of heat transfer [24]. Their analytical approach shows that the flux at a point a distance χ along the electrode is given by the approximation,

$$\frac{(\partial u/\partial \xi)\chi, \tau}{(\partial u/\partial \xi)\chi, \tau \to \infty} \sim \frac{1.048}{\sqrt{\tau'}} \tag{21}$$

which is valid for $\tau' < 1.0$ where $\tau' = \tau/\chi^{2/3}$. For $\tau' > 1.0$ eqn. (21) was shown to be an underestimate [24].

Thus for points on the electrode surface sufficiently downstream of the leading edge the transient shows a "Cottrell equation" type behaviour in its early stages. This is not true of Fig. 1 which shows the flux integrated over the electrode surface. The contribution of points near the leading edge of the electrode for which eqn. (21) is a poor approximation causes the total current at the electrode to deviate from $(\text{time})^{-1/2}$ behaviour even at small times.

Note that the above theory is also applicable to tubular electrodes in this case Fig. 1 still describes the transient response but now τ is defined by:

$$\tau = \left(4v_0^2 D/x_E^2 r_0^2\right)^{1/3} t$$

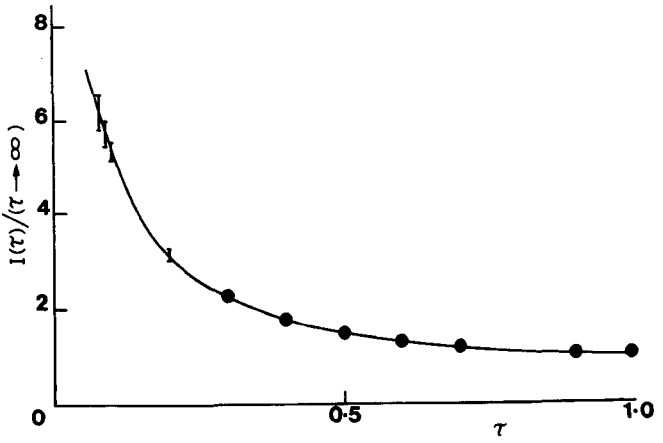

Fig. 1. Theoretical current transients calculated from eqn. (18).

where r_0 is the radius of the tubular electrode and v_0 is the flow velocity (cm s^{-1}) at the centre of the tube.

EXPERIMENTAL

The design of the channel electrode unit and the associated flow system has been described previously [5,6]. The channel unit had approximate cross-sectional dimensions of 0.4 mm × 7.0 mm. A precise value for the short dimension was obtained each time the channel unit was assembled by measuring the diffusion-limited current from a species of known concentration and of known diffusion coefficient as before [6]. Polished platinum foils of approximate dimensions 5.0 mm × 5.0 mm were used as electrodes. Flow rates in the range 5×10^{-3} to 10^{-1} cm^3 s^{-1} were obtained by gravity feed through capillaries of different diameters.

Solutions were made up using twice-distilled deionised water and typically contained ca. 3×10^{-3} *M* potassium ferricyanide and 0.1 *M* potassium chloride. Reagent grade chemicals were used throughout. Solutions were thoroughly purged of oxygen by bubbling through the solution nitrogen which had been purified by passage over BTS catalyst.

RESULTS AND DISCUSSION

The above theory was tested by studying the reduction of potassium ferricyanide in 0.1 *M* potassium chloride,

$$Fe(CN)_6^{3-} + e^- = Fe(CN)_6^{4-}$$

at a platinum channel electrode. Steady-state measurements showed the diffusion-limited current to vary as the cube root of the flow rate as predicted by the Levich equation [9]:

$$I_{lim} = 1.165\, nFcD^{2/3}\overline{U}^{1/3}b^{-1/3}wx_E^{2/3}$$

where w is the width of the electrode. Figure 2 shows a log–log plot of I_{lim} against volume flow rate ($V_f = 2bw'\overline{U}$, w' = width of channel); the slope is close to the expected value of ($\frac{1}{3}$). The intercept allows us to calculate the diffusion coefficent of ferricyanide as 7.5×10^{-6} cm^2 s^{-1} in excellent agreement with the literature value of 7.63×10^{-6} cm^2 s^{-1} [25]. Current–time curves were obtained for flow rates between 5×10^{-3} and 10^{-1} cm^3 s^{-1} by stepping the potential from a value at which no current passed to a potential where the current was diffusion-limited, and recording the entire transient. This was analysed by finding the time, t_2, taken for the current to fall from the initial very large value to twice the final steady-state value. From Fig. 1 we see that this is given by:

$$0.35 = \left(9\overline{U}^2D/x_E^2b^2\right)^{1/3}t_2 \qquad (22)$$

In Fig. 3 the experimental determined values of t_2 are plotted against the volume

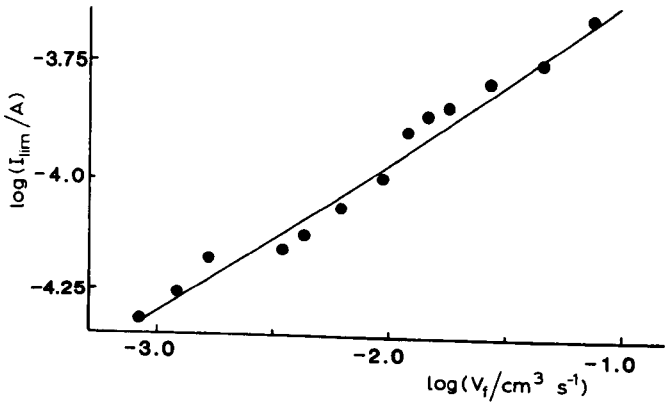

Fig. 2. The steady state limiting currents obey the Levich equation. The line has the expected slope of (1/3).

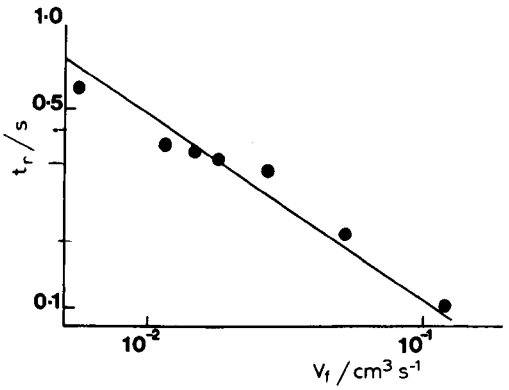

Fig. 3. Experimentally determined values of t_2 vary as $V_f^{-2/3}$

flow rate V_f. The slope of the log–log plot is close to the $(-\frac{2}{3})$ predicted by eqn. (21). The line drawn is that calculated from eqn. (21) together with the experimentally determined values of D and the measured values for the geometry of the electrode. Good agreement between theory and experiment is seen.

ACKNOWLEDGEMENT

We thank the Freshwater Biological Association and SERC for a CASE studentship for a CASE studentship for P.J.D. We also thank a referee for drawing our attention to ref. 24.

REFERENCES

1 B.H. Vassos and G.W. Ewing, Electroanalytical Chemistry, John Wiley, New York, 1983, p. 167.
2 W.J. Blaedel and L.N. Klatt, Anal. Chem., 38 (1966) 879.
3 W.J. Blaedel and S.L. Boyer, Anal. Chem., 43 (1971) 1538.
4 W.J. Blaedel and G.W. Schieffer, Anal. Chem., 49 (1977) 49.
5 R.G. Compton and B.A. Coles, J. Electroanal. Chem., 144 (1983) 87.
6 R.G. Compton, D.J. Page and G.R. Sealy, J. Electroanal. Chem., 161 (1984) 129.
7 R.G. Compton and B.A. Coles, J. Electroanal. Chem., 127 (1981) 37.
8 R.G. Compton and G.R. Sealy, J. Electroanal. Chem., 145 (1983) 35.
9 H. Matsuda, J. Electroanal. Chem., 15 (1967) 325.
10 R.E. Meyer, M.C. Banta, P.M. Lantz and F.A. Posey, J. Electroanal. Chem., 30 (1971) 345.
11 F.A. Posey and R.E. Meyer, J. Electroanal. Chem., 30 (1971) 359.
12 K. Aoki and H. Matsuda, J. Electroanal. Chem., 90 (1978) 333.
13 K. Aoki, K. Tokuda and H. Matsuda, J. Electroanal. Chem., 76 (1977) 217.
14 K. Tokuda, K. Aoki and H. Matsuda, J. Electroanal. Chem., 80 (1977) 211.
15 K. Aoki, K. Tokuda and H. Matsuda, J. Electroanal. Chem., 79 (1979) 49.
16 K. Aoki and H. Matsuda, J. Electroanal. Chem., 94 (1978) 157.
17 T. Tsuru, T. Nishimura, K. Aoki and S. Haruyama, Denki Kagaku, 50 (1982) 712.
18 S. Bruckenstein and S. Prager, Anal. Chem., 39 (1967) 1161.
19 I.M. Longman, SIAM J. Appl. Math., 24 (1973) 429.
20 M. Abramowitz and I.A. Stegun, Handbook of Mathematical Functions, Dover, New York, 1970, p. 446.
21 I.M. Longman, Int. J. Comp. Math., (1971) 53.
22 I.M. Longman, J. Comp. Phys., 10 (1972) 224.
23 D. Levin, Int. J. Comp. Math., (1973) 371.
24 M. Soliman and P.L. Chambre, Int. J. Heat Mass Transfer, 10 (1967) 169.
25 M. von Stackelberg, M. Pilgram and V. Toome, Z. Elektrochem., 57 (1953) 342.